UNIVERSITÀ
DEGLI STUDI
FIRENZE

Università degli Studi di Firenze
Dipartimento di Ingegneria dell'Informazione (DINFO)
Corso di Dottorato in Ingegneria dell'Informazione
Curriculum: Elettronica, Elettromagnetismo ed Elettrotecnica

Prognosis and diagnosis of electrical power systems using machine learning methods

Candidate
Marco Bindi

Supervisors
Prof. Antonio Luchetta

Prof. Stefano Manetti

PhD Coordinator
Prof. Fabio Schoen

ciclo XXXV, 2019-2022

Università degli Studi di Firenze, Dipartimento di Ingegneria
dell'Informazione (DINFO).

Acknowledgments

First and foremost I am extremely grateful to my supervisors, Prof. Antonio Luchetta and Prof. Stefano Manetti for their invaluable advice, continuous support, and patience during my PhD study. Their immense knowledge and plentiful experience have encouraged me in all the time of my academic research and daily life. I would like to thank also Prof. Francesco Grasso for his invaluable supervision and support during the course of my PhD degree, Prof. Maria Cristina Piccirilli and Prof. Alberto Reatti for the introduction of multidisciplinary aspects in my research and all my colleagues of the Smart Energy Lab, who were of great help during these years. In particular, my thanks go to Giacomo Talluri, Fabio Corti, Carlos Iturrino Garcia and Libero Paolucci who collaborated in many parts of my research work. I would like to thank also Prof. Igor Aizenberg for his kind support and hospitality during my stay at Manhattan College in New York.

Contents

Chapter 1

Introduction

1.1 The objective

The main objective of this research is the development of a prognostic approach capable of detecting and localizing malfunctions in electrical power systems using machine learning methods. The theoretical basis of the monitoring method proposed here is the analysis of analog circuits, in which the variation of the passive components caused by ageing shifts the operating point from the nominal one. These working conditions are called malfunctions and usually precede the occurrence of catastrophic failures. Therefore, the detection and localization of malfunctions allow the prevention of faults, thus decreasing recovery times and increasing the reliability of the system. The prognostic procedure developed in this research can be applied to many different electrical systems and power devices while maintaining three basic steps, which are: the study of the main failure modes and failure mechanisms of the systems under test, the selection of the best measurements for the detection of malfunctions and the development of a classifier based on artificial intelligence. The main field of application presented in this work is the monitoring of electrical transmission and distribution lines, where the localization of problems plays a fundamental role in order to organize maintenance operations. Furthermore, since the recent development of smart grids and smart cities involves the integration of renewable energy sources, battery-powered loads and non-linear loads, the effectiveness of the prognostic procedure is also verified on DC-DC converters and in the field of Power Quality (PQ) analysis.

1.2 Contributions

The current PhD thesis aims to introduce a new method to analyse the health status of electrical systems, thus preventing failures and avoiding catastrophic consequences.

In the field of electrical grid monitoring, the first approach proposed here is the detection and localization of malfunctions starting from measurements of the line frequency response. In fact, the most common failure mechanisms affecting electrical infrastructures can be linked to variations in the line parameters and, consequently, to the changes in the measured frequency response. The development of a machine learning method capable of detecting these variations and their causes is the final purpose of the work. Initially, High Voltage (HV) overhead lines are considered and the main subjects of the study are the junction regions between successive sections of the same phase conductor. Therefore, the main contribution in this field of application is the introduction of a prognostic procedure organized as follows:

- definition of the equivalent line circuit with lumped parameters and modelling of the effects of ageing and deterioration;
- selection of the best test points in order to detect variations in electrical parameters (Testability analysis);
- development of a classifier based on machine learning techniques capable of identifying the state of health of the joints.

The main theoretical results obtained in this type of applications show the great potential of Multi-Layer neural networks with Multi-Valued Neurons (MLMVN). The algorithm on which these classifiers are based is presented and developed in the continuation of the Thesis, highlighting the excellent performance in the recognition of electrical measurements.

Once the main phases of the prognostic method have been defined, it can be used to develop monitoring systems capable of preventing catastrophic failures in many different types of electrical infrastructures. In this sense, underground distribution lines are considered, since access to Medium Voltage (MV) cables is usually very complicated and the location of problems plays a fundamental role in the organization of maintenance operations. Therefore, a monitoring system based on the evaluation of the line frequency response is simulated in Matlab-Simulink environment. In this case, the main technical

aspect is the implementation of Power Line Communication (PLC) technologies to obtain the necessary measurements. Hence, the most important contributions of this study are:

- to propose an overview of the main problems in MV cables and their effects on the equivalent lumped circuit;
- to develop a measurement system based on low-level intrusive PLC instrumentation;
- to propose a simulation procedure easily adaptable to different line topologies;

The classification results obtained through MLMVN and other machine learning techniques confirm the effectiveness of the proposed monitoring system and highlight the need for a model based on distributed parameters to extend the length of the line branch under consideration.

The transition from lumped to distributed parameters allows the use of higher frequencies and requires the measurements of the transmitted signals to be processed instead of the frequency response values. In this case, the MLMVN-based monitoring system focuses on the detection and localization of overheating situations in underground MV lines. In fact, abnormal working temperatures can be considered as one of the main causes of cable degradation and the identification of thermal malfunctions allows the prevention of catastrophic failures. To improve the quality of the simulations, the experimental characterization of several MV cables is proposed. Therefore, the behaviour of electrical parameters in the frequency domain is defined by using a Vector Network Analyser (VNA) both in nominal and overheating conditions. In this way, it is possible to set the values of the distributed elements according to the frequencies of the transmitted signals and simulate their variations as the working temperature increases. This allows the introduction of further contributions:

- development of a prognostic method for underground medium voltage cables focused on the working temperature of the line;
- definition of an experimental procedure for the frequency characterization of MV cables both in nominal and overheating conditions;
- development of a complete simulation model for the MLMV-based monitoring system that uses measurements of PLC signals;

Thanks to the experimental measurements obtained, it is possible to study different uses of high frequency signals in the failure prevention and fault localization. These applications are investigated in the following chapters.

To increase the fields of use of the proposed prognostic method, the monitoring of DC-DC converters is considered. These power devices are widely used in all battery-powered systems and will play a fundamental role in the development of smart grids and smart cities, enabling the integration of renewable energy sources that produce direct current. In this case, since power converters are time variant circuits, a time-domain analysis is required and some characteristics of the prognostic approach need to be modified. The main objective of this application is to detect the ageing of passive components before they can take the converter out of service. To achieve this purpose, deviations of passive elements with respect to their nominal values must be identified and classified. Therefore, the main contributions of this work can be summarized as follows:

- to propose a graphical method for the Testability analysis in time-variant circuits, which facilitates the selection of test points avoiding ambiguity situations;
- to develop a monitoring system based on MLMVN capable of identifying the passive component in the worst state of health by processing time-domain measurements;
- to validate experimentally the proposed prognostic approach on a Zeta converter;

By generalizing this procedure it is possible to define the working conditions of many different DC-DC converters during their normal operation. The possibility of working on-line is one of the most important aspects of the monitoring system developed.

Finally, given the growing use of non-linear loads, power electronic devices and electrical machines, the quality of the energy in distribution lines can decrease introducing large malfunctions. Again, the early detection of voltage and current distortions allows the prevention of hard faults and the organization of countermeasures. For example, in the industrial sector, the presence or harmonic contents different from the fundamental waveform ($50Hz$) introduces overheating in power transformers and causes energy losses in rotating electrical machines. Identifying this problem and fixing it would improve

overall performance and reduce manufacturing costs. Therefore, a further application of machine learning methods, including MLMVN, is presented in the field of Power Quality analysis.

The overall structure of the Thesis can be summarized as follows.

In the second Chapter, an extensive literature review is presented in order to introduce the main theoretical concepts necessary to understand the proposed prognostic procedures. Therefore, the most important definitions in the field of electrical system monitoring are presented, clarifying the differences between *failure* and *malfunction* as well as those between *prognosis* and *diagnosis*. The basic concepts of multi-frequency parametric analysis of analog circuits are also presented and the main simulation tools used to perform this study are introduced. Finally, the fields of application taken into consideration are described: monitoring of electrical infrastructures, prognosis of DC-DC converters and analysis of Power Quality disturbances.

In the third Chapter, the main aspects of the proposed methodology are introduced. Then, once the prognostic procedure is illustrated, the neural classifier developed to apply it is presented in detail. This algorithm is based on a complex neural network and has been entirely developed in Matlab code to allow easy adaptation in the various fields of application. In addition, lumped and distributed parameter modelling methods of overhead and underground power lines are proposed to allow training of the neural network. Finally, since the training phase must be preceded by a specific Testability analysis, a new graphical method is proposed to perform this evaluation in time-variant circuits.

The fourth Chapter presents the first application examples. These are completely simulated procedures which aim to verify the theoretical effectiveness of the method. In particular, a system for monitoring joints in overhead high voltage lines and for detecting overheating in medium voltage underground lines is proposed. In both cases, the method is based on the lumped parameter modelling presented in the third section.

In order to facilitate the training procedure using higher frequencies, the use of the distributed parameter model is presented in the fifth Chapter. In this case, an experimental characterization procedure for medium voltage cables is also proposed. The main objective of this process is to define the electrical parameters of the cable per unit of length in the nominal working conditions and in the presence of an over-temperature. The results obtained experimentally are integrated in the simulations to verify the effectiveness of

the method in situations closer to the real ones.

The sixth Chapter presents the possible application of the prognostic method on a Zeta converter. Therefore, the graphical method for the Testability assessment presented in the third section is applied for the selection of optimal test points. Subsequently, the performance of the prognostic system is experimentally verified on a real prototype of the converter.

The seventh Chapter shows the possible application of the classifier for the identification of disturbances in low voltage distribution networks. Also in this case an experimental set-up is used to verify the effectiveness of the method. Two different configurations of the classifier are proposed: the first directly processes data in the time domain while the second involves a preprocessing phase through Discrete Fourier Transform.

Finally, the eighth Chapter contains the conclusions and possible future developments of the research.

Chapter 2

Theoretical Aspects: Literature Review

This chapter provides a brief overview of the main theoretical concepts and related works in the field of failure analysis. The first part of the chapter introduces a general classification of faults based on the type of electrical systems considered and the severity of the deviation from the nominal conditions. This allows the introduction of the term Malfunction, which is one the most important concepts in failure prevention systems. Starting from this, it is possible to define different types of maintenance operations depending on the final purpose and the time in which they occur. These interventions are based on monitoring methods that employ different measurements and analysis techniques to define the health status of the system under test. The most useful approaches proposed in the literature are presented in this chapter together with the main aspects of the developed prognostic procedure. In this sense, the introduction of artificial intelligence algorithms plays a fundamental role and represents one of the most challenging aspects for researchers in various sectors. [1]

[1]The part of this chapter related to the detection of parametric failures in analog circuits has been published as "A neural network classifier with multi-valued neurons for analog circuit fault diagnosis" in *Electronics (Special Issue: Diagnosis in Analog Electronic Circuits, Electrical Power Systems and Smart Grids), vol. 10, iss. 3, 2021* [1].

2.1 Faults and Malfunctions

Fault diagnosis is a multidisciplinary term widely used in the literature to describe a huge number of methods and applications. To understand the correct meaning of this wording it is necessary to consider the main characteristics of the System Under Test (SUT). For example, in the electrical sector, the first aspect taken into consideration is the digital or analog nature of the SUT. In the first case, a limited variety of faults can be found, such as short circuits and open circuits, which determine a complete loss of functionality or a situation very far from the nominal condition. Therefore, the presence of a fault in digital systems is usually evident and diagnostic methods have the main objective of locating the problem, avoiding its extension and securing the entire system. In fact, the growing miniaturization and complexity of electronic devices, makes the localization and limitation of faults essential to reduce recovery times in corrective maintenance operations. In many cases, these types of failures are not easily predictable since they do not represent consequences of ageing and degradation of components. Therefore, the small amount of failure models has led to the development of fully automated test methodologies that are easily adaptable to many different types of digital systems. Instead, in the field of analog circuits, most catastrophic faults occur due to the presence of failure mechanisms, which are chemical or physical processes capable of gradually changing the values of the electrical components. Therefore, ageing and deterioration caused by failure mechanisms introduce deviations of the operating point, thus resulting in performances different from the nominal ones. The persistence of this situation can lead to catastrophic consequences with total loss of functionality. This means that the concept of failure in analog systems is very broad and includes many different situations. For this reason, the term *Parametric Fault* is introduced, which is used to describe the deviation of at least one characteristic property of the circuit from the allowed range. In this sense, the tolerances of the passive electrical components play a fundamental role in distinguishing the nominal state and the degradation.

2.1.1 Main Definitions

Starting from the general observations, the following classification can be introduced:

- **Manufacturing Tolerances**

This term describes the nominal ranges of the passive components belonging to the Circuit Under Test (CUT). When all the electrical elements are in these intervals, the overall system works correctly according to the design assumptions.

- **Soft Faults**

  In this condition, one or more electrical components exceed the manufacturing tolerances and this produces a slight deviation of the operating point. The whole system is still functioning but some features differ from the desired behaviour. Soft faults can be caused by temporary abnormal working conditions or the initial stages of ageing and deterioration.

- **Hard Faults**

  This term is used to describe significant deviations of the circuit parameters with respect to the nominal intervals. In this condition, the CUT does not work completely and corrective maintenance operations are required. Usually, hard faults are caused by severe component deterioration, long-term overload or a drastic change in environmental conditions.

- **Catastrophic Faults**

  A catastrophic fault (or fatal failure) represents the total loss of functionality, usually accompanied by the destruction of a circuit component and can be modelled using a short or open circuit. The change in the circuit topology makes the failure condition evident and no further measurements are required.

Assuming this classification, it is possible to use the term *Malfunctions* to indicate all working conditions different from the nominal ones that precede the occurrence of a catastrophic fault. These conditions result in a partial loss of functionality, thus shifting the operating point towards a low efficiency or less effective configuration. Therefore, the detection of malfunctions allows the prevention of catastrophic failures introducing specific maintenance operations. Figure 2.1 summarizes the evolution of operating conditions due to the occurrence of a specific failure mechanisms.

From a general point of view, *Maintenance* can be defined as the combination of all technical, administrative and managerial actions during the life cycle of an item intended to retain it in, or restore it to, a state in which

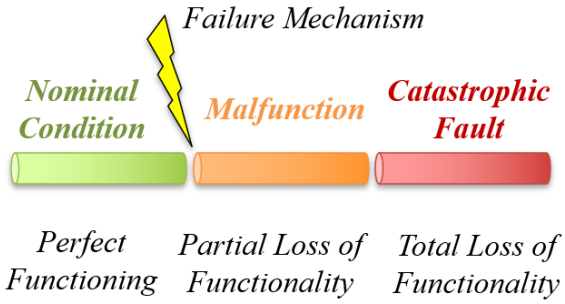

Figure 2.1: Evolution of operating conditions due to the occurrence of failure mechanisms.

it can perform the required function [2]. Several approaches can be used to define a maintenance strategy: reactive approach, preventive approach, condition-based interventions and predictive approach. Starting from this, it is possible to summarize the maintenance operations in the following categories:

- **Corrective Maintenance**

  This is the result of a reactive approach. It concerns all the operations necessary to restore the SUT and all its functionalities after a problem has occurred. In this case, the term problem is used to describe a hard fault or a catastrophic fault. The main benefit of this strategy is the minimization of costs for the monitoring systems, while the main disadvantage is the inability to avoid system shut-downs. For these reasons, this solution is adopted in low complexity systems with easily replaceable parts.

- **Preventive Maintenance**

  The main aspect of this strategy is to use an inspection and activity program to find and fix small issues before they turn into big problems.In this case, the main advantage is the possibility of avoiding catastrophic consequences caused by the ageing of the system elements, while the main drawbacks are the costs of inspections and the need to partially or totally interrupt the operation of the system for testing activities.

- **Predictive Maintenance**

  In this case, when the SUT is fully functional, specific monitoring systems are used to predict the residual useful life of its components and organize future maintenance operations. Furthermore,this approach allows the identification of anomalous working conditions that increase the degradation of the components without compromising the current functioning of the system. The main advantage of this solution is the ability to prevent hard failures without interrupting the normal operation of the system and to identify potentially harmful situations. The main drawback is the complexity of the monitoring systems introduced and their intrusive level in the SUT.

In order to complete the dissertation about maintenance operations it is necessary to highlight that some technical standards divide predictive maintenance into two categories: predetermined and condition based. In the first case, each intervention is planned over time and carried out according to a specific program without considering the current state of the system. This approach is characterized by a low level of flexibility and can sometimes lead to unnecessary operations. The condition-based strategy involves maintenance when a specific condition occurs. The event used to start the maintenance operations can be set by knowing the degradation model of the system components or their average useful life, or it can be a particular working condition that indicates the achievement of an unacceptable failure probability. This approach is particularly flexible and can be implemented with different levels of complexity.

In the case of complex systems, consisting of numerous subsystems, corrective maintenance can also be divided into programmable and non programmable. Obviously, when a catastrophic failure occurs, maintenance operations must begin immediately and last as little as possible. On the other hand, when a hard failure concerns a subsystem that is not essential for the overall functioning, it can be decided to postpone the interventions and schedule them at the best time.

The concepts introduced in this paragraph are the basis of any failure analysis and can be applied to many different systems. The multiple aspects of failure diagnosis have been addressed by researchers for many decades [3] [4], and some modern papers offer interesting reviews that facilitate the classification of possible approaches [5] [6]. In the field of analog systems, the concept of malfunction plays a fundamental role. Therefore, the

transient and sensitivity analyses proposed by Tadeusiewicz et al. in [7] they are essential for introducing the concept of soft fault and deviation with respect to nominal conditions in analog electrical circuits. Given the growing complexity and miniaturization of these systems, analysis and monitoring techniques must constantly be updated and developed. For example, the same authors in [8] present an improvement of the parametric failure detection method based on the solution of a failure equation along a spatial curve. Similar approaches are used in other papers, such as in [9], where Tian et al. propose a method of modelling the continuous displacements of analog components and offer a graphical description. Failure analysis represents a fundamental theoretical aspect in the development of this Thesis, which aims to propose innovative monitoring methods for different types of electrical systems. Based on the type of failure considered and the characteristics of the monitoring system, the most appropriate maintenance strategy can be defined. Therefore, the failure analysis elements presented above are also a fundamental prerequisite for reading technical standards on maintenance such as [10] and [11].

2.2 Diagnosis and Prognosis

Considering the definitions presented in the previous section, it can be stated that corrective maintenance focuses on hard and fatal faults. In this case, one of the most important tasks is the localization of the faulty components, because it allows the reduction of recovery times and increases the availability of the system [12]. On the other hand, preventive and predictive maintenance are focused on the detection of malfunction conditions. In this way, catastrophic consequences can be avoided and restoration interventions can be organized and planned [13].

In general, it can be said that monitoring systems aimed at detecting and locating catastrophic faults perform a diagnostic operation, while those focused on malfunction conditions carry out a prognostic evaluation [14]. Figure 2.2 offers a brief explanation of this difference.

One of the main objectives of this Thesis is the definition of prognostic procedures for electrical power systems on which maintenance operations can be based. In the continuation of the work these definitions are often recalled:

- **Diagnostic Method**

This term indicates a set of devices and operations aimed at detecting and locating hard and catastrophic faults.

- **Prognostic Method**

  This term indicates a set of devices and operations aimed at detecting and locating malfunctions, thus predicting the residual useful life on the basis of parametric failure models.

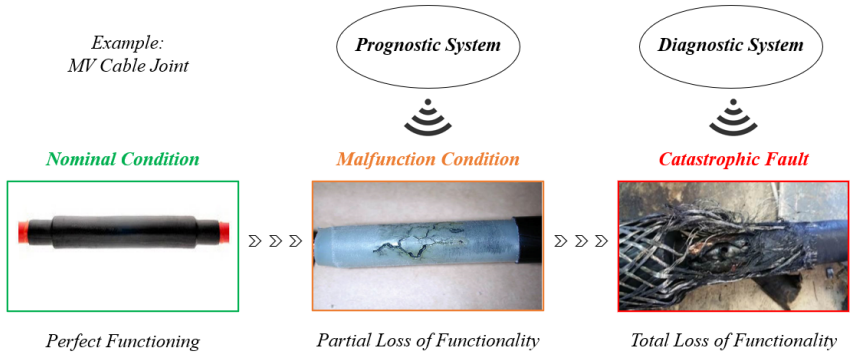

Figure 2.2: Main difference between prognostic and diagnostic system.

2.2.1 Theoretical Basis of Monitoring Systems

From a theoretical point of view, modern monitoring systems for electrical devices can follow two different approaches: Simulation Before Test (SBT) and Simulation After Test (SAT) [15]. SBT requires a large number of simulations on all possible failures and the collection of the circuit responses in a dedicated dictionary. Therefore, the behaviour of the circuit is compared with information from the dictionary to locate problems. This approach is usually suitable for single catastrophic faults, because the size of the dictionary becomes very large in the case of multiple parametric fault situations. In the SAT approach, the first step is to observe the response of the faulty network to a specific test stimulus, then all elements can be identified by comparing the behaviour of the circuit with the analytical form of the network function. This approach is suitable for detecting parametric faults. To

better understand these concepts and the subsequent discussion it is necessary to clarify the meaning of *Single Failure Hypothesis* and *Multiple Failure Hypothesis*.

- **Single Failure Hypothesis**

  Working under these assumptions means that only one component of the circuit can be faulty at a time. Therefore, the number of abnormal working conditions that the monitoring system must recognize is equal to the number of possible defective elements.

- **k-Fault Hypothesis (or Multiple Failure Hypothesis)**

  In this case, more than one component can be considered faulty at the same time. This means that an abnormal operating condition is added for each combination of defective elements, up to a maximum of k components at the same time.

It should be noted that in the case of parametric faults, more than one abnormal condition can be associated with the same circuit component, based on the extent of the variation. This introduces further complications and makes studying the multiple failure hypothesis very difficult.

In both SBT and SAT strategies, circuit modelling plays a fundamental role as well as the definition of appropriate simulations [16]. In the case of digital systems, failure conditions of internal components are limited and this makes the simulation procedure easy from the analytical point of view. The most critical aspect in defining failure models is the selection of measurements. In fact, the circuit responses taken into consideration must allow the cause of the failure to be defined without ambiguity. For example, using SBT approach in digital systems, each measurement of a circuit response belonging to the fault dictionary refers to a problem on a specific component. If two defective elements produce the same circuit response it is necessary to change or add different measurements [17]. Furthermore, if more than one component is considered faulty at the same time, the complexity level increases and specific methods must be introduced for selecting measurements.

In the case of analog circuits, where parametric faults can occur, the modelling operations are very complicated and require accurate theoretical descriptions of the network functions. In fact, the gradual deviations of the electrical components with respect to their nominal values introduce a series of successive operating states that depend on the extent of the changes. The

continuous shift of the working point must be analysed by the monitoring systems in order to detect the presence of a soft fault before it becomes a serious problem [18]. Furthermore, the localization of the cause (degraded component) allows the organization of specific maintenance operations. This prognostic approach requires a very careful choice of measurements, since different variations of the various components can produce the same effect. Again, switching to the multiple failure hypothesis makes the process more complex.

The treatment of analog circuits represents the theoretical basis of the Thesis. Here, the modelling operations can essentially be divided into two phases: modelling of parametric failures and modelling of the circuit response. In the first case, the main step is the study of the failure mechanisms for each possible component. Therefore, once the effects of the degradation processes have been defined, it is possible to calculate the variations of the electrical parameters according to the physical characteristics of the materials and their ageing. The second phase of the modelling procedure consists in defining the best way to represent the overall behaviour of the circuit. Basically, the characteristics of analog circuits can be described using models in the time or frequency domain. In the time domain, the circuit description is based on a set of differential equations, whose order depends on the number of independent energy storage components [19]. These equations can be solved by numerical integration and the solutions are generally very expensive from the computational point of view, potentially unstable or non-convergent. However, this approach can be applied to linear and non-linear circuits. Instead, in the frequency domain, the behaviour of the circuit is described using phasors and algebraic equations in symbolic form [20]. This approach has great advantages from the computational point of view but can only be applied to linear (or linearised) circuits.

2.2.2 Frequency Domain Representation

Considering the representation in the frequency domain, the first step to develop a monitoring system focused on parametric faults is the selection of suitable test points, each of which allows the measurement of specific network functions $H_i(j\omega, \mathbf{p})$. Given a set of n_H different network functions, their analytical form (2.1) is used to describe the behaviour of the CUT and the effects of parameter variations.

$$H_i(j\omega, \mathbf{p}) = \frac{N_i(j\omega, \mathbf{p})}{D_i(j\omega, \mathbf{p})} = \frac{a_{i0}(j\omega, \mathbf{p}) + \cdots + a_{in}(j\omega, \mathbf{p})(j\omega)^n}{b_{i0}(j\omega, \mathbf{p}) + \cdots + b_{in}(j\omega, \mathbf{p})(j\omega)^n} \quad (i = 1, \ldots n_H) \tag{2.1}$$

In fact, $\mathbf{p} = (p_1, \cdots p_{n_p})$ is the vector containing all possible defective elements. Each of these components can change its value due to a specific failure mechanism, thus introducing possible variations in one or more functions $H_i(j\omega, \mathbf{p})$. Therefore, a series of non-linear equations in the form (2.2) can be written, where $M_i(j\omega)$ are the measurements of the corresponding network functions.

$$H_i(j\omega, \mathbf{p}) - M_i(j\omega) = 0 \quad (i = 1, \ldots n_H) \tag{2.2}$$

For these reason, they are called failure equations and should contain all the information necessary to detect and locate malfunctions. To achieve this purpose, each faulty element must introduce variations distinguishable from those produced by the other components. Therefore, the choice of the network functions used to create the failure equations plays a fundamental role and it is made by means of a study called *Testability Assessment*. This study allows the definition of how many and which components can be considered faulty as they introduce distinguishable effects in the measurements of certain network functions [21]. In the case of circuit elements that produce the same variations on the measures, it is possible to adopt two strategies: change the network functions considered or increase the number of test points and therefore the number of equations. Sometimes, due to the limited availability of test points, only a few network functions can be used. In these cases, different test frequencies are considered to write n_p equations in the form (2.2). The concept of *Multi-Frequency Parametric Analysis* is then introduced [22].

In general, therefore, all prognostic and diagnostic methods start from a system of failure equations (2.3) obtained using fixed test points and test frequencies. Under specific mathematical conditions, the inversion of this system allows the precise identification of the electrical components. At first, the total number of equations, which is the sum of the number of network functions considered n_H and that of frequencies n_f, must be greater than (or at least equal to) the number of all possible defective elements. Then, in case of unavoidable ambiguities found during the testability assessment, a reduction of the fault causes is introduced. This means that the number of

possible defective elements n_p is less than the total number of components belonging to the CUT. In fact, one or more elements, those that introduce ambiguity, are fixed in their nominal intervals.

$$\begin{cases} H_1(j\omega_1, \mathbf{p}) - M_1(j\omega_1) = 0 \\ \vdots \\ H_1(j\omega_{n_f}, \mathbf{p}) - M_1(j\omega_{n_f}) = 0 \\ \vdots \\ H_{n_H}(j\omega_{n_f}, \mathbf{p}) - M_{n_H}(j\omega_{n_f}) = 0 \end{cases} \tag{2.3}$$

The basic characteristics of the monitoring systems for electrical lines proposed in this Thesis are well summarized in [23], where all the main phases of the symbolic analysis in the frequency domain and in the case of multiple failure are presented. This fully automated method with reduced computational complexity was developed by Fedi et al. introducing new aspects related to the selection of test points to achieve maximum fault location capability, as shown in [24] and [25]. Further developments were introduced by the research group of the University of Florence, which created specific software for circuit analysis [26] and integrated the symbolic approach with modern artificial intelligence algorithms [25].

2.3 Multi-Frequency Parametric Analysis

As mentioned in the previous sections, prognostic and diagnostic techniques are mainly based on mathematical methods for solving a system of failure equations in which the unknowns are the possible defective elements. For example, a bilinear decomposition of the failure equations can be easily applied under single and double failure hypothesis, but the computational cost becomes too high when more than two components can be simultaneously defective. Therefore, more robust mathematical methods are usually proposed for solving a system of failure equations assuming any *k-fault hypothesis*. If the number of selected measurements is sufficient to create a system of linearly independent failure equations, all electrical components can be calculated through a parameter identification technique and this means that all unknowns are defined uniquely. This mathematical condition must be compared to the practical possibility of acquiring the selected quantities. In

fact, some required test points may not be available or it may be very problematic or expensive to include them into the measurements. If one or more test points cannot be used and an alternative system of linearly independent equations cannot be created, the calculation of the parameters does not have a unique solution. In this case, there is a reduction in the Testability level and one or more electrical components must be considered in their nominal ranges. Therefore, the definition of a set of testable parameters plays a fundamental role and it is a preliminary step for each diagnostic or prognostic method. In this sense, the Testability assessment provides information about the solvability degree of the system of equations and represents the base of any monitoring system.

Another important step is to minimize the effects caused by measurement noise and tolerances on analog components. In fact, these factors can lead to an incorrect classification of the health status of the CUT. To limit these problems, a widely used solution is the introduction of specific algorithms for the selection of test frequencies.

2.3.1 Testability Analysis

As said above, Testability assessment is the first fundamental step for any type of monitoring system because it provides information about the solvability degree of the selected failure equations [27]. In fact, the unknowns to be defined are the possible faulty elements belonging to the CUT and their values can be uniquely calculated only if the failure equations are linearly independent. It should be noted that the equations taken into account are the result of a preliminary selection of the test points. This means that specific quantities are initially supposed to be measured on the basis of the accessibility level, the cost of the metering devices and the complexity of the operation. Starting from this, a system of failure equations is created using the corresponding network functions, and the Testability evaluation is required to verify the effectiveness of the choice.

From a mathematical point of view, the main purpose is the calculation of the Testability index (T), which is defined as the rank of the Jacobian matrix (2.4) obtained from the system of failure equations [28].

$$T = rank \begin{bmatrix} \frac{\partial H_1(j\omega,\mathbf{p})}{\partial p_1} & \dots & \frac{\partial H_1(j\omega,\mathbf{p})}{\partial p_{n_p}} \\ \vdots & \dots & \vdots \\ \frac{\partial H_{n_H}(j\omega,\mathbf{p})}{\partial p_1} & \dots & \frac{\partial H_{n_H}(j\omega,\mathbf{p})}{\partial p_{n_p}} \end{bmatrix} \tag{2.4}$$

Given n_{CUT} the total number of electrical components belonging to the CUT, one of the following conditions can be obtained:

- $T = n_{CUT}$ (Maximum Testability)

  In this case, all the elements can be considered faulty because they introduce distinguishable effects on the selected measurements. Therefore, the presence of n_{CUT} linearly independent equations guarantees the solvability of the system and, consequently, the number of possible faulty elements n_p can be chosen equal to the total number of components n_{CUT}. This result positively verifies the choice of test points.

- $T < n_{CUT}$

  In this case there are situations of ambiguity because two or more electrical components introduce indistinguishable variations in the selected measurements. Therefore, some elements must be fixed in their nominal range and excluded from the system unknowns. Consequently, the number of components belonging to the vector $\mathbf{p}$ is $n_p = n_{CUT} - T$.

Based on this, the concept of *Ambiguity Group* (AG) is introduced, which is used to indicate a set of parameters where it is not possible to uniquely identify the defective one. Note that the order of a given AG is the number of electrical parameters it contains. Furthermore, an Ambiguity Group is defined as Canonical (CAG) when it does not contain ambiguity groups of lower order. Note that the calculation of T and the definition of ambiguity groups belong to the stage commonly called *Testability Analysis*. Thanks to this analysis, it is possible to confine the presence of problems to well-defined groups of components, called Fault Classes (FCs). In the absence of AGs, each electrical component constitutes a FC while, if one or more AGs are present, there will be at least one FC with at least two elements whose variations cannot be distinguished.

One of the most important concepts in the field of Testability analysis is that of the Gloabal Ambiguity Group (GAG), which is a set of components derived from the union of two or more CAGs with at least one common

element. Starting from this definition it is possible to introduce the following considerations related to the case of single failure hypothesis.

1. It is possible to monitor all the components of the CUT if all the GAGs are made up of CAGs of order at least equal to 3. Therefore, if there is no CAG of order 2, all the parameters are identifiable and each of them is a FC.

2. If there are CAGs of order 2, it is not possible to uniquely identify variations of their components. In this case, all the elements not belonging to CAGs of order 2 are identifiable and each of them is a FC. Meanwhile, for the components belonging to CAGs of order 2, there are two cases:

   (a) Each CAG is a FC if all the CAGs of order 2 do not intersect;

   (b) Each GAG constituted by CAGs of order 2 intersecting each other are considered a FC.

The theoretical aspects reported above can be found in [29], where, starting from the definition of Sean and Saeks, a Testability calculation algorithm is proposed that overcomes the problem of the loss of accuracy due to the rounding typical of numerical techniques and the high computation cost of standard symbolic analysis when circuit size increases. It should be noted that various definitions of Testability can be found in the literature. In its guidance document [30], Berkowitz introduces the concept of solvability as the ability to uniquely define the entire set of network parameters from measurements to its terminals. Subsequently, definitions based on sensitivity matrices and topological approaches have been formulated, as shown in [31] and [32] respectively. However, the definition of Sean and Saeks is the most general and versatile, and it can be used to easily extend the concept of Testability to DC-excited periodically switched networks, as shown in [28].

2.3.2 Test Frequency Selection

From a theoretical point of view, therefore, the diagnosis of parametric faults in analog circuits is carried out by identifying the values of certain components. The identification process requires the solution of the so-called fault equations measured at specific test points. As previously stated, the Testability study offers a possible criterion for choosing these points. Observing

the system of failure equations it can be seen that the measures and symbolic functions refer to certain frequencies. The total error in the component identification process is given by numerical errors, which are caused by uncertainties in fixed network parameters and measurements. All these perturbations can be significantly reduced by a suitable choice of test frequencies. For this reason, the test frequency selection plays a fundamental role in parametric fault diagnosis. This issue is still highly challenging and numerous different approaches can be found in the literature [33] [22].

A method that minimizes the condition number of the Jacobian matrix extracted from [22] is introduced in this Thesis. Referring to the Jacobian matrix (J_M) presented in (2.4), the condition number can be defined as shown in (2.5),

$$k(J_M) = \|J_M\|_2 \|J_M^{-1}\|_2 \tag{2.5}$$

This result is obtained starting from the solution of the failure equations by the Newton-Raphson method and applying the mathematical procedure shown in [22]. Consequently, the Test Index (T.I.) is defined as follows,

$$T.I. = (k(J_M) - 1)\|J_M^{-1}\|_2 = \frac{\sigma_{max} - \sigma min}{\sigma_{min}^2} \tag{2.6}$$

where σ_{max} and σ_{min} are respectively the maximum and the minimum singular value of the Jacobian matrix. The term $T.I.$ it can be minimized through the algorithm shown in [22] to obtain the optimal frequencies. However, it is necessary to introduce the following consideration: the Jacobian matrix depends on both frequencies and component values. At the first step of the Newton–Raphson algorithm, an initial value for the unknown vector of parameters has to be chosen. This value corresponds to the vector of the nominal component values. On the other hand, the Newton–Raphson algorithm needs measurement values for starting. So, initially, it is necessary to minimize the $T.I.$ that is relevant to the nominal component values to determine the frequencies where the measurements have to be carried out. At the second step, the Jacobian matrix is evaluated in the component value vector determined in the previous step, i.e., the Jacobian matrix changes. This means that, at the second step, the condition number is different from that relevant to the first step, and so on, for the subsequent steps. So, a possible way to apply the Newton–Raphson algorithm could consist of the minimization of the $T.I.$ for each step to determine step by step the better

measurement frequencies. However, this approach has two practical drawbacks: the repeated application of the $T.I.$ minimization algorithm and the consequent repetition of the measurements at different frequencies for each step. So, it is preferable to minimize the $T.I.$ only at the first step for the nominal component values, as a simplified Newton inverse algorithm.

The minimization procedure is implemented in the first application proposed in this Thesis using a specific algorithm developed by the authors of [22]. Even if the presented prognostic procedure does not require the mathematical solution of the system of failure equations, good performance is achieved by selecting the test frequencies used to train the neural classifier.

2.3.3 Introduction of Computational Intelligence

The analytical procedure presented in this chapter for the detection of malfunctions in analog circuits and the recognition of the causes through a multi-frequency parametric analysis represents the starting point of the Thesis. In fact, the theoretical rules described here are used to develop monitoring methods for different types of electrical systems. When the SUT is an electrical circuit, the analysis in the frequency domain can be applied directly by defining the best test points, the best frequencies for measurements and a suitable method for solving the system of failure equations. If, on the other hand, the SUT is a plant or infrastructure where electrical tests can be made, the first step is always the creation of the equivalent circuit and, subsequently, the same approach can be used. Figure 2.3 summarizes the main steps of the parametric analysis.

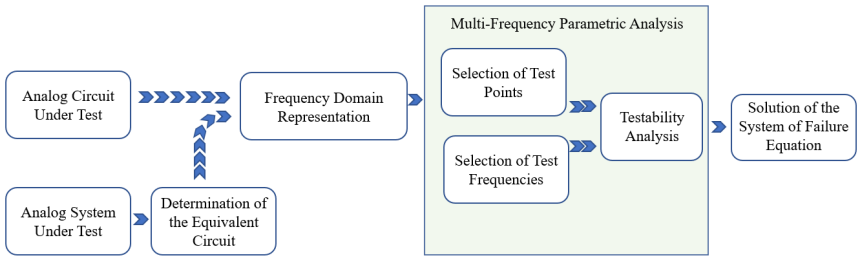

Figure 2.3: Summary of the main phases of multi-frequency parametric analysis for analog circuits and systems.

Also in this field, as in many industrial sectors, the growing diffusion of machine learning and deep learning methods has led to the introduction of new monitoring approaches [34]. Even if the solvability conditions are still valid, neural algorithms offer new prospectives with respect to the mathematical solution of the failure equations. Essentially, these computational models can be introduced in multi-frequency parametric analysis to improve the measurement selection phase and classify health status without the need for a deterministic mathematical method (Figure 2.4).

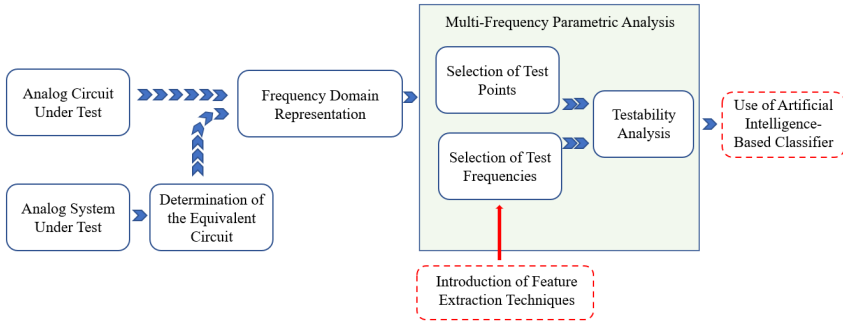

Figure 2.4: Introduction of artificial intelligence techniques in multi-frequency parametric analysis.

Artificial Neural Networks (ANNs), for example, can be used to define the state of health of the SUT using the same measurements presented in (2.3). This approach does not require the analytical solution of the system of equations and is based on the associative memory of neural algorithms. In fact, these are computational models inspired by the biological neural networks that constitute animal brains and have elementary units called neurons connected through links called synapses. Each of these connections is characterized by a weight, which is a number initially set randomly and then adjusted during the training phase to achieve the desired goal. Therefore, each neuron receives the weighted sum of the information transmitted by the other elementary units and processes it through a specific activation function. The training procedure gives the necessary experience for the neural algorithm to process new data and provide correct outputs. A possible organization of neural networks widely used in literature consists in creating successive layers and specific connections between the neurons belonging to them. Different types of ANNs can be obtained based on the

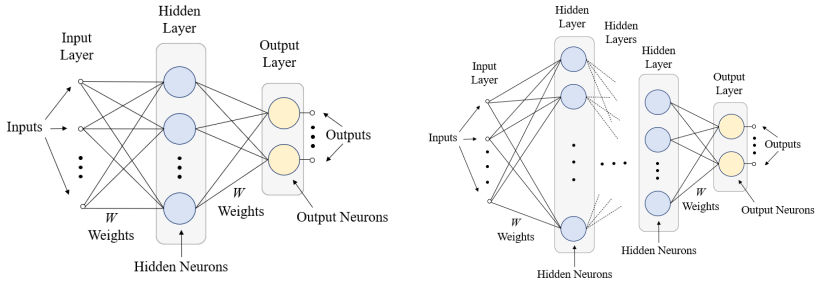

Figure 2.5: Main categories of computational intelligence methods. (a) Standard machine learning structure. (b) Standard deep learning structure.

overall structure of the computing system. From a general point of view, the neural algorithms characterized by less than three layers belong to the category of machine learning methods [35], while the more complex structures characterized by a large number of neurons and layers are called deep learning techniques [36]. Typically, given their thin structure, machine learning methods require short training times and are easier to implement from a hardware point of view. Figures 2.5(a) and 2.5(b) show two standard examples of machine learning and deep learning structures respectively.

Considering the connections between neurons, ANNs can be divided essentially into two categories: feed-forward and recurrent neural networks. In the first case, the information moves in only one direction (forward) from the elementary units belonging to the input layer, through the hidden neurons, to the output ones. This means that connections between nodes do no form cycles. On the other hand, recurrent neural networks are computational models in which some neurons are connected forming a loop. Typically, one or more outputs of an upper layer are used as inputs of a lower layer and this allows the introduction of a state memory element. Therefore, by applying a time series as an input, it is possible to represent a dynamic behaviour in which the output at a given instant depends on the current inputs and on the previous state. Figure 2.6(a) and Figure 2.6(b) summarize the main aspects of the feed-forward and recurrent structure respectively. Starting from these macro-categories it is possible to obtain many different types of neural networks by introducing time delay elements or by organizing a particular

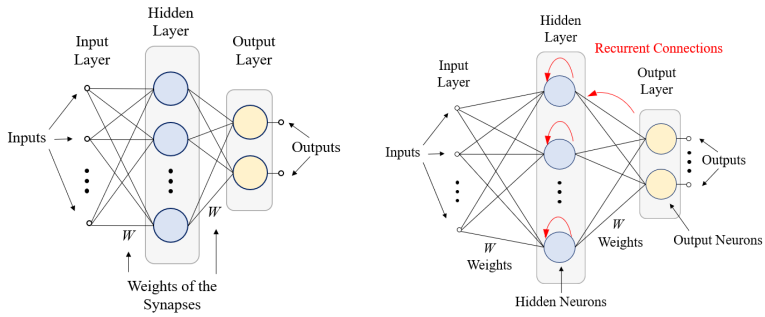

Figure 2.6: Neural network structures. (a) Feed-forward. (b) Recurrent.

structure of neurons.

Using the type of training as a distinctive parameter, it is possible to divide the ANNs into the following categories: supervised learning, unsupervised learning, reinforcement learning and self-associative learning [35]. In the first case, the correction of the weights is carried out by using several input-output examples. Therefore a dataset matrix is used, where the input samples and the corresponding desired outputs belong to the same row. At each step of the training procedure the inputs are processed obtaining the current outputs. This values are then compared with the desired ones obtaining the error terms used for the correction of the weights. This correction is the core of the training and can be done using different procedures, such as the back-propagation technique. This rule is widely used in feed-forward neural networks and provides the propagation of calculated errors from the output layer to the input one. Several methods, characterized by different formulas, can be used to achieve this goal and the weight adjustment can be performed recursively or using batch algorithms. In the first case each weight is corrected during the back-propagation while, in the second case, all the errors are saved in a specific matrix and then the corrections are calculated at the end of the training epoch, i.e. when all the input samples have been processed. Figure 2.7 highlights the main phases of the back-propagation procedure.

If unsupervised learning is used, the dataset matrix does not contain the desired output labels and the primary goal of the training is to develop the

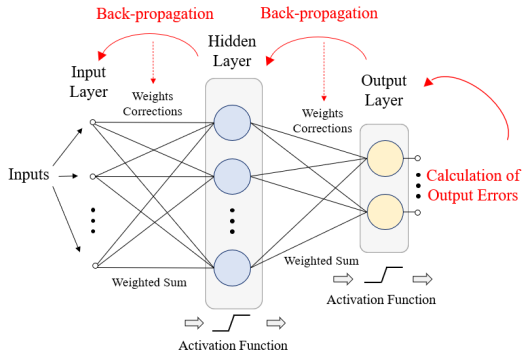

Figure 2.7: Back-propagation procedure.

clustering capability of the ANN. Therefore, the main objective is to classify inputs with similar characteristics and allow future recognition of new data. Multiple networks with different structures can be used and usually a graphical representation is performed to clarify the distribution of the resulting cluster. For example, in Kohonen maps and in self-organizing maps in general, closed neurons react to specific inputs and their weights are corrected to strengthen this link. The concept of neighborhood changes according to the network considered and it can be a Euclidean distance in the n-dimensional space of the inputs or a similar output obtained by means of the same activation function. Figures 2.8(a) and 2.8(b) present two possible unsupervised learning structures.

In reinforced learning, there are no predefined targets for the desired outputs, but an objective function is used to define the configuration that best fits the final purpose. Finally, in the ANNs characterized by self-associative learning, the target signals and the inputs coincide, while the outputs are taken from a specific level inside the network. In this sense, one of the most used configurations is that of bottleneck networks (Figure 2.9), in which the outputs are extracted from an internal layer characterized by a low number of neurons in order to reduce the dimensionality while maintaining the information content.

Considering the activation function of the elementary units, ANNs can be divided into continuous [37] and discrete [38]. In the first case, the output of each neuron varies continuously over a wide range of possible values. These configurations are usually used to represent the input-output relationships of

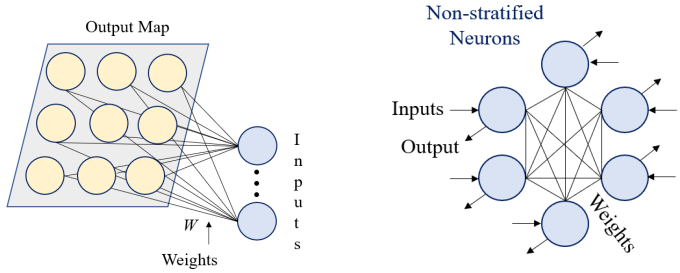

(a) (b)

Figure 2.8: Examples of neural networks trained through unsupervised learning procedures. a) Kohonen maps. b) Hopfield neural network.

complex physical systems without building a mathematical model. The numerous examples of input-output pairs used during the training phase make it possible to replicate the functioning of the system under consideration. Another important task in which continuous versions of neural networks are widely used is the definition of control strategies for analog and digital devices [39]. In this case, the control action is learned by the algorithm to obtain the desired behaviour from the examined system. On the other hand, the discrete output of neurons is usually used to perform classification tasks. This means that neurons can only provide a limited number of values corresponding to specific categories.

In the field of prognosis and diagnosis, ANNs can be used in many different ways. Mainly, the discrete version of these computational models is used to classify the state of health of the SUT starting from the selected measurements [40]. To achieve this goal, a preliminary simulation procedure is required, focused on representing the system under nominal and abnormal working conditions to create the dataset matrix. Therefore, the values of the selected measurements are extracted from the simulation and used as input of the neural classifier, while the label of the corresponding health status is saved as desired output. Each input-output pair is processed during the training procedure to obtain a neural network capable of identifying the operating conditions of the SUT [41]. Therefore, the difference between prognosis and diagnosis consists in the simulated situations: considering the malfunction conditions it is possible to recognize operational states that pre-

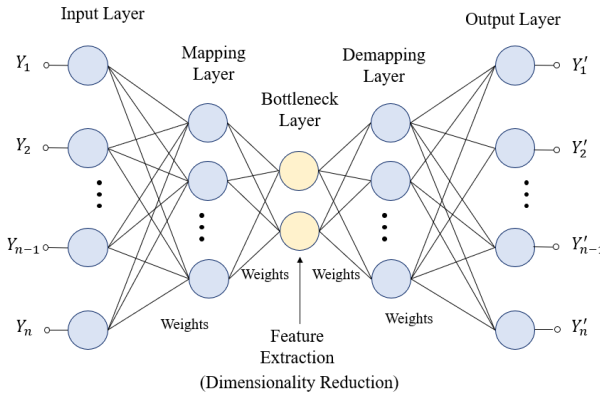

Figure 2.9: Example of bottleneck network.

cede catastrophic consequences. Note that continuous neural networks can also be adapted to achieve this purpose. For example, in the case of diagnosis for analog circuits, it is possible to use output neurons with continuous activation functions to define the exact value of each electrical component [42]. In this case, the outputs used during the training procedure are not the corresponding health status labels but the electrical parameters of the CUT. Therefore, by analyzing the results obtained, it is possible to find the defective element that falls beyond the nominal range. This approach is used when the precise identification of electrical components plays a fundamental role in the organization of maintenance operations and provides useful information on the effectiveness of the system and its residual life.

Sometimes, in very complex and articulated systems where different variables change rapidly defining numerous operational configurations it is not possible to label each of them and the best solution is to group the system conditions through a self-organizing map [43]. In this way it is not necessary to know the exact status of each node of the system but the working conditions are clustered by similarity based on the effects produced. Subsequently, knowing only a few situations, it is possible to identify the overall state of health.

Finally, another possible application of artificial intelligence techniques in diagnostic and prognostic systems is the reduction of input samples while maintaining the informative content. As mentioned above, ANNs characterized by self-associative learning, such as bottleneck networks, can be used to

achieve this goal [44]. In complex systems, characterized by a large number of measurements, these computational models allow a preliminary reduction of the dimensionality without affecting the subsequent classification carried out, for example, by a discrete neural network. Thanks to this operation it is possible to simplify the structure of the neural classifier and, in particular, that of its input level. Note that this type of application plays a fundamental role in monitoring systems that require the transmission or storage of measurements. In fact, the first reduction of dimensionality (encoding) carried out by these algorithms facilitates data management, while the second phase of self-associative training (decoding) allows the initial information to be recovered. Another important technique used to reduce the number of inputs in many different applications is the Principal Component Analysis (PCA). It consists in calculating the principal components and using them to perform a change of basis on the data, sometimes using only the first few principal components and ignoring the rest [45]. In its linear version it aims to identify the best linear transformation to translate an n-dimensional vector with an average value equal to zero into an m-dimensional vector where $m < n$ or $m \ll n$. In other words, the PCA projects the input data from the original space, in which they are highly correlated with each other, into another one of smaller dimensions, in which they are instead loosely correlated, keeping as much as possible the information contained in the origin. Given a set of s n-dimensional inputs, the standard method for extracting the principal components is based on the computation of the covariance matrix. In particular, the eigenvalues and eigenvectors of this matrix are calculated, and the space identified by the eigenvectors associated with the most significant m eigenvalues is used to map the original space. Therefore, once the eigenvalues have been calculated, they are organized in an increasing sense and the larger ones contain the greatest information content. Then, a specific number of eigenvalues are selected and the corresponding eigenvectors represent the new space. Obviously, by limiting the number of components taken into consideration, an error is introduced which corresponds to a partial loss of information content. In prognosis and diagnosis systems, these techniques can be used for example to replace the selection of optimal frequencies. In fact, assuming that it is possible to easily perform numerous simulations of the SUT for various test frequencies, it is possible to subsequently reduce the measurements performed by eliminating all unnecessary information contents.

2.4 Simulation Tools

All the theoretical information necessary to develop a monitoring system on a specific CUT must be obtained using simulation programs. The growing computing power has led to the spread of complete software in many fields of applied sciences and electrical engineering. However, in the sector of analog circuits, given the complex succession of operations to be performed, it is necessary to combine functions from different simulation programs. For example, the most used circuit simulator, SPICE, is very powerful but being a numerical calculation program it does not allow the evaluation of intermediate steps in solving a specific problem and, in many cases, it cannot provide the designer with the necessary explanatory keys. More general packages, for example Matlab/Simulink and its electrical expansion Simscape, can be very useful for speeding up the simulation procedure and complex steps such as creating datasets and extracting features. However, a preliminary study of the CUT is needed along with a deep experience in handling Matlab codes. For these reasons the use of the software SapWin (Symbolic Analysis Program for Windows) is proposed in this Thesis [26]. The program was developed by the Department of Information Engineering of the University of Florence and allows the symbolic simulation of analog circuits by carrying out specific tasks related to the diagnosis and prognosis of faults.

2.4.1 SapWin

The symbolic approach is the main aspect that makes the circuit analysis performed through Sapwin different from that carried out through SPICE, where the analytical associations between the circuit parameters are lost when the simulation begins the first phase. Design of electrical circuits and verification of their operation, Testability assessment and model identification are the main functionalities available in SapWin. Thanks to a user friendly interface, this program can be used by beginners without a specific background and represents a very useful tool for educational applications [46].

Circuit Modelling

As described in the previous sections, the development of a monitoring system for electrical circuits requires a set of simulations and measurements on the CUT at different frequencies. The number of simulations can be very large, because they have to be repeated for a large number of random

variations in component values over a given range. Sapwin allows the rapid calculation of multiple responses following a single simulation and provides their description in symbolic form. The representation of the circuit is given by means of a Spicelike net list or directly inside the schematic editor of the program, which then performs a translation of the scheme into an ASCII net list. All the standard two-terminal or two-port elements can be taken from a component list. Sub-circuits can be created by the user as a two-port combination of available components. The circuit under simulation must include at least one output probe (voltage or current) in order to set up the simulation. In the last version of the program, multiple outputs are allowed. In the same editor, it is possible to create and save sub-circuit schemes. Approximation of output expression can be performed, in order to improve the manageability of the generated functions. The simulation generates two different output files, in binary format, which can constitute an interface to other programs, and in ASCII format. The ASCII file contains the resulting expression of the simulation in the Laplace/frequency domain and they can be extracted in Matlab format. The responses can be elaborated also in a graphical way, to obtain different diagrams: magnitude response, losses, phase response, time delay, poles/zeroes, step response, impulse response, relative sensitivity (of Magnitude and Phase).

Time-Domain Simulations

One of the most important developments recently introduced in SapWin is the possibility of performing simulations in the time domain. This allows the study of time-variant circuits such as for example DC-DC power converters, which are electronic devices designed to convert a source of direct current from a voltage level to another and keep it stable within given specifications [47].

The DC-DC switching power converters, also called Pulse Width Modulation(PWM) DC-DC converters, are a widely used category of linear, time variant devices, which are not easy to model and simulate. The actual operation of these circuits is largely influenced by parasitic parameters and, therefore, the simulation results in the time and frequency domain are accurate only if the non-idealities of the converters are adequately modelled. Note that in the frequency domain analysis the poles and/or zeros are not included in the transfer functions of the converter when the parasitic effects are neglected. However, when these parasitic components are considered,

the expressions of the converter transfer functions become very complex and cannot be easily derived. A DC-DC converter simulator that uses a symbolic approach is something totally new and essential for these derivations.

A PWM DC-DC power converter switches high voltages and currents in a very short time. This causes several numerical simulators to have convergence problems that break the simulation in the time domain after it has been run for some time. Convergence problems are often overcome by reducing the accuracy of the simulation. SapWin is based on a numerical solution of symbolic functions rather than numerical approximations of the circuit waveforms and thus results in fast and accurate simulations without convergence problems.

Testability Assessment and Ambiguity Group Calculation

In order to calculate the Testability level of the CUT, a further version of SapWin can be used, which is called *SapWin PET*. Here, the program LINFTA (Linear Invariant Network Fast Testability) is implemented to calculate the rank of the Jacobian matrix obtained by setting specific test points. In fact, the current and voltage probes used in the electrical diagram allow the calculation of specific network functions with respect to the imposed source. The symbolic form of these functions, containing all the lumped components as unknowns, is used to calculate the derivative terms shown in (2.4) and define any linearly dependent columns. Starting from this information it is possible to find all the ambiguity groups and testable components. The latter represent all the possible combinations of elements that can be considered defective, while guaranteeing the solvability of the system of failure equations.

2.4.2 Integration Between SapWin and MatLab

The basic form of the procedure proposed in this Thesis to perform multi-frequency parametric analysis and train the neural classifier exploits the integration of SapWin and Matlab. In particular, the discrete complex-valued neural network is entirely developed on Matlab to offer a versatile and easily applicable tool in the various fields of interest. Furthermore, to facilitate its use, a specific Matlab application has been developed. This program allows the processing of dataset matrices in .txt format. As for the generation of the dataset matrix, several methods can be used. When the system under test is

an analog circuit or can be associated with an analog circuit, the parametric faults can be simulated directly on SapWin PET, where it is possible to generate the dataset matrix. In order to facilitate this process and very quickly integrate new parametric variations, the most suitable procedure proposed here is to extract the symbolic form of the selected frequency responses and import them into Matlab. In this way, it is possible to introduce variations of the parameters according to specific rules. For example, it is possible to vary the resistance values according to the working frequency by modelling the skin effect. Therefore, the integration between the two simulation software can be summarized in Figure 2.10.

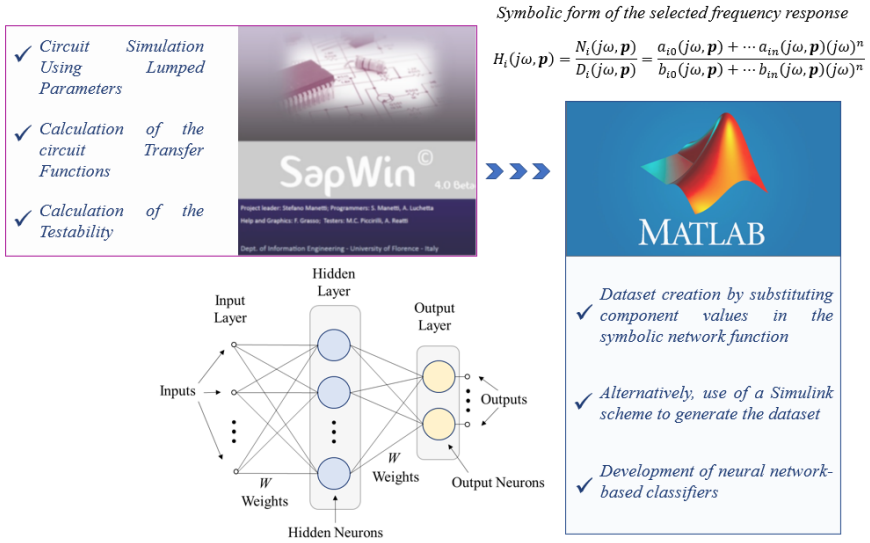

Figure 2.10: Simulation procedure based on SapWin and Matlab.

The main limitation of this procedure is the high computational cost for the extraction of the symbolic function when the dimensions of the circuit are very large. In these cases, the proposed solution is to use SapWin for the Testability study, keeping only the faulty parameters in symbolic form, and to create the dataset completely on Matlab by exploiting the potential of Simulink/Simscape.

2.5 Fields of Application

All the theoretical concepts presented in the previous sections are used in this Thesis to develop monitoring methods on different types of electrical systems. The main application taken into consideration is the prognosis of faults in power transmission and distribution lines. In this case, the final purpose is to prevent catastrophic failures avoiding blackouts for thousands of users. To achieve this goal, malfunctions must be detected and localized. Therefore, the most important failure mechanisms of the various electrical infrastructures are considered: first the high voltage overhead lines are studied in their most stressed parts and then the underground medium voltage networks are taken into account, focusing attention on their operating temperature. In these cases, prognostic procedures in the frequency domain are proposed, where the equivalent model of the system under test presents electrical components sensitive to the failure mechanisms. Therefore, changes in these elements introduce variations in the overall frequency response and a neural classifier is used to define the health status of the system. This means that all the theoretical steps of the multi-frequency parametric analysis are performed, from the Testability assessment for the correct selection of the available test points to the definition of testable and ambiguity groups. In the proposed approach, the use of artificial intelligence techniques replaces the solution of failure equations through a mathematical method.

A similar prognostic procedure is presented to monitor the operating conditions of power converters. In this case, the analysis is carried out in the time domain and a new graphical approach is proposed for the Testability assessment. This means that voltage and current waveforms are sampled and then processed by the neural classifier to detect changes in the electrical components of the circuit. DC-DC converters are mainly taken into consideration, given their importance for all battery-powered electrical devices and their fundamental role in integrating renewable energy sources that produce direct current. The analysed converters are time-variant circuits connected to the low voltage distribution network, where the quality of the energy depends on the various non-linear loads and controllers installed by the users. In fact, many electronic devices and electrical machines can inject harmonic disturbances or modify the waveforms of voltage and current producing wide problems for all connected systems. For this reason, the detection of power quality disturbances can also be considered a useful monitoring operation to organize maintenance interventions and locate critical nodes of the distribu-

tion networks. This problem is addressed in the final part of the Thesis by proposing a neural classifier capable of recognizing line voltage distortions.

Therefore, all phases related to energy delivery are studied in this work using different approaches to introduce predictive maintenance operations. In fact, all national electrical systems can be divided into three main steps: Generation, Transmission and Distribution. Once the power has been generated, its supply begins through High Voltage (HV) electrical transmission lines, which are characterized by a great length and allow the losses reduction by using high voltage and low current (the Italian standard essentially provides three voltage values: $132kV$, $220kV$ and $380kV$). As for the distribution system, it consists of two main parts: medium voltage and low voltage networks. Formally, from $1kV$ to $33kV$ the line under test is a Medium Voltage (MV) infrastructure, while any voltage level below this threshold is considered Low Voltage (LV). The structure described is based on centralized distribution, which means that the overall organization of the electrical system involves a low number of generation plants characterized by high power and many passive users. However, in recent years, the growing diffusion of renewable energy sources has led to the evolution of passive users into active ones. Therefore, the unidirectional flow of energy typical of centralized generation is replaced by the bidirectional flows of distributed generation. This change introduces new challenges from the point of view of grid management and diagnosis, making the electricity system more complex and variable. The use of new devices for the integration of generators and the management of bi-directional energy flows could reduce the reliability of the entire system by introducing many different possible defective elements. For this reason new monitoring systems and prognostic procedures are necessary to maintain the performance and stability of electrical system. Figure 2.11 presents a summary of the main fields of application considered in this Thesis for the introduction of prognostic analysis.

2.5.1 Transmission and Distribution Lines

Currently, many different techniques are used in electrical transmission and distribution lines to detect problems, but most of these methods focus on catastrophic faults, which produce the interruption of the electricity service. In this case, the main objective is the correct localization of faults to avoid the extension of the problem and to take out of service only the network branch in which it occurs. In the literature, many papers are present to

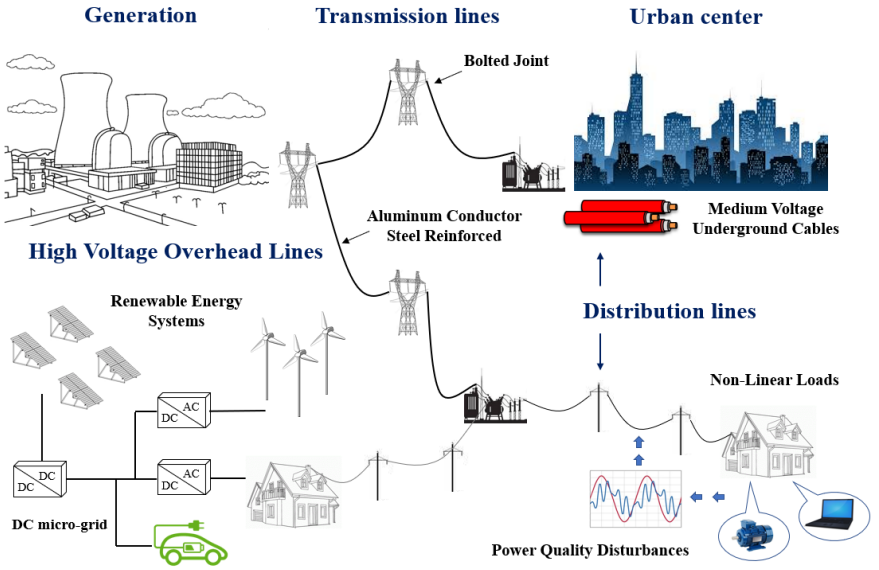

Figure 2.11: Summary of the main topics covered in the Thesis.

develop these protection techniques. For example, an advanced system for classifying and locating faults in power transmission lines is presented in [48]. This method integrates two sophisticated machine learning algorithms to distinguish the type of failure and indicate the affected network branch: Summation-Wavelet Extreme Learning Machine and Summation-Gaussian Extreme Learning Machine. Other approaches, such as the one presented by Huang in [49] and Li in [50], show specific techniques for detecting high impedance faults and arc faults. All these methods are very effective in identifying the problem and limiting it, but the prognostic aspect is totally absent.

To develop the concept of prevention in electrical power lines it is necessary to study the causes of the main problems. A partial review of the information contained in [51] is proposed below:

- Overvoltages

  In this case the mains voltage exceeds the nominal design value. Based on the nature of the causes, they can be divided into internal and external.

  - External

    They are caused by induction phenomena or direct lightning strikes that determine the so-called overvoltages of atmospheric origin. The biggest damage they can cause is the failure of the insulation of one or more components. Lost of insulation is serious as it can produce short circuits in which a large amount of energy is dissipated and this can lead to explosions. Usually, to prevent damage to the insulation of electrical components, they are rated for voltages several times greater than the nominal ones, in order to guarantee a high margin of safety.

  - Internal

    They are caused by closing and opening operations of circuits and, therefore, they are also called switching overvoltages. They can also be determined by rapids load variations or from resonance phenomena. Finally, surges can be caused by faults, such as accidental contacts and insulation losses. These overvoltages can exceed nominal values by a few times and generally have a duration of the order of milliseconds.

- Overcurrents

  In this case the mains current exceeds the nominal design value. Depending on the causes that generate them, they can be divided into permanent, transient and fault overcurrents.

  - Caused by permanent overloads

    They are mainly due to operations such as starting asynchronous motors, which it involves inrush currents up to ten times higher than the nominal ones and lasting a few seconds, or the insertion of vacuum transformers, which it can involve currents up to three times larger than the rated ones and that ends in a short time. Both of these overcurrent causes are linked to transient phenomena, it is therefore not appropriate to adopt protections for the line that lead to the opening of the branch in which the overcurrent circulates. This operation would be harmful, as it causes an unnecessary out of service.

  - Caused by transient overloads

    They occur when there are loads that draw higher power to that used in the dimensioning of the line. They involve a slow heating

of the conductors and, when this thermal overload is prolonged for a long time, it is necessary to break the circuit.

– Caused by faults

When an accidental electrical connection occurs between two points normally at different potentials, a low impedance mesh is created, called a fault loop, in which a short-circuit current circulates. This current has a much larger Root Mean Square (RMS) value than the nominal one. Normally, a short circuit can occur due to a lack of insulation caused by accidental contacts, rain and overheating produced by long overloads, but, more frequently, from overvoltages that cause the striking of arcs between points with different potential. Many different types of short circuits can occur in electrical lines and, for each of them, specific protections must be adopted.

The response of the protection systems to the most serious problems must be the rapid and automatic disconnection of the faulty section of the line. This operation must be performed while minimizing the disconnection of non-faulty equipment and ensuring the availability of the electricity service to users without overloads in the functioning part of the network. The overall performance of a protection system can be assessed on the basis of three criteria:

- Discrimination

  It represents the ability of the protection system to decide whether to intervene or not in the event of a specific operating condition detected. For example, anomalous situations may occur due to faults on other parts of the line (protected by other systems) which do not immediately require the circuit to be opened.

- Stability

  It is a measure of the system's ability not to intervene under certain conditions, such as transient overloads and failures protected by other systems.

- Sensitivity

  It is the system's ability to detect fault conditions close to the nominal situation. The correct design of the protections allows, for example,

the detection of the short-circuit current that circulates in the furthest point from the protection itself.

- Operating time

  It is the total time that elapses from the beginning of the fault to the sending of the trip signal from the relay to the circuit-breaker. Intervention times must be low enough to ensure the safety of the system, equipment and personnel, but the use of intentional time delays in protection systems allows high levels of discrimination.

The protection systems change according to the configuration of the network considered and the characteristics of the fault sought. However, it is possible to define a general structure of this equipment [52]. First, it is necessary a measuring device to detect the status of the network (e.g. voltage and current transformers). Then, equipment must be used to make decisions and translate measures into corrective actions on the line (e.g. relays). Obviously, suitable circuit breakers must be used to carry out the actions controlled by the relays. Finally, the communication systems between the various protection systems located in different points of the line play an increasingly fundamental role for coordination on a large scale.

Monitoring of High Voltage Lines

High voltage electrical lines represent the first phase of energy delivery and are used to cover long distances from the production centers to the primary stations. The overall structure of the transmission system is meshed and it is used in this mode to optimize power flows and ensure continuity of power supply. This is a fundamental infrastructure for which long periods of interruption are not allowed and in which complex systems of communication and remote management are implemented. Most of the equipment used in high voltage networks are protected through specific devices and are designed with the criterion of redundancy to ensure continuity and increase the availability of the entire service. Given the need to cover long distances, transmission lines are generally overhead, while HV cables (much more expensive) are used only in special cases and in submarine connections.

Basically, there are two different types of protections in high voltage transmission lines: distance protection and differential protection [53]. In some situations and on specific devices, overcurrent protection can be added.

The distance protections are based on the evaluation of the line impedance calculated through the voltage and current measurements at the starting point of the line. When a short circuit occurs, magnitude and phase of the line quantities vary and, consequently, the global impedance changes. In the event of a fault with zero resistance, the line impedance decreases with respect to the nominal situation and this allows the detection of the problem. Likewise, if the fault introduces a resistive term, it modifies magnitude and phase of the impedance and causes the protection to trip. The coordination of the distance protections plays a fundamental role in isolating only the part of the line where the fault occurs. In fact, the impedance values used as activation thresholds and the corresponding opening times can be set to trip only the protection closest to the failure point.

As for the differential protection, it can be used to protect lines, busbars, power transformers and other HV equipment. The main theoretical concept on which this protection is based is the measurement of a characteristic quantity, generally current, across the protected area and the subsequent comparison to activate the opening of the circuit. If a difference in magnitude and/or phase is detected between the two measurements, it is considered a fault symptom and the opening of the protections is activated. Also in this case it is possible to use specific settings of the differential current relays, such as the use of an increasing threshold if the measured current values are very high. In some situations, a back-up protection with overcurrent relays is implemented to correct any faults in the differential protection. In this type of protections for high voltage electrical lines, delay times are generally not included.

The presented protections are used to detect catastrophic faults and represent the first step of a corrective maintenance procedure. Overhead transmission line operators typically introduce a preventive maintenance program based on thermal inspections. To carry out these operations, drones equipped with thermal imaging cameras are used or helicopter inspections are scheduled. The main subjects of these analysis are the joints of the line, that is the connection points of between two different parts of the phase conductor.TERNA, which is the operator of the Italian transmission network, carries out this type of inspection every two years and the check becomes more frequent for the sections of the network located in areas with critical environmental conditions.

Monitoring of Medium Voltage Lines

Distribution networks represent the last part of the energy chain and can be divided into MV lines and LV lines. The former are used to connect primary and secondary stations, secondary stations to each other, and secondary stations with large users. This is done by reducing the voltage and increasing the current. In fact, these infrastructures are usually close to urban centers and are also used inside them to cover medium distances. For this reason, the energy lost due to the Joule effect is considered acceptable. In rural contexts, medium voltage lines are made up of overhead conductors to easily reach all users along irregular paths determined by the characteristics of the territory. These networks are more exposed to accidental direct contact and lightning, but can be visually analysed in the event of a failure. In addition, the overhead structure is the cheapest choice compared to other solutions. Instead, in large urban areas, MV lines are made up of underground cables and this makes them safer, guaranteeing a low impact on cities and citizens. However, cables are difficult to reach and inspections are time-consuming and resource-intensive. In this case, correctly identifying the broken branch plays a fundamental role.

From a general point of view, medium voltage lines have a mesh structure but operate in radial mode. Their extremely branched and complex configuration requires the exclusion of the faulty branch and its safety before the utilities can be powered by alternative routes. Furthermore, the presence of generators from renewable sources that feed into the distribution network introduces a further factor of complexity for the management of the line in fault conditions.

Basically, in MV networks, the main protection activities are carried out by means of overcurrent relays in conjunction with auto-reclosers, fuses and/or section switches [54]. This allows protection of the line from long-lasting overcurrents and poly phase short circuits by putting out of service the branch of the grid in which they occur. Furthermore, by applying directional relays it is possible to detect the single-phase earth fault and, consequently, by using the same type of circuit-breakers, the faulty line section can be isolated.

The current overload relays introduced above play a fundamental role in increasing the selectivity of the protection system. In fact, these devices are characterized by a so-called inverse current-time operating curve. This curve results in slower tripping for low overcurrent levels and immediate trip-

ping for critical values. The overcurrent relays can operate in two different programmable modes: pickup and time-multiplyer configurations. In the first case, the characteristic curve is moved along the horizontal axis thus increasing the current value for which intervention is required in a given time. By applying this strategy to the upstream relays, the necessary time is granted to those downstream to intervene without putting the entire distribution network out of service. In the second mode, the characteristic curve is shifted vertically and, therefore, the tripping time is increased for the same overcurrent. By combining these functions it is possible to achieve a high level of selectivity even in very branched networks such as medium voltage distribution lines.

In order to obtain a rapid resolution of transient faults, the auto-reclosers are applied downstream of the primary station protections, in intermediate points of the line. These devices are used to trip before the primary station protections in the event of earth faults (characterized by currents lower than the polyphase faults). After a first opening, these devices attempt two successive closings to restore network functionality in the shortest possible time. If the transient fault has not yet been resolved after the second closing attempt, the MV line is definitively opened without triggering the protections in the primary station. In this way the selectivity is increased.

Functions similar to those of auto-reclosers can also be implemented in the primary station to develop extremely detailed and precise systems for selecting the faulty branch. To obtain this result, it is necessary to introduce communication and remote control systems in the secondary stations of the network considered. In this way, it is possible to manage the switches of the substations during the opening periods and to localize the problem exactly. This type of management is implemented in modern Supervisory Control And Data Acquisition (SCADA) to optimize the operation of the network and all connected devices, including those of distributed generation.

All the functions described above are essential to ensure the safe availability of the electricity service but are focused on catastrophic failures (temporary or not) of the line. When these fault conditions are caused by situations of accidental contact or lightning, it is not possible to adopt preventive countermeasures. However, it is possible to introduce predictive maintenance to avoid failures due to infrastructure wear. This Thesis addresses this challenge and in particular considers underground MV networks. In cable lines, in addition to the protections mentioned above, it is possible to use off-line

fault localization systems. In fact, given the difficulty of accessing cables, once the faulty branch has been identified, it is essential to locate the section of cable where the damage occurred. Generally, the degradation of the insulation due to thermal effects causes the phenomenon of partial discharges and, subsequently, the formation of so-called water trees. The persistence of this situation during the operation of the line can lead to the breaking of the cable and the opening of the protections. The use of TDR meter (Time Domain Reflectometry) on the disabled cable allows the localization of the breaking point thanks to the study of the signal reflected at high frequencies.

In this thesis a preventive approach is proposed to identify and localize the initial degradation of the cable and allow prompt intervention before the failure occurs.

2.5.2 DC-DC Converters

As previously mentioned, the distribution system also includes the low voltage lines that carry out the final delivery of the energy. This part of the electricity system is extremely branched and has become very complex in recent decades due to the increasing installation of renewable energy sources. In fact, the transition to distributed generation has converted many passive users into active users and this requires the introduction of specific systems to manage the new energy flows. In this scenario, DC-DC power converters play a fundamental role, since they can be used as interface between DC renewable sources and micro grids and in all battery-powered systems to guarantee different voltage values. Many monitoring methods for power converters focus on active components, but they can only detect fault conditions characterized by a total loss of functionality. The identification of these conditions and the consequent detection of the defective element is of great importance, but does not prevent the interruption of operation. As for passive components, fewer techniques are available for detecting early malfunctions and, in this case, the concept of parametric fault must be resumed. In fact, the passive components of the DC-DC power converters can be studied with the already discussed rules of the multi-frequency parametric analysis. The most important aspect in this case is the time-variant nature of the CUT. Since PWM converters switch between two or more different states during their operation and since each state corresponds to a specific circuit topology, it is necessary to evaluate which is the best interval in which the prognostic analysis can be carried out. In fact, the testability evaluation

and the definition of the ambiguity groups can provide different results in each operating state of the converter. Obviously, the network functions considered in the frequency domain are different according to the corresponding topology and the choice of test points can also vary. As an alternative to the frequency domain approach, a time domain analysis can be adopted for this type of circuit. Starting from these considerations, this Thesis shows a monitoring system based on neural networks for DC-DC power converters and a possible graphic study of testability.

Testability Analysis for Time-Variant Circuits

The testability analysis presented above is widely used in the literature to study linear time-invariant circuits while the treatment of non-linear and time-varying devices is not widespread. In [55] and [56] a possible approach for non-linear analog circuits is presented, based on an input-output model in a Hilbert space setting. Regarding the time-variant circuits, it is not possible to directly apply the standard analysis based on the Laplace transform due to the presence of multiple topologies. Taking into account PWM DC-DC converters, the number of topologies depends on the operating mode. In fact, two topologies can be obtained when the converter considered works in Continuous Conduction Mode (CCM) while three different configurations are available in Discontinuous Conduction Mode (DCM). As regards the study of these circuits, the main reference taken into consideration is [28], where a possible analysis linked to the standard Testability assessment is proposed. The theoretical foundations of this method are developed in the time domain and the results can be translated into the Laplace domain providing also a possible graphic approach. Therefore, the circuit is analysed in the steady-state conditions using the following steps, extracted from [47].

- Selection of a certain working phase, which corresponds to a specific configuration of switches.
- Determination of the vector $\mathbf{u}_0$ corresponding to the constant input samples.
- The CUT is studied in the selected configuration for a fixed time interval by sampling the electrical quantities in n different instants.
- Determination of the output vector (2.7), which contains the samples of the electrical quantities used as outputs that depend on the inputs

$\mathbf{u}_0$ and on the vector of n_p unknown parameters $\mathbf{p}$.

$$\mathbf{y}_T(\mathbf{p}, \mathbf{u}_0) = [\mathbf{y}(t_1, \mathbf{p}, \mathbf{u}_0)^{tr}, \mathbf{y}(t_2, \mathbf{p}, \mathbf{u}_0)^{tr}, \ldots, \mathbf{y}(t_n, \mathbf{p}, \mathbf{u}_0)^{tr}]^{tr} \quad (2.7)$$

- Determination of the fault diagnosis equations (2.8), where $\mathbf{y}_T^*$ is the vector of the measurements corresponding to the output vector.

$$\mathbf{y}_T(\mathbf{p}, \mathbf{u}_0) = \mathbf{y}_T^* \quad (2.8)$$

- Evaluation of Testability through the Jacobian matrix associated with the failure equations evaluated using the nominal parameters of the circuit $\mathbf{p}_0$.
- Determination of the CAGs corresponding to the minimal set of linearly dependent columns of the Jacobian matrix.

The Testability obtained is independent of measurement errors, sampling times, and nominal values of parameters. Furthermore, testability analysis can give different results moving from a time interval to another one. Therefore, by suitably choosing the time interval, it is possible to increase the number of distinguishable parameters by considering a higher Testability and/or a smaller number of second order CAGs. In [28], it has been demonstrated that the simplest way to realize a computer program implementing this algorithm is based on the equivalence, in terms of Testability and ambiguity group determination, of the above-mentioned Jacobian matrix to the Laplace transform of its extension to all the positive time semi-axis. In this way, a link with the frequency domain may be built up, which can exploit the results in [47] for setting up a fully numerical algorithm for the testability analysis of DC-DC converters. The program implementing this algorithm is called TAPSLIN (Testability Analysis for Periodically Switched Linear Networks) and it is able to identify the correct fault classes and the best test points in these types of devices. TAPSLIN is implemented in the program SapWin PET to integrate the Testability assessment of time-variant circuits.

2.5.3 Power Quality

Finally, a very important field of application considered in this Thesis is the evaluation of the Power Quality (PQ) level in low voltage distribution networks. This is a significant task due to the increasing presence of non-linear

loads and variable generators in power systems. For example, as shown in [57] and [58], charging stations for electric vehicles and renewable energy production systems have a strong impact on the quality of the grid energy. Since these sectors are growing rapidly to contain greenhouse gasses emission, several efforts have been made to minimize the impact of these Power Quality Disturbances (PQDs). Fast and automatic classification of PQDs allows proper countermeasures to be applied to maintain the stability of the grid avoiding plant shut-downs and economic losses. Therefore, the assessment of the PQ level in distribution networks can be considered a monitoring operation aimed at preventing failures for thousands of users. The EN 50160 [59], IEC 61000 [60], and IEEE-1159 standards [61] provide a detailed description of all PQDs. One of the most common causes of power quality degradation is the use of non-linear loads that inject distorting electrical components into the electrical grid, affecting voltage and current waveforms [62]. Consequently, power network quantities present some distortions with respect to the nominal condition and this introduce problems for all connected users [63]. The most important PQ disturbances considered in the literature can be summarized in five different categories: voltage sag, voltage swell, harmonic distortion, voltage notch and interruption.

In this case the main objective is the development of a classification tool, usually based on machine learning or deep learning techniques, capable of identifying the presence of PQDs. The typical procedures usually proposed in the literature consist in applying a feature extraction method and then processing data through one or more neural networks. Initial data is always measurements of voltage and/or current waveforms with a specific sample rate. After the feature extraction process, the data can be expressed in different domains. For example, the simplest signal processing technique to apply to sampled data is the Fourier Transform (FT) [64]. This is a powerful technique for periodic time series where the characteristics of the signal do not change with time [65]. In practice, the disturbances lead to non-stationary signals. To overcome this issue, Short Time Fourier Transform (STFT) is used by introducing a sliding window to obtain time and frequency information [66]. Alternative techniques are based on Wavelet Transform (WT). In this method, the sampling window is changed according to the frequency content of the signal [67]. A short window is used for high frequency, while a long window is used for low frequencies. This adaptation makes the technique particularly suitable for monitoring transient behaviour and disconti-

nuities in the signal, but it is more complex than FT-based approaches and is more sensitive to noise [68]. To decrease the sensitivity to noise, the S-Transform (ST) technique can be used. Although this technique overcomes the limitations of FT, STFT and WT, its adoption is limited due to high computational costs [69]. Additional techniques have been proposed over the years based on statistical approaches [70] or including machine learning for feature extraction [71]. However, FT, STFT and WT are the most used techniques in the literature and, since they represent simpler solutions from the computational point of view, they can be practically implemented in real-time applications.

As for the classification of PQDs, many different algorithms can be used. In particular, numerous studies show that Convolutional Neural Networks (CNNs) have strong learning and generalization capabilities, making them the most used techniques [72].

Chapter 3

Theoretical Aspects: Proposed Methodology

This chapter presents in detail the preliminary steps for introducing different monitoring methods in the field of power lines and power devices. Starting from the theoretical concepts covered in the previous chapter, the most important developments necessary for the introduction of predictive maintenance are illustrated here. In the case of electrical lines, the first objective is to detect the degradation of the main grid components by studying their equivalent models. In fact, variations in the electrical characteristics of the line can be considered as parametric faults in analog circuits. The main idea is to inject high frequency signals into the grid and use a complex-valued neural networks to detect and locate malfunctions. A similar concept can be applied to switching power devices, such as DC-DC converters, by introducing a specific time-domain preprocessing. Since the neural network proposed here is a discrete classifier, it can be adapted to process many different types of data. Therefore, a possible application in the field of Power Quality analysis is also taken into consideration. To achieve these objectives, the main theoretical steps can be summarized in three categories: system modelling, selection of measures and creation of a suitable classifier. [1]

[1] Part of this work was conducted while the author was a visiting Ph.D. student at Manhattan College, New York (USA), on November 2022 (working with. Prof. Igor Aizenberg).

3.1 Introduction

The purpose of this chapter is to present the main theoretical aspects, simulation models and algorithms developed to classify the operating conditions of many different electrical systems.

Therefore, the first section presents all the most important characteristics of the complex-valued neural network used to create suitable intelligent classifiers. Initially, the main theoretical concepts on which this computational model is based are briefly recalled and subsequently the proposed configuration and training algorithms are presented in detail. In particular, three possible configurations have been developed to analyse different situations: single failure hypothesis, multiple failure hypothesis and multiple malfunction severities. The latter allows the prognostic aspect to be improved and plays a fundamental role for the introduction of predictive maintenance operations. The complete procedure required to train the neural network and translate the input samples into the most suitable form has been integrated into a Matlab application that allows immediate use of the classifier in different applications. Therefore, once a very versatile and easily usable classifier has been created, the correct modelling of the problem under examination is essential.

Regarding the monitoring of power lines, the modelling phase is divided into three main steps:

- realization of the equivalent circuit of the network branch taken into consideration;
- analysis of the most common failure mechanisms;
- study of the relationships between failure mechanisms and electrical components;

In fact, the deviations of the electrical parameters with respect to the nominal conditions can be used as an index of degradation and anomalous working conditions. Once the modelling phase is complete, various simulation tools can be used to perform parametric analysis, select the best test points, and create a significant dataset for neural network training. This chapter presents the models developed in SapWin and Matlab/Simulink to study high voltage overhead lines and medium voltage underground lines. Furthermore, to simulate the injection of high frequency signals, a possible modelling of Power Line Communication (PLC) systems is proposed.

Regarding the parametric analysis of DC-DC converters, a new method for performing Testability analysis in graphical form is presented below. This greatly facilitates the selection of test points in the case of time-variant circuits and can be easily applied to different circuit topologies.

3.2 Complex-Valued Neural Network

As described in section 2.3.3, artificial intelligence techniques are usually used in monitoring systems to process and classify extracted measurements, thus obtaining the state of health of the system under test. The most important algorithm proposed in this Thesis is that of Multi-Layer neural network with Multi-Valued Neurons (MLMVN). Different configurations have been developed for all the applications taken into consideration starting from the basic form presented in [73]. This section presents the main theoretical aspects of the algorithm and describes in detail the most important developments introduced to obtain specific classification tools.

From a general point of view, MLMVN is a feed-forward neural network organized in three layers: input layer, hidden layer and output layer. This means that information is processed from the input layer to the output one without neuronal connections forming loops and feedback. Therefore, it can be considered as a standard machine learning structure, in which each neuron of a specific layer is connected with those belonging to the higher level and all these connections are characterized by weights.

The values of the weights are modified during the training phase forming the associative memory typical of artificial intelligence algorithms. A back-propagation procedure based on a supervised approach is used for MLMVN and this means that the dataset contains many examples of input data and the corresponding desired outputs.

In the initial steps of the training phase, the weights are set randomly and the inputs are processed to obtain the network outputs. Therefore, errors can be calculated by comparing the actual and desired outputs. Consequently, these errors are back-propagated from the last layer to the input level by using specific formulas and the correction of the weights are defined to minimize the difference between calculated and desired outputs. Hereafter, this part of the training is called learning phase and each output error is also used to get an overall performance assessment when all inputs have been processed. To achieve this goal, different indexes can be used, such as

for example the Root Mean Square Error (RMSE) or the Classification Rate (CR) in discrete problems.

Often, the dataset is divided into two different parts and one of these is used to perform the learning phase while the input data belonging to the other part are used to evaluate the neural network performance without correcting the values of the weights (testing phase). This approach is called hold out validation and usually involves the use of high percentages of the dataset for the learning phase and the remaining inputs for the testing phase. In general, the term training epoch is used to describe a complete learning and testing cycle using all available inputs. As previously mentioned, at the end of each training epoch a specific index is calculated for the evaluation of the overall learning performance and the same happens for the data used in the testing phase. The latter represents the most important information because it describes the generalization capability of the neural network with data not used for weight correction.

Generally, the overall results obtained during the learning phase are used to decide whether the training phase should be interrupted or not and those obtained during the testing phase are used to describe the performance of the algorithm. In fact, thresholds can be set to assess the need for further weight corrections. Moreover, the difference between the performances obtained during the learning phase and the testing phase allows the detection of over-fitting problems: when the results obtained in the learning phase are much better than those obtained during the test phase, the neural algorithm it is over-adapted to the learning data. Over-fitting reduces the performance of the neural network on new measurements and can be avoided by using several techniques [74], [75]. Certainly, the number of neurons or the hyper-parameters of the algorithm play a fundamental role. A high amount of neurons in the hidden layer of machine learning techniques with respect to the dimensionality of the inputs can lead to hyper-adaptation.

A more consistent evaluation of the neural network results can be achieved by replacing the hold out validation described above with a cross validation method. In this case, the division of the dataset into two parts is repeated several times ensuring the use of each input both in the learning phase and in the testing phase. In this way, a better performance evaluation is obtained avoiding the problems introduced for example by the heterogeneity of the data used in the two phases. A summary of these concepts is presented below.

- **Learning Phase:** this is the first phase of the training procedure in which the output errors are calculated and used for weight correction. Once all the inputs have been processed, the performance is evaluated through the learning error.

- **Testing Phase:** it consists in processing a part of the dataset not used during the learning phase in order to evaluate the performance on new data. Also in this case, at the end of each training epoch, an error called test error is calculated.

- **Hold Out Validation:** in this case, the dataset is divided into two different parts, one used for the learning phase and the other used for the testing phase. Performance is evaluated using the learning error and the testing error at the end of each training epoch without changing the division of the data used in both phases.

- **Cross Validation:** in this case all inputs are used both in the learning and testing phase. Therefore, once the fixed error threshold has been reached, the hold out procedure is repeated by modifying the data used in the two phases.

MLMVN training is managed using these considerations but, compared to other feed-forward neural networks, these structures have two main characteristics: they are complex-valued models and use a derivative free learning algorithm. The complex nature of these neural networks implies that the inputs, weights and outputs are complex numbers. For this reason, MLMVN can be easily applied to electrical problems, where all the quantities are usually expressed by phasors. This means that electrical measurements can be processed directly trough MLVMN without introducing the necessary coding phase in real-valued neural networks. Furthermore, the correction of complex weights can be performed using the procedure shown in [73] which does not require the calculation of derivative terms. Therefore, the computational cost of this training procedure compared to those based on the gradient rule is extremely advantageous.

In order to study the main characteristics of these neural networks, the elementary unit called Multi-Valued Neuron (MVN) must be analysed in detailed.

3.2.1 Multi-Valued Neurons

Before studying the overall structure of MLMVN and the theoretical developments introduced in the output layer to obtain suitable classification tools, it is necessary to analyse the functioning of the MVN. This type of neurons can implement a continuous or discrete activation function for processing complex inputs.

Continuous Activation Function

In their continuous version, MVNs are usually used to solve regression problems and describe the input/output relationships typical of many different systems. If the System Under Test (SUT) is an electrical device, coding phases could be avoided and the inputs correspond to the extracted measurements. Similarly, the outputs can be directly compared to the system responses. Referring to Figure 3.1, where a single MVN with n complex inputs $(X_1, \dots X_n)$ is presented, the continuous activation function is (3.1),

$$Y = P(z) = \frac{z}{|z|} = \exp(jArg(z)) = cos(Arg(z)) + jsin(Arg(z)) \tag{3.1}$$

where Y is the complex number representing the output of the neuron, $Arg(z)$ is the argument of the weighted sum of the inputs called z. This term is a complex number calculated by (3.2),

$$z = W_0 X_0 + \sum_{i=1}^{n} W_i X_i \tag{3.2}$$

where W_i describes the i^{th} weight and X_i represents the corresponding i^{th} input. Using this continuous activation function, MVNs move the weighted sum of the inputs to the unit circle and most of the information content is represented by the result phase. When these neurons are used in the output layer of MLMVN, each output error is the difference between the desired number located on the unit circle and that obtained by applying the activation function (3.1). Therefore, the desired outputs are reported on the unit circle to start the correction process.

Discrete Activation Function

When the number of possible outputs is finite or the main objective is the classification of the input data, it is possible to use MVNs characterized

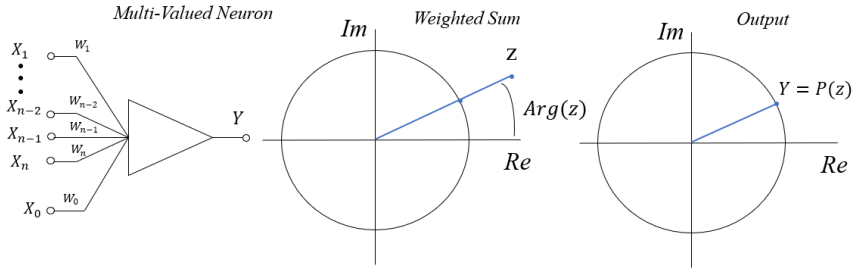

Figure 3.1: Multi-Valued Neuron with continuous activation function.

by the discrete activation function. In this case, each neuron divides the complex plane into b equal sectors, and the output corresponds to the lower border of the sector that contains the weighted sum of the inputs. Formally, the expression of the discrete activation function is (3.3),

$$P(z) = \varepsilon_b^Y = \exp\left(j2\pi\frac{Y}{b}\right) \quad if \quad \frac{2\pi Y}{b} \leq Arg(z) < 2\pi\frac{(Y+1)}{b} \tag{3.3}$$

where z is the weighted sum of the inputs calculated as shown in (3.2), b is the total number of sectors created by the considered MVN and Y is the index of the sector that contains the weighted sum of the inputs. Therefore, the lower border of Y is chosen as the output of the neuron if the argument of the weighted sum belongs to this sector. Figure 3.2 describes the main characteristics of the discrete activation function. For example, in prognostic and diagnostic systems, one of the most common solutions is to use a discrete neuron in the output layer and use a number of sectors equal to that of the fault classes. Consequently, the desired outputs used to calculate the errors in the back-propagation procedure are complex numbers located on the unit circle and corresponding to the beginning of the sectors.

3.2.2 Multi-Layer Neural Network with Multi-Valued Neurons

As previously mentioned, the most important neural classifier used in this Thesis is the MLMVN presented in Figure 3.3.

First of all it should be noted that the index m indicates the output layer of the neural network, the index $(m-1)$ is used to describe the hidden layer

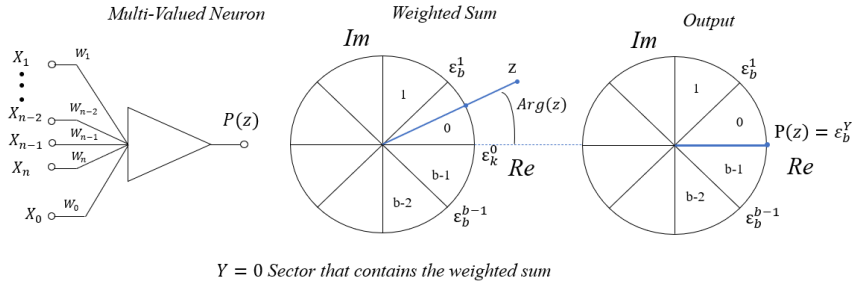

Figure 3.2: Multi-Valued Neuron with discrete activation function.

while the input layer receives the n inputs $(X_1^s, X_2^s, \ldots, X_n^s)$ of each example belonging to the dataset. Therefore, the index s indicates the currently processed example and varies in the range $(s = 1, \ldots, n_s)$, where n_s is the total number of cases considered in the dataset matrix.

Regarding the weights, a generic $W_i^{k,m}$ represents the i^{th} weight of the k^{th} neuron belonging to the last layer m. In this case, the index k varies in the range $(k = 1, \ldots, n_m)$, where n_m is the total number of neurons belonging to the output layer, while the index i indicates one of the neuron outputs of the hidden layer and varies in the range $(i = 1, \ldots, n_{m-1})$.

Likewise, the term $W_i^{k,m-1}$ is used to describe the i^{th} weight of the k^{th} neuron belonging to the layer $(m-1)$. In this case, the maxim value of k is the total number on neurons belonging to the hidden layer (n_{m-1}), while the index i varies in the range $(i = 1, \ldots, n)$.

Since the MLMVN training procedure is based on a supervised algorithm, the dataset matrix must contain many examples of input data and the corresponding desired outputs. In (3.4) an example of a dataset containing n_s different examples is provided,

$$\begin{bmatrix} X_1^1 & X_2^1 & \ldots & X_n^1 & D_{1,m}^1 & D_{2,m}^1 & \ldots & D_{n_m,m}^1 \\ X_1^2 & X_2^2 & \ldots & X_n^2 & D_{1,m}^2 & D_{2,m}^2 & \ldots & D_{n_m,m}^2 \\ & & \ldots & & & & \ldots & \\ X_1^{n_s} & X_2^{n_s} & \ldots & X_n^{n_s} & D_{1,m}^{n_s} & D_{2,m}^{n_s} & \ldots & D_{n_m,m}^{n_s} \end{bmatrix} \tag{3.4}$$

where a generic $D_{k,m}^s$ is the desired output of the k^{th} neuron belonging to the last layer, obtained by processing the inputs of the s^{th} row. It should be noted that the inputs of the neurons belonging to the output layer correspond

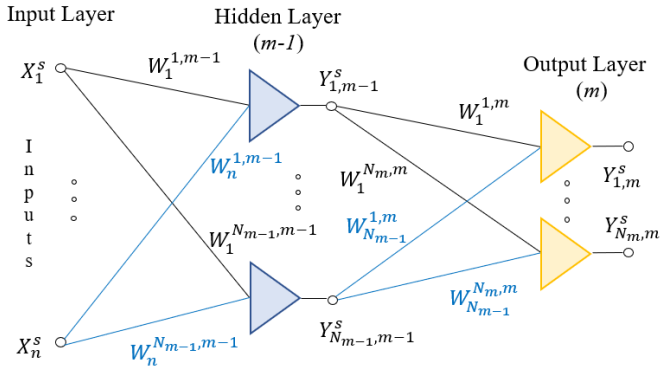

Figure 3.3: General structure of the MLMVN-based classifier.

to the outputs of the hidden layer and, therefore, they are indicated as $(Y^s_{k,m-1}, \ldots, Y^s_{n_{m-1},m-1})$.

In the case of continuous activation function, output errors are calculated by (3.5),

$$\delta^s_{k,m} = \frac{D^s_{k,m} - Y^s_{k,m}}{(n_{m-1}+1)} \tag{3.5}$$

where $\delta^s_{k,m}$ is the output error of the k^{th} neuron belonging to the layer m obtained by processing the s^{th} input sample of the dataset, $D^s_{k,m}$ is the corresponding desired output reported on the unit circle and $Y^s_{k,m}$ is the current output calculated by (3.1). If, on the other hand, discrete neurons are considered, the calculation of the errors is replaced by the following relation,

$$\delta^s_{k,m} = \frac{\varepsilon_b^{D^s_{k,m}} - \varepsilon_b^{Y^s_{k,m}}}{n_{m-1}+1} \tag{3.6}$$

where $D^s_{k,m}$ is the index of the desired sector, $Y^s_{k,m}$ is the index of the sector containing the current weighted sum, $\varepsilon_b^{D^s_{k,m}}$ is the complex number corresponding to the lower border of the desired sector and $\varepsilon_b^{Y^s_{k,m}}$ is that of the sector containing the current weighted sum. The normalization presented in (3.5) and (3.6) with respect to the number of inputs of the neuron considered $(n_{m-1}+1)$ is the starting point of the back-propagation procedure. Note that the number of inputs corresponds to the number of neurons belonging

to the hidden layer plus the bias input. Figure 3.4 shows the definition of the error in the case of continuous neuron and discrete neuron.

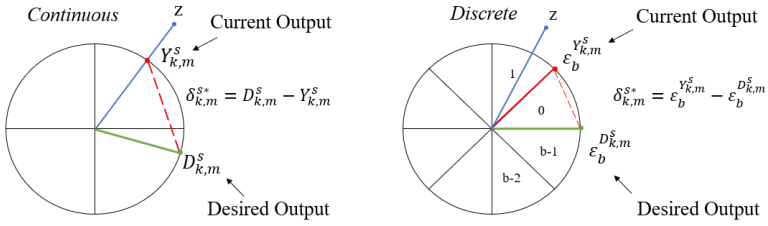

Figure 3.4: Definition of the error.

The standard rules of the back-propagation procedure demonstrated in [73] require the calculation of the errors in the hidden layer by (3.7),

$$\delta^s_{k,m-1} = \frac{1}{(n+1)} \sum_{i=1}^{n_m} \delta^s_{i,m} (W^{i,m}_k)^{-1} \tag{3.7}$$

Once the errors have been calculated for all neurons it is possible to start the iterative correction of the weights using the following formulas. In particular, for neurons belonging to the last layer, the correction of the weight $W^{k,m}_0$ can be calculated as shown in (3.8) while the corrections of the other weights are defined by (3.9),

$$\Delta W^{k,m}_0 = \frac{\alpha_{k,m}}{(n_{m-1}+1)} \delta^s_{k,m} \tag{3.8}$$

$$\Delta W^{k,m}_i = \frac{\alpha_{k,m}}{(n_{m-1}+1)} \delta^s_{k,m} \overline{Y}^s_{i,m-1} \tag{3.9}$$

where $\Delta W^{k,m}_i$ is the correction for the i^{th} weight of the k^{th} neuron belonging to the layer m, $\alpha_{k,m}$ is the corresponding learning rate and $\overline{Y}^s_{i,m-1}$ is the conjugate-transposed of the current input. These rules can be easily adapted for the correction of hidden neuron weights. Formulas (3.10) and (3.11) show the corrections for the bias weight and those for the other weights respectively.

$$\Delta W^{k,m-1}_0 = \frac{\alpha_{k,m-1}}{(n+1)|z^s_{k,m-1}|} \delta^s_{k,m-1} \tag{3.10}$$

$$\Delta W_i^{k,m-1} = \frac{\alpha_{k,m-1}}{(n+1)|z_{k,m-1}^s|}\delta_{k,m-1}^s \overline{X}_i^s \tag{3.11}$$

The main advantages of this back-propagation procedure with respect to the standard approach based on the gradient rule can be summarized as follows:

- the absence of partial derivatives allows the problem of local minima to be avoided, thus increasing the effectiveness of the training phase;
- since the calculation of the derivative terms is not necessary to define the corrections of the weights, the computation cost is very low and the training phase is faster than the canonical method.

Finally, note that all these formulas can be easily extended to train MLMVN with more than three layers, thus obtaining deep learning algorithms.

Iterative Training Procedure

The approach proposed above consists of an iterative procedure in which each weight is corrected step by step during the back-propagation of the output errors. This process is stopped when the error made in the regression or classification activities is low enough. Typically, this condition is evaluated by setting a specific threshold for the RMSE. The Algorithm 1 summarizes the overall procedure in the case of continuous neurons. In the discrete case it is sufficient to replace the error definition with (3.6).

Training Procedure Based on Batch Algorithms

In order to speed up the MLMVN learning phase, it is possible to introduce batch algorithms in the calculation of the weight corrections. In this case, the previously described iterative procedure is replaced by several mathematical methods capable of solving oversized systems of linear equations. In fact, the weight corrections are not calculated during the back-propagation procedure but at the end of each training epoch. Therefore, the error calculation rules are still valid and also the propagation from the last layer to the input one takes place as described above. However, in this case, all errors are saved in a specific matrix and used to calculate the best corrections at the end of

Algorithm 1 Iterative Training Procedure

Require: Dataset matrix (n_s examples, n input samples for each example, n_m desired outputs for each example)
Ensure: Learning rate $\alpha_{k,m}$ for each neuron belonging to the output layer
Ensure: Learning rate $\alpha_{k,m-1}$ for each neuron belonging to the hidden layer
Ensure: Initial weights $W_i^{k,m}$ of the output layer
Ensure: Initial weights $W_i^{k,m-1}$ of the hidden layer
Ensure: Threshold for the Root Mean Square Error $RMSE_{tr}$

while $RMSE \leq RMSE_{tr}$ **do**
  for $s = 1, \ldots, n_s$ **do**
    $X_1 = X_1^s$
    $\vdots$
    $X_n = X_n^s$
    for $k = 1, \ldots, n_{m-1}$ **do**
      $z_{k,m-1}^s = W_0^{k,m-1} X_0 + \sum_{i=1}^{n} W_i^{k,m-1} X_i$
      $Y_{k,m-1}^s = P(z_{k,m-1}^s)$
    end for
    for $k = 1, \ldots, n_m$ **do**
      $z_{k,m}^s = W_0^{k,m} X_0 + \sum_{i=1}^{n_{m-1}} W_i^{k,m} Y_{i,m-1}^s$
      $Y_{k,m}^s = P(z_{k,m}^s)$
      $\delta_{k,m}^s = \frac{D_{k,m}^s - Y_{k,m}^s}{(n_{m-1}+1)}$
      $\Delta W_0^{k,m} = \frac{\alpha_{k,m}}{(n_{m-1}+1)} \delta_{k,m}^s$
      for $i = 1, \ldots, n_{m-1}$ **do**
        $\Delta W_i^{k,m} = \frac{\alpha_{k,m}}{(n_{m-1}+1)} \delta_{k,m}^s \overline{Y}^s{}_{i,m-1}$
      end for
    end for
    for $k = 1, \ldots, n_{m-1}$ **do**
      $\delta_{k,m-1}^s = \frac{1}{(n+1)} \sum_{i=1}^{n_m} \delta_{i,m}^s (W_k^{i,m})^{-1}$
      $\Delta W_0^{k,m-1} = \frac{\alpha_{k,m-1}}{(n+1)|z_{k,m-1}^s|} \delta_{k,m-1}^s$
      for $i = 1, \ldots, n$ **do**
        $\Delta W_i^{k,m-1} = \frac{\alpha_{k,m-1}}{(n+1)|z_{k,m-1}^s|} \delta_{k,m-1}^s \overline{X}_i$
      end for
    end for
    $\Delta_s = \frac{1}{n_m} \sum_{k=1}^{n_m} (D_{k,m}^s - Y_{k,m}^s)$
  end for
  $RMSE = \sqrt{\frac{1}{n_s} \sum_{s=1}^{n_s} \Delta_s}$
end while

the training epoch, i.e. when all the examples belonging to the dataset have been processed.

From a general point of view, the main characteristics of this method can be extracted from [76] and can be summarized as follows:

- a change is introduced in the calculation of the output errors and formula (3.12) is presented;

$$\delta_{k,m}^{s} = D_{k,m}^{s} - z_{k,m}^{s} \tag{3.12}$$

- output errors are calculate by (3.12) and back-propagated by (3.7) without correcting the weights;
- all errors for the hidden and output layer are saved in two specific matrices and are used to create an oversized system;
- the system of equations is solved with a mathematical method to obtain the best correction of the weights after processing all the inputs;
- note that this method can be applied only to the output layer of the neural network while the iterative procedure can be still valid for the hidden one.

From the mathematical point of view, focusing on the output layer, the weighted sums $z_{k,m}^{s}$ for a generic input s are calculated as follows,

$$z_{k,m}^{s} = W_{0}^{k,m} + \sum_{i=1}^{n_{m-1}} W_{i}^{k,m} Y_{i,m-1}^{s} \tag{3.13}$$

where k is still the index that identifies the number of the neuron in the last layer m and the bias input is considered to be always active. Considering the new error definition (3.12), the desired outputs can be written as follows,

$$D_{k,m}^{s} = \widetilde{W}_{0}^{k,m} + \sum_{i=1}^{n_{m-1}} \widetilde{W}_{i}^{k,m} Y_{i,m-1}^{s} \tag{3.14}$$

where the terms $\widetilde{W}$ indicate the correct weights, which are the values that allow the desired outputs to be obtained. Consequently, by introducing formulas (3.13) and (3.14) in (3.12), it is possible to obtain the following relationship:

$$
\begin{aligned}
&\delta^s_{k,m} = D^s_{k,m} - z^s_{k,m} = \\
&(\widetilde{W}^{k,m}_0 + \sum_{i=1}^{n_{m-1}} \widetilde{W}^{k,m}_i Y^s_{i,m-1}) - (W^{k,m}_0 + \sum_{i=1}^{n_{m-1}} W^{k,m}_i Y^s_{i,m-1}) = \\
&\widetilde{W}^{k,m}_0 + \widetilde{W}^{k,m}_1 Y^s_{1,m-1} + \ldots - W^{k,m}_0 - W^{k,m}_1 Y^s_{1,m-1} - \ldots - W^{k,m}_{n_{m-1}} Y^s_{n_{m-1},m-1} = \\
&\widetilde{W}^{k,m}_0 - W^{k,m}_0 + (\widetilde{W}^{k,m}_1 - W^{k,m}_1) Y^s_{1,m-1} + \ldots + (\widetilde{W}^{k,m}_{n_{m-1}} - W^{k,m}_{n_{m-1}}) Y^s_{n_{m-1},m-1} = \\
&\Delta W^{k,m}_0 + \Delta W^{k,m}_1 Y^s_{1,m-1} + \ldots + \Delta W^{k,m}_{n_{m-1}} Y^s_{n_{m-1},m-1}
\end{aligned}
\tag{3.15}
$$

where the terms $\Delta W^{k,m}_i Y^s_{1,m-1}$ are the corrections to be calculated for each neuron of the output layer ($i = 1, \ldots, n_{m-1}$). Therefore, by considering all neurons belonging to the output layer, the errors committed can be expressed using a set of equations as shown in (3.16).

$$
\begin{cases}
\delta^s_{1,m} = \Delta W^{1,m}_0 + \Delta W^{1,m}_1 Y^s_{1,m-1} + \ldots + \Delta W^{1,m}_{n_{m-1}} Y^s_{n_{m-1},m-1} \\
\delta^s_{2,m} = \Delta W^{2,m}_0 + \Delta W^{2,m}_1 Y^s_{1,m-1} + \ldots + \Delta W^{2,m}_{n_{m-1}} Y^s_{n_{m-1},m-1} \\
\vdots \\
\delta^s_{n_m,m} = \Delta W^{n_m,m}_0 + \Delta W^{n_m,m}_1 Y^s_{1,m-1} + \ldots + \Delta W^{n_m,m}_{n_{m-1}} Y^s_{n_{m-1},m-1}
\end{cases}
\tag{3.16}
$$

Starting from these considerations it is possible to write a system of n_s equations for each error. These systems are oversized because the number of examples belonging to the dataset matrix is commonly greater than the number of unknowns which, in this case, correspond to the corrections of the weights ($n_s \gg n_{m-1} + 1$). In (3.17) and (3.18) two of these systems are presented, respectively one for the first neuron of the output layer and the other for the last neuron.

$$
\begin{cases}
\delta^1_{1,m} = \Delta W^{1,m}_0 + \Delta W^{1,m}_1 Y^1_{1,m-1} + \ldots + \Delta W^{1,m}_{n_{m-1}} Y^1_{n_{m-1},m-1} \\
\delta^2_{1,m} = \Delta W^{1,m}_0 + \Delta W^{1,m}_1 Y^2_{1,m-1} + \ldots + \Delta W^{1,m}_{n_{m-1}} Y^2_{n_{m-1},m-1} \\
\vdots \\
\delta^{n_s}_{1,m} = \Delta W^{1,m}_0 + \Delta W^{1,m}_1 Y^{n_s}_{1,m-1} + \ldots + \Delta W^{1,m}_{n_{m-1}} Y^{n_s}_{n_{m-1},m-1}
\end{cases}
\tag{3.17}
$$

$$\begin{cases} \delta^1_{n_m,m} = \Delta W_0^{n_m,m} + \Delta W_1^{n_m,m} Y^1_{1,m-1} + \ldots + \Delta W^{n_m,m}_{n_{m-1}} Y^1_{n_{m-1},m-1} \\ \delta^2_{n_m,m} = \Delta W_0^{n_m,m} + \Delta W_1^{n_m,m} Y^2_{1,m-1} + \ldots + \Delta W^{n_m,m}_{n_{m-1}} Y^2_{n_{m-1},m-1} \\ \vdots \\ \delta^{n_s}_{n_m,m} = \Delta W_0^{n_m,m} + \Delta W_1^{n_m,m} Y^{n_s}_{1,m-1} + \ldots + \Delta W^{n_m,m}_{n_{m-1}} Y^{n_s}_{n_{m-1},m-1} \end{cases} \tag{3.18}$$

Many methods can be used to solve these systems in the sense of Linear Least Squares (LLS). In this Thesis, the QR decomposition is used and it has been introduced in the training algorithm of the MLMVN.

QR Decomposition

In order to apply the QR decomposition, the system taken into consideration must be written in matrix form. For example, in (3.19), the system corresponding to the error on the first neuron of the output layer is presented.

$$\begin{bmatrix} \delta^1_{1,m} \\ \delta^2_{1,m} \\ \vdots \\ \delta^{n_s}_{1,m} \end{bmatrix} = \begin{bmatrix} 1 & Y^1_{1,m-1} & Y^1_{2,m-1} & \ldots & Y^1_{n_{m-1},m-1} \\ 1 & Y^2_{1,m-1} & Y^2_{2,m-1} & \ldots & Y^2_{n_{m-1},m-1} \\ \vdots & \vdots & \vdots & \vdots & \vdots \\ 1 & Y^{n_s}_{1,m-1} & Y^{n_s}_{2,m-1} & \ldots & Y^{n_s}_{n_{m-1},m-1} \end{bmatrix} \begin{bmatrix} W_0^{1,m} \\ W_1^{1,m} \\ \vdots \\ W^{1,m}_{n_{m-1}} \end{bmatrix} \tag{3.19}$$

It can be written in its compact version (3.20),

$$\delta_{\mathbf{1}} = A_1 \; \Delta \mathbf{W^1} \tag{3.20}$$

where $\delta_{\mathbf{1}}$ is the vector of dimension n_s containing the errors calculated for each input example, A_1 is the matrix of dimension $(n_s \cdot n_{m-1})$ containing all the inputs of the neuron considered and, finally, $\Delta \mathbf{W^1}$ is the vector of dimension n_{m-1} containing the unknowns (which are the corrections of the weights).

Since the system is oversized, there is no single solution but the QR decomposition can be used to obtain a solution that minimizes the root mean square error. Therefore, the goal is to calculate the vector $\Delta \mathbf{W^1}$ by minimizing the residual vector $\mathbf{r}$.

$$\mathbf{r}(\Delta \mathbf{W^1}) = \delta_{\mathbf{1}} - A_1 \; \Delta \mathbf{W^1} \tag{3.21}$$

In general, the QR decomposition of a square matrix A_1 consists in the definition of an orthogonal matrix Q and of an upper triangular matrix R such that $A_1 = QR$. In case A_1 is a complex valued matrix, then Q is a unitary matrix and the following relation is valid.

$$A_1 \ \textit{complex} \Rightarrow Q \ \textit{unitary} \Rightarrow Q^T Q = Q Q^T = I \tag{3.22}$$

In the specific case of weight correction, the matrix A_1 is rectangular of dimension $(n_s \cdot n_{m-1})$. This means that the matrix R is triangular and consists of an upper triangular $R_{n_{m-1}+1}$ matrix and an identically null matrix.

$$R = \begin{bmatrix} R_{n_{m-1}+1} \\ - - - \\ 0 \end{bmatrix} \tag{3.23}$$

The matrices R and Q can be calculated through the Householder method [77]. Table 3.1 summarizes the dimension of the matrices.

$A_1 \in \Re^{(n_s)\cdot(n_{m-1}+1)}$
$Q \in \Re^{(n_s)\cdot(n_s)}$
$R \in \Re^{(n_s)\cdot(n_{m-1}+1)}$
$R_{n_{m-1}+1} \in \Re^{(n_{m-1}+1)\cdot(n_{m-1}+1)}$
$0 \in \Re^{(n_s-(n_{m-1}+1))\cdot(n_s-(n_{m-1}+1))}$

Table 3.1: Matrix size summary.

Therefore, the residual vector $\mathbf{r}$ can be expressed as follows,

$$\mathbf{r}(\Delta \mathbf{W^1}) = \delta_\mathbf{1} - A_1 \ \Delta \mathbf{W^1} = \delta_\mathbf{1} - QR \ \Delta \mathbf{W^1} \tag{3.24}$$

and multiplying both sides by Q^T yields two vectors $\mathbf{u}$ and $\mathbf{v}$ as shown in (3.25).

$$Q^T \mathbf{r} = Q^T \delta_\mathbf{1} - Q^T Q R \Delta \mathbf{W^1} = \begin{bmatrix} [Q^T \delta_1]_{n_{m-1}+1} - R \Delta \mathbf{W^1} \\ [Q^T \delta_1]_{n_s - n_{m-1}+1} \end{bmatrix} = \begin{bmatrix} \mathbf{u} \\ \mathbf{v} \end{bmatrix} \tag{3.25}$$

Since Q is orthogonal, formula (3.26) is obtained.

$$\| \mathbf{r} \|^2 = \mathbf{r}^T \mathbf{r} = \mathbf{r}^T Q Q^T \mathbf{r} = \mathbf{u}^T \mathbf{u} + \mathbf{v}^T \mathbf{v} \tag{3.26}$$

Therefore, since $\mathbf{v}$ does not depend on $\Delta \mathbf{W^1}$, the minimum value of $\| \mathbf{r} \|^2$ is obtained when $\mathbf{u} = 0$.

$$\mathbf{u} = 0 \Rightarrow R_{n_{m-1}+1} \Delta \mathbf{W^1} = [Q^T \delta_1]_{n_{m-1}+1} \tag{3.27}$$

Finally, the vector $\mathbf{\Delta W^1}$ calculated from (3.27) allows the minimization of the residual vector and represents the best solution of the oversized system in the sense of linear least squares. The algorithm 2 shows the introduction of QR decomposition in the training procedure. Note that the correction of the hidden neurons is carried out through the standard iterative procedure.

Discrete MLMVN with Soft Margin

As previously mentioned, the discrete version of the MLMVN is used in this work to create monitoring methods capable of identifying the state of health of several electrical systems. The activation function shown in (3.3) provides for the division of the complex plane into a certain number of equal sectors and the neuron output corresponds to the lower border of the sector that contains the weighted sum of the inputs. As mentioned above, this type of neural networks can be used to solve classification problems and, usually, a neuron is implemented in the output layer by dividing the complex plane into a number of sectors equal to that of the classes. Figure (3.2) clarifies the characteristics of the discrete activation function and Table (3.2) summarizes the meaning of the main terms.

b	Total number of sectors
D	Index of the desired sector
Y	Index of the sector obtained with the current input
ε_b^D	Desired output (complex number)
ε_b^Y	Current output (complex output)
γ	Sector error
δ	Error to back-propagate

Table 3.2: Meaning of the main terms.

Therefore, the last column of the dataset matrix contains the desired sectors indices for all input examples. These indices are translated into the desired complex outputs and the errors used in the back-propagation procedure is calculated by (3.28).

$$\begin{aligned} \delta &= \varepsilon_b^D - \varepsilon_b^Y = \exp\Big(j2\pi\frac{D}{b}\Big) - \exp\Big(j2\pi\frac{Y}{b}\Big) = \\ &= cos\Big(2\pi\frac{D}{b}\Big) + jsin\Big(2\pi\frac{D}{b}\Big) - cos\Big(2\pi\frac{Y}{b}\Big) - jsin\Big(2\pi\frac{Y}{b}\Big) \end{aligned} \tag{3.28}$$

Algorithm 2 Training Procedure Based on Batch Algorithms

Require: Dataset matrix (n_s examples, n input samples for each example, n_m desired outputs for each example)
Ensure: Learning rate $\alpha_{k,m}$ for each neuron belonging to the output layer
Ensure: Learning rate $\alpha_{k,m-1}$ for each neuron belonging to the hidden layer
Ensure: Initial weights $W_i^{k,m}$ of the output layer
Ensure: Initial weights $W_i^{k,m-1}$ of the hidden layer
Ensure: Threshold for the Root Mean Square Error $RMSE_{tr}$

while $RMSE \leq RMSE_{tr}$ **do**
  for $s = 1, \ldots, n_s$ **do**
    $X_1 = X_1^s$
    $\vdots$
    $X_n = X_n^s$
    for $k = 1, \ldots, n_{m-1}$ **do**
      $z_{k,m-1}^s = W_0^{k,m-1} X_0 + \sum_{i=1}^{n} W_i^{k,m-1} X_i$
      $Y_{k,m-1}^s = P(z_{k,m-1}^s)$
    end for
    for $k = 1, \ldots, n_m$ **do**
      $z_{k,m}^s = W_0^{k,m} X_0 + \sum_{i=1}^{n_{m-1}} W_i^{k,m} Y_{i,m-1}^s$
      $Y_{k,m}^s = P(z_{k,m}^s)$
      $\delta_{k,m}^s = D_{k,m}^s - z_{k,m}^s$
    end for
    for $k = 1, \ldots, n_{m-1}$ **do**
      $\delta_{k,m-1}^s = \frac{1}{(n+1)} \sum_{i=1}^{n_m} \delta_{i,m}^s (W_k^{i,m})^{-1}$
      $\Delta W_0^{k,m-1} = \frac{\alpha_{k,m-1}}{(n+1)|z_{k,m-1}^s|} \delta_{k,m-1}^s$
      for $i = 1, \ldots, n$ **do**
        $\Delta W_i^{k,m-1} = \frac{\alpha_{k,m-1}}{(n+1)|z_{k,m-1}^s|} \delta_{k,m-1}^s \overline{X}_i$
      end for
    end for
    $\Delta_s = \frac{1}{n_m} \sum_{k=1}^{n_m} (D_{k,m}^s - z_{k,m}^s)$
  end for
  $\delta_{\mathbf{1}} = A_1 \, \Delta \mathbf{W^1}$
  $\vdots$
  $\delta_{\mathbf{n_m}} = A_{n_m} \, \Delta \mathbf{W^{n_m}}$
  for $k = 1, \ldots, n_m$ **do**
    $\Delta \mathbf{W^k} = [Q^T \delta_k]_{n_{m-1}+1} (R_{n_{m-1}+1})^{-1}$
  end for
  $RMSE = \sqrt{\frac{1}{n_s} \sum_{s=1}^{n_s} \Delta_s}$
end while

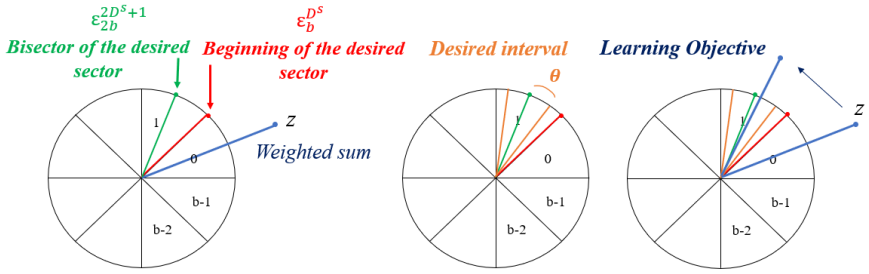

Figure 3.5: Soft margin technique.

In this case, there is another important index called sector error which is used to decide whether or not to stop the learning process. This error is calculated by (3.29),

$$\gamma = (D - Y) mod(b) \tag{3.29}$$

where the *mod* function gives the remainder of the division between $(D-Y)$ and b, which represents the error in terms of number of sectors. The first and most stringent solution is to require all input examples to be correctly classified. Equation (3.30) shows this condition.

$$\gamma^s = 0 \quad \vee s = 1, \ldots, n_s \tag{3.30}$$

On the other hand, as shown in the previous algorithms, it is possible to use the evaluation of the root mean square error at the end of each training epoch. In this case, all the terms γ^s are used as shown in (3.31) and a specific threshold is set ($RMSE_{\gamma tr}$).

$$RMSE_\gamma = \sqrt{\frac{1}{n_s}\sum_{s=1}^{n_s}(\gamma^s)^2} \leq RMSE_{\gamma tr} \tag{3.31}$$

In order to improve the classification performance it is possible to introduce the *Soft Margin* technique [78]. In this case, the beginning of the sector is not used as the desired output, but its bisector. Therefore all the weighed sums are moved towards the center of the desired sectors during the training phase. Figure 3.5 clarifies this concept.

The goal of learning is to move as many weighted sums as possible into the 2θ amplitude interval centred in the bisector. This allows the reduction

of classification errors caused by the weighed sums that are positioned near the boundaries between two successive sectors. Therefore a new error term is introduced (3.32),

$$\varphi^s = |arg(z^s) - arg(\varepsilon_{2b}^{2D^s+1})| \tag{3.32}$$

where $\varepsilon_{2b}^{2D^s+1}$ is the complex number on the unit circle that corresponds to the bisector of D^s. The soft margin technique requires a certain number of weighted sums in the 2θ interval before stopping the training phase. Therefore, in addition to the $RMSE_\gamma$ condition, the following soft margin error limitation is required.

$$RMSE_\theta = \sqrt{\frac{1}{n_s}\sum_{s=1}^{n_s}(\varphi^s)^2} \leq \theta \tag{3.33}$$

Alternatively, it is possible to use the so-called hard margin rule, in which all weighted sums must fall within the 2θ interval. In this case, the formula (3.34) is used as an error condition.

$$\varphi^s = |arg(z^s) - arg(\varepsilon_{2b}^{2D^s+1})| \leq \theta \quad \vee s = 1, \ldots, n_s \tag{3.34}$$

3.2.3 Proposed Configuration of MLMVN

The main configuration developed in this Thesis to create different monitoring systems is a hybrid structure in which the neurons of the hidden layer have a continuous activation function while those of the output layer are characterized by a discrete activation function. Furthermore, more than one neuron are used in the last layer and all the possible fault classes are obtained as combinations of the outputs. Since the soft margin rule is implemented, the formulas presented above must be extended to n_m output neurons. Remember that the subscript (k, m) indicates the k^{th} neuron of the output layer.

$$\begin{aligned} &\varphi_{k,m}^s = |arg(z_{k,m}^s) - arg(\varepsilon_{2b}^{2D_{k,m}^s+1})| \Rightarrow \phi^s = \frac{1}{n_m}\sum_{k=1}^{n_m}(\varphi_{k,m}^s)^2 \Rightarrow \\ &\Rightarrow RMSE_\theta = \sqrt{\frac{1}{n_s}\sum_{s=1}^{n_s}\phi^s} \leq \theta \end{aligned} \tag{3.35}$$

The best solution proposed here in terms of classification rate presents binary neurons in the output layer. This type of structure has been used in all the applications considered and different configurations have been proposed based on the following criteria:

- single or multiple failure hypothesis;
- severity levels of the parametric faults considered.

Configuration Developed in the Single Failure Hypothesis

The use of binary neurons in the case of single failure hypothesis requires the presence of one neuron for each fault class in the output layer. Each neuron divides the complex plane into two sectors: the first corresponds to the upper half plane $[0, \pi)$ and is usually called *Sector 0* while the second is the lower half plane $[\pi, 2\pi)$ and it is called *Sector 1*. Figure 3.6 describes the situation.

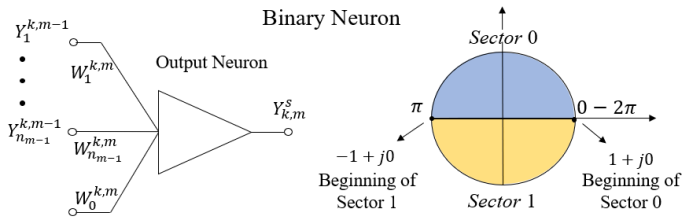

Figure 3.6: Binary neuron.

Many different interpretations of the outputs can be used in the case of single failure hypothesis. Two examples are proposed below:

- in the case of a monitoring system for electrical circuits, each output neuron corresponds to a possible faulty element and the output 0 describes its nominal condition while the output 1 is used to indicate a parametric fault;
- in the case of a monitoring system for electrical disturbances, each neuron corresponds to a specific problem and the upper half plane indicates the absence of the distortion while the lower half plane indicates its presence.

In these examples, it is assumed that two faulty components cannot be present at the same time and that two disturbances cannot occur at the same time. Therefore, the nominal conditions of the overall system are represented by a succession of zeros while the fault classes that indicate a malfunction have an output equal to 1. Table 3.3 presents a possible organization of the outputs in the case of three malfunctions.

Configuration of the outputs			
Nominal conditions	0	0	0
Malfunction 1	0	0	1
Malfunction 2	0	1	0
Malfunction 3	1	0	0

Table 3.3: Example of output coding.

The values presented in Table 3.3 are used as indices $D^s_{k,m}$ for the three output neurons belonging to the last layer.

Configuration Developed in the Multiple Failure Hypothesis

The configuration described above is also used in the case of multiple faults, where the number of classes corresponds to every possible combination of faulty components or possible disturbances. Therefore, the number of fault classes in the case of three malfunctions becomes 8 and they can be summarized as shown in Table 3.4. As in the previous case, even now the succession

Configuration of the outputs			
Class 0 (Nominal conditions)	0	0	0
Class 1	0	0	1
Class 2	0	1	0
Class 3	0	1	1
Class 4	1	0	0
Class 5	1	0	1
Class 6	1	1	0
Class 7	1	1	1

Table 3.4: Example of output coding in the case of multiple failure hypothesis.

of three zeros is used to describe the nominal conditions of the system while the presence of two or more high-level outputs indicates the presence of simultaneous malfunctions. The weight correction technique follows the same procedure presented in the previous sections and, in this case, the use of more neurons in the output layer produces obvious advantages. In fact, the use of a single neuron and eight sectors would have increased the classification errors between successive sectors.

Case of Multiple Severities

In order to develop the prognostic aspect of monitoring systems, it is often required to classify the extent of the malfunctions. In this case, the simplest and most used classification presents the division into three levels: nominal conditions, soft faults and hard faults. According to the definitions proposed in the previous chapter, this division can be applied to circuits containing analog components and subject to parametric faults. The main idea is still to use a combination of binary neurons in the output layer to describe any possible state of health of the system. Now, two neurons are used for each defective element as shown in Figure 3.7: the first is used to indicate the possible presence of a soft fault, i.e. a slight deviation with respect to the nominal interval, the second neuron describes a critical situation (hard fault) that usually precedes catastrophic failures. As usual, sector 0 is used to describe the absence of the problems while the lower half plane is an alert state. Since the most common failure mechanisms of analog components gradually lead from a soft failure to a hard fault, the latter condition is described using both high-level neurons. Consequently, the 01 combination cannot be used. In other words, it is not possible to have a hard fault without going through a soft fault condition.

Interpretation of the Measurements

The MLMVN developed in this Thesis and described above is used to process complex inputs. This aspect makes it particularly suitable for dealing with problems in the electrical sector because all the quantities are expressed in the form of phasors and correspond to complex numbers. These measurements have informative content both in the magnitude and in the phase and can be processed directly without a preliminary coding phase.

However, it is also possible to process real measurements with great ac-

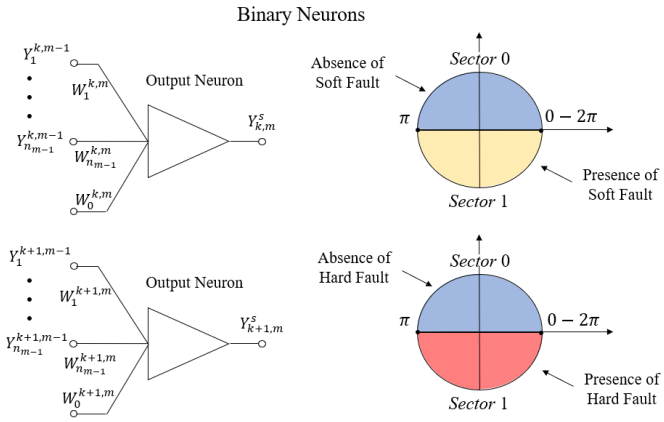

Figure 3.7: Configuration of the output neurons in the case of multiple severities.

curacy. For example, the main procedure used in this Thesis is to associate each real sample to the phase of a complex number having a unitary magnitude. Another approach is to create complex inputs after placing the real samples in dataset (3.4). These techniques are summarized below:

1. **Single Input mode**: each real measurement belonging to the dataset is used as phase of a complex number with magnitude equal to 1.

2. **Magnitude-Phase mode**: In this case, the columns of the dataset are considered in pairs. The numbers belonging to the first column of each pair is the magnitude of the complex numbers, while the second column contains the phases.

3. **Real-Imaginary mode**: In this case, the columns of the dataset are considered in pairs. The numbers belonging to the first column of each pair is the real parts of the complex numbers, while the second column is used to create the imaginary parts.

Therefore, even real measurements and time domain sampled waveforms can be processed by the complex-valued neural network in various ways.

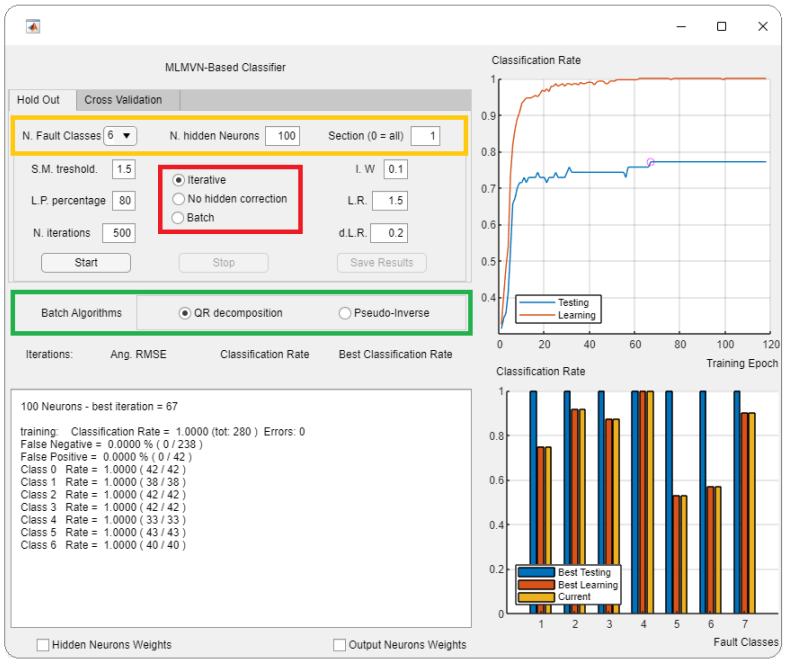

Figure 3.8: Matlab application developed for using MLMVN-based classifier.

3.2.4 MATLAB application for using MLMVN-based classifier

In order to develop the complex neural network configurations described above and make them easily usable for different purposes, a Matlab application has been created. Therefore, the learning algorithms with the various weight correction rules have been written in Matlab code and integrated into the platform shown in Figure 3.8. This makes them more intuitive and facilitates the evaluation of results while all the different ways of creating complex inputs are easily selectable. The red box shown in the Figure 3.8 allows the selection of the weight correction method: by clicking *Iterative* it is possible to follow the standard weight correction rule based on the iterative procedure; by selecting *Batch*, the weights are corrected at the end of each training epoch using the QR decomposition or the calculation of the pseudo-inverse matrix (green box); finally, the tick on *No hidden correction* can be used to solve over-fitting problems without correcting the hidden layer weights.

The number of fault classes and the number of neurons belonging to the hidden layer can be easily selected as shown in the yellow box. The *I.W.* indicates the magnitude of the initial weights, *L.R.* is the learning rate used in the correction procedure and *d.L.R.* is the percentage reduction of this index at the end of each training epoch. Furthermore, it is possible to choose the maximum number of iterations to be carried out without improvement of the classification rate (*N. iterations*), the percentage of data to be used in the learning phase of the hold out validation (*L.P. percentage*) and the width of the interval centred on the bisector for the soft margin rule (*S.M. threshold*).

The two windows on the right side of the interface allow the evaluation of the classification results. In particular, the top window shows the evolution of the classification rate according to the learning periods: the red line indicates the results obtained during the learning phase while the blue line those of the testing phase. In addition, the best test result is indicated with a circle. In the lower window, a histogram graph is presented to evaluate the classification results obtained for each class of failure considered. Also in this case, the best learning result, the test result and the current classification rate are indicated. Remember that in any phase, the classification rate is defined as the ratio between the corrected classified samples and the total number of processed samples.

3.3 Modelling of Electrical lines

Once the classification tool has been defined and a suitable platform for its use has been created, it is necessary to model the electrical systems under test to apply the main steps of the parametric analysis. In this section, the modelling procedure for electrical transmission and distribution networks is carried out by considering the physical characteristics of the most important grid components and their failure mechanisms.

Initially, a possible procedure is proposed to simulate the electrical behaviour of high voltage overhead lines in SapWin. The model obtained can be used to represent a specific network branch and perform its frequency response analysis. In fact, in order to develop a monitoring method based on the classification of the frequency response it is necessary to carry out the Testability assessment, select the best test points and create a specific dataset. In this case, the proposed prognostic method consists in injecting

high frequency signals into the line and classifying the health status of the infrastructure through the previously described MLMVN.

In order to improve modelling capabilities and include other components of the electrical network without increasing the computational cost excessively, the use of a Simulink model is also proposed. In particular, this solution is used for the study of medium voltage underground lines and for the introduction of the PLC systems necessary for the transmission of high frequency signals.

3.3.1 High Voltage Overhead Lines

In the case of overhead power lines, junction regions and conductor sections are the main physical elements. Their equivalent models represent the starting point for the development of a prognostic procedure and, therefore, the relationships between all possible malfunctions and electrical components must be defined. Only the joint degradation is considered in this study and two different failure mechanisms are introduced: oxidation process and partial breakage of the joint structure. In this way, three different working conditions can be defined for a generic junction region, corresponding to the nominal situation, the oxidation condition and the presence of a partial breakage. A specific type of conductor and bolted joint is considered below, but the modelling procedure can easily be extended to elements with different characteristics.

Conductor Modelling

This section deals with the Aluminium Conductor Steel Reinforced (ACSR) shown in Figure 3.9(a), characterized by a diameter of 22.8$[mm]$. The equivalent model of the conductor is the canonical π-model, which contains four electrical elements: the longitudinal resistance and inductance, R'_l and L'_l respectively, take into account the voltage drops along the line, while the transversal conductance and capacitance, G'_l and C'_l, describe the current losses. This equivalent circuit, shown in Figure 3.9(b), is usually used to study wave propagation and power flow analysis. The values of the electrical parameters R'_l, L'_l, C'_l and G'_l are defined per unit of length and depend on the mechanical characteristics of the phase conductor. Note that the conductance G' is usually neglected when considering overhead lines.

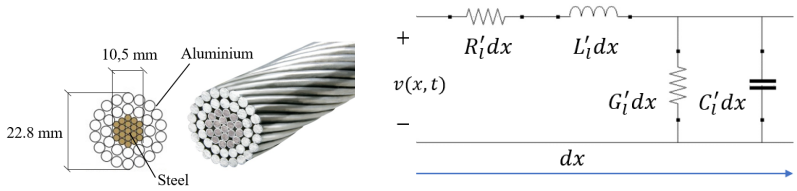

Figure 3.9: Equivalent lumped circuit of the line conductor: (a) physical characteristics; (b) equivalent π-model.

Joint Modelling

Junction regions are the main subjects of the prognostic analysis proposed here. They represent the connection points between two different parts of the same phase conductor and must guarantee the electrical continuity along the line. Usually, two different types of joint are used in high voltage overhead transmission lines: bolted joints and compression joints. The latter can be used in various positions because their geometrical structure is similar to that of the phase conductor but the low mechanical resistance makes them unsuitable for installation near pylons. On the other hand, bolted joints consist of two aluminium plates fixed by steel bolts and present a high mechanical strength. Therefore, they are mounted on the pylons at the beginning of each span. These junction regions are considered for the prognostic analysis but no available literature exists that describes their electrical behaviour. An acceptable solution proposed here is to model bolted joints with the better known equivalent circuit of solder joints, for which some information on the degradation mechanisms is available [79]. Therefore, the equivalent model is shown in Figure 3.10(a), where R_{sj} is the joint resistance, L_{sj} its inductance and C_{sj} its capacitance. In order to relate the electrical characteristics of the joints with their physical structure, Figure 3.10(b) is considered, where $\Delta\lambda$ is the length of the junction region, d is its width and H is the height. Assuming the flow of current from the upper surface of the joint to the lower one, the equivalent resistance R_{sj} can be calculated as shown in (3.36),

$$R_{sj} = \frac{\rho H}{\Delta\lambda d} \tag{3.36}$$

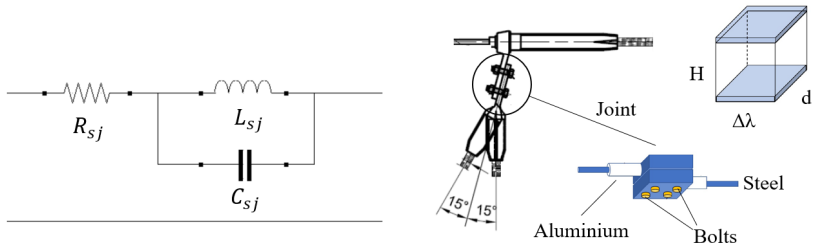

(a) (b)

Figure 3.10: Equivalent model of bolted joints: (a) electrical circuit; (b) physical characteristics.

where ρ is the electrical resistivity of the joint material. As for the joint inductance L_{sj}, geometrical characteristics and magnetic permeability can be combined as shown in (3.37),

$$L_{sj} = \frac{\mu_0 \mu_r H}{2\pi} \left[\ln\left(\frac{2H}{\Delta\lambda + d} \right) + 0.5 \right] \tag{3.37}$$

where μ_0 is the vacuum magnetic permeability and μ_r is the relative permeability of aluminium. Regarding the joint capacitance C_{sj}, it could be neglected in nominal operating conditions due to its extremely low value. In this study, C_{sj} is assumed non-zero in all possible situations to maintain the topology shown in Figure 3.10(a) and its value will be calculated below.

Elementary Section of the Line

The main objective of the prognostic method proposed here is to identify the state of health of the joints belonging to a specific network branch. For this reason, the equivalent circuits presented above are connected in cascade to obtain the elementary section of the line. Figure 3.11 shows the equivalent model of the elementary section, the repetition of which allows the global representation of the network branch.

Calculation of Parameters

Once the equivalent lumped circuits of joint and conductor have been created, it is possible to describe the whole network branch by connecting in

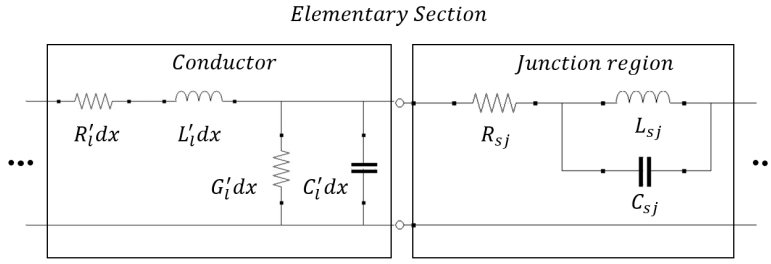

Figure 3.11: Elementary section of an overhead line.

cascade several elementary sections, each of which represents a line stretch between two pylons: the conductor circuit describes the span while the model of the joint corresponds to the pylon position. In this case, an acceptable simplification is used, as there should be two joints and a short length of conductor for each support. First of all, it is necessary to calculate the values of the electrical components in order to distinguish nominal conditions and those of malfunction. For this reason, the geometrical characteristics of joints and conductors taken into consideration are presented in Table 3.5 and Table 3.6.

	$H[m]$	$\Delta\lambda[m]$	$d[m]$
Bolted joint	0.038	0.008	0.008

Table 3.5: Geometrical characteristics of joints.

Geometrical characteristics	ACSR
Outer Diameter $[m]$	$22.8 \cdot 10^{-3}$
Wire diameter (Aluminium)$[m]$	$3.5 \cdot 10^{-3}$
Wire diameter (Steel)$[m]$	$2.8 \cdot 10^{-3}$
Number of wires (Aluminium)	26
Number of wires (Steel)	7

Table 3.6: Geometrical characteristics of conductors.

Joint Parameters in Nominal Conditions

First of all, the nominal values of R_{sj}, L_{sj} and C_{sj} must be defined considering the characteristics of the material, the physical structure of the joint and the test frequency used for the measurements. As for the resistance R_{sj}, (3.36) must be modified introducing the skin effect. In fact, the penetration depth of the current decreases as the frequency of the signal increases and this produces a reduction in the surface available for conduction, thus increasing the resistance R_{sj}. Formula (3.38) allows the calculation of the penetration depth δ using the information on the material conductibility σ, on the magnetic permeability in the vacuum μ_0, on the relative permeability of the material μ_r and on the frequency used for the measurements f.

$$\delta = \frac{1}{\sqrt{\pi \sigma \mu_0 \mu_r f}} \tag{3.38}$$

Consequently, formula (3.39) shows the correct way to calculate the joint resistance under nominal condition.

$$R_{sj}(f) = \frac{\rho H}{2\delta(\Delta\lambda + d - 2\delta)} \tag{3.39}$$

Regarding the term L_{sj}, formula (3.37) does not require any changes and it can be used to calculate the joint inductance in nominal condition. On the other hand, to define the capacitance value, it is necessary to introduce the effects of the failure mechanisms on the joint structure. As said before, two different causes of malfunctions are considered in this work: oxidation and partial breakage of the structure. It should be noted that these processes are consequential, and this means that the first stage of degradation during the useful life of the joint is the oxidation of the aluminium parts. Hence, when the oxide layer in the joint structure has become dominant, it reduces the overall mechanical strength and partial fractures may occur. The effects of these failure mechanisms on the electrical parameters of the joint are summarized below.

Oxidation Process

The main effect produced by the oxidation process on the joint structure is the increase in electrical resistivity. Both aluminium plates and steel bolts are subject to this phenomenon and the overall resistance increases as the amount of oxide increases. The variations in resistivity can be calculated

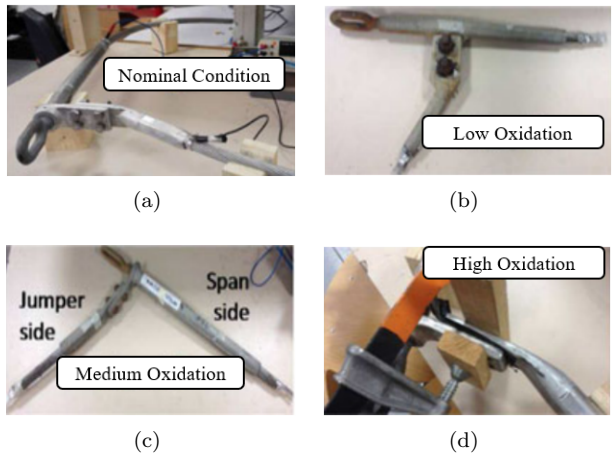

Figure 3.12: Bolted joints used in the experimental measurements presented in [80]: (a) nominal condition; (b) low oxidation; (c) medium oxidation; (d) High oxidation.

by inverting the formula (3.36), referred to the DC resistance of the joint, and introducing the experimental measurements presented in [80]. Table 3.7 presents the DC resistance values and the corresponding resistivity levels for four different operating conditions: nominal condition, low oxidation condition, medium oxidation condition and high oxidation condition. Starting from these intervals it is possible to quantify the effects of the oxidation process and define the limit situation that precedes a partial breakage of the joint structure. Figures 3.12(a), (b), (c), (d) show the bolted joints used in the experimental measurements presented in [80].

Operating conditions	$R_{sj}[\Omega]$	$\rho_{sj}[\Omega m]$
Nominal condition	$60 \cdot 10^{-6} \div 2.5 \cdot 10^{-3}$	$10^{-7} \div 4.2 \cdot 10^{-6}$
Low oxidation	$2.5 \cdot 10^{-3} \div 5 \cdot 10^{-3}$	$4.2 \cdot 10^{-6} \div 8.5 \cdot 10^{-6}$
Medium oxidation	$5 \cdot 10^{-3} \div 100 \cdot 10^{-3}$	$8.5 \cdot 10^{-6} \div 1.7 \cdot 10^{-4}$
High oxidation	$100 \cdot 10^{-3} \div 2$	$1.7 \cdot 10^{-4} \div 3.4 \cdot 10^{-3}$

Table 3.7: DC joint resistance and resistivity in different oxidation conditions.

Partial Damage to the Joint Structure

The most critical situation taken into consideration is the presence of a fracture in the joint structure. In order to define the severity of the damage, the width and height of the crack are introduced as shown in Figure 3.13 and they are indicated by the terms x and h respectively. This malfunction introduces variations in all the electrical parameters of the joint, which can be calculated by still exploiting the equivalence between solder joints and bolted joints [79]. Therefore, the value of the joint resistance $R_{sj}(f)$ in the presence of a partial breakage is calculated by (3.40) as a function of the crack size.

$$\begin{cases} R_{sj}(f) = \rho\left[\frac{H-h}{2\delta(\Delta\lambda+d-2\delta)} + \frac{h}{2\delta(\Delta\lambda+d-x-2\delta)}\right] & (d-x) \geq 2\delta \\ R_{sj}(f) = \rho\left[\frac{H-h}{2\delta(\Delta\lambda+d-2\delta)} + \frac{h}{\Delta\lambda(d-x)}\right] & (d-x) < 2\delta \end{cases} \tag{3.40}$$

As for the joint inductance L_{sj}, the influence of the damage is introduced by means of equation (3.41).

$$L_{sj} = \frac{\mu_0\mu_r(H-h)}{2\pi}\left[\ln\left(\frac{2(H-h)}{\Delta\lambda+d}\right)+0.5\right] + \frac{\mu_0\mu_r h}{2\pi}\left[\ln\left(\frac{2h}{\Delta\lambda+d-x}\right)+0.5\right] \tag{3.41}$$

Regarding the capacitance C_{sj}, formula (3.42) is used to calculate its value both in nominal operating conditions and in the presence of a breaking mechanism.

$$C_{sj} = \frac{\varepsilon_0\varepsilon_r x\Delta\lambda}{h} \tag{3.42}$$

From a general point of view, C_{sj} could be neglected in nominal working conditions. However, in order to maintain the same equivalent circuit topology of the joint in all possible operating conditions, the capacitance value in the nominal ones is calculated assuming x and h less than 1% of the total width d and of the total height H. Considering higher percentages, the severity of the damage increases and it is possible to calculate the corresponding value of C_{sj}.

Conductor Parameters in Nominal Conditions

As previously mentioned, only the degradation of the joints is considered in this study because they represent one of the most stressed parts in high

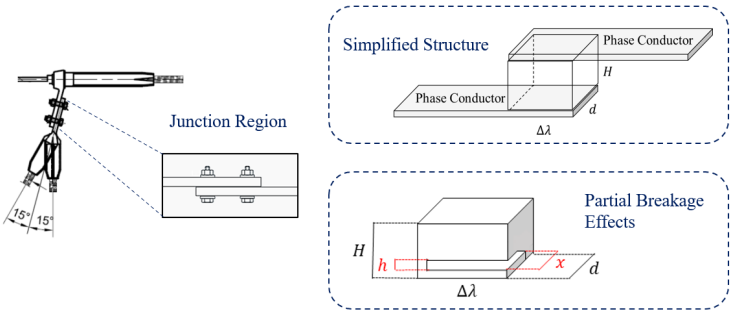

Figure 3.13: Joint modelling in the event of a partial breakage.

voltage overhead lines and are usually prone to catastrophic failures. Regarding the electrical parameters of the phase conductor, they are assumed in nominal conditions without introducing any particular failure mechanism. However, other external effects need to be considered to make the model as close to a real situation as possible. Therefore, the incidence of the working temperature and the skin effect is introduced to calculate the exact value of the resistance R'_l in different operating conditions. First of all, it is necessary to define the apparent reduction of the surface available for conduction caused by the high frequency of the signal used for the measurements. Generally, the data sheets provided by the ACSR manufacturers contain only the resistance value at $50Hz$ and in standard environmental conditions. In order to define the penetration depth of the current in the aluminium wires, formula (3.43) can be used,

$$\delta_l = \sqrt{\frac{\rho_l}{\pi \mu_l f}} \tag{3.43}$$

where ρ_l and μ_l are the electrical resistivity and the magnetic permeability of the aluminium part respectively, and f is the frequency of the signal. Once the penetration depth of the current has been defined, a parameter called K_0 is calculated as shown in (3.44) using the outer diameter of the conductor D.

$$K_0 = \frac{D/2}{\sqrt{2\delta_l}} \tag{3.44}$$

Consequently, the correction factor to be applied to the $50Hz$ resistance is defined as shown in (3.45).

$$\begin{cases} K = \left[1 + \frac{K_0^4}{3}\right] & K_0 \leq 1 \\ K = \left[0.25 + K_0 + \frac{3}{K_0}\right] & K_0 \geq 1 \end{cases} \tag{3.45}$$

Therefore, once the frequency used for the measurements has been selected, the resistance value at $50Hz$ in standard environmental conditions ($20°C$) is extracted from the technical data sheet of the conductor and corrected using the term K.

$$R'_{lf} = KR'_l \tag{3.46}$$

The value calculated by (3.46) can be considered the nominal level of the conductor resistance at $20°C$ for a specific test frequency. Since the environmental conditions along the line path are extremely variable and the load current is not constant, it is essential to calculate the influence of the working temperature on the conductor resistivity. In fact, the heat produced by the Joule effect and that induced by external factors produce variations in the resistivity and, consequently, in the resistance of the conductor. This change can be calculated using (3.47) and introducing the aluminium thermal coefficient α and the conductor temperature T_c.

$$R'_{lfT} = R'_{lf}[1 + \alpha(T_c - 20)] \tag{3.47}$$

This means that the operating temperature of the line shifts the nominal resistance of the conductor introducing variations in its response to the high frequency signal. By quantifying these changes, it is possible to define a tolerance interval for the parameter R'_{lf}. In this way, the neural classifier is trained with variable values of the conductor resistance around its nominal value, thus reproducing different situations and making the prognostic procedure robust with respect to environmental and load conditions. The main step in calculating this interval is the definition of a heat balance equation, in which all internal and external contributions are taken into account. Equation (3.48) is used in this study,

$$\begin{aligned} C_m v \pi A_t \frac{\partial T_c}{\partial t} =& R'_l[1 + \alpha(T_c - 293.15)]I^2 + \alpha_s Q_s A_s - \\ & - \alpha_c (T_c - T_\alpha) A_s 5.67 \alpha_r [(\frac{T_c}{100})^4 - (\frac{T_\alpha}{100})^4] A_r \end{aligned} \tag{3.48}$$

where: T_c is the temperature of the conductor expressed in Kelvin degrees, T_α is the air temperature surrounding the conductor expressed in Kelvin degrees, C_m is the specific heat of the conductor materials, v is the density of the conductor materials, A_t is the conductor section, A_s is the surface area receiving illumination per unit of length, A_c is the convection surface area, A_r is the radiation surface area per unit of length, αc is the coefficient of convective heat, α_r is the radiation factor of the conductor materials, α_s is the sunshine absorption rate of the conductor, Q_s is the radiation intensity of the sun and sky. As shown in (3.48), the energy balance equation contains the term R'_l, which is the conductor resistance at $50Hz$ and causes, together with the fundamental component of the phase current, the heat dissipation due to the Joule effect. As for the characteristics of the conductor material, they are summarized in Table 3.8. Therefore, the value of the conductor temperature

C_m $[J/(kgK)]$	v $[kg/m^3]$	A_t $[m^2]$	A_s $[m^2/m]$	A_r $[m^2/m]$
$0.88 \cdot 10^{-3}$	$2.7 \cdot 10^3$	$\pi(D/2)^2$	$\pi(D/2)$	πD
A_c $[m^2/m]$	α_s $[-]$	α_c $[W/(kg/m^3)]$	α_r $[-]$	R'_l $[\Omega/km]$
πD	0.6	5.8	0.2	0.12

Table 3.8: Characteristics of the conductor materials.

can be calculated by solving the energy balance equation (3.48). To achieve this goal, the initial conditions of the conductor, the radiation intensity Q_s and the air temperature T_α must be known. Typical values of Q_s and T_α are used in this study based on real measurements performed in Italy in 2011. In general, Q_{smax} represents the average of the maximum radiation levels for a specific month and $T_{\alpha max}$ that of the maximum air temperatures. The average of the minimum temperature levels T_{min} is considered as the mean temperature in the night period and, for this reason, it is associated with a zero-radiation level. For simplification, the average values for each season are considered in Table 3.9. Therefore, the following procedure can be used to define the impact of environmental conditions on the resistance value:

- set a value for the load current;
- solve the heat balance equation under extreme conditions $(Q_{smax}, T_{\alpha max})$ and $(Q_{smin}, T_{\alpha min})$;

	$Winter$	$Spring$	$Summer$	$Autumn$
$Q_{max}[W/m^2]$	392	753	753	357
$T_{\alpha max}[K]$	281	295	301	284
$Q_{min}[W/m^2]$	0	0	0	0
$T_{\alpha min}[K]$	275	286	292	279

Table 3.9: Average values of solar radiation and temperature for each season

- use the conductor temperatures defined in the previous step to calculate the resistances R'_{lfT} through (3.47);
- calculate the percentage error.

For example, during the summer season, the conductor temperature can be calculated using $(Q_{smax}, T_{\alpha max}) = (750, 301)$ and the maximum resistance error with respect to the night period is approximately 16%. Furthermore, considering the interval $(0 \div 500)A$ for the load current and setting specific environmental conditions, it is possible to obtain the incidence of the load on the resistance value. In this case, the procedure is the following:

- set a specific environmental condition (Q_s, T_α);
- solve the heat balance equation in the absence of load current and by setting the maximum value $I = 500A$;
- use the conductor temperatures defined in the previous step to calculate the resistances R'_{lfT} through (3.47);
- calculate the percentage error.

Still, during the summer period, the influence of the load current is approximately 7%. The worst situation for each season is presented in Table 3.10. It should be noted that the maximum error is obtained during the spring period and its percentage value is about 25.16%.

Error % winter	Error % spring	Error % summer	Error % autumn
17.34	25.16	24.92	16.1

Table 3.10: Maximum errors for all seasons

In conclusion, by calculating the temperature with intermediate initial conditions between $(Q_{smax}, T_{\alpha max})$ and $(Q_{smin}, T_{\alpha min})$ and fixing the current at $250A$, it is possible to consider a 15% variation range for the conductor resistance. The same variation range is extended to each electrical parameter of the conductor. Regarding the capacitance C_l' and the inductance L_l', they are calculated assuming the transposition of the conductors and considering a typical transmission line constituted by three phases [54]. Formulas (3.49) and (3.50) are used in this model to calculate the inductance and capacitance of the conductor expressed in $[\mu F/km]$ and $[mH/km]$ respectively,

$$C_l' = \frac{0.024}{\ln\left(\frac{\Delta'}{D/2}\right)} \tag{3.49}$$

$$L_l' = 0.46 \log\left(\frac{\Delta'}{D/2}\right) \tag{3.50}$$

where Δ is the equivalent distance between the conductors, defined as shown in (3.51) using the reciprocal distances of the phases Δ_{12}, Δ_{23} and Δ_{31}.

$$\Delta' = \sqrt[3]{\Delta_{12}\Delta_{23}\Delta_{31}} \tag{3.51}$$

Simulations on SapWin

As indicated in the previous chapter, the SapWin software can be used to simulate the equivalent circuit and perform the main steps of the parametric analysis. Figure 3.14 shows the equivalent circuit of an elementary section of overhead power line created on SapWin. To facilitate the study of network branches characterized by several elementary sections, it is possible to save the schematic of Figure 3.14 as a sub-circuit and use it as a generic 4-port network.

In order to perform the parametric analysis of the circuit under test, it is necessary to insert a source (voltage or current) and specific test points characterized by voltage and/or current measurements. Figure 3.15 shows an example using the elementary line section, a voltage source V_{in} and a voltage measuring point V_0. Note that each inductor belonging to the circuit also represents a current measurement point, while each capacitor is a voltage measurement point. Using the analysis command, it is possible to obtain all the possible transfer functions in symbolic form by considering the measured variables as outputs and the source as input.

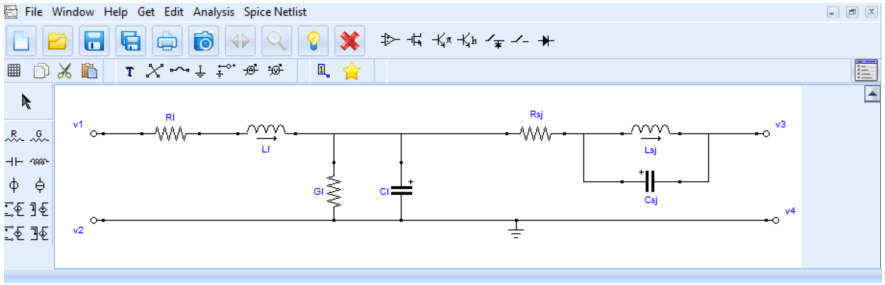

Figure 3.14: Sub-circuit of an elementary section of the line on SapWin.

For example, the voltage transfer function extracted from SapWin for the case shown in Figure 3.15 is as follows,

$$\frac{V_0}{V_{in}} = \frac{1 + (C_{sj}L_{sj})s^2}{(G_lR_l + 1) + (C_lR_l + G_lL_l)s + (C_lL_l + G_lC_{sj}L_{sj}R_l + C_{sj}L_{sj})s^2 + \\ (C_{sj}C_lL_{sj}R_l + G_lC_{sj}L_lL_{sj})s^3 + (C_{sj}C_lL_lL_{sj})s^4} \tag{3.52}$$

where all the electrical components are expressed in symbolic form. This network function can be expressed in the frequency domain by replacing s with $j\omega$ and can be extracted in Matlab code.

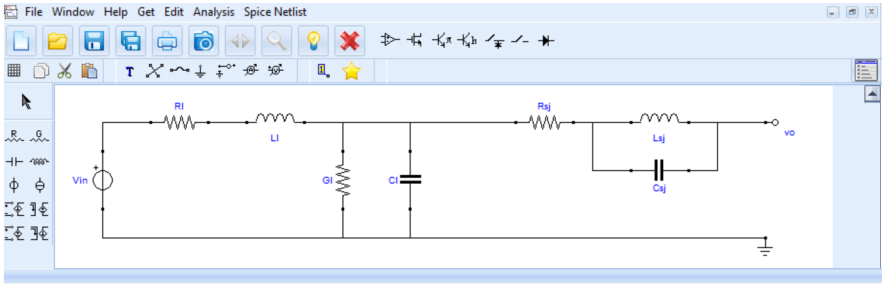

Figure 3.15: Example of circuit for parametric analysis.

By setting certain frequency limits and component values, it is possible to plot the trend of the voltage gain, of the magnitude and of the phase of the selected transfer function as well as the sensitivity of these quantities with

respect to each circuit element. Furthermore, SapWin allows the testability assessment by implementing the method described in section 2.3.1. Note that in the SapWin schemes proposed above, the conductance of the line was maintained, which is generally neglected in the modelling of high voltage overhead networks.

3.3.2 Medium Voltage Underground Lines

As regards the modelling of medium voltage lines, underground cables are taken into consideration, which generally have the following structure from the inside to the outside (see Figure 3.16):

- copper or aluminium core (it may be solid, formed from several layers of concentric spiral wound wires, or consist of sector shaped conductors that help make the cable flexible while minimizing its overall diameter for a given current carrying capacity);
- first extruded semiconductor screen;
- insulation layer (nowadays in Hard Ethylene Propylene Rubber (HEPR) or cross-linkable polyethylene (XLPE));
- second extruded semiconductor screen;
- external protective rubber/PVC (quality G7).

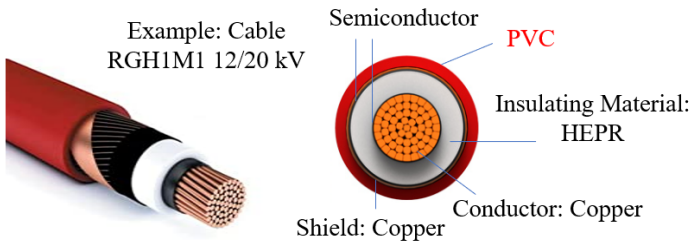

Figure 3.16: General structure of a Medium Voltage cable.

The main cause of failure in underground medium voltage cables is the degradation of the insulating material. In fact, the ageing of the HEPR or XLPE layer entails the occurrence of partial discharges and the formation

of water trees. These phenomena, if not detected promptly, can lead to the definitive loss of insulation and therefore to catastrophic failures. From the theoretical point of view, the equivalent circuit of a cable stretch is still the π-model. This means that the electrical characteristics of the line can be expressed by four parameters per unit of length: resistance R'_c, inductance L'_c, capacitance C'_c and conductance G'_c. In this case, the transversal parameters C'_c and G'_c play a fundamental role in detecting the state of health of the insulating material. In fact, many off-line analysis methods are focused on studying these parameters to define the residual useful life of the cable. However, since the goal of the prognostic method is to prevent insulation problems, the longitudinal resistance of the model plays a fundamental role. In fact, it increases with increasing temperature and can be used as an indication of abnormal operating conditions. These situations, if neglected, can produce premature ageing of the cable.

In order to facilitate the modelling of MV power lines, a specific Matlab application has been developed, which takes into account the effects of the type of laying, environmental conditions and load current. As shown in Figure 3.17, the main window of this application allows the selection of all the line characteristics, including the cable materials, the shape of the conductor wires, the possible presence of a metal sheath for mechanical protection, the depth of installation and the type of soil in which it is made.

In this way, it is possible to obtain the characteristic parameters of the cable considered at the mains frequency and evaluate the incidence of internal and external factors. As mentioned above, the effects of ambient temperature and load current on conductor resistance play a fundamental role for the prognostic procedure. To obtain this information, the Matlab application solves the heat balance equation of the cable using all the thermal resistances of the materials, that of the soil and the heat generated by the Joule effect [54]. As is known, once the operating temperature of the cable T has been obtained, the conductor resistance can be calculated by means of (3.53),

$$R'_T = R'_{20}[1 + \alpha(T - 20)] \tag{3.53}$$

where R_{20} is the resistance of the conductor material at $20°C$ per unit of length and α is its thermal coefficient. As for the calculation of the cable capacitance C'_c, the following equation is introduced,

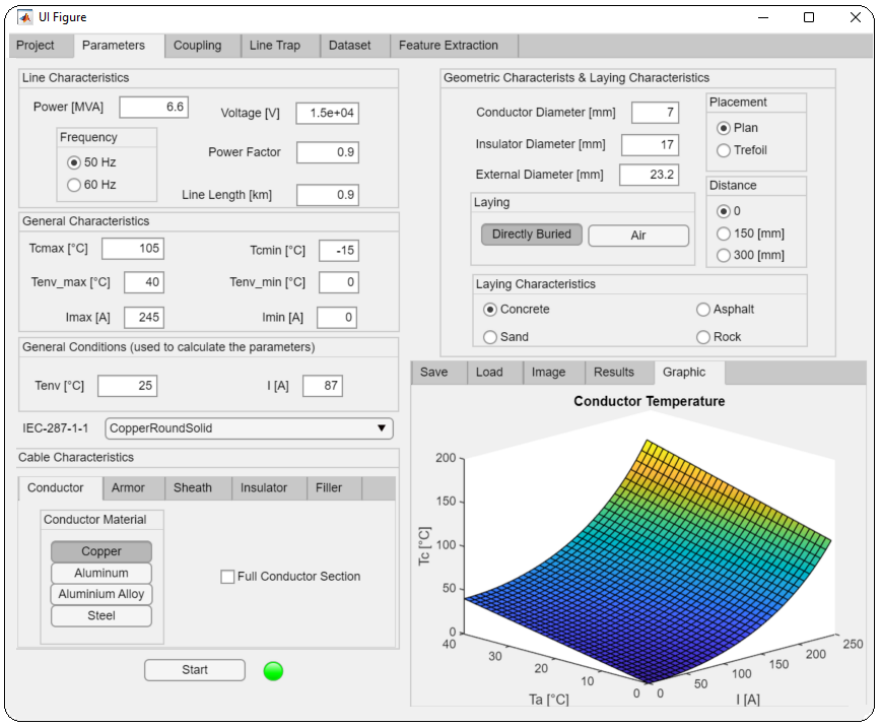

Figure 3.17: Matlab application for modelling medium voltage cable power lines.

$$C'_c = \frac{2\pi\varepsilon_0\varepsilon_r}{\ln\left(\frac{r_s}{r_c}\right)} = \frac{0.0242\varepsilon_r}{log\left(\frac{r_s}{r_c}\right)} \tag{3.54}$$

where the term r_s is the radius of the sheath, r_c is that of the conductor, ε_r the relative magnetic permeability of the insulating material and ε_0 is that of the vacuum. The results obtained by (3.54) is expressed in $[\mu F/km]$. To calculate the characteristic conductance of the cable, it is necessary to introduce the term $tan(\delta)$, also called tangent loss, which is often used as an index of the insulation quality. Tangent loss can be expressed as,

$$tan(\delta) = \frac{I_R}{I_C} = \frac{\sqrt{I^2 - I_C^2}}{I_C} \tag{3.55}$$

Material	$tan(\delta)$	ε_r
HEPR	0.003	2.6
XLPE	0.0007	2.3
PVC	\	5.5
Impregnated Paper	0.006	3.5
Fluid Oil	0.002	\

Table 3.11: Typical values of tangent loss and relative magnetic permeability

where the currents I_C and I_R are the charge component and the loss component of the total current I respectively, obtained by the phasor method [81]. Since the equivalent circuit of the insulation system corresponds to the parallel connection between a capacitance and a voltage-dependent resistance, the value of the term $tan(\delta)$ at a specific pulsation ω and at a certain voltage V is obtained as shown in (3.56).

$$tan(\delta) = \frac{I_R}{I_C} = \frac{\frac{V}{R}}{\frac{V}{1/\omega C}} = \frac{1}{\omega RC} \tag{3.56}$$

Finally, the value of the conductance G'_c in $[\mu S/km]$ and that of the inductance L'_c in $[mH/km]$ at the mains frequency can be calculated as shown in (3.57) and (3.58) respectively.

$$G'_c = \omega \; C'_c \; tan(\delta) \tag{3.57}$$

$$L'_c = 0.05 + 0.46 \; log \frac{2\sqrt[3]{2}a}{d_c} \tag{3.58}$$

Where a is the distance between the axes of two cable conductors expressed in $[mm]$ and d_c is the diameter of the conductors in $[mm]$. It should be noted that these equations are used by the application in order to study MV lines constituted by three unipolar cables. Table 3.11 shows some typical values of tangent loss and relative magnetic permeability commonly used in literature.

On the basis of the calculated values it is possible to simulate the operation of a MV line in the Simulink/Simscape environment. In fact, as shown in Figure 3.18, the *AC cable* block can be used to represent a complete network branch. These blocks require the sheath and conductor electrical resistances,

the physical characteristics of the cable and the relative permittivity of insulation to perform the simulation with lumped parameters according to the π-model. This solution represents a possible alternative to the use of SapWin in the simulation of electrical networks, as it allows the introduction of many other line components without requiring a high computational cost for the calculation of the network function in symbolic form. However, SapWin remains fundamental for the study of Testability.

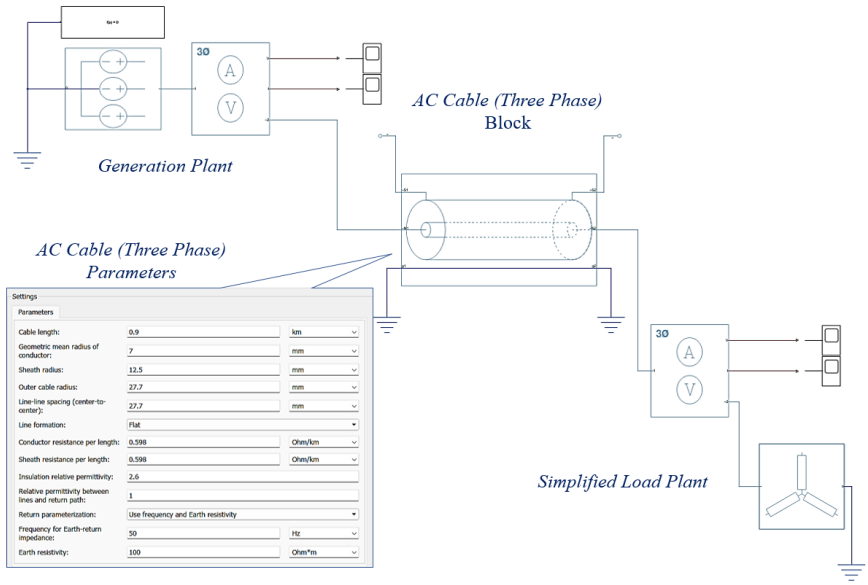

Figure 3.18: Example of Simulink/Simscape model of a medium voltage line created using AC cable blocks.

3.4 Modelling of Power Line Communications

The Simulink/Simscape model presented in Figure 3.18 can be used to study many different line topologies and operating situations. For example, the conductor and sheath resistances can be calculated under different environmental conditions and applying various load currents using the Matlab application presented in section 3.3.2 and then implemented in the Simulink/Simscape diagram. In addition to the power devices shown in Figure 3.18 it is

possible to simulate the injection of high frequency signals required in the proposed monitoring method. In fact, the *AC cable* blocks offer the possibility of treating each phase separately and, consequently, make the core and sheath of each cable available. Therefore, by modelling suitable coupling devices, it is possible to extract the required measurements directly from Simulink. To achieve this goal, Power Line Communication (PLC) systems are taken into consideration, which are used in power transmission and distribution lines to send information through the phase conductors.

In this work PLC systems are considered from a theoretical point of view using the information extracted from [82] and other research papers [83] [84]. However, this is a general approach that will need further development in the future to bring the modelling closer to real situations.

The overall structure of a communication system can be divided into three main parts: transmitter device, coupling circuits and receiver. It should be noted that the issue of signal modulation is not considered in this study as the main goal is to inject high frequency carriers to classify the line response. This means that the purpose of the PLC devices presented here is not to transmit information but to provide a stable platform for injecting measurement signals. In fact, being already used in many power lines for communication between substations, it could be possible to integrate the prognostic method ensuring a low level of intrusion.

In order to introduce a PLC system into the Simulink/Simscape diagram of the medium voltage line, the transmitter device is modelled as an AC voltage generator with a series output resistor of 50Ω or 75Ω. This resistance is usually matched to the characteristic impedance of the power line via a transformer [82]. Since several factors can influence the value of the characteristic impedance, it is necessary to choose the turn ratio carefully. If introducing a variable turn ratio is too complex, a possible solution is to choose a sufficiently large frequency range where the return loss is greater than $15dB$. Obviously this is a general indication that can be used in the simulation phase and requires further investigations in the case of specific applications.

As for the coupling circuits, they must connect PLC transmitters to the power line ensuring the lowest possible losses and protect both humans and the PLC transmitter/receiver from the mains voltages. Two different types of coupling can be adopted: capacitive or inductive. The capacitive type is frequently used in high and medium voltage lines in combination with a high

pass filter such as in the ABB A9BS [82] couplers, or with a band pass filter as in the ABB A9BP model. Capacitive couplers are convenient to use when the active conductor of the power line is easily accessible, as is the case of overhead power lines. However, for MV lines, specialized line personnel can mount the couplers under voltage and no power interruption is required. In addition, the substations of the HV and MV lines are generally prepared for mounting the couplers when they are built. Figure 3.19 shows the simplified electrical diagram of a capacitive coupler with a high pass filter, while Figure 3.20(a) shows a physical model of it (CAMS 10K produced by the company Ziv).

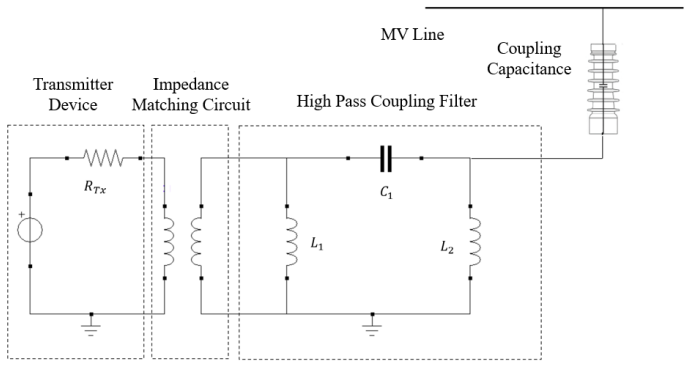

Figure 3.19: Equivalent model of a capacitive coupler.

Therefore, in the case of capacitive coupling, the last element of the connection circuit is a fixed value capacitance and the other components can be modelled as a high pass filter needed to remove the mains voltage. A possible procedure is to dimension a ladder network according to the Butterworth approximation respecting specific criteria. In this sense, one of the most common choices is to attenuate power mains voltage to a level $10dB$ lower than PLC voltage amplitude [82]. However, depending on the application considered, further requirements can be introduced, such as for example the verification of attenuation on specific harmonic components of the mains voltage.

When the active conductor of a power line has an insulation material covering, it is more difficult to safely connect a capacitive coupler to the power line. In that case an inductive coupler is easier to fit to the power

line. The inductive coupler consists of a split ferrite toroid, with a coil wound on it. That coil is connected to a BNC connector (see Figure 3.20(b) relating to the MICU 300A S LF model).

(a) (b)

Figure 3.20: Coupling devices: a) capacitive type; b) inductive type.

Finally, it is necessary to observe that the so-called Narrow Band PLC (NBPLC) is considered in this Thesis, which corresponds to the interval $(3 \div 500)kHz$. In Europe, the band available for PLC communications is divided into three levels: CENELEC A $(3 \div 91)KHz$, CENELEC B $(95 \div 125)kHz$, CENELEC C $(125 \div 140)kHz$ and CENELEC D $(148 \div 148.5)kHz$. The Japanese standard for power line communications is called ARIB and corresponds to the band $(10 \div 450)kHz$, while the United States and other countries use the FCC band $(10 \div 500)kHz$. Furthermore, the Chinese standard includes all the NPLC band. The frequency range corresponding to the Broadband PLC $(1.7 \div 250)MHz$ is not taken into consideration.

Based on these considerations, a PLC system can be integrated into the Simulink/Simscape scheme shown in Figure 3.18 to simulate the injection of high frequency signals. In particular, the configuration called *line-ground* is taken into consideration, in which the signal is transmitted between the core of the cable and its sheath [83]. Figure 3.21 shows the modified Simulink/Simscape diagram, in which for greater clarity only one cable of the three-phase line is considered and the part relating to power devices is omitted. It is necessary to underline that in the third window of the Matlab application presented in Figure 3.17, an algorithm has been integrated that allows the dimensioning of the coupling system by choosing the filter order, the cut-off frequency and the attenuation level required for the line voltage.

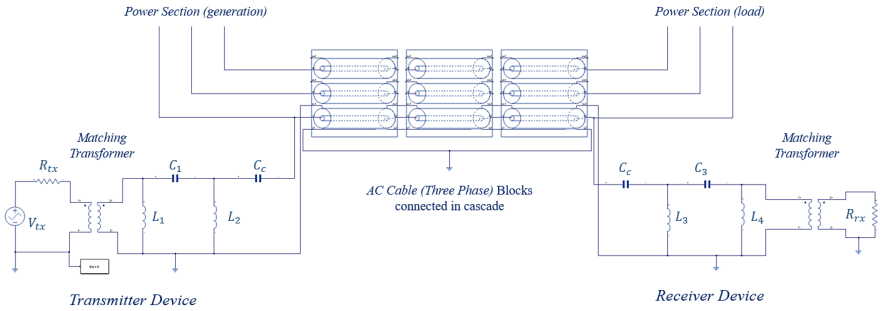

Figure 3.21: Simulink/Simscape model of a medium voltage line with a PLC system.

Note that the line can be divided into successive cable sections as in Figure 3.21. This allows the simulation of different operating conditions in various parts of the network. This lumped parameter model is used in the continuation of the Thesis to verify the effectiveness of MLMVN in localizing malfunctions using the measurements of the voltage transfer function at different frequencies. From the simulation point of view, the main limitation of this configuration consists in the impossibility of freely setting all the parameters of the π-model. For this reason, only changes in resistances (conductor and sheath) as a function of temperature are considered as an indication of malfunction in the initial simulations. In order to overcome this limitation, use the entire available bandwidth and bring the simulation closer to a real situation, a distributed parameter model of the line can be used. Numerous examples of distributed parameter modelling can be found in the literature, in particular in [83] and [84] a very detailed Simulink scheme is presented which also includes a high frequency model of the power transformers and the model of a real power line transceiver. In [83], the *distributed parameter line* block belonging to the Specialized Power Systems library of Simscape is used. In order not to lose the information of the conductance of the cable in the event of a thermal malfunction, in this Thesis a similar structure is reproduced using the *transmission line* blocks of the Electrical Simscape library. Figure 3.22 shows the simplified Simulink diagram of a single phase.

In conclusion, it should be noted that the Matlab application presented in section 3.17 allows the dimensioning of a specific *line trap* for the power line taken into consideration. Usually, this type of circuits are used in high

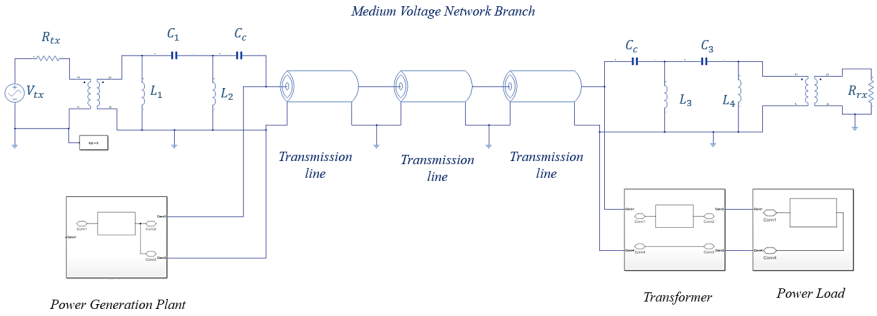

Figure 3.22: Simulink/Simscape model with distributed parameters of a medium voltage line with a PLC system.

voltage overhead lines to avoid transmission of high frequency carriers to unwanted destinations. However, the same operating principle can also be used in distribution lines. From a theoretical point of view, they consist in double resonant circuits as shown in Figure 3.23(a), which offer high reactances to high-frequency signals and low reactances to mains frequency. The physical structure of these devices is a cylinder consisting of three main components: the main coil, the tuning device and the protective device (also known as a surge arrester). The protection and tuning devices are mounted inside the main coil and are connected in series to a phase of the transmission line (see Figure 3.23(b)).

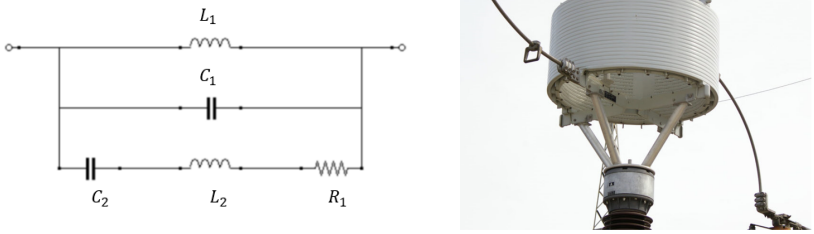

(a) (b)

Figure 3.23: Line traps: a) equivalent circuit; b) physical structure.

3.5 Graphical Testability Assessment

An interesting technique for Testability analysis of linear time-invariant networks under the single-input, single-output, and single-fault hypothesis is proposed in [85], where the fault model in the form of a geometric locus in the complex plane is based on the following reasoning. Consider a circuit represented by a frequency response $h(j\omega, \mathbf{p})$ relevant to an input-output pair. At a fixed frequency value ω_t, it is possible to obtain a locus in the complex plane for each parameter of the circuit $p_i \in \mathbf{p} = [p_1, p_2, \ldots, p_{np}]^T$ keeping all the others fixed. So the parameter taken into consideration is the only variable of $h(j\omega, \mathbf{p})$:

$$L_i^+|_{\omega t} = \{h \in C | h = h(j\omega_t, \mathbf{p}_0^i), p_i \in [0, +\infty]\} \tag{3.59}$$

where $\mathbf{p}_0^i = [p_{1,0}\ p_{2,0}\ \cdots\ p_{i-1,0}\ p_{i+1,0}\ \cdots\ p_{n_{p,0}}]^T$ is the vector of the nominal values with the exception of p_i. If n_p is the parameter number, the obtained loci are n_p and are defined signature curves. For each locus, when the corresponding variable parameter assumes its own nominal value, the nominal value $\mathbf{h}_0 = h(j\omega_t, \mathbf{p}_0)$ evaluated at the chosen frequency value is obtained. This means that all the signature curves $|L_1^+|_{\omega t}, |L_2^+|_{\omega t}, \ldots, |L_{n_p}^+|_{\omega t}$, must pass through the point representative $\mathbf{h}_0 = h(j\omega t, \mathbf{p}_0)$, in the complex plane, where p_0 is the vector of nominal values, with dimension n_p. Now, let p^* and h^* be the actual value assumed by $\mathbf{p}$ and the experimentally measured counterpart of $h(j\omega t, p^*)$, respectively. Then, under the single-fault hypothesis, only one of the two situations can occur:

- $\mathbf{p}^* = \mathbf{p}_0$ and hence $\mathbf{h}^* = \mathbf{h}_0$
- $\mathbf{p}^* \neq \mathbf{p}_0$ and then there must exist exactly one $i \in \{1, 2, \ldots, n_p\}$ such that $h^* \in L_i^+|_{\omega t}$

this means that, if $h^* = h_0$, then the circuit is healthy, if $h^* \neq h_0$ and $h^* \in |L_i^+|_{\omega t}$, then the circuit is faulty and p_i is the fault source. This observation means also that, if, for a certain i, one k exists such that $|L_i^+|_{\omega t} = |L_k^+|_{\omega t}$, p_i and p_k constitute a Canonical Ambiguity Group (CAG) of order two in correspondence of the frequency ωt, because they produce the same fault situation. Furthermore, the number of distinct signature curves gives the number of identifiable parameters, i.e. it gives the Testability measure. If more than two signature curves overlap, this means that the corresponding parameters form a Global Ambiguity Group (GAG) derived from the union

of CAGs of order two constituted by all the possible couples of the involved parameters. In this way, an alternative method for testability analysis under the hypothesis of a single fault has been introduced. The application of this technique to the fault location is not as easy as it could appear. In fact, in the case of fault diagnosis, it is not possible to disregard the effects of parameter tolerances and measurement errors differently from testability analysis, and this requires some precautions which are yet to be analysed in depth. The above-described method requires drawing the variation of the input/output relationship versus each circuit parameter in a unique plane. In the case of linear, time-invariant, analog circuits a network function represents the required equation. In the frequency domain, once the frequency value has been fixed, it is possible to draw, for each parameter p_i within the range $[0, +\infty]$, the imaginary part versus the real part of $h(j\omega_t, \mathbf{p})$, thereby obtaining the signature curves. As for time-variant circuits, the standard analytical methodology presented in section 2.5.2 demonstrates how, once steady state is reached, Testability behaviour can change from interval to interval. Therefore, the graphical method described above can be applied considering only the network function relating to a specific working interval. The steady state operation is guaranteed by the use of the frequency response, which can be obtained by SapWin. As previously described, this program can determine the network functions of DC–DC converters in the Laplace domain, and then, by replacing the Laplace variable with $j\omega$, the frequency responses. They depend on the parameters representing the state of switch and diode in each working interval and on the initial conditions of inductor and capacitor. For each working interval, both switch and diode parameters and initial conditions change. This means that these network functions do not have the classical meaning and then cannot be used for determining the frequency domain behaviour of the whole circuit. If a traditional frequency domain simulation is required, it is necessary to replace the switch-diode cell with a time-invariant equivalent circuit so that the circuit is linearised. However, the SapWin network functions can be used to determine the signature curves, as described above, within each of two or three possible working intervals of a converter, depending on the operating mode. This is due to the independence of Testability analysis from parameter values and time instants and to its dependence on circuit topology, which in turn also justifies the possibility of having different testability analysis results in different converter working phases. Nevertheless, this way of proceeding is

very onerous in terms of time consumption. Starting from these considerations, in this thesis a new graphic method is proposed to evaluate Testability in DC-DC converters. Therefore, the main idea is to select specific network functions in the time domain and analyse them in every possible operating interval. In fact, the signature curves need only to draw circuit characteristics with respect to each parameter variation independently on the domain. In the case of DC–DC converters, it is easier obtain steady state responses in time rather than in frequency. In the time domain, different characteristics of the typical quantities (for example mean value, maximum value and ripple) of the steady state response can be considered and the signature curves can be obtained by drawing one versus the other for each parameter variation once a time is fixed for every operation mode. Proceeding in this manner, different groups of signature curves are obtained, each group corresponding to a different working interval. The results, in terms of testability and ambiguity groups, are equal to those obtained by using frequency responses. The advantages consist in the fact that time domain simulations are faster, and any simulation program can be used for the extraction of the required quantities. In the following a brief example on a Buck converter is presented.

Illustrative Example on a Buck Converter

The topology taken into consideration is shown in Figure 3.24, in which there are three passive components: two reactive elements ($L1$ and $C1$) and a resistive load $R1$. This is a switching converter driven by a Pulse Width Modulation (PWM) capable of reducing the input DC voltage with high efficiency. The output voltage V_{out} is measured at the ends of the resistive load and, in Continuous Conduction Mode (CCM), it can be calculated as

$$V_{out} = DV_{in} \tag{3.60}$$

where D is the duty cycle of the PWM signal and V_{in} is the DC source. During the operation of the converter, it is possible to distinguish two different periods: switch-on period and switch-off period. They are related to the state of the active components ($B1$ and $A1$), which are alternately conductive and interdicted. During the switch-on period, $B1$ is in conduction, while $A1$ is off; during the switch-off period, the state of the active elements is opposite. As said before, the time-varying nature of DC–DC converters makes the testability analysis more complex, because different topologies are obtained depending on the time interval taken into consideration. In the pro-

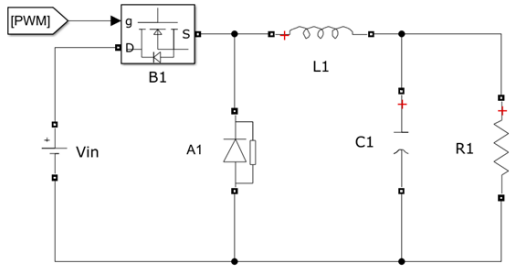

Figure 3.24: Buck topology.

posed approach, the Simulink/Simscape model of the buck converter is used to extract the voltage and current waveforms by varying the values of the passive components. Therefore, by processing these quantities, it is possible to create graphs in which the ripple is on the ordinate axis and the average value is on the abscissa axis. By analysing these curves, it is possible to obtain information about testability and testable groups. In fact, when two or more curves are superimposed or very close together, the corresponding components cannot be considered faulty at the same time. Note that in this example the converter operation in CCM is considered, using a DC source of $20V$ and $D = 0.6$. This procedure requires several simulations carried out by varying the values of the passive components one at a time. The selected measurements are then extracted when the steady state condition is reached by the converter. Finally, the measured quantities are processed to obtain the ripple and the mean value.

In this example, the output voltage and the current on the capacitor are considered. Figure 3.25(a) and Figure 3.25(b) show the corresponding testability curves. Note that the starting point where all curves converge represents the nominal condition of the circuit (all components are at their nominal values).

The curves presented in Figures 3.25 show that the testability value is 2 and each pair of passive components can be considered as a testable group. The curves obtained during the switch-off period offer the same results.

As regards the use of the output voltage and current on the inductor as test points, the curves shown in Figure 3.26(a) and Figure 3.26(b) are obtained during the switch-on period. In this case, the effect of the variations of $C1$ in Figure 3.26(b) is absolutely negligible. This determines maximum

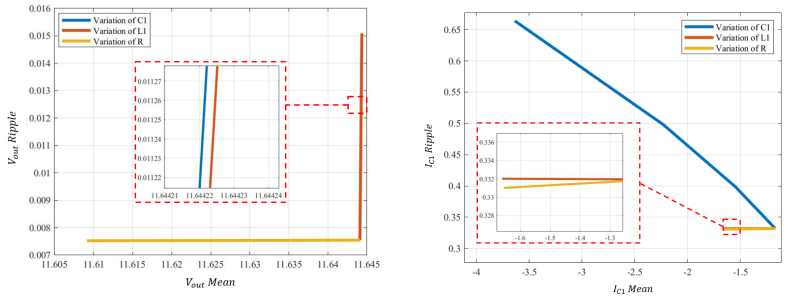

(a) (b)

Figure 3.25: Testability curves: a) output voltage; b) current on $C1$.

testability and, consequently, there is only one testable group containing all three passive components, if both the test points are simultaneously considered. These results can be easily verified by means of the completely symbolic procedure on SpWin.

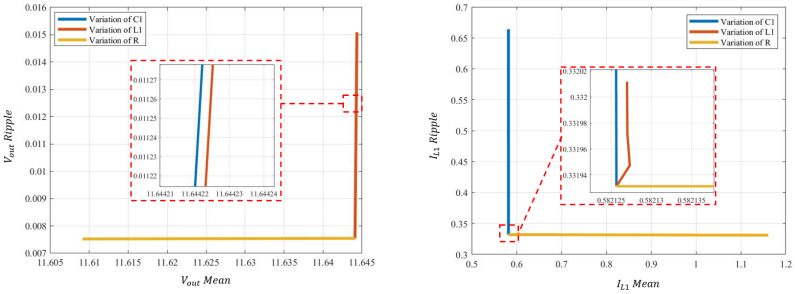

(a) (b)

Figure 3.26: Testability curves using different test points: a) output voltage; b) current on $L1$.

3.6 Conclusion

The results shown in this chapter allow to carry out the main phases of the prognostic analysis in all the fields of application considered. In particular,

the modelling proposed for bolted joints and phase conductors of overhead lines allows the simulation of network sections under nominal and malfunctioning conditions. The proposed circuit diagrams allow the development of the multi-frequency parametric analysis and the evaluation of the Tesatability. Furthermore, the formulas introduced for the modelling of failure mechanisms allow the definition of the corresponding failure classes.

As regards underground medium voltage lines, the Matlab application presented in this section allows the calculation of the line parameters in different operating situations. These values represent the starting point to use the proposed Simulink/Simscape schemes and generate the dataset necessary to train the Multi-Layer neural network with Milti-Valued Neurons.

The neural classifier is used in subsequent chapters thanks to the Matlab application described above. All the proposed configurations can be easily implemented to perform the training phase.

In the case of DC-DC converters, this training phase is preceded by the graphical testability analysis using the new method proposed in this chapter.

Chapter 4

Application: Prognosis of Joints in High Voltage Electrical Lines and Medium Voltage Underground Cable

This chapter proposes a classification method based on the complex-valued neural network described above to asses the health status of the junction regions in high voltage overhead lines and that of insulating materials in medium voltage underground networks. The purpose of this method is to prevent breakage of joint structures and abnormal degradation of underground cables by using frequency response measurements. Therefore, a possible extension of the parametric analysis usually used in the field of circuit diagnosis is proposed to monitor electrical infrastructures. The main idea on which this approach is based is to detect changes in electrical characteristics by injecting high frequency signals into the line. To achieve this purpose, the equivalent model of the network branch taken into consideration must be used. In fact, the electrical components belonging to this circuit are sensitive to specific failure mechanisms and change as they occur. These variations introduce changes in the frequency response and a Multi-Layer neural network with Multi Valued Neurons (MLMVN) is used to detect and locate malfunctions. This chapter presents a

simulation procedure necessary to define all the steps of the prognostic method, highlighting their potential and limitations. These considerations will be developed in the following chapters by introducing experimental tests. [1]

4.1 Introduction

The first objective of this chapter is to present the theoretical basis of a prognostic method capable of identifying the state of health of electrical infrastructures using frequency response measurements.

First, the study of the junction regions in overhead transmission lines is proposed to carry out a detailed description of the prognostic procedure, starting from the modelling of the system under test up to the development of a specific classification tool. Therefore, the field of application is the management of electrical transmission lines, which are characterized by a great length and connect the generation plants to the distribution networks. In this type of power lines, the detection and localization of problems play a fundamental role by reducing recovery times and increasing system availability. In fact, transmission lines guarantee electricity service to thousands of users and maintenance operations should be as rapid as possible. As described in section 2.5.1, high voltage overhead networks are currently protected by devices capable of identifying the fault position and putting the non-functioning part of the grid out of service. For example, distance protections use Intelligent Electronic Devices (IEDs) to estimate the impedance between the installation point and the failure point by measuring the phase voltage and current. In this way, the distance from the fault is calculated considering the correspondence between the conductor impedance and the length of the line section. Furthermore, new protection devices have been introduced in the last years, based on travelling wave detection. These techniques allow the impulsive signals generated by faults to be measured with great precision. However, all of these methods focus on the fault condition only once it has occurred and can be used to organize corrective maintenance operations. The monitoring procedure proposed here allows the introduction

[1] This chapter has been published as "Neural network-based fault diagnosis of joints in high voltage electrical lines" in *Advances in Science, Technology and Engineering Systems Journal Vol. 5, No. 4, 488-498 (2020)* [86] and "Failure Prevention and Malfunction Localization in Underground Medium Voltage Cables" in *Energies, (Special Issue: Power Transmission Line Simulation), vol. 14, iss. 85, 2020* [87].

of a predictive approach, thus increasing the reliability of the entire electrical system. The joints of overhead lines are therefore considered, as they represent one of the most stressed parts and their correct functioning guarantees electrical continuity between two different parts of the same phase conductor. The main objective of this theoretical method is the detection and localization of the joints in the worst state of health by means of frequency response measurements. For this reason, the equivalent lumped circuit of the junction regions presented in the previous chapter is used (see section 3.3.1), thus also introducing the effects of ageing and deterioration. Therefore, the changes introduced by the failure mechanisms in the frequency response measurements can be simulated and used to train the neural classifier. The most important characteristics of the technique proposed here are the low intrusive level and the prognostic aspect. In fact, the measurement of the frequency response requires at most two test points at the ends of the line and the detection of the failure mechanisms in their initial phase allows catastrophic failures to be avoided. As for the classification tool, the MLMVN presented in section 3.2.3 is used, whose complex nature makes it very suitable for processing electrical measurements expressed by phasors. The output configuration suitable for multiple severities and for the k-fault hypothesis is considered, which consists in the use of two binary neurons for each junction region belonging to the network branch studied. In this case, the SapWin software is used to perform the Testability assessment and extract the selected transfer functions in symbolic form. Next, a Matlab script is used to process these functions and create the dataset matrix. Note that the values of the test frequencies are selected through the mathematical procedure shown in 2.3.2.

The second application presented in this chapter concerns the monitoring of medium voltage underground cables. In this case, the lumped model presented in section 3.3.2 is used to detect abnormal operating temperatures and locate the cable section in the worst state of health. The prognostic method is still based on the analysis of the frequency response but, in this application, only the variations of the conductor resistance due to the increase in temperature are considered. Overheating situations can be caused by several internal and external factors, such as overload currents and variations in environmental conditions, which produce a rapid deterioration of the insulating materials. In turn, damage to the insulation increases current leakage and contributes to the temperature rise. In order to prevent the

formation of water trees and partial discharge phenomenon and avoid catastrophic events, the increase in resistance can be used as an indication of malfunction. As described above, variations in resistance produce changes in the frequency response that the neural network must classify to detect and locate problems. In this case, SapWin is used to provide the Testability study while the realization of the dataset is performed on Matlab/Simulink by integrating the typical devices of a Power Line Communication (PLC) system, as shown in 3.4. Note that in this case Principal Component Analysis (PCA) is used instead of the mathematical procedure for selecting test frequencies.

This chapter is organized as follows: initially, the lumped models presented in section 3.3.1 are used to calculate the failure classes considered in the joint prognosis problem. Subsequently, three case studies are proposed and the operations for assessing testability and selecting the optimal frequencies are described. Finally, the simulation procedure required to obtain the classification results is illustrated in detail. As regards the study of underground medium voltage lines, the modelling proposed in 3.3.2 is resumed and the prognostic procedure is developed using the Simulink model in the creation of the dataset. Furthermore, a different configuration of the neural network is used.

4.2 Prognosis of Joints in Power Transmission Lines

This section proposes the application of the prognostic procedure based on the frequency response analysis to obtain the health status of bolted joints in high voltage overhead lines. The equivalent circuits of junction regions and phase conductor have been developed in section 3.3.1, where the effects of the two main failure mechanisms are described through mathematical formulations. Remember that only the joint degradation is considered, while the electrical parameters of the phase conductor are fixed in their nominal ranges defined taking into account the variability introduced by the load current and environmental conditions. Two failure mechanisms are considered in this study: oxidation process and partial breaking mechanism. Starting from the description of these phenomena presented in section 3.3.1, the following simulation procedure is proposed:

- definition of the fault classes;
- testability assessment and test frequency selection for the case study considered;
- definition of MLMVN set-up;
- dataset creation;
- training results;

4.2.1 Definition of the Fault Classes

Since the main objective of the prognostic method is the detection of the failure mechanisms before they can produce catastrophic consequences, the MLMVN must be able to distinguish the nominal condition of the joints from that of oxidation and to recognize the presence of a partial breakage. The proposed classifier uses frequency response measurements to define the state of health of the junction regions and, therefore, several examples must be generated in all possible working conditions by varying the electrical parameters of the equivalent circuit. The entity of these variations is defined using the formulas and the physical characteristics presented in 3.3.1.

First of all, it is necessary to define the values of the joint parameters in nominal working conditions. Starting from the DC resistance measurements proposed in Table 3.7 and the relative calculations of the joint resistivity, it is possible to define the nominal range of the parameter R_{sj} taking into account the skin effect. Therefore, using formulas (3.38) and (3.39), the results shown in Table 4.1 are obtained for the joint resistance in the range $(3 \div 60)kHz$. In this case, it is assumed that the relative permeability is equal to 100 to take into account the presence of aluminium and steel parts, while the vacuum magnetic permeability is fixed at $4\pi \cdot 10^{-7}$ $[N/A^2]$.

Therefore, the upper limit of the joint resistance in nominal working conditions depends on the frequency used for the measurements and it can be calculated using the following interpolation (4.1).

$$R_{sjmax}(f) = 4.78 \cdot 10^{-5}\sqrt{f} + 7.77 \cdot 10^{-4} \tag{4.1}$$

Regarding the inductance L_{sj} in nominal working conditions, there are no particular effects to consider and its value can be calculated by (3.37) using the physical characteristics of the joints shown in Table 3.5 and the

Nominal conditions				
Frequency $[kHz]$	ρ_{min} $[\Omega m]$	ρ_{max} $[\Omega m]$	R_{sjmin} $[\Omega]$	R_{sjmax} $[\Omega]$
3	10^{-7}	$4.2 \cdot 10^{-6}$	$4.24 \cdot 10^{-4}$	$3.5 \cdot 10^{-3}$
10	10^{-7}	$4.2 \cdot 10^{-6}$	$7.61 \cdot 10^{-4}$	$5.6 \cdot 10^{-3}$
20	10^{-7}	$4.2 \cdot 10^{-6}$	$1.1 \cdot 10^{-3}$	$7.5 \cdot 10^{-3}$
30	10^{-7}	$4.2 \cdot 10^{-6}$	$1.3 \cdot 10^{-3}$	$9 \cdot 10^{-3}$
40	10^{-7}	$4.2 \cdot 10^{-6}$	$1.5 \cdot 10^{-3}$	$10.3 \cdot 10^{-3}$
50	10^{-7}	$4.2 \cdot 10^{-6}$	$1.7 \cdot 10^{-4}$	$11.5 \cdot 10^{-3}$
60	10^{-7}	$4.2 \cdot 10^{-6}$	$1.8 \cdot 10^{-4}$	$12.5 \cdot 10^{-3}$

Table 4.1: Joint resistance values in nominal conditions as the frequency varies.

magnetic permeabilities described above. Therefore, the nominal inductance is $1.56[\mu F]$ and does not change due to the oxidation process. As for the capacitance C_{sj}, a nominal value of $0.01[pF]$ is obtained using formula (3.42) and setting very low levels of the fracture parameters ($x = 0.5\%d$ and $h = 0.5\%H$). Also in this case, the skin effect does not produce variations in the electrical parameter.

In order to define the resistance value in oxidation conditions, the maximum resistivity value of $3.4 \cdot 10^{-3}[\Omega m]$ shown in Table 3.7 is considered, which corresponds to a R_{sj} of $2[\Omega]$. It should be noted that the influence of the skin effect when the resistivity of the material is minimal produces a significant increase in joint resistance, but this variation decreases as oxidation progresses. In fact, this failure mechanism causes an increase in resistivity and, consequently, an increase in the penetration depth of the current. This means that the oxidation of the joint structure produces a partial compensation of the skin effect and the resistance R_{sj} can be considered not-sensitive to the frequency when a significant degradation occurs. Therefore, the resistance value R_{sj} in case of oxidation can vary in the interval between $R_{sjmax}(f)$ and $2[\Omega]$. As mentioned above, inductance and capacitance do not change due to the oxidation process and therefore only a range of 10% around their nominal values is considered.

In the case of a partial fracture in the joint structure, equations (3.40), (3.41) and (3.42) are used to calculate the electrical parameters of the circuit. Since the consequentiality between oxidation process and partial breaking

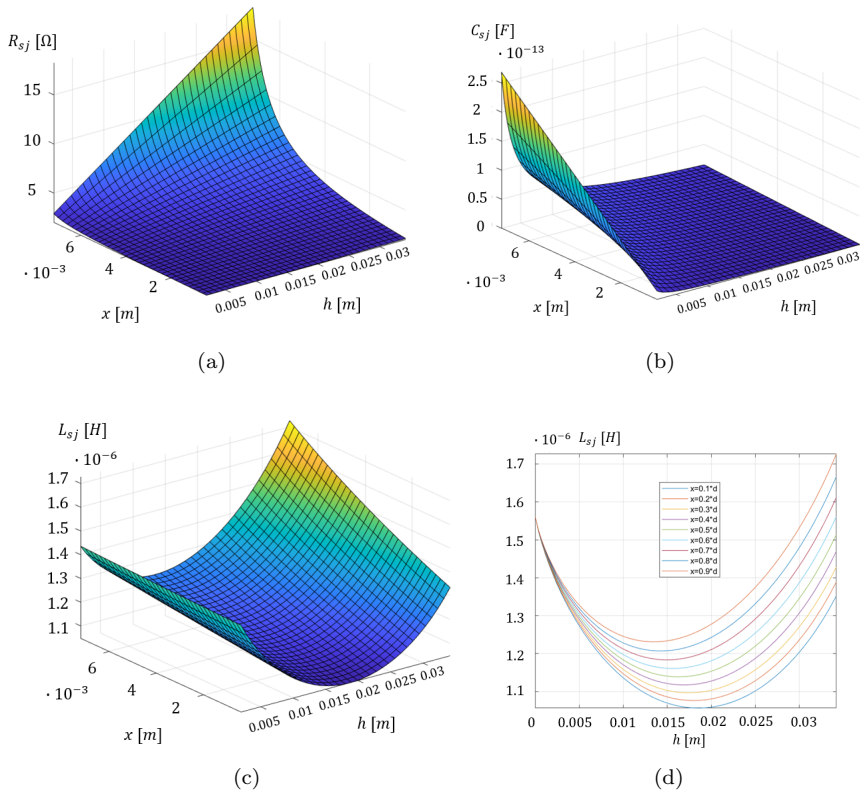

Figure 4.1: Joint parameters with respect to crack height and crack width: (a) resistance; (b) conductance; (c) inductance; (d) inductance.

mechanism is assumed in this study, the presence of a damage can only occur in oxidation conditions. This means that the incidence of the skin effect can be neglected and the second equation presented in (3.40) is used to calculate R_{sj}. Inductance and capacitance can be evaluated considering different percentages of the fracture parameters x and h up to 90% of the total height H and width d respectively. Figures 4.1(a-c) show the variation of the electrical parameters as a function of the extent of the break.

Observing the behaviour of L_{sj} in Figure 4.1(d), it can be seen that the maximum difference with respect to the nominal value is obtained with $h = 50\%H$ and $x = 10\%d$. Exceeding these values, the inductance increases

and approaches again the nominal range. Then, when the extent of the break is very high, the value of L_{sj} increases significantly. Since the purpose of the prognostic analysis is to prevent catastrophic failures, the following maximum values of the fracture parameters are used: $h = 65\%H$ and $x = 65\%d$. Based on these considerations, the fault classes shown in Table 4.2 are defined.

As regards the phase conductor, once the resistance value at $50Hz$ has been extracted from the datasheet, formulas (3.44) and (3.46) are applied to obtain the value at the frequency used for the measurements. Subsequently, applying a tolerance of 15% on the calculated value, the nominal range is obtained which takes into account the effects of the load current and environmental conditions (see section 3.3.1). Note that the same tolerance is also applied to line inductance and capacitance. Table 4.3 presents the nominal values for the ACSR considered.

Nominal conditions	
$R_{sj}[\Omega]$	$60 \cdot 10^{-6} \div (4.78 \cdot 10^{-5}\sqrt{f} + 7.77 \cdot 10^{-4})$
$L_{sj}[H]$	$(1.3 \div 1.7) \cdot 10^{-6}$
$C_{sj}[F]$	$(0.0099 \pm 0.011) \cdot 10^{-12}$
Oxidation conditions	
$R_{sj}[\Omega]$	$(4.78 \cdot 10^{-5}\sqrt{f} + 7.77 \cdot 10^{-4}) \div 2$
$L_{sj}[H]$	$(1.3 \div 1.7) \cdot 10^{-6}$
$C_{sj}[F]$	$(0.0099 \div 0.011) \cdot 10^{-12}$
Partial breaking conditions	
$R_{sj}[\Omega]$	> 2
$L_{sj}[H]$	$(1 \div 1.3) \cdot 10^{-6}$
$C_{sj}[F]$	$(0.011 \div 0.16) \cdot 10^{-12}$

Table 4.2: Fault classes and corresponding parameter values.

R'_l $[\Omega/km]$	L'_l $[mH/km]$	C'_l $[\mu F/km]$
0.12	1.28	$9.74 \cdot 10^{-3}$

Table 4.3: Electrical parameters of the phase conductor.

4.2.2 Case Studies

Once the fault classes and the corresponding intervals for the joint parameters have been defined, three case studies are introduced, each of which presents a different number of elementary sections. In particular, situations characterized by three, four and five junction regions are considered. Remember that a single elementary section is constituted by the cascade connection of the equivalent circuit of the conductor and that of the joint. Considering the case of three elementary sections, the overall equivalent model can be summarized as shown in Figure 4.2. Note that a length of approximately 200 meters is considered for each conductor stretch.

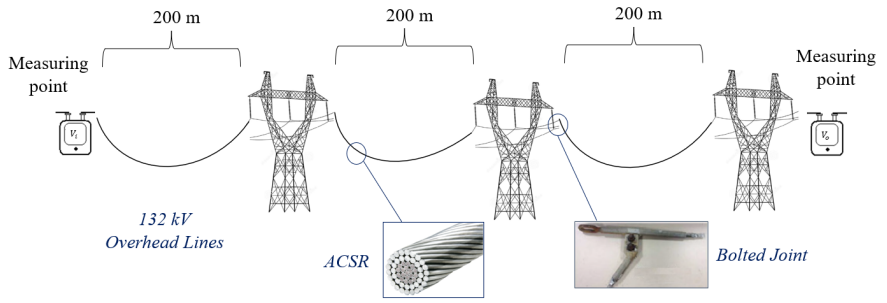

Figure 4.2: First case study considered: three conductor stretches and three bolted joints.

In this application, the measuring points are fixed at the ends of the network branch taken into consideration. The main idea of the monitoring method is to inject high frequency signals and measure the voltage transfer function (magnitude and phase) in order to recognize the state of health of the junction regions. To achieve this purpose, it is necessary to study the Testability level associated to the network function $F(s) = V_o(s)/V_i(s)$ considering all the possible variable elements. Note that the term *variable elements* is used to indicate electrical parameters that change their values

when a malfunction occurs. In the case of bolted joints, for example, there are three defective elements for each junction region.

Therefore, in the case study characterized by three joints there are nine variable components, which increase to twelve in the case of a network branch with four junctions and become fifteen when considering five junction regions.

The prognostic goal has a high level of complexity as it refers to the multiple severity condition. In fact, two consequential failure mechanisms are considered, and this involves the presence of three possible health conditions for each joint: nominal conditions, oxidation and partial damage.

Furthermore, the k-fault hypothesis is introduced and this means that more than one joint can be affected by malfunctions at the same time. Consequently, using the term n_j to indicate the number of joints belonging to the network branch considered, the total number of conditions to be recognized is defined by (4.2).

$$N \ \ conditions = 3^{n_j} \tag{4.2}$$

4.2.3 Testability analysis

As extensively described in previous chapters, Testability analysis is one of the most important steps in all diagnostic/prognostic procedures. In this case, it provides information about the effects produced by the variable components in the line transfer function. To obtain the classification of all the possible operating conditions described above, the electrical parameters of the different junction regions must introduce different variations in the network function $F(s)$. Furthermore, to distinguish the oxidation condition from the partial breakage of the structure, it is necessary to separate the variations of the resistive and reactive parameters of the same joint.

Therefore, the connection in cascade of the SapWin scheme proposed in Figure 3.14 is carried out n_j times, keeping in symbolic form the electrical parameters of the joints and setting those of the conductor stretches to the nominal values. To simplify the reading of the circuit, each elementary section is used in the form of a sub-circuit (Figure 4.3). Note that to study the voltage transfer function it is necessary to use a voltage source at the first end of the line and a voltage measurement point at the other. Furthermore, it should be noted that in this case the introduction of the coupling circuits necessary for PLC devices is not considered, but only the equivalent scheme of the network branch is studied from a theoretical point of view.

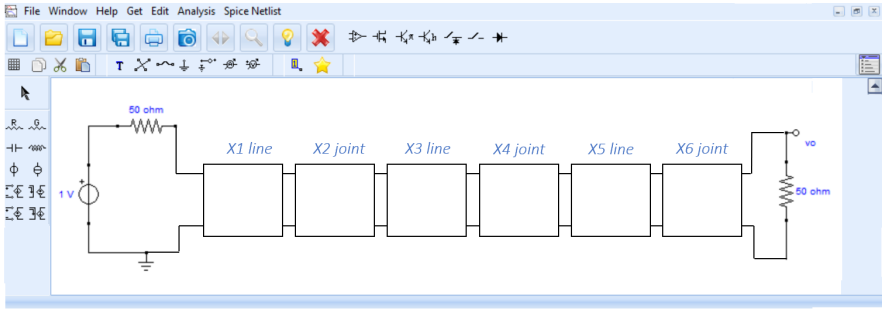

Figure 4.3: Circuit configuration used in SapWin to study the overall Testability of the first case study.

Consequently, using the LINFTA program implemented in the SapWin PET version, the testability of the overall circuit is calculated by evaluating the rank of the Jacobian matrix in symbolic form. Analysing the results obtained, it is possible to state that the Testability is maximum in all the case studies considered. In fact, the Testability index calculated through (2.4) is always equal to the maximum number of variable components and no ambiguity groups are found.

Case study	N. joints	N. faulty elements	N. conditions	Testability
1	3	9	27	9
2	4	12	81	12
3	5	15	243	15

Table 4.4: Summary of case studies and Testability analysis results.

4.2.4 Optimal frequency selection

As previously mentioned, the identification of malfunctions is carried out by classifying the line frequency response obtained at different frequencies. As reported in section 2.3.2, measurement errors and manufacturing tolerances similarly affect the result and depend on the choice of frequencies. Proper selection minimizes the effect of these errors, thus increasing the probability of detecting malfunctions. A method for making this selection is presented in 2.3.2 and is used to obtain the best test frequencies in the range $(3 \div 60) kHz$.

This technique exploits the Jacobian matrix associated with the failure equations evaluated at different frequencies. The use of multiple frequencies has the purpose of increasing the number of equations, so that their number is at least equal to that of the variable parameters (unknowns). Starting from the Jacobian matrix, an index called Test Index ($T.I.$) is introduced, whose minimization allows the selection of optimal frequencies. $T.I.$ can be calculated as follows,

$$T.I. = (k(J_M) - 1)\|J_M^{-1}\|_2 = \frac{\sigma_{max} - \sigma min}{\sigma_{min}^2} \tag{4.3}$$

where σ_{max} and σ_{min} are respectively the maximum and the minimum singular value of the Jacobian matrix (J_M) and k is its condition number (4.4).

$$k(J_M) = \|J_M\|_2\|J_M^{-1}\|_2 \tag{4.4}$$

The index $T.I.$ is then minimized with respect to the frequency range. Note that there is no parameter identification in the prognostic procedure presented here, so there are no fault diagnosis equations to solve. However, the analytical calculation of the symbolic network function is necessary to evaluate the Testability level and calculate the best test frequencies, thus allowing adequate training of the complex neural network. Using the mathematical approach just proposed, the best test frequency is about $55kHz$. Since the additional frequencies are concentrated in the range $(40kHz \div 60kHz)$, the following values are used: $(40, 45, 50, 55, 60)kHz$

4.2.5 Classification Results

The following are the main characteristics of the neural classifier proposed to prevent catastrophic failures in bolted joints. In this case, the configuration for multiple severities presented in section 3.2.3 is used to detect the oxidation and partial breaking conditions considering their possible contemporaneity on different junction regions. This require a specific configuration of the MLMVN output layer.

Neural Network Set-Up

The main peculiarity of the MLMVN-based classifier used in this application is the presence of two binary neurons for each junction region in the output layer (Figure 4.4).

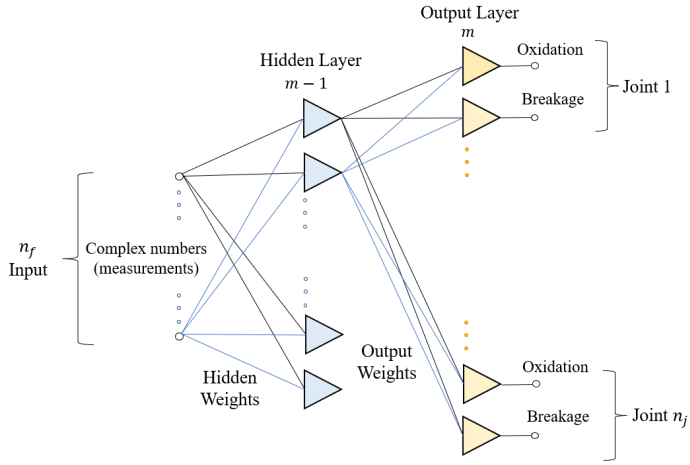

Figure 4.4: Overall structure of the MLMVN-based classifier.

The first neuron of each pair is used to indicate the oxidation or not of the corresponding joint, while the second neuron is used to indicate a possible fracture. Since these are binary units, each output can be a high level (1) or a low level (0). The latter corresponds to the upper half of the complex plane $[0, \pi)$ and is used to describe the nominal conditions, while the value 1 is used to code the presence of the malfunction and corresponds to the lower half plane $(\pi, 2\pi]$. Figure 4.5 describes the output configuration used for each joint.

Regarding the training procedure, there are no substantial changes compared to the algorithm presented in 3.2.3. Therefore, all errors calculated in the output layer are back-propagated and saved in a specific matrix. Subsequently, when all the examples contained in the dataset have been processed, the QR decomposition is used to calculate the best corrections of the weights in the sense of least squares. Remember that the dataset must contain many examples of each possible condition and the related binary code necessary to perform the supervised learning procedure. The structure of the dataset for all three considered case studies is generalized below.

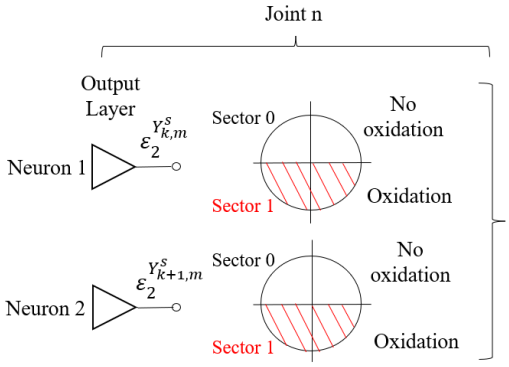

	Neuron 1	Neuron 2
Nominal Condition	0	0
Oxidation	1	0
Breakage	1	1
	0	1

Not used due to the consequentiality between oxidation and breaking mechanism

Figure 4.5: Output configuration for each pair of neurons.

Dataset Creation

As mentioned above, the dataset for this type of application is created using the fully symbolic network function extracted from SapWin and a Matlab script to simulate all possible operating conditions. The main task of the Matlab code is to randomly generate the values of the conductor parameters in the nominal range and those of the joints in all possible fault classes: nominal conditions, oxidation and partial breakage. Remember that the nominal range of the conductor parameters is established by applying a tolerance of 15%, which takes into account the effects of the load current and environmental conditions. As for the joint parameters, once the test frequencies have been selected, the three intervals for each parameter are defined as indicated in Table 4.2. The Matlab script substitutes all parameters in the symbolic voltage transfer function and calculates its amplitude and phase. This operation is repeated for all n_f test frequencies in order to obtain n_{rs} random samples of every possible working condition. Figure 4.6 clarifies the structure of the dataset matrix.

In the input section of the dataset there are $(2 \cdot n_f)$ columns: each pair contains magnitude and phase of the corresponding measure. The output section contains the indices of the desired sectors for each neuron of the last layer. Since they are binary neurons, all the possible working conditions are described by a succession of 1 and 0 according to the rules shown in Figure 4.5. The total number of rows (examples) is given by the product $(n_{rs} \cdot 3^{n_j})$.

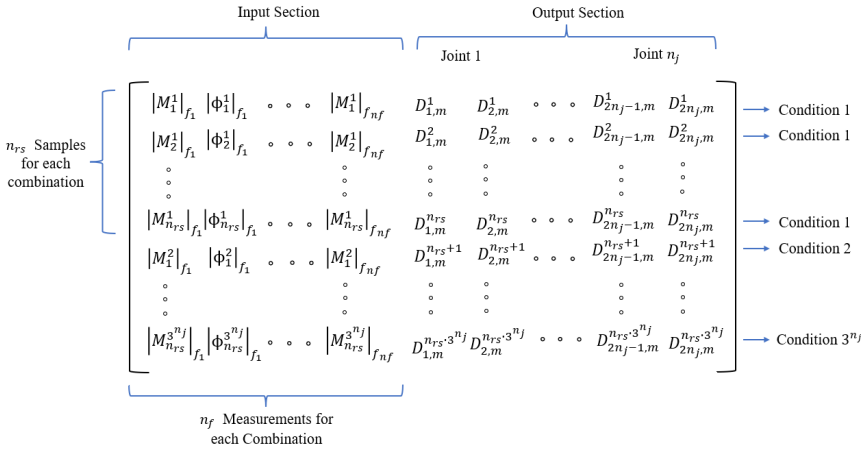

Figure 4.6: Description of the dataset structure.

Training Phase

Once the dataset matrix has been created, the MLMVN-based classifier is trained using the Matlab application described in section 3.2.4. In this case, 100 samples are generated for each possible operating condition of the network branch studied. Then, the hold out validation technique is applied: 80% of the data is used during the learning phase to correct the weights and the remaining 20% is used in the test phase to verify the performance of the classifier. Below are the results of the test phases relating to the three case studies examined. Note that the performance of the prognostic method is expressed in terms of Classification Rate (CR), which corresponds to the ratio between the number of correctly classified samples and the total number of samples.

Table 4.5 shows the global classification rate obtained in the cases of network branches with three and four junction regions. In this case, performing a correct classification means recognizing the exact combination of the state of all joints. Therefore, a single mistake made on an output neuron results in the misclassification of the entire input example.

For a more accurate analysis of the results, Table 4.6 and Table 4.7 are presented, where the classification rate is calculated for each neuron and for each joint.

Case study	N. joints	N. conditions	N. hidden neurons	$CR\%$
1	3	27	200	85.11
2	4	81	250	72.44

Table 4.5: Global classification rate obtained in the cases of three and four junction regions.

Fault Classes	Neuron	$CR\%$ for each neuron	Joint	$CR\%$ for each joint
Oxidation	1	95.11	1	94.07
Partial Breakage	2	99.37		
Oxidation	1	92.85	2	91.30
Partial Breakage	2	99.22		
Oxidation	1	97.89	3	96.70
Partial Breakage	2	99.81		

Table 4.6: Classification results obtained for each output neuron and for each joint in the first case study: three junction regions.

Fault Classes	Neuron	$CR\%$ for each neuron	Joint	$CR\%$ for each joint
Oxidation	1	97.72	1	95.45
Partial Breakage	2	98.89		
Oxidation	1	93.03	2	90.52
Partial Breakage	2	98.33		
Oxidation	1	94.38	3	92.34
Partial Breakage	2	98.21		
Oxidation	1	91.67	4	90.13
Partial Breakage	2	98.33		

Table 4.7: Classification results obtained for each output neuron and for each joint in the second case study: four junction regions.

The results obtained show the excellent potential of the prognostic method in the analysis of network sections containing three and four junction regions. The global classification rates are excellent considering the high number of conditions to be classified, 27 in the case of three joints and 81 in the case

of four junction regions. Furthermore, by analysing in detail the results obtained for each joint, extremely better performances can be noted. The reason is that the error in the classification of a joint is considered as the wrong classification of the whole input example in the calculation of the overall CR. Therefore, the specific analysis reveals the possibility of classifying the health status of each individual joint with an accuracy level greater than 90%. The results calculated for each output neuron are even better. This means that the configuration of the neural network and the training method used allow an excellent minimization of errors. The reduction in the overall classification rate is essentially due to the complexity of the problem (multiple failure hypothesis with multiple severities).

As regards the case with five junction regions, it can be said that it represents the limit of the prognostic method proposed here. In fact, as shown in Table 4.8, a general decrease in CR is obtained and an accuracy level of no more than 70% in the two neurons corresponding to the fifth joint. Given the impossibility of increasing the frequency of the transmitted signals to maintain the validity of the lumped parameter model, the prognostic method must be modified and adapted to allow the monitoring of longer network branches.

Fault Classes	Neuron	$CR\%$ for each neuron
Oxidation	1	99.36
Partial Breakage	2	99.97
Oxidation	1	99.49
Partial Breakage	2	99.89
Oxidation	1	60.35
Partial Breakage	2	59.95
Oxidation	1	67.35
Partial Breakage	2	68.51
Oxidation	1	83.55
Partial Breakage	2	96.23

Table 4.8: Classification results obtained for each output neuron in the third case study: five junction regions.

4.3 Prognosis of Medium Voltage Underground Cables

In this section, the prognostic method based on the use of MLMVN is adapted to monitor the health status of underground Medium Voltage (MV) lines. The definition of the problem is simplified compared to the previous treatment and, therefore, the hypothesis of single failure is introduced. Furthermore, in this application, the junction regions are not considered and the main subjects of the analysis are the successive cable sections. The idea is to extend the length of the network branch examined by focusing on the working temperature and avoiding the consideration of specific junction points. The theoretical concept on which this method is based is still the analysis of the frequency response. Therefore, the voltage transfer function is used to identify the operating temperature of the line, which depends on several factors, such as overload currents and variations in environmental conditions. These phenomena produce a rapid degradation of the insulating materials, thus reducing the useful life of the electrical infrastructure. As shown in [88], the distribution of catastrophic failures in different areas of the Italian medium voltage grid indicates that most of the problems occur during the summer period. In this sense, more than 60% of cable failures occur from June to August. This means that the high ambient temperature and the consequent thermal characteristics of the arid soil increase the failure rate of underground medium voltage cables. Another factor that affects the working temperature of the line is the load current. High values of transmitted power increase losses due to the Joule effect, and this means that the cable temperature depends on the load current. This is not an external factor, and it should be considered during the dimensioning of the line. In fact, the section of the cables is defined on the basis of the line rated current for specific laying characteristics in order to reduce the voltage drop and not to exceed the maximum temperature provided by the manufacturers. Generally, short overloads do not represent a problem for the underground cables but, the persistence of this situation, can cause an excessive increase in temperature especially in the summer months.

4.3.1 Initial Case Study

An underground medium voltage line of 900 meters consisting of three $35mm^2$ RG7H1M1 single-core cables represents the initial case study analysed here.

Cable length $[km]$	Conductor radius $[mm]$	Sheath radius $[mm]$	Outer radius $[mm]$
0.3	7	17	23.2
Line-line spacing $[mm]$	Line formation	Insulation relative permittivity	Cable section $[mm^2]$
46.4	Flat	2.4	35

Table 4.9: Characteristic of a single cable part.

Three successive cable parts are considered in the hypothesis of single failure, which assumes that the overheating can affect only one of them at a time. This means that four fault classes are used. The first of them is called *class 0* and it describes the nominal operating condition of each cable part. The other n classes are used to describe the abnormal working temperature of each cable section ($n = 1, 2, 3$). Table 4.9 summarized the characterises of a single cable part and Figure 4.7 shows the case study. Note that each cable section is represented by a π-model in which the variable element is the longitudinal resistance. In fact, the main physical phenomenon considered in this application is the relationship between cable temperature and cable resistance: as the working temperature increases, the resistance of the conductor also increases.

Therefore, a significant variation in the conductor resistance produces a corresponding change in the frequency response, which means that the line transfer function measurements contain all the information about the cable temperature. In order to obtain this measurements, the injection of high frequency signals into the line through PLC devices is considered in this application. Then, magnitude and phase of the voltage transfer function are processed by the neural classifier to understand in which of the cable parts the over-temperature is occurring. Unlike the case analysed above, in this application the creation of the dataset is completely performed on Matlab/Simulink. The SapWin software is obviously used to verify the Testability of the overall circuit, and the result obtained indicates the possibility of distinguishing the four fault classes through the selected measurement.

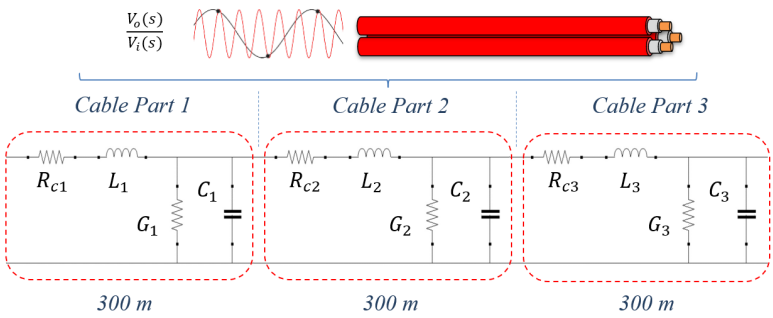

Figure 4.7: Case study: medium voltage underground line divided into three sections.

4.3.2 Cable Parameters and Fault Classes

In order to calculate the operating temperatures of the cable and consequently the resistance interval for each fault class, the Matlab application described in section 3.3.2 is used. The main purpose of the application is to facilitate the parametrization of the equivalent cable model in any condition other than that reported on the technical datasheet. Therefore, starting from the physical characteristics provided by the manufacturer, it is possible to calculate the cable parameters in a specific grid configuration, with particular load currents and environmental conditions.

In the case study considered, the cables of the underground line have the physical characteristics shown in Table 4.9, and the nominal ambient temperature into the concrete channel is assumed equal to $20°C$. Therefore, the calculated cable temperature corresponding to a rated load current of $200A$ is equal to $70°C$ and the resistance value at $50Hz$ obtained through equation (3.53) is $0.64[\Omega/km]$. Any change in environmental conditions or load current that produce a temperature above $70°C$ is considered as a malfunction. Identifying this condition allows the monitoring of the cable behaviour and the prevention of catastrophic failures. When a malfunction occurs, the resistance of the conductor exceeds the value of $0.64[\Omega/km]$ and produces a variation in the frequency response that must be classified by the complex neural network. Furthermore, by dividing the branch of the line into three parts, it is possible to locate the malfunction and intervene promptly, reduc-

ing recovery times. Figure 4.8 summarizes the possible operating conditions of each cable section. Note that only one severity of malfunction is considered at this stage. In fact, the objective is to monitor the line and intervene as soon as the temperature exceeds the nominal level, thus maximizing the prevention aspect of the method.

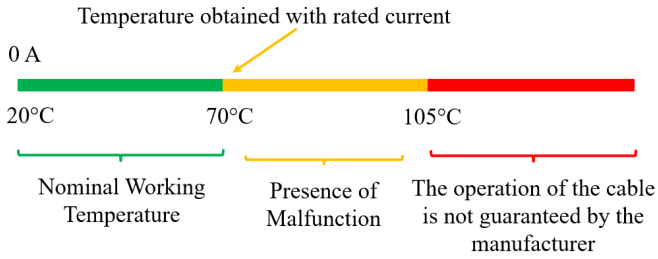

Figure 4.8: Operating conditions.

Consequently, the meaning of the four classes of failure can be summarized as follows.

- Class 0: the working temperature of each cable section is lower than $70°C$.
- Class 1: the working temperature of the first cable section is higher than $70°C$.
- Class 2: the working temperature of the second cable section is higher than $70°C$.
- Class 3: the working temperature of the third cable section is higher than $70°C$.

4.3.3 Classification Procedure

Once the fault classes have been defined, it is possible to use the Matlab application mentioned above to set up the PLC system and create the dataset matrix. Therefore, the turn ratio of the matching transformers is fixed to adapt the transmitter/receiver resistance with the characteristic line impedance. The coupling circuit used in this case is capacitive and presents a

fourth order high pass filter with a minimum bandwidth frequency of $3kHz$. In fact, to inject the measurement signals, the $(3 \div 50)kHz$ band is taken into consideration.

To create the dataset matrix, the Simulink/Simscape scheme proposed in Figure 4.9 is managed by the Matlab application, which varies the resistance values to simulate all the different classes of failure. The corresponding values of the voltage transfer function ($F(s) = V_o(s)/V_i(s)$) are measured in magnitude and phase for n_f test frequencies belonging to the band $(3 \div 50)kHz$.

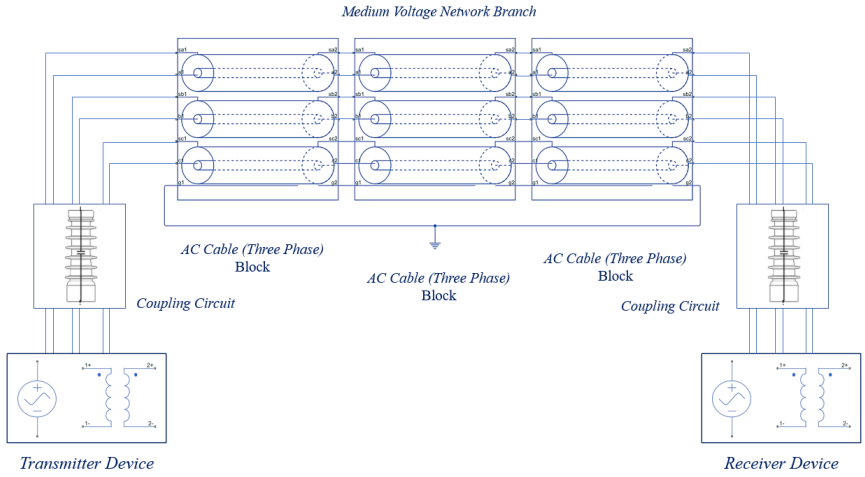

Figure 4.9: Simulink/Simscape model used for creating datasets.

In this procedure, the preliminary selection of test frequencies is compared with a Principal Component Analysis (PCA). Initially, the analytical method described in 2.3.2 is used to select 4 test frequencies. These frequencies are used in the Simulink/Simscape diagram to extract transfer function measurements and create a dataset containing 300 random samples for each class of failure. Then, 100 frequencies are considered, obtained by dividing the band used in equal parts. Again 1200 examples are generated from the four failure classes at the test frequencies.

Therefore, a linear PCA (see appendix A) is applied to the dataset matrix containing the measurements relating to 100 frequencies, maintaining the 98% of the informative content. This produces the reduction of the

dimensionality of each input from 100 complex numbers to 4.

This means that two dataset are available to classify the state of health of the line using four complex numbers for each input. In the first case, these numbers correspond to magnitudes and phases of the measured transfer function. In the second case they are obtained following the projections of the measurements obtained for 100 frequencies in a space with reduced dimensionality. In the new coordinate system, the physical meaning of the measurements is not maintained but a certain percentage of the information content is preserved (98% in this case).

MLMVN Set-Up

In this case, the output configuration of the MLMVN-based classifier is the one for the single fault situation. Therefore, three binary neurons are used in the output layer, one for each cable section taken into consideration. These neurons are used to distinguish the nominal condition of the corresponding cable section from the over temperature situation. In particular, the value 0 corresponding to the beginning of the upper half plane is used to indicate the nominal working temperature, while the lower border of the second sector indicates the overheating.

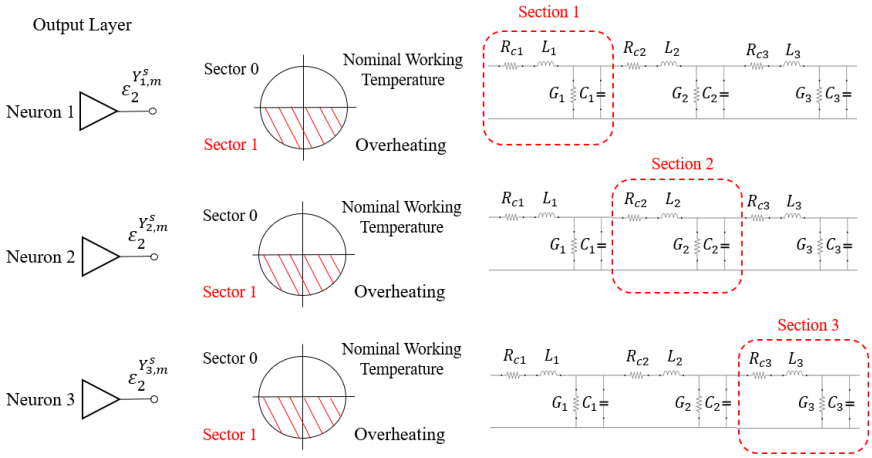

Figure 4.10: Configuration of the output layer of the MLMVN-based classifier.

Training Phase

As previously mentioned, two datasets are used in this case to evaluate the performance of the MLMVN-based classifier. In the first case, the transfer function measurements obtained at 4 test frequencies selected by the mathematical method are used. The results obtained in terms of the overall classification rate are shown in Figure 4.11(a), while Figure 4.11(b) presents the performance of the complex neural network for each class separately. These results are obtained by setting 20 neurons in the hidden layer and using the hold out validation technique: 80% of data is used for weight correction (learning) while the remaining 20% is used for further validation of the performance (test). In Figure 4.11(a), the red line is used to describe the classification rate obtained during the learning phase while the blue one refers to the testing phase.

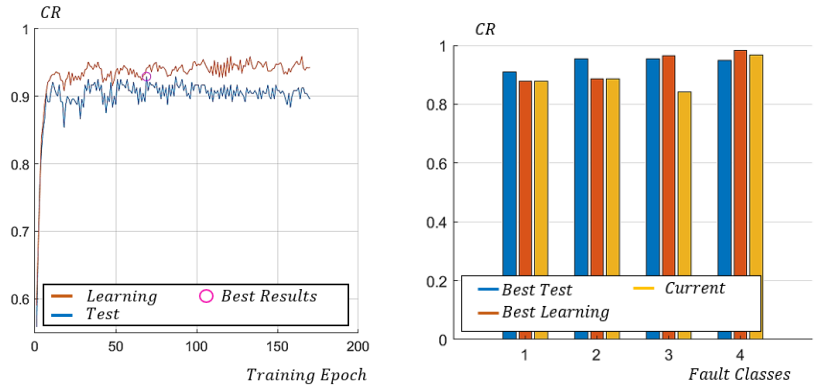

(a) (b)

Figure 4.11: Classification results obtained using 4 frequencies selected by the mathematical method: (a) global classification rate; (b) classification rate for each output neuron.

Finally, the training procedure is repeated by applying a linear PCA to the simulated measurements obtained at 100 frequencies. By maintaining 98% of the information content, the results shown in Figure 4.12(a) and Figure 4.12(b) are obtained. The performance obtained by keeping 20 neurons in the hidden layer is slightly better than that obtained in the previous case.

Therefore, the use of a linear PCA can be considered a valid alternative

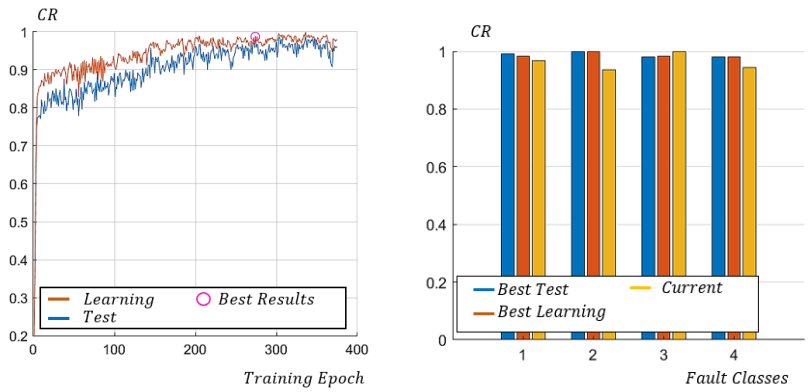

(a) (b)

Figure 4.12: Classification results obtained by PCA: (a) global classification rate; (b) classification rate for each output neuron.

to the frequency selection method during training and use of the neural classifier. Instead of implementing a rather complex mathematical method, it is possible to perform measurements at multiple frequencies and then reduce the dimensionality of the inputs to avoid a heavy structure of the MLMVN. On the other hand, to obtain a comparable result using all the measurements obtained at 100 frequencies, it is necessary to use a number of neurons in the hidden layer 3 times higher. Table 4.10 summarizes these considerations, where *No PCA* indicates the used of four test frequencies selected through the mathematical method, *Linear PCA* indicates the use of a linear PCA to the dataset containing simulated measurements at 100 frequencies and *100 Frequencies* indicates direct used of this dataset. The main theoretical aspects of the PCA used in this case are reported in appendix A.1.4.

4.4 Conclusion

The theoretical results presented in this chapter offer a possible approach for the detection and localization of malfunctions in transmission and distribution lines. The goal of the simulations performed was to demonstrate that the MLMVN-based classifier allows the identification of the state of the line using measurements of its frequency response. In the case of the

Configuration	Clasification Rate (CR%)	N. Hidden Neurons	N Complex Inputs
No PCA	92.92	20	4
Linear PCA	98.75	20	4
100 Frequencies	96.70	60	100

Table 4.10: Summary of the results obtained with and without applying the PCA.

prognosis of joints on overhead lines, the hypothesis of multiple failure with multiple severities was adopted. In this situation, the method allows the correct monitoring of the joints contained in a branch of 800 meters. Exceeding this limit, the performance in recognizing the operating conditions of all joints decreases. It is still possible to study a single joint with good accuracy but the overall performance is not sufficient. As regards the monitoring of underground lines, the single failure hypothesis was assumed and the prognostic method was focused on the detection of overheating. In this case, the classifier allows the correct monitoring (accuracy greater than 95%) of approximately $1km$ of line divided into three successive sections. The increase in the length of the line branch considered and therefore in the number of successive sections determines the reduction of the classification rate and requires further developments. For this reason, in the continuation of the thesis the hypothesis of using higher frequencies and moving to distributed parameter modelling is investigated.

Chapter 5

Application: Localization of Malfunctions in Medium Voltage Underground Cables

This chapter proposes a new prognostic approach capable of preventing catastrophic failures in Medium Voltage (MV) power cables by overcoming the limitations occurred in the study of the frequency response. The main objective is the development of a monitoring system focused on the detection and localization of cable over-temperatures in underground distribution networks. The predictive analysis proposed here is based on a Multi-Layer neural network with Multi-Valued Neurons (MLMVN), which elaborates measurements of high frequency signals transmitted through Power Line Communication (PLC) devices. Therefore, the prognostic method does not require the introduction of additional components since the power line is already equipped through a communication system. This allows a low intrusive level and the possibility of working on-line during the operation of the network without service interruption. Furthermore, the MLMVN-based classifier processes magnitude and phase of the received signals without preliminary coding steps and ensures a low computational cost. Again, the main theoretical concept on which the predictive analysis is based is the detection of malfunctions starting from their effects on the cable parameters. For this reason,

an RG7H1M1 cable has been experimentally characterized in the range $(90kHz \div 1MHz)$ *both in nominal conditions and in overheating situations generated by means of a climatic chamber. The changes in the electrical parameters of the cable modify the transmitted signal and the monitoring system proposed here allows the identification and localization of the overheated section with high accuracy.* [1]

5.1 Introduction

As extensively described in the literature review, the detection and localization of faults in electrical power systems plays a fundamental role for the development of modern smart grids and smart cities [89]. The growing complexity of power distribution networks due to the integration of renewable energy sources and the new challenges in managing power flows must be addressed while maintaining the reliability of the electricity service [90]. The innovative devices introduced in electrical lines allow an improvement in many technical aspects and in the services offered to users, but require specific maintenance operations and monitoring systems [91]. In this sense, the prevention of faults is essential to avoid long interruptions in the electricity service and limit the area affected by the outage. The main objective of this application is the development of a prognostic method capable of preventing catastrophic failures in MV underground cables using PLC technologies and a neural classifier based on MLMVN. Communication devices are usually used in high voltage transmission lines to transfer control signals between primary stations. In distribution networks, PLC technologies are used to exchange information between line operators and users and between secondary substations. Therefore, the main idea behind this monitoring method is to use existing communication systems to detect malfunctions in underground power cables. This allows a low intrusive level and ensures the possibility of working on-line during the normal operation of the network. The use of PLC signals for fault detection in power lines is a research topic of increasing interest [92] [93]. Most of the papers in the literature focus on identifying

[1] This chapter has been submitted as "Frequency Characterization of Medium Voltage Cables for Fault Prevention through Multi-Valued Neural Networks and Power Line Communication Technologies" in *IEEE Transactions on Power Delivery* and it is still under review.

and locating high impedance faults and catastrophic damage to conductors [94] [95]. In these cases, the information provided by the monitoring systems allow the reduction of recovery times by detecting the fault position but do not avoid the interruption of the service because the preventive aspect is missing. The proposed prognostic method focuses on the detection and localization of malfunctions, which are operating conditions different from the nominal ones and involve a partial loss of functionality. These working conditions usually precede catastrophic failures and, in the case of medium voltage cables, over-temperatures are taken into consideration. In fact, situations of overheating can introduce an anomalous deterioration of the insulating materials, thus facilitating the formation of water trees and partial discharges [96] [97]. The joints of the underground lines are the components subjected to the greatest thermal stress [98], and their working temperature depends on various factors [99]. Unfortunately, in many MV lines the position of the joints is unknown, and this makes it impossible to develop punctual monitoring systems for their predictive maintenance. Therefore, the main objective of the prognostic approach proposed here is the localization of the cable section affected by over-temperature and the evaluation of its extension. To achieve this goal, the experimental characterization of an RG7H1M1 cable has been performed in the range ($90kHz \div 1MHz$) using a Vector Network Analyser (VNA). The same practical measurements have been repeated by reproducing critical working conditions using a climatic chamber. In this way, it is possible to define the values of the cable parameters as a function of the frequency both in nominal and overheating situations. Therefore, once the cable parameters have been obtained and the frequency of the PLC signal has been selected, it is possible to simulate the behaviour of the cable under malfunction conditions and train the MLMVN to recognize such situations. Since this classifier is a complex-valued neural network, magnitude and phase of the received signals are directly used as inputs without introducing coding steps or feature extraction techniques. The main theoretical concept behind this prognostic method is is that the over-temperatures produce changes in the electrical parameters of the cable and, consequently, on the signals propagating along the line. The effects of these variations on signal magnitude and phase are used by the classifier to identify position and entity of the malfunction. A possible alternative proposed in the literature to achieve a similar classification is the use of optical fibres in the insulating material or buried with the cable [100] [101]. However,

these methods are expensive, requiring additional devices to inject laser pulse signals and process the backscatter components. In addition, the physical application of optical fibers to existing lines requires access to cables along the entire path. The use of high frequency and pulse signals for detecting problems in power cables is also a topic covered in the literature [102] [103]. Most of these techniques rely on Time Domain Reflectometry (TDR) and allow the detection of problems that produce large variations in the characteristic impedance of the line. These situations often coincide with serious faults and can be correctly located by detecting the signal reflected at the point of impedance discontinuity. The magnitude of the reflected signal depends on the distance of the fault and, in the event of small malfunctions, it is difficult to detect the peak of the reflected signal. For this reason, the attention to the working temperature of the cable allows the identification of the anomalies in the initial phases, thus avoiding a strong deterioration of the insulation. In this work, MLMVN is used to process received signals and classify the state of health of the line. In order to train this classifier, a dataset matrix is created using the Simulink model of the network branch considered. This matrix contains magnitude and phase information, as obtained from measurements, of the received signals, at different frequencies and at nominal and non-nominal working conditions of the electrical network. In these simulations, the presence of the over-temperature in a specific cable section is created using the experimental measurements previously described. Therefore, the main contributions of this application are:

- to propose a prognostic method for underground medium voltage cables focused on the working temperature of the line;
- to develop an experimental procedure for the frequency characterization of MV cables both in nominal and overheating conditions;
- to overcome the limits occurred in the frequency response analysis proposed in chapter 4;
- to present a non-intrusive and low-cost computational monitoring system based on MLMVN and PLC technologies to locate the cable section in the worst operating condition.

The chapter is organized as follows: in the second section the main theoretical concepts related to the PLC are recalled, in the third section the experimental procedure for the cable characterization is proposed, in the

fourth section the main aspects of the MLMVN used in this case are discussed, in the fifth section a case study is presented and, finally, the last section contains conclusions and possible future works.

5.2 Power Line Communication and Cable Parameters

The theoretical model used to describe the behavior of transmission lines is based on the equivalent π-circuit shown in Figure 5.1 and on the telegrapher's equations (5.1) and (5.2).

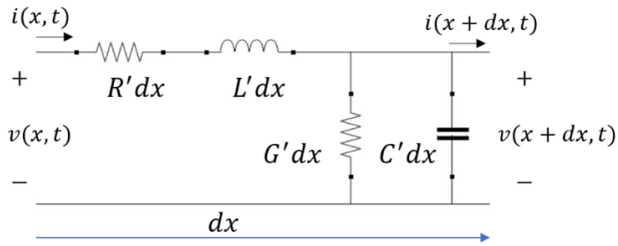

Figure 5.1: Equivalent π-model for a transmission line.

$$\frac{\partial v(t,x)}{\partial x} + R'i(t,x) + L'\frac{\partial i(t,x)}{\partial t} = 0 \tag{5.1}$$

$$\frac{\partial i(t,x)}{\partial x} + G'v(t,x) + C'\frac{\partial v(t,x)}{\partial t} = 0 \tag{5.2}$$

The terms R', L', G' and C' are the line parameters per unit of length: R' is the longitudinal resistance expressed in $[\Omega/m]$, L' is the longitudinal inductance measured in $[H/m]$, G' is the transversal conductance expressed in $[S/m]$ and C' is the transversal capacitance in $[F/m]$. The longitudinal parameters are used to describe the voltage drop along the line section having length dx, while the transversal ones take into account losses of the insulating materials. The term x indicates a specific section along the longitudinal direction of the line and, therefore, the quantities $v(x,t)$ and $i(x,t)$ respectively express the voltage and current at that section at instant t. Similarly, $v(x+dx,t)$ and $i(x+dx,t)$ are the simultaneous voltage and current at the section $(x+dx)$. By introducing the longitudinal impedance

($Z' = R' + j\omega L'$) and the transversal admittance ($Y' = G' + j\omega C'$) and using the phasor form of the sinusoidal electrical quantities, equations (5.1) and (5.2) can be written as follows.

$$\frac{\partial V(x)}{\partial x} = -Z'I(x) \tag{5.3}$$

$$\frac{\partial I(x)}{\partial x} = -Y'V(x) \tag{5.4}$$

By deriving (5.3) and (5.4) with respect to x, two second order homogeneous differential equations are obtained, which depend on the coefficient γ, where γ is called propagation constant and is calculated as shown in (5.5).

$$\gamma = \sqrt{Z'Y'} = \sqrt{(R' + j\omega L')(G' + j\omega C')} = \alpha + j\beta \tag{5.5}$$

The general solution of these differential equations with constant coefficients is presented in (5.6) for the line voltage, where α and β are the real and imaginary parts of the propagation constant respectively.

$$V(x) = A_1 \exp(-\alpha x) \exp(-j\beta x) + A_2 \exp(\alpha x) \exp(j\beta x) \tag{5.6}$$

The coefficient α is called attenuation constant and affects the amplitude of the signal along the line section considered, while β is called phase constant and describes the phase shift of the sine wave. Finally, the physical solution can be written as follows,

$$v(x,t) = |A_1| \exp(-\alpha x) cos(\omega t - \beta x + \varphi_1) + |A_2| \exp(\alpha x) cos(\omega t + \beta x + \varphi_2) \tag{5.7}$$

where $A_1 = |A_1| exp(j\phi_1)$ and $A_2 = |A_2| exp(j\phi_2)$, the first term is the forward wave function and the second term represents the backward wave function. Note that (5.7) describes two sinusoidal waves with respect to both time and space. The speed of the signals along the transmission line can be calculated by setting the constant phase condition and the final result is shown in (5.8),

$$c' = \pm \frac{\omega}{\beta} \tag{5.8}$$

where ω is the angular frequency ($\omega = 2\pi f$) and f is the frequency of the signal. By fixing the time t and studying the periodicity along x it is possible

to calculate the wavelength λ expressed in meters (5.9).

$$\lambda = \frac{2\pi}{\beta} = \frac{c'}{f} \tag{5.9}$$

Considering a line section of total length l, if $\lambda \gg l$ the circuit can be studied using the lumped parameters and the exponential attenuation in (5.7) is not considered. As for the PLC, several standards can be used (CENELEC, ARIB, FCC and Chinese Band), where the lowest frequency is that of the CENELEC A sub-band, which is 3 kHz. Considering this lower limit, the use of lumped parameters could allow the analysis of about 5 km long line section. Since higher frequencies must be used to exploit the minimum attenuation of the most common coupling circuits, strong limitation occurs in the length of the network branch considered. For this reason, the entire simulation procedure presented in the next sections is based on the use of distributed parameters. Since the propagation characteristics depend on these electrical parameters and their values change when a malfunction occurs, the main idea of the prognostic method is to detect the presence of problems by studying the characteristics of the high-frequency signals transmitted.

5.2.1 Cable Parameters

In this work, the transmission lines taken into consideration are constituted by MV cables, whose structure can be related to that of a coaxial cable. A possible simplified model is proposed in [104], where the presence of the semiconductor screens interposed between the inner conductor and the insulation layer and between the insulation layer and the shield is neglected. In this model, the dependence on signal frequency of resistance and inductance is modelled as shown in (5.10) and (5.11),

$$R'(f) = \left(\frac{1}{2r_c} \sqrt{\frac{\mu_0}{\pi\sigma_c}} + \frac{1}{2r_s} \sqrt{\frac{\mu_0}{\pi\sigma_s}} \right) \sqrt{f} \tag{5.10}$$

$$L'(f) = \frac{1}{4\pi f r_c} \sqrt{\frac{\pi f \mu_0}{\sigma_c}} + \frac{1}{4\pi f r_s} \sqrt{\frac{\pi f \mu_0}{\sigma_s}} + \frac{\mu_0}{2\pi} \ln\left(\frac{r_s}{r_c}\right) \tag{5.11}$$

where r_c is the conductor radius, σ_c is the conductivity of the conductor material, r_s is the radius of the shield, σ_s is the conductivity of the shield and μ_0 is the vacuum magnetic permeability. As for the capacitance, the

standard formula (5.12) is adopted, where ϵ_0 is the dielectric constant of the vacuum and ϵ_r is the relative dielectric constant of the insulating material. Finally, the conductance can be calculated by multiplying the term $\omega C'$ by the loss factor $\tan\delta$ [81].

$$C'(f) = \frac{2\pi\varepsilon_0\varepsilon_r}{\ln\left(\frac{r_s}{r_c}\right)} \tag{5.12}$$

These parameters can be used to define the characteristic impedance of the MV cable. Starting from (5.3) and using equations (5.5) and (5.6) it is possible to express the current $I(x)$ as follows.

$$\begin{aligned} I(f) = \frac{\gamma}{Z'}(A_1\exp(-\gamma x) - A_2\exp(-\gamma x)) = \\ \sqrt{\frac{Y'}{Z'}}(A_1\exp(-\gamma x) - A_2\exp(-\gamma x)) \end{aligned} \tag{5.13}$$

Finally, characteristic impedance can be introduced, which is a complex quantity and can be calculated by means of (5.14). Strong variations of Z_0 at one point cause reflected signals detected by TDR systems.

$$Z_0 = \sqrt{\frac{Z'}{Y'}} = \sqrt{\frac{R' + j\omega L'}{G' + j\omega C'}} \tag{5.14}$$

To obtain impedance matching in PLC systems, it is necessary to close the transmission line on an impedance equal to Z_0.

5.2.2 Power Line Communications

As previously mentioned, PLC technologies are considered in this application as the main method for injecting high frequency signals into electrical networks [105] [106]. These communication systems are widely used in MV and High Voltage (HV) lines in order to transfer control information between power substations and between the Distribution System Operator (DSO) and users. From a general point of view, the structure of a PLC system can be summarized in three main parts: transmitter (TX), coupling circuits and receiver (RX). Transmitter and receiver are located at the opposite ends of the network branch taken into consideration and, to achieve the goal of this application, no modulation techniques are necessary. Therefore, the main task of transmitter modem is the creation of a carrier wave with

a specific frequency. As for the coupling circuits, they must connect PLC modems to the power line ensuring the lowest possible losses. Capacitive coupling is considered and this means that the final element used to connect the transmitter/receiver and the power line is a fixed value capacitor (Figure 5.2). The other fundamental parts of the coupling circuit are the high pass filter used to attenuate the mains voltage and the impedance matching transformer. The high-pass filter is a LC ladder network designed using the Butterworth approximation, where the last element is the fixed capacitor. The order of the filter must guarantee the safety of human operators and low voltage devices by significantly reducing the quantities at 50 Hz and their harmonics. A common rule is to attenuate power mains voltage to a level 10 dB lower than PLC voltage amplitude [82]. In some specific applications, a further verification of the attenuation up to the $50th$ harmonic is required and, possibly, an increase in the order of the filter is introduced to avoid interference with the PLC signal. Regarding the turns ratio of the impedance matching transformer, it is chosen to adapt the output resistance of the modems, typically 50Ω or 75Ω, to the characteristic impedance of the MV cable considered. Unfortunately, several factors may affect the value of the cable impedance, such as the frequency used for the transmission, and this means that a frequency independent match might not be effective. Since the introduction of a variable turns ratio is often too complex, a sufficiently wide frequency range where the return loss is higher than $15dB$ is considered acceptable for the PLC.

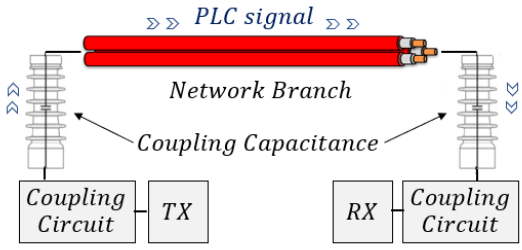

Figure 5.2: General model of a PLC system.

5.3 Cable Characterization

In this application, a specific prognostic procedure is proposed for a RG7H1M1 cable with a cross-section of $35mm^2$. Since the main goal is to detect the over-temperatures of the cables during normal line operation, it is necessary to define the electrical parameters in nominal conditions and in critical situations to train the neural classifier. Therefore, one of the main contributions of this work is to propose an experimental procedure for the frequency characterization of MV cables.

5.3.1 Experimental Set-Up

A $10m$ long cable section is used in this case to characterize the behaviour of the electrical parameters with respect to the signal frequency. The measurement device used to achieve this purpose is a *Rohde&Schwarz* Vector Network Analyzer (VNA), model ZNB 8, operating in the frequency range $(9kHz \div 8.5GHz)$. The band considered in this application is $(90kHz \div 1MHz)$. Since a unipolar cable is used, a line-to-ground configuration is tested, where the signal is injected between cable core and shield. The connection between power cable and VNA is created using a female N-type connector as shown in Figure 5.3. The inner conductor of the N connector is connected to one of the central wires in the cable structure. The parasitic parameters (residual resistance, inductance and capacitance) of the connection assembly are neglected since its length (a few centimetres) is much smaller than the 10 m cable length.

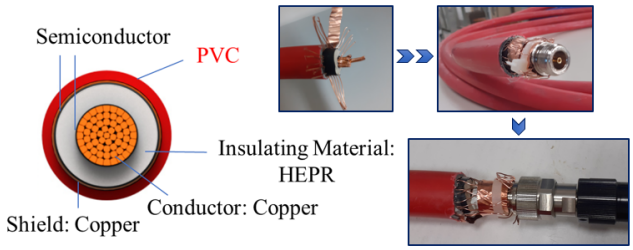

Figure 5.3: Measurement set-up: interface between cable and VNA.

5.3.2 Measurement Procedure

As previously mentioned, the line-to-ground configuration is considered, where the starting point of the cable stretch is connected to the VNA by means of the N connector and the opposite end is used to create two different loading conditions: short circuit and open circuit. The short circuit condition between the cable core and the shield allows the determination of the longitudinal parameters R' and L'. This measurement set-up is shown in Figure 5.4(a) and is used to extract the impedance Z'_{11} of the corresponding two port network in the frequency domain from $90kHz$ to $1MHz$. The real part of the measured impedance corresponds to the cable resistance R' and the imaginary part is related to the cable inductance L', see (5.15). On the other hand, the open circuit configuration (Figure 5.4b) is used to determine the behaviour of the capacitance C' and that of the conductance G' with respect to the signal frequency by measuring the admittance Y'_{11}, see (5.16).

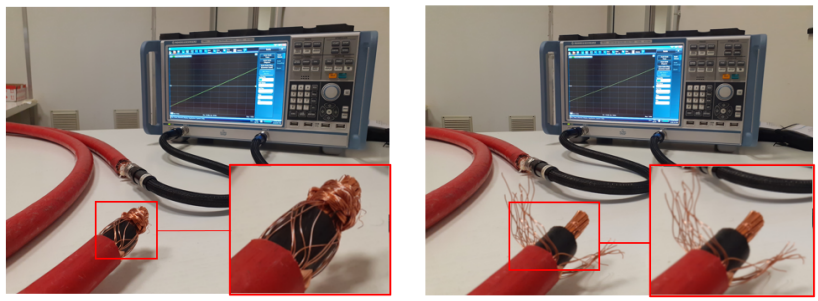

(a) (b)

Figure 5.4: Measurements configuration: (a) short circuit; (b) open circuit.

$$Z'_{11} = Z'_{sc} = R' + jX' = R' + j\omega L' \tag{5.15}$$

$$Y'_{11} = Y'_{oc} = G' + jB' = G' + j\omega C' \tag{5.16}$$

5.3.3 Characterization Results

The measurement procedure described above is performed at ambient temperature ($20°C$) obtaining the results shown in Figures 5.5.

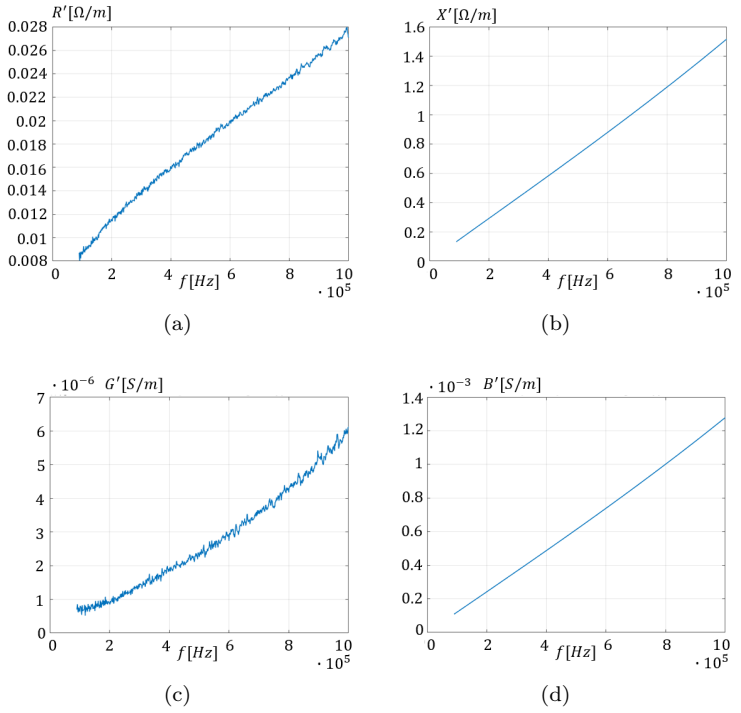

Figure 5.5: Measurement results: a) real part of the impedance; b) imaginary part of the impedance; c) real part of the admittance; d) imaginary part of the admittance.

The real part of the impedance and that of the admittance can be used directly to define the resistance and conductance of the cable (Figure 5.5(a) and Figure 5.5(b) respectively). The behaviours of R' and G' are consistent with the theoretical concepts described in section 5.2.1, where the resistance is proportional to the square root of the frequency and the conductance is proportional to frequency.

By fitting the measured curves (Figure 5.6 and Figure 5.8), it is possible to express the behaviour of R' and G' in the frequency domain using (5.17) and (5.18), note that R' and G' are expressed in $[\Omega/m]$ and $[S/m]$ respectively.

$$R' = (2.765 \cdot 10^{-5})\sqrt{f} - 0.0011 \tag{5.17}$$

$$G' = (5.835 \cdot 10^{-12})f - 3.477 \cdot 10^{-7} \tag{5.18}$$

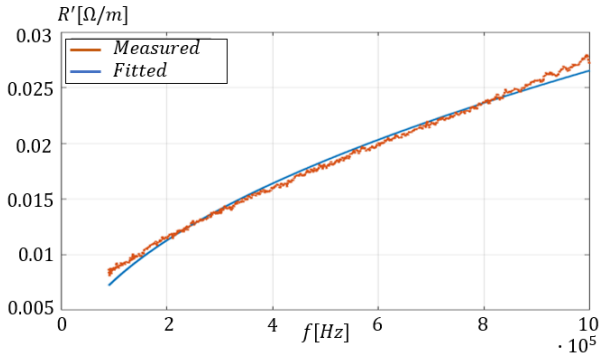

Figure 5.6: Resistance per unit of length.

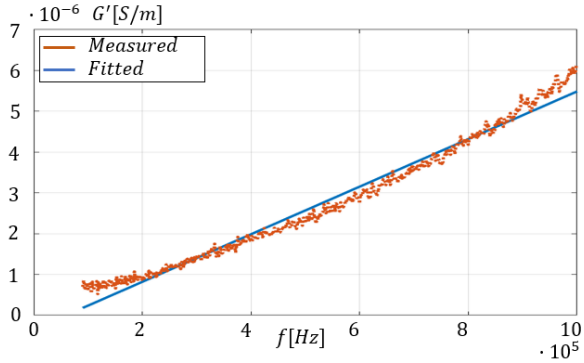

Figure 5.7: Conductance per unit of length.

It should be noted that a second order (quadratic) dependence on frequency can improve the fitting of the model of conductance to measurement results (see Figure 5.9). The simple linear dependence is however sufficient to capture the essential behaviour. In order to obtain inductance L' and capacitance C' from measurement results, it is necessary to introduce some

considerations. First of all, the measured imaginary parts are not directly $\omega L'$ and $\omega C'$. Indeed, the effects of electric field in the short circuit configuration and those of magnetic field in the open circuit set-up are significant at high frequencies. Equations (5.19) and (5.20) show the analytical form of the measured imaginary parts (L'_{mis} and C'_{mis}), where l is the cable length.

$$L'_{mis} = \frac{1}{1 - \omega^2 L' C' l^2} L' \tag{5.19}$$

$$C'_{mis} = \frac{1}{1 - \omega^2 L' C' l^2} C' \tag{5.20}$$

To calculate L' and C' it is necessary to solve a system of two equations containing (5.19) and (5.20) for each test frequency. The final results for inductance and capacitance are shown in Figure 5.8 and Figure 5.9 respectively.

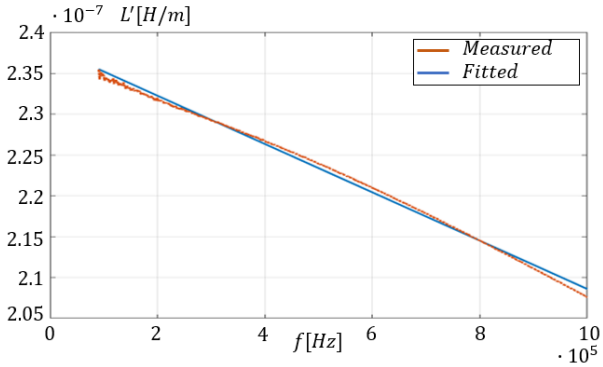

Figure 5.8: Inductance per unit of length.

Once the electrical parameters of the cable at the ambient temperature have been obtained, the initial values of the nominal conditions are known. In order to derive the variations of the electrical components with respect to the cable temperature, the same procedure can be repeated using a climatic chamber. These measurements are used in simulations to represent abnormal (overheating) working conditions.

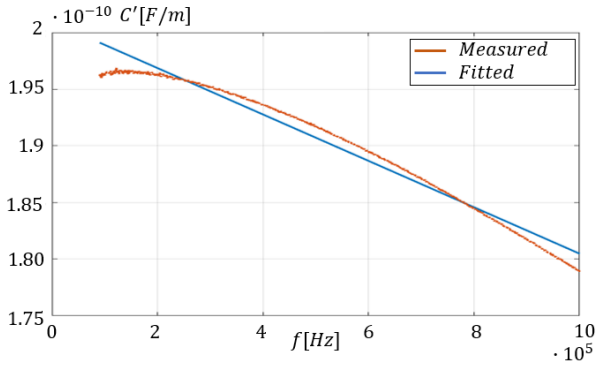

Figure 5.9: Capacitance per unit of length.

5.3.4 Temperature Effects

The behaviour of the electrical parameters with respect to the working temperature is investigated using the experimental set-up shown in Figure 5.10. A climatic chamber is used to create an increasing thermal stress from $20°C$ to $120°C$. Once a certain temperature is set via the chamber controller, two additional thermocouples are used to measure the temperature of the inner conductor and that of the interface between the cable and the VNA.

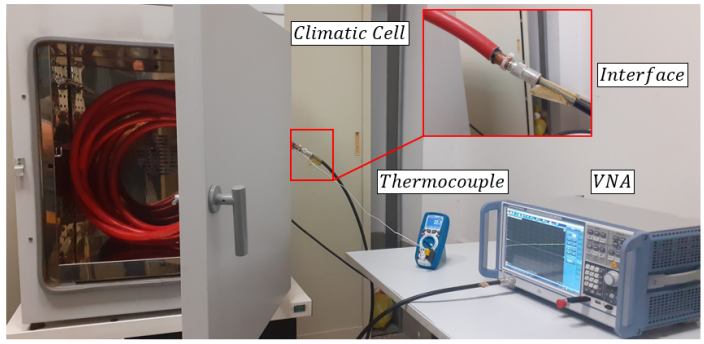

Figure 5.10: Experimental set-up.

The results of the characterization in the range $(90kHz \div 1MHz)$ demonstrate a linear dependence of the parameters R', L' and C' with respect to the cable temperature. In particular, the resistance and inductance increase

as the thermal stress increases while the capacitance decreases when the working temperature increases. Since the behaviour of the conductor resistance is usually expressed by (5.21), the same formulation can be used both for inductance and capacitance.

$$R'_T = R'_{20}[1 + \alpha_R(T - 20)] \tag{5.21}$$

Therefore, three different thermal coefficients $(\alpha_R, \alpha_L, \alpha_C)$ can be obtained through interpolation in the analysed frequency range to calculate the variations of R', L' and C' respectively. These results are shown in Figures 5.11.

Regarding the conductance of the cable under test, it is not possible to define a linear dependence with respect to the working temperature. However, the behaviour of G' presents some interesting characteristics and it is shown in Figure 5.11(d). In particular, the increase in conductance before reaching the maximum operating temperature of the cable could represent a fundamental index for the detection of abnormal over-temperatures. In fact, in order to improve the prognostic aspect of the monitoring procedure, it is important to detect variations in electrical components which do not introduce permanent degradation of the cable characteristics. In the following, for example, the limit temperature between nominal conditions and over-temperature corresponds to the conductance peak, which therefore contributes to the identification of the malfunction. This conductance behaviour is related to the cross-linking process of the insulation structure, which involves density variations due to the partial melting of the crystals [107].

5.4 Use of Multi-Layer Neural Network with Multi-Valued Neurons

In this section, the main characteristics of the MLMVN-based classifier are recalled and a specific organization of the output layer is described to achieve the identification and localization of over-temperatures.

5.4.1 Summary of the Main Theoretical Features

The configuration presented in section 3.2.3 is still used in this case. Therefore, the overall structure of the classifier is that of a feed-forward neural network with three layers, trained through a supervised learning algorithm

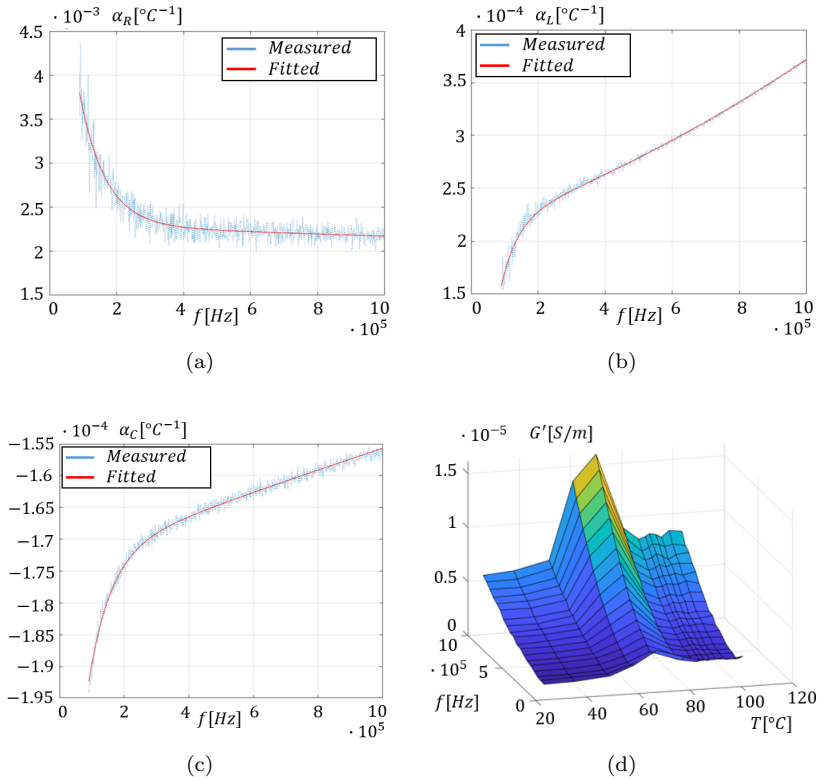

Figure 5.11: Thermal characteristics: a) thermal coefficient of the cable resistance; b) thermal coefficient of the cable inductance; c) thermal coefficient of the cable capacitance; d) behaviour of the cable conductance with respect to temperature and frequency.

based on the backpropagation procedure described in [73]. Remember that the main characteristics of this classifier compared to other machine learning techniques are the absence of derivative terms during the training phase and its complex nature. In fact, the gradient rule is not used for the correction of weights, which are complex numbers as well as the inputs and outputs. Figure 5.12 recalls the overall structure of the neural classifier, where $W_i^{k,m}$ is the i^{th} weight of the k^{th} neuron belonging to the layer m, $N_{(m-1)}$ is the number of neurons belonging to the hidden layer, N_m is the number of neu-

rons belonging to the output layer and $(X_1^s, X_2^s, \cdots, X_n^s)$ are the complex inputs.

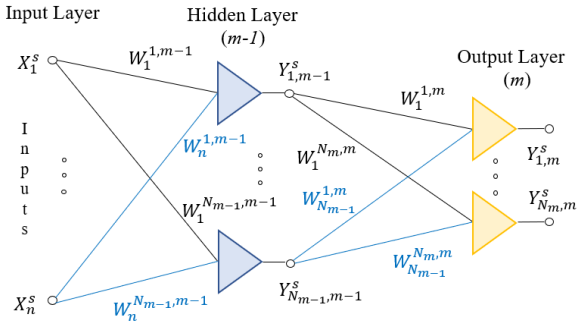

Figure 5.12: Global structure of the MLMVN.

Since a supervised learning algorithm is used, the dataset matrix must contain a significant number of samples ($s = 1, \cdots, N_s$) and the corresponding desired outputs on the last layer $D_{k,m}^s$. Again, since discrete neurons are used in the output layer, the terms $D_{k,m}^s$ correspond to the indexes of the desired sectors. Consequently, the error on the k^{th} neuron of the layer m obtained by processing the sample s is calculated by (5.22),

$$\delta_{k,m}^s = \frac{\varepsilon_b^{D_{k,m}^s} - \varepsilon_b^{Y_{k,m}^s}}{N_{m-1} + 1} \tag{5.22}$$

where $\varepsilon_b^{Y_{k,m}^s}$ is the lower border of the sector that contains the current weighted sum, $\varepsilon_b^{D_{k,m}^s}$ is that of the desired sector and b is the total number of sectors created by each neuron on the complex plane. These errors are backpropagated from the last layer to the input one using (5.23).

$$\delta_{k,m-1}^s = \frac{1}{N_{m-1} + 1} \sum_{i=1}^{N_m} \delta_{i,m}^s (W_k^{i,m})^{-1} \tag{5.23}$$

Remember that the training procedure presented in section 3.2.3 involves the calculation of the weight corrections by means of a batch algorithm. Therefore, all the errors are saved in a specific matrix and the corrections of the weights are calculated at the end of each training epoch.

5.4.2 Setting Up the Neural Classifier

In this application, the main objective of the MLMVN is the detection and localization of cable sections characterized by over-temperatures. To achieve this purpose, magnitude and phase of the received PLC signals are used as inputs of the neural classifier. The complex nature of these measurements makes MLMVN easily adaptable to the classification problem and no preliminary coding steps are required. Therefore, a generic input X_i is a complex number created by (7.5),

$$X_i = M_i \exp j\phi_i = M_i cos(\phi_i) + jM_i sin(\phi_i) \tag{5.24}$$

where M_i is the magnitude of the signal and ϕ_i is its phase. Multiple signals with different frequencies can be considered and the index i is used to distinguish them ($i = 1, \cdots, N_f$). As for the neurons belonging to the hidden layer, they are characterized by the continuous activation function shown in (5.25).

$$Y = P(z) = \frac{z}{|z|} = \exp(jArg(z)) = cos(Arg(z)) + jsin(Arg(z)) \tag{5.25}$$

Therefore, the outputs of the hidden neurons are complex numbers located on the unit circle. These values are processed by the neurons belonging to the output layer using the discrete activation function (5.26).

$$P(z) = \varepsilon_b^Y = \exp\Big(j2\pi\frac{Y}{b}\Big) \quad if \quad \frac{2\pi Y}{b} \leq Arg(z) < 2\pi\frac{(Y+1)}{b} \tag{5.26}$$

Note that binary neurons are used in the following simulation procedure, each of which divides the complex plane into 2 sectors (high level and low level). This means that one neuron is implemented for each possible malfunction. When a neuron is at a high level it indicates the presence of the corresponding problem. The nominal situation presents all neurons at a low level. In this case, the output errors are defined as shown in Figure 5.13.

5.5 Simulation Results

5.5.1 Case Study

In order to verify the performance of the proposed prognostic method, the monitoring of a $5km$ long medium voltage network is proposed. The main

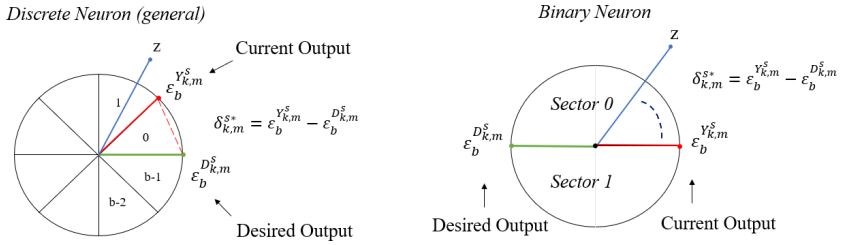

Figure 5.13: Representation of the discrete activation function.

idea is to demonstrate the effectiveness of the neural classifier to prevent abnormal cable degradation in a network branch between two secondary substations. The monitoring activity is divided into two phases: identification of the overheating entity and localization of the overheated cable section. First of all, the Simulink model of the electrical infrastructure is built using functional blocks called *Transmission Line*, belonging to the Simscape library. The use of three blocks connected in cascade as shown in Figure 5.14 allows to simulate all the possible positions of an overheated cable section with different extensions. In order to bring the simulation closer to a real situation, the interpolations of the experimental measurements presented in section 5.3.3 are used to define the values of R', L', C' and G'. The communication system model is created in Simulink on the basis of the information reported in section 5.2.2. Therefore, the transmitter consists of an alternating voltage source, a series resistance of 50Ω and a matching transformer whose winding ratio is calculated using the nominal characteristic impedance of the line Z_0. As for the coupling circuit, it is a fourth order high pass filter dimensioned using Butterworth approximation with a fixed cut-off frequency at $15kHz$. On the opposite side of the line, the structure of the communication system is mirrored, and the last element of the receiver is a resistance of 50Ω. The propagation constant of the transmission line can be evaluated as described in [83] and [84], taking into account the topology of the network branch and the presence of other power devices. In this application, the Simulink model summarized in Figure 5.14 is managed by a Matlab script in order to create the dataset matrix needed for MLMVN training. As mentioned above, this matrix contains magnitude and phase measurements of the transmitted voltage waveforms. Three signals with three different frequencies are used: the two extremes and the central value of the band considered. Once the

frequencies of the signals are defined, various simulations are performed to create two datasets. The first is used to identify the extent of the possible thermal malfunction while the second allows its localization.

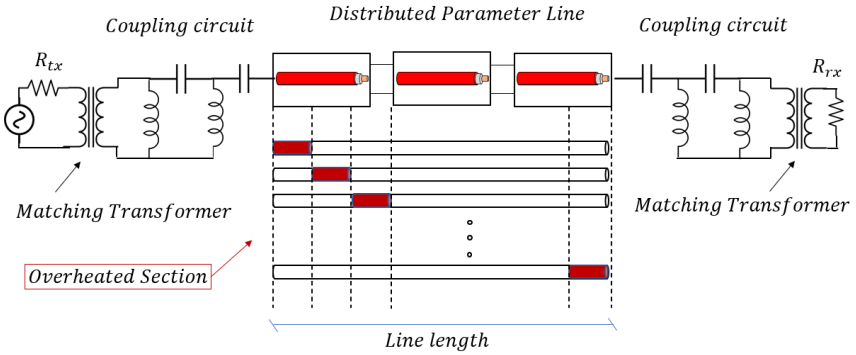

Figure 5.14: Overall model of the network branch considered.

5.5.2 Classification results

The first phase of the proposed monitoring method is aimed at classifying the extent of the over-temperature. Therefore, different lengths of thermal malfunction are simulated starting from $250m$ up to $1km$ with a $250m$ step. Since the maximum operating temperature provided by the cable manufacturer is $105°C$, the highest level used in these simulations is $110°C$. As regards the nominal conditions, the range $(50°C \div 70°C)$ is considered, which can be obtained using 70% of the nominal current in standard installation conditions. In this case, the main objective of the classifier is to distinguish the four possible malfunction conditions and the nominal situation. Therefore, four binary neurons are used in the output layer of the MLMVN-based classifier. The percent Classification Rate ($CR\%$) obtained for the $(95 \div 148.5)kHz$ and $(95 \div 400)kHz$ bands is presented in Table 5.1. The first interval corresponds to the sub-bands CENELC B, C and D while the second is included in all other PLC standards.

In this configuration, the monitoring system can be used to modify the maintenance schedule. For example, when the system detects an over-temperature of 250 meters, the line operator can intervene in the following ways:

Band	$(95 \div 148.5)kHz$	$(95 \div 450)kHz$
$CR\%$	97.68	98.61

Table 5.1: Classification results: severity recognition

- check the line current to verify the presence of a temporary overload condition;
- in the case of overload, investigate the causes;
- if the current is normal, it is possible to intervene or monitor the evolution of the phenomenon; in fact, the classifier allows the monitoring of the increase in extension of the overheated section at $500m$, $750m$ and $1km$.

To intervene as quickly as possible, it is useful to locate the section along the line. A second neural classifier is therefore proposed, capable of recognizing the presence and position of a $250m$ long cable section characterized by over-temperature. To achieve this purpose, 20 binary neurons are used in the output layer of the MLMVN, each of which corresponds to a specific position of the thermal malfunction from the starting point of the line to the opposite end. The classification results obtained during the training procedure in the frequency range $(95 \div 450)kHz$ are shown Figure 5.15 and the main characteristics of the MLMVN are summarized in Table 5.2.

CR% Training	CR% Validation	Hidden Neurons	Output Neurons	Training Time
98.02	96.03	45	20	4'40"

Table 5.2: Classification results: severity recognition

Finally, a comparison between MLMVN and other classifiers commonly used in the literature is presented in Table 5.3.

	MLMVN	SVM	Decision Tree
$CR\%$	96.03	93.65	84.92

Table 5.3: Comparison between MLMVN and other techniques.

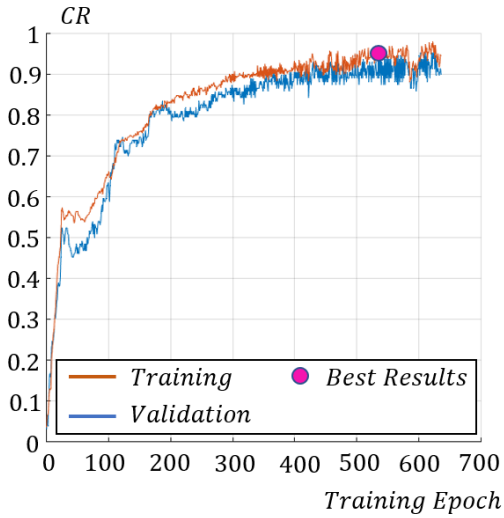

Figure 5.15: Classification results: detection and localization.

5.6 Conclusion

In conclusion, it can be stated that the prognostic method proposed here allows the detection and localization of thermal malfunctions in MV underground networks with a high level of accuracy (96%). The MLMVN-based classifier focuses on the localization of cable over-temperatures $(105 \div 110)°C$ when they concern $250m$ of a $5km$ long line. The monitoring procedure is based on the transmission of high frequency signals through PLC systems and allows the identification of abnormal working temperatures thanks to the variation of the received voltage waveforms. In order to define these variations, a complete experimental procedure was presented, aimed at characterizing the cable considered under nominal conditions and in situations of high thermal stress. The experimental procedure and measurement results can be easily adapted to many different cables and represent one of the main contributions of this work. Furthermore, the Simulink model used for simulations represents a very useful tool for studying communications on power lines and allows the development of the monitoring method for different line topologies.

Chapter 6

Application: Experimental Prevention of Zeta Converter Failures

This chapter develops the main steps of the prognostic procedure applied to DC-DC power converters. Multi-Layer neural network with Multi-Valued Neurons (MLMVN) is used to process time-domain measurements, thus detecting and locating any possible malfunction. Thanks to the low computational complexity, the proposed method operates on-line, estimating the deviations of the passive components from their nominal values: this allows control strategies to be promptly adopted and operation of the DC-DC converter to be kept in high-efficiency and reliability conditions. Since measuring the voltage and current on each component increases the complexity of the system, a testability analysis is proposed with the aim of identifying the minimum number of measurements needed to distinguish the fault classes. To make the testability phase easier and more intuitive, a graphical approach is used. As a case study, prognostic analysis has been applied to prevent catastrophic failures in a synchronous Zeta converter. Several fault conditions have been analysed through simulations and experimental tests. The results obtained show that MLMVN offers better performance than other solutions commonly used in

the literature, such as the Support Vector Machine (SVM). [1]

6.1 Introduction

Power converters have a large application in fields like automotive, renewable energies, aircraft, smart grid and other industrial and consumer applications. These circuits are the most vulnerable parts of integrated power systems [108] [109], and their failures often produce damages or downtimes which requires costly maintenance procedures. To avoid these problems, redundancy has historically been adopted by increasing the reliability of the entire system. Although this solution allows for greater fault tolerance capacity, it also increases the cost and size of the power converters. To overcome this limitation, the design for reliability approach has been developed in recent years, which consists in explicitly considering reliability during the design process. This approach together with continuous monitoring of DC-DC converters allows an increase in the expected lifetime. The monitoring can be implemented through different approaches, such as model-based, signal-based, or knowledge-based techniques [5] [6]. The recent diffusion of artificial intelligence in the industrial sector has led to the development of monitoring systems based on neural networks [110] and other machine learning algorithms [111], focusing on the data-driven approach. Most of these techniques focus on power semiconductors, such as MOSFETs and IGBTs [112] [113]. Usually, the monitored parameter is the conduction resistance of these active components, which increases with ageing [114]. As shown in [115], the conduction resistance is approximately constant when the semiconductor operates in healthy conditions, while it exponentially increases just before its failure. Consequently, the failure of a switching semiconductor is easily detected because it quickly affects the power converter operation. This behaviour justifies the large number of papers related to the use of redundancy of semiconductor components to make the systems fault-tolerant, usually connecting modules in parallel to guarantee the functioning of the system until the repair, allowing continuity of service.

To obtain a monitoring system capable of preventing catastrophic failures in DC-DC converters it is crucial to consider passive components, whose

[1] This chapter has been published as "Failure prevention in DC-DC converters: theoretical approach and experimental application on a Zeta converter" in *IEEE Transactions on Industrial Electronics (2022).*

variations from the nominal values represent possible malfunctions and occur over a longer time [116]. Therefore, this application focuses on detecting changes of passive component values using MLMVN.

In the literature there are some works related to the monitoring of power converters using machine learning algorithms [117] [118]. One of the most critical aspects is the number of measurements required to identify different failure scenarios and the absence of the prevention aspect. In [42] a possible monitoring approach for two different DC-DC power converters is proposed, where a continuous version of a MLMVN is used for the parametric identification of passive components. This neural network is used to solve a regression problem that requires a large number of measurements to identify the exact values of a few elements. In particular, current and voltage measurements are used to obtain the identification of two passive components in a Buck and in a Boost topology [42]. To overcome these limitations, the prognostic procedure proposed here is based on a discrete MLMVN, which allows the detection of malfunctions and the localization of their causes using a small number of voltage measurements. Therefore, the main objectives can be summarized as follows:

- To propose a practical application of the graphical Testability assessment method, which facilitates the selection of test points avoiding ambiguity situations. In fact, variations on different passive components could introduce indistinguishable effects on measured quantities. The Testability study determines how many and which measurements are required for the detection and exact localization of malfunctions [119]. Differently from existing testability analysis [28] [29], the proposed graphical representation does not require the extraction of the analytical transfer function. The testability curves obtained with the proposed method are suitable for DC-DC power converters, where different topologies alternate during normal operation and the mathematical approach may be not easily applicable.

- To develop a neural classifier based on a three-layer MLMVN capable of processing time-domain measurements. The overall structure contains continuous neurons in the hidden layer and binary neurons with discrete activation function in the output one. Therefore, the proposed classifier has one output for each passive component and allows the localization of malfunctions, thus reducing recovery times and increasing the reliability of the converter. During the training phase

of the MLMVN the batch algorithms presented in [76] are used, after adapting the error calculation to the structure of the classifier and introducing the *winner takes all* rule.

- To validate experimentally the proposed failure prognosis technique on a Zeta converter.

6.2 Zeta Converter

In recent years DC-DC conversion has been greatly developed in many sectors of the industrial world and the Zeta converter has been applied with excellent results in terms of power density and output ripple [120]. Thanks to its simple structure and its ability to operate as a buck-boost converter with a non-inverted output, it has been used in many different applications: as an electric vehicle battery charger powered by a PV array [121], as a DC motor controller [122] and as grid interface in a standalone DC microgrid [123]. The elementary circuit of the synchronous Zeta converter is shown in Figure 6.1.

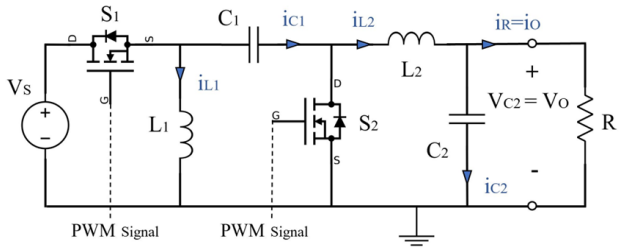

Figure 6.1: Topology of Zeta converter.

The circuit results in a fourth-order step-up/step-down converter characterized by two inductors (L_1 and L_2) and two capacitors (C_1 and C_2). This topology guarantees a non-inverted polarity of the output voltage, and this represents one of the most important advantages over other transformerless DC-DC buck-boost converters. The Pulse Width Modulation (PWM) technique is used to drive MOSFETs S_1 and S_2 at a switching frequency f. Assuming the converter is operated under a Continuous Conduction Mode (CCM), during a switching period $T = 1/f$, two topologies alternate depending on $S1$ state: On period (S_1 ON and S_2 OFF) and Off period (S_1

OFF and S_2 ON). The first one, the Switch-On period, lasts $t_{on} = DT$, and the second one, the Switch-Off period, lasts $t_{off} = (1-D)T$. During DT, L_1 is charged by the input voltage source and L_2 by capacitor C_1. This means that both inductors are in the charging state and their currents linearly increase. During Off-mode, L_1 and L_2 discharge through C_1 and the resistive load R respectively. Figure 6.2(a) shows the topology of the Zeta converter during the On period while Figure 6.2(b) shows the topology during the Off period.

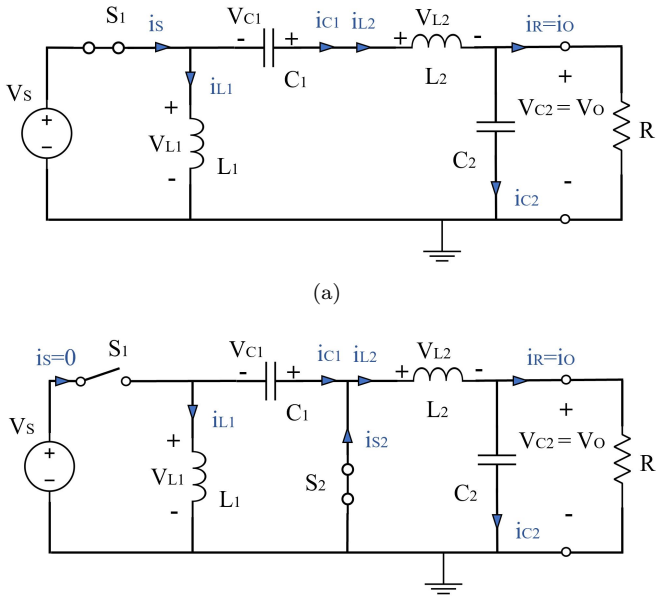

Figure 6.2: Circuit topologies: a) On period; b) Off period.

6.2.1 Dimensioning and simulation

To develop the prognostic procedure focused on the passive component variations a Simulink model of the synchronous Zeta converter has been implemented. By using this model, the operation of the circuit in every working condition is verified and the dataset matrix, needed for the training phase of the classification tool, is generated. The Simulink-Simscape library is used to

achieve this purpose and common Simulink blocks are introduced to generate the PWM signal driving S_1 and S_2 with opposite phases. The design procedure shown in [124] has been used. Table I summarizes the nominal values of the converter components, ensuring operation in CCM and a peak-to-peak output ripple lower than 5%.

$L_1[\mu H]$	$L_2[\mu H]$	$C_1[\mu F]$	$C_2[\mu F]$	$R[\Omega]$
380	380	1.4	1.4	10

Table 6.1: Converter components.

To derive a monitoring method capable of detecting changes in passive components, a set of acceptable intervals around their nominal values must be defined. These intervals are called nominal ranges and have been chosen as $\pm 15\%$. Variations inside the specified ranges are considered acceptable as they guarantee an output ripple of less than 10% and CCM operation.

6.2.2 Prototype of the Synchronous Zeta Converter

To verify the performance of the prognostic method, a physical Zeta converter prototype has been built as shown in Figure 6.3. Given the simple topology of the converter, a single Printed Circuit Board (PCB) has been used, and several test points have been included to obtain the measurements of all voltages across the components, while current measurements are not needed by the proposed method.

Since the main purpose of the analysis is to detect the variation of the passive components, the positioning of the inductors has been chosen to facilitate their replacement and different capacitor values have been obtained by connecting several elements in parallel. The two switches are N-channel STC3022AL power MOSFETs. The other elements of the circuit are given in Table 6.2.

As shown in Figure 6.3 there are four different Input/Output (I/O) sections in the PCB: an external 24 V power supply is used to supply the integrated power MOSFET gate drivers. Two BNC connectors are used to inject the control signals with opposite phases and, finally, the other two I/O sections are used to apply the DC source and power the load.

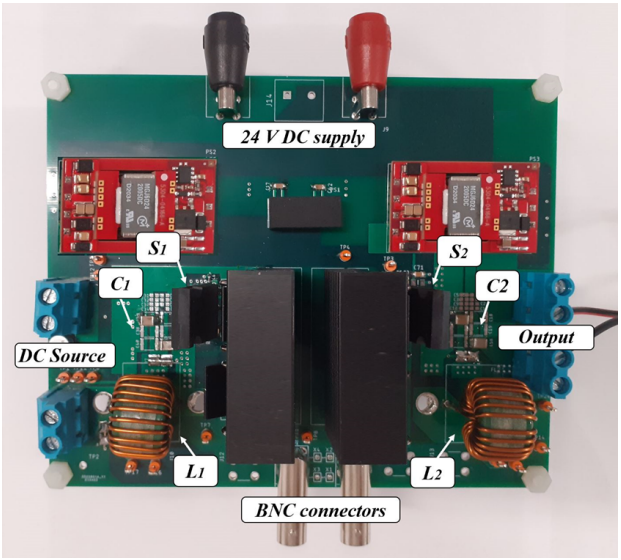

Figure 6.3: Experimental prototype of the synchronous Zeta converter.

Sign	Full Name	Type
E1-E2	MGJ6D242005DC	5.7kVDC Isolated 6W Gate Drive SIP DC-DC Converter
E3	TEC 3-2411WI	Isolated 3W DC-DC Converter
E4-E5	1EDC60H12AHXUMA1	Single Channel Isolated IGBT Driver

Table 6.2: Circuit elements.

6.3 Prognostic Procedure: Theoretical Concepts

6.3.1 Fault Classes

This application proposes a prognostic approach based on time domain measurements of four voltages. The main objective is to identify the variation of the components outside the nominal range in the case of a single failure hypothesis. This means that only one component can change at a time and five classes of failure are considered. Table 6.3 summarizes these classes, where

the malfunction condition of the inductors shows a reduction in a proportion $(15 \div 90)\%$ with respect to the nominal value, and that of the capacitors in a proportion $(15 \div 40)\%$. These intervals were chosen to test the effectiveness of the prognostic method even during Discontinuous Conduction Mode (DCM).

N class	L_1 $[\mu H]$	L_2 $[\mu H]$	C_1 $[\mu F]$	C_2 $[\mu F]$
0	$(323 \div 437)$	$(323 \div 437)$	$(1.2 \div 1.6)$	$(1.2 \div 1.6)$
1	$(38 \div 323)$	$(323 \div 437)$	$(1.2 \div 1.6)$	$(1.2 \div 1.6)$
2	$(323 \div 437)$	$(38 \div 323)$	$(1.2 \div 1.6)$	$(1.2 \div 1.6)$
3	$(323 \div 437)$	$(323 \div 437)$	$(0.8 \div 1.2)$	$(1.2 \div 1.6)$
4	$(323 \div 437)$	$(323 \div 437)$	$(1.2 \div 1.6)$	$(0.8 \div 1.2)$

Table 6.3: Fault classes.

Many factors such as ageing or deterioration due to abnormal environmental conditions can lead to the variation of the passive component values and this modifies the converter working conditions. The most common failure modes for inductors are short circuits between turns and the saturation of the magnetic core. Therefore, the malfunction conditions of L_1 and L_2 only result in a reduction of the inductance value below the nominal range. For capacitors C_1 and C_2 the most common causes of failure are ageing, overload and over-temperature. All these situations can produce a deterioration of the dielectric with a consequent reduction of their capacitance.

Several techniques can be found in the literature to introduce a prognostic method in passive circuits [8] [125]. However, the main problems are the ability of these methods to work on-line and their capability of identification of the components in the worst state of health. Moreover, these frequency-domain based methods can fail when applied to time-varying circuits as DC-DC converters are. Recalling that the MLMVN-based classifier falls in the category of supervised learning algorithms, it is necessary to use a dataset containing several examples of correct classifications. Therefore, the dataset matrix contains a high number of examples n_s for each fault class and the corresponding index in the last column (6.1). Each example consists of eight measurements: average values and ripples of the four voltages. The voltages used are those across the passive components, and to understand their effectiveness, it is necessary to perform the testability evaluation.

$$\begin{bmatrix} V_{L_1m}^1 & V_{L_1r}^1 & V_{L_2m}^1 & V_{L_2r}^1 & V_{C_1m}^1 & V_{C_1r}^1 & V_{C_2m}^1 & V_{C_2r}^1 & 0 \\ V_{L_1m}^2 & V_{L_1r}^2 & V_{L_2m}^2 & V_{L_2r}^2 & V_{C_1m}^2 & V_{C_1r}^2 & V_{C_2m}^2 & V_{C_2r}^2 & 0 \\ \vdots & \vdots & \vdots & \vdots & \vdots & \vdots & \vdots & \vdots & \vdots \\ V_{L_1m}^{5n_s} & V_{L_1r}^{5n_s} & V_{L_2m}^{5n_s} & V_{L_2r}^{5n_s} & V_{C_1m}^{5n_s} & V_{C_1r}^{5n_s} & V_{C_2m}^{5n_s} & V_{C_2r}^{5n_s} & 4 \end{bmatrix} \tag{6.1}$$

6.3.2 Testability Assessment

As mentioned before, the main idea of prognostic analysis is to use the voltages across the passive components to identify the working condition of the Zeta converter. In this sense, the choice of test points plays a fundamental role because it makes the fault classes distinguishable. In fact, the variation of one component introduces a change in multiple measurements. This change must be different from that introduced by the variation of other components. If the choice of measurements allows the identification of all classes without ambiguities, the circuit under test is completely testable.

In this application, the graphical method presented in section 3.5 is used. Since it is based on the less common time domain approach, the most important theoretical concepts are recalled below. Testability is still linked to the solvability degree of the failure equations which, in this case, refer to time-dependent quantities. In fact, as shown in [28], input/output relationships or specific waveforms are sampled in steady state conditions and the analytical form of these quantities is used to obtain a set of failure equations in which the unknowns are the components and the inputs are kept constant. Therefore, the symbolic vector of the sampled quantities is (6.2),

$$\mathbf{y}_T(\mathbf{p}, \mathbf{u}_0) = [\mathbf{y}(t_1, \mathbf{p}, \mathbf{u}_0), \cdots, \mathbf{y}(t_{n_t}, \mathbf{p}, \mathbf{u}_0)] \tag{6.2}$$

where $\mathbf{u}_0$ contains the constant input samples and $\mathbf{p}$ is still the vector of the unknown parameters. Introducing the vector of the measurements $\mathbf{y}_T^*$ it is possible to obtain the system of the fault diagnosis equations (6.3) whose Jacobian allows the calculation of Testability.

$$\mathbf{y}_T(\mathbf{p}, \mathbf{u}_0) = \mathbf{y}_T^* \tag{6.3}$$

In general, if the system of equations is completely solvable the Testability is maximum and equal to the total number of passive components belonging to the circuit. If, on the other hand, the Testability is less than

the total number of variable components, there are two or more elements that introduce the same variation on the measurements. This means that it is possible to detect the problem, but the specific component causing the improper converter operation cannot be located. In such a case, these elements belong to the same Ambiguity Group (AG), which is defined as set of components that cannot be simultaneously considered defective because they introduce indistinguishable variations on the selected measurements. In the case of time-variant circuit, the complexity of the method increases because the converter circuit goes through multiple topologies inside a switching period. This means that different testability ratings can be obtained in each situation, and the computational cost significantly increases, as reported in [28] [47]. For this reason, a graphical evaluation of Testability is proposed for the prognostic analysis of the Zeta converter. To achieve this goal, the Simulink model described above is managed by a Matlab script, which sets the gradual variation of the components from the nominal value up to the malfunction conditions shown in Table 6.3. According to the single failure hypothesis, these variations are not simultaneous. For each situation, measurements of the four voltages are carried out and, consequently, the corresponding ripples and mean values are calculated. By plotting these measurements in a $2D$ graph with the average values on the horizontal axis and the ripples on the vertical axis, the Zeta converter Testability is studied. Figures 6.4 show the plots obtained by setting $V_s = 15V$. Here, the Testability is maximum because there are no overlapping curves repeated in all the situations. In general, the presence of two or more curves very close to each other indicates a possible reduction in Testability, because the variations of the components introduce the same effect on the measurement. If this situation is repeated for each graph, the corresponding components are indistinguishable, and it is necessary to add new measurements or modify some test points. In the case of the Zeta converter, there are no critical situations, and the Testability is maximum. Furthermore, the analysis of Figure 6.4 allows the reduction of the measurements to only two voltages. In fact, the situation of partial ambiguity shown in Figure 6.4(a) between the red and purple lines could be compensated by the distance of these curves in Figure 6.4(b). The same is for purple and yellow plots in Figure 6.4(c) and Figure 6.4(d). Therefore, the possibility of monitoring the Zeta converter by using only two voltage measurements is one of the crucial aspects to verify through experimental tests.

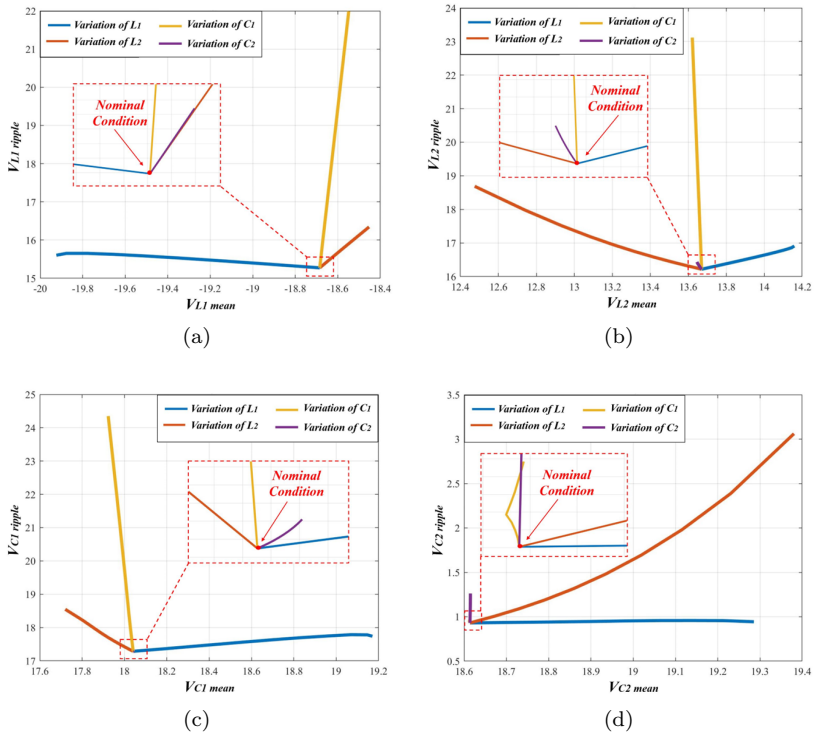

Figure 6.4: Testability curves: a) voltage on L_1; b) voltage on L_2; c) voltage on C_1; d) voltage on C_2.

This not only avoids current measurements but also significantly reduces the number of test points.

6.3.3 Neural Classifier

The smart tool used in this application is the MLMVN based classifier presented in section 3.2.3, which can detect parametric faults under the single failure hypothesis. Figure 6.5 recalls the global structure of the classifier, where $W_i^{k,m}$ is the i^{th} weight of the k^{th} neuron belonging to the last layer (called layer m), $n_{(m-1)}$ is the number of neurons belonging to the hidden layer, n_m is the number of neurons belonging to the output layer and $(X_1^s, X_2^s, \ldots, X_n^s)$ are the inputs. Note that the superscript s is used to

indicate the processed example of the dataset.

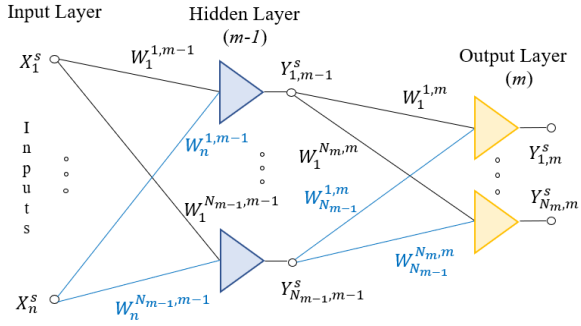

Figure 6.5: General structure of the MLMVN-based classifier.

This computational algorithm uses continuous neurons in the hidden layer and discrete binary neurons in the output layer. This means that each output neuron creates two sectors in the complex plane: the first corresponds to the upper half plane $[0, \pi)$ and is encoded by the value 0, the second corresponds to the lower half plane $[\pi, 2\pi)$ and is identified by the value 1. Consequently, the first sector of each neuron indicates the nominal condition of the corresponding analog component, while the second sector is used to describe the presence of a malfunction. This means that four neurons are used in the output layer, one for each electrical component, and the nominal condition of the converter corresponds to a combination of four zeros. It should be noted that the first output neuron is used to detect a malfunction on the inductor L_1, the second neuron is used to detect a problem on C_1, the third output indicates a change in L_2, and the last neuron is used to describe an abnormal working condition of the capacitor C_2. Table 6.4 summarizes the fault classes used in this case and the corresponding values of the outputs.

When the output of a binary neuron is 0 it means that the weighted sum z falls in the upper half plane and the complex value of this output is $(1+j0)$. When the output of a binary neuron is 1 it means that the weighted sum z falls in the lower half plane and the complex value of this output is $(-1+j0)$. Therefore, the desired classes shown in the last column of the dataset matrix (6.1) must be converted in the corresponding output combinations during the training phase. In this way, it is possible to calculate the error for each output neuron and apply the backpropagation procedure.

Class	Neuron 1	Neuron 2	Neuron 3	Neuron 4
0	0	0	0	0
1	1	0	0	0
2	0	1	0	0
3	0	0	1	0
4	0	0	0	1

Table 6.4: Fault classes and output values.

Remember that the error terms in the case of discrete neurons can be calculated through (6.4),

$$\delta_{k,m}^{s} = \frac{\varepsilon_b^{D_{k,m}^{s}} - \varepsilon_b^{Y_{k,m}^{s}}}{n_{m-1}+1} \tag{6.4}$$

where $\varepsilon_b^{D_{k,m}^{s}}$ is the complex number corresponding to the lower border of the desired sector and $\varepsilon_b^{Y_{k,m}^{s}}$ is that of the sector containing the current weighted sum of the inputs. By using the backpropagation procedure presented in section 3.2, the errors on the hidden layer are calculated by (6.5).

$$\delta_{k,m-1}^{s} = \frac{1}{(n+1)} \sum_{i=1}^{n_m} \delta_{i,m}^{s} (W_k^{i,m})^{-1} \tag{6.5}$$

Figure 6.6 summarizes the functioning of the output neurons. Since in this application the QR decomposition is implemented as a batch algorithm, the corrections of the weights are calculated at the end of each training epoch. Therefore, the standard procedure used to train the MLMVN-based classifier can be summarized as follows: each example belonging to the dataset is processed individually and the last element of the row is used to calculate the desired combination of the outputs as shown in Table 6.4. Since binary neurons are used in the last layer, all the desired outputs equal to zero correspond to the lower border of the upper half plane $(1 + j0)$, while the desired output equal to 1 corresponds to the lower border of the interval $[\pi, 2\pi)$, which is $(-1 + j0)$. Once the desired outputs are calculated, all complex weights are initialized to random values and the inputs are processed to obtain the current outputs. Starting from these values, output errors are calculated (6.4) and back-propagated (6.5) without any correction. The use of the QR decomposition in this last phase allows the reduction of the

computational cost and the speeding up of the training process.

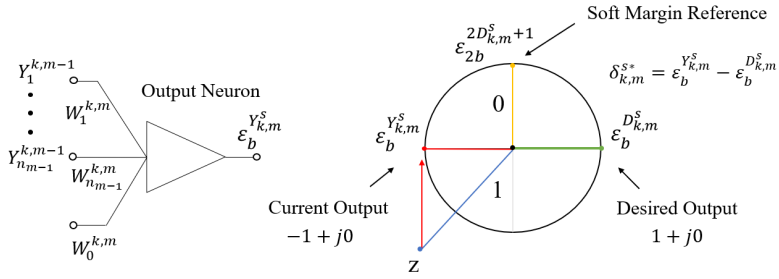

Figure 6.6: Functioning of output neurons.

6.4 Prognostic Procedure: Experimental Validation

The experimental procedure proposed here is organized as follows:

1. the first step is the Testability evaluation of the Zeta converter using its Simulink model;
2. starting from the Testability curves it is possible to select the best test points avoiding ambiguity situations and to create the dataset matrix directly from the Simulink model;
3. the simulated voltage measurements belonging to the dataset refer to every possible working condition of the converter, and they are used to train the MLMVN based classifier in the Matlab environment;
4. once the training phase has been completed, the performance of the classifier in recognizing the state of health of the Zeta converter is verified using real measurements extracted from the prototype;
5. to obtain real measurements of each possible working condition, passive components are substituted with others having different values.

Note that the creation of the dataset is completely carried out in Simulink by using the Zeta converter model without introducing real measurements in the training phase. Therefore, a Matlab script is used to generate 100

samples ($n_s = 100$) for each fault class. This means that for any class of Table 6.3, 100 random values are generated for each component in both the nominal and the malfunction ranges. These values are used in Simulink to simulate the operation of the converter and extract the voltages across the passive components with a switching frequency of $50kHz$ and a fixed $D = 0.6$. As a result, the dataset matrix is created as shown in (6.1). A $(5 \div 20)V$ range is considered for the input voltage. In this way, it is possible to simulate the operation of the monitoring system in the presence of a variable power source. During the training phase, only four values are used: 5, 10, 15, 20 V. Instead, different values than those utilized for the training, belonging to the range $(5 \div 20)V$ are used in the experimental validation. This verifies the generalization capability of the classifier and facilitates the training phase. Similarly, to obtain a robust classification system with respect to load variations, it is necessary to include resistance R values different from the nominal one during the training phase. In particular, to maintain a high classification rate, all possible operating conditions must be considered in correspondence with all possible combinations of input voltage/load resistance. Therefore, variations in input source and load resistance pose no problem for classification performance when properly considered during the training phase. Obviously, the greater is the number of possible variations, the more time it takes to create the dataset matrix and train the neural classifier. The computation cost in extremely variable situations represents the main limitation of the proposed classifier, whose hidden layer must be modified according to the case studied. Once the dataset has been obtained, the Matlab application presented in section 3.2 is used to train the MLMVN. As said above, the implemented learning procedure is based on the QR decomposition, and this allows the reduction of training times and computational efforts. It should be noted that 80% of the dataset is processed to calculate the corrections (learning-phase) and the remaining 20% is used to verify the classifier performance (testing phase). The succession of the learning phase and the testing phase represents a training epoch. The quality of the classification is evaluated in both phases through the Classification Rate (CR), which is defined as the ratio between the correctly classified samples and the total number of samples. The most significant CR is calculated during the testing phase because it refers to data not used for the correction of the weights during the previous training epochs. The Cross Validation method can be introduced to process all the information belonging to the dataset for

both the training and testing phases, obtaining a more accurate performance evaluation. The Matlab application used here offers both types of validation and the CR considered below is the one obtained in the test phase through the Cross Validation method. Remember that the proposed MLMVN can use the input measurements in three different ways. The first of them is the most used in the literature and generates a complex number starting from each real measurement. In the other two cases, each pair of dataset columns is used to create the corresponding complex numbers. The main characteristics of these methods are recalled below.

1. *Single Input* mode: each real measurement belonging to the dataset is used as phase of a complex number with magnitude equal to 1.
2. *Magnitude-Phase* mode: In this case, the numbers belonging to the first column of each pair is the magnitude of the complex numbers, while the second column contains the phases.
3. *Real-Imaginary* mode: the numbers belonging to the first column of each pair is the real parts of the complex numbers, while the second column is used to create the imaginary parts.

These three solutions are considered and compared during the simulations and the experimental tests. The first result shown in Figure 6.7 refers to the training procedure performed with 60 neurons in the hidden layer and setting the *Magnitude-Phase* mode of the MLMVN.

The CR obtained during the test-phase (blue line) is higher than 94% and a good performance is confirmed from a practical point of view using the experimental set-up shown in Figure 6.8.

Two external generators are used to apply the DC source and the PCB $24V$ supply voltage; a function generator with a specific auxiliary circuit is used to create the phase-opposite $5V$ control signals. The voltages on the passive components are measured by an oscilloscope and imported to Matlab to be processed by the neural classifier. It is necessary to point out that, to obtain the measurements in the fault conditions, the analog components are replaced with others having a different value or, as in the case of capacitors, one of the elements in parallel is eliminated. The results obtained during the training phase and those obtained by processing real measurements are summarized in Table 6.5. It should be noted that the hyper-parameters of the classifier are chosen through a heuristic approach, starting from a given number of neurons, 20 in this case, and increasing up to 120.

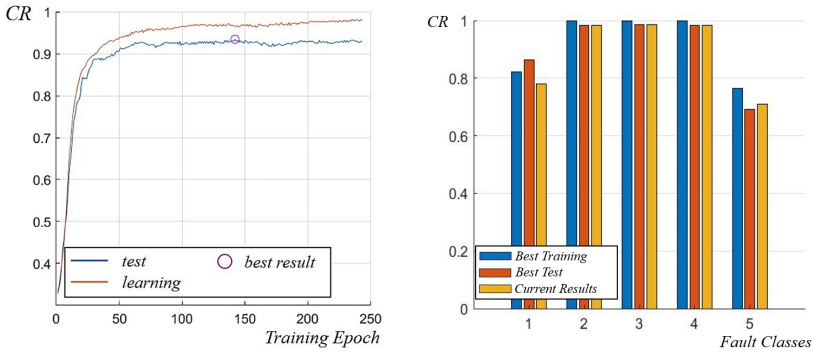

(a) (b)

Figure 6.7: Results obtained during the training phase using the MLMVN with 60 neurons in the hidden layer and setting *Magitude-Phase* mode: a) classification rate with respect to the training epochs; b) classification rate for each fault class.

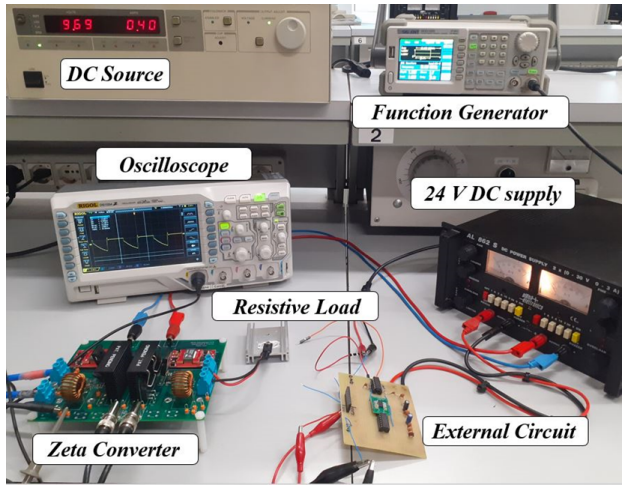

Figure 6.8: Experimental set-up to obtain real measurements.

These results are obtained using ripples and mean values of the voltages extracted from four test points. 60 neurons are used in the case of *Magnitude-Phase* mode and 90 neurons in the case of *Real-Imaginary* and

MLMVN set-up	$CR\%$ learning phase	$CR\%$ test phase	$CR\%$ real measures
Magnitude-Phase	96.5	94.75	89.47
Real-Imaginary	98.25	97.75	78.95
Single-Input	92	87.5	73.68

Table 6.5: Classification results obtained using ripples and mean values of the voltages extracted from four test points.

Single Input modes. Since the testability curves show the possibility of using only two measurements, two experimental tests have been carried out separately considering the voltages on the inductors and those on the capacitors. The results obtained in these cases are shown in Table 6.6.

MLMVN set-up	Ripple Voltages	$CR\%$ learning phase	$CR\%$ test phase	$CR\%$ real measures
Mag-Phase	V_{L_1}, V_{L_2}	68.13	67.75	47.37
Mag-Phase	V_{C_1}, V_{C_2}	82.25	80.25	78.95

Table 6.6: Classification results obtained using ripples and mean values of the voltages extracted from two test points.

These results are obtained using ripples and mean values of the voltages extracted from two test points. 30 neurons are used in the hidden layer to process V_{L_1} and V_{L_2}. 60 neurons are used for V_{C_1} and V_{C_2}. The results obtained by using only two measurements confirm the testability assessment described above. As for the voltages on the inductors, the ambiguity shown in Figure 6.4(a) and Figure 6.4(b) does not allow to exceed a 50% classification rate with real measurements. Therefore, this solution cannot monitor the operation of the Zeta converter with an acceptable level of accuracy. On the other hand, by using the voltages across the capacitors, it is possible to reach a CR as high as 80%. In this case the designer can decide whether to prefer the classification accuracy by measuring 4 voltages, or to reduce the intrusive level and accept a lower accuracy. Furthermore, the results shown in Table 6.5, allows to conclude that the performances obtained in *Real-Imaginary* mode are slightly better than those obtained in *Magnitude-Phase* during the training procedure. On the other hand, by processing real measurements, the best result is obtained in *Magnitude-Phase* mode. This

situation is caused by the small differences between the Zeta converter model and its prototype. In fact, the presence of parasitic effects makes the real behaviour of the converter slightly different than that simulated, and this mostly affects the average value of the voltages. Since the *Magnitude-Phase* mode creates complex inputs without changing the information content of the ripple measurements, it results in better classifications with real measurements. Starting from these considerations new tests have been carried out using only ripples in the dataset matrix. These results are shown in Table 6.7.

MLMVN set-up	$CR\%$ learning phase	$CR\%$ test phase	$CR\%$ real measures
Magnitude-Phase	96.88	95	94.74

Table 6.7: Classification results obtained using only ripples of the voltages extracted from four test points.

These results are obtained using only ripple measurements and four test points. 70 neurons belong to the hidden layer of the MLMVN. Therefore, the best classification result obtained on real measurements is carried out considering only ripples. In this case, four test points are still used but the processing of the measurements is facilitated. To compare the best performance of the MLMVN with those of other machine learning techniques, several algorithms based on different theoretical approaches were applied to the same dataset. Results obtained with Bayesian classifiers and Decision Tree-based classifiers are not presented because they do not exceed 80% classification rate during the training phase. The performances of a quadratic Support Vector Machine and a K-Nearest Neighbor (KNN) classifier are presented in Table 6.8, because they are comparable with those of the MLMVN. In particular, the SVM algorithm is slightly better than the KNN classifier and very close to the MLMVN performance using both ripples and average voltage values. However, the best result obtained by applying MLMVN on ripple measurements is not achieved by any other technique.

Summing up, the neural classifier based on MLMVN results in an excellent performance by using four test points: CR is close to 95% during the training phase and 90% with real measurements. The monitoring method does not use current measurements, which are more difficult to obtain, but only the voltages across all the passive components. Using only the voltages

	MLMVN real measurements	SVM real measurements	KNN real measurements
Mean Values and Ripples	89.47%	89.47%	84.21%
Only Ripples	94.74%	78.95%	75%

Table 6.8: Comparison between MLMVN and other machine learning techniques.

across the capacitors, the intrusive level of the prognostic system is lowered and the accuracy of the classification reduced by 10%.

6.5 Conclusion

The prognostic analysis based on MLMVN proposed in this chapter allows the monitoring of DC-DC converters by locating the occurrence of malfunctions in specific components. This method is suitable to organize maintenance and plan the replacement of the component in the worst state of health, thus reducing recovery times and damages inside the system the converter is utilized in. The experimental results obtained on a Zeta converter confirm that the proposed method is an excellent tool for the classification of malfunctions, because it results in a high accuracy level and, also, requires a low computational effort and a very fast classifier training phase as well. In addition, the low intrusive level and the use of voltage measurements facilitate the application of the procedure in very complex circuits. In this sense, the proposed testability study results in a tool useful for practical applications, by providing a procedure that is easily extractable to other converter topologies. As a further development, the performance obtained with real measurements could be improved by modelling the parasitic components typical of any practical converter circuit and the fault prevention referred to semiconductor devices will be explored.

Chapter 7

Application: Detection of Power Quality Disturbances

This chapter proposes two different ways to use a classifier based on Multi-Layer neural networks with Multi-Valued Neurons to detect electrical disturbances in low voltage power grids. Nowadays, the massive use of electronic loads and controllers introduces several distortions in the electrical distribution grid due to the non-linear behaviour of these devices. Machine learning methods are currently being exploited to obtain detection and classification of disturbances. This application presents two possible uses of a complex-valued neural network: in the first case, the inputs of the classification tool are time-domain samples of the line voltage, while in the second application, the magnitude and phase in the frequency domain are used. The training phase of these classifiers is carried out in the Matlab environment using the analytical form of five disturbances: voltage sag, voltage swell, harmonic distortion, voltage notch and interruption. The performances of the monitoring systems are analysed during the training phase using simulated data and subsequently through experimental measurements, obtained from an artificial generator of disturbances and variable loads. [1]

[1]This chapter has been published as "Classification of Power Quality disturbances using Multi-Valued Neural Networks and Convolutional Neural Networks" in *Proceedings of WCCI2022 IEEE World Congress on Computational Intelligence (2022).*

7.1 Introduction

Malfunctioning of electric loads in residential and industrial environments has become a concerning issue. This kind of problems can be caused by electrical disturbances in the power grid that degrades Power Quality (PQ) levels [126]. Moreover, high energy demanding companies are becoming more sensitive to loss of profit margins due to power losses and plant shutdowns [127] [128]. A degradation of PQ can be caused using non-linear loads that affects the sinusoidal waveform by injecting distorting electrical components in the power grid [62] [129]. Furthermore, the integration of renewable energy systems leads to an increase in disturbances of the distribution and transmission networks and this plays a fundamental role in the diffusion of distributed generation [58] [130]. These distortions or disturbances pull away voltages and currents from their nominal amplitude and frequency levels [61]. Therefore, the PQ analysis will be a fundamental aspect in the management of smart grids and smart cities in the near future, as well as the optimization of energy flows and the prevention of faults in electrical infrastructures [86]. The most important PQ disturbances considered in the literature can be summarized in five different categories: voltage sag, voltage swell, harmonic distortion, voltage notch and interruption [60] [59]. To assess these problems and to compensate for any power loss, it is important to detect and classify these disturbances. In [131] and [132], different machine learning techniques are presented in order to recognize disturbances. This application proposes two different uses of the MLMVN as a PQ problem classifier.

- In the first application, the inputs of the neural network are time-domain samples of the line voltage extracted from a distribution grid and converted into complex numbers through a specific coding procedure.

- The second application proposed here consists in processing the Fourier Transform (FT) of the measured voltage waveforms.

7.2 Power Quality Disturbances and Dataset Creation

7.2.1 Summary of PQ Disturbances

From a general point of view *Power Quality is a term used to broadly encompass the entire scope of interaction among electrical suppliers, the environment, the systems and products energized, and the users of those systems and products* [62]. In order to improve the PQ level, it is necessary to detect any problem in the grid manifested in voltage, current, or frequency deviations that result in failure or faulty operations of customer equipment [63]. In this work, the classification of disturbances is based on the analysis of the line voltage waveform. As mentioned before, these disturbances can be summarized in five categories and their main characteristics are presented here:

- voltage sag is a reduction of the Root Mean Square (RMS) value of the phase voltage between 10% and 90% of the nominal value;
- voltage swell represents an increase in voltage level greater than 10% of the nominal value;
- interruption is a term used to describe a complete loss of power and this means that the phase voltage drops below 10% of its nominal value for a time not exceeding one minute;
- notch is a condition when the magnitude of voltage decreases towards zero for a short period of time, usually microseconds;
- harmonic distortion describes the presence of components at frequencies other than the fundamental ($50Hz$ in Italy) in the waveform of the phase voltage.

Figures 7.1 show an example of each possible voltage distortion in the Italian distribution grid, characterized by a nominal V_{RMS} value of $230V$ and a frequency of $50Hz$.

7.2.2 Dataset Creation

In both cases proposed here, the dataset used to train the MLMVN-based classifiers is carried out in the Matlab environment starting from the analyt-

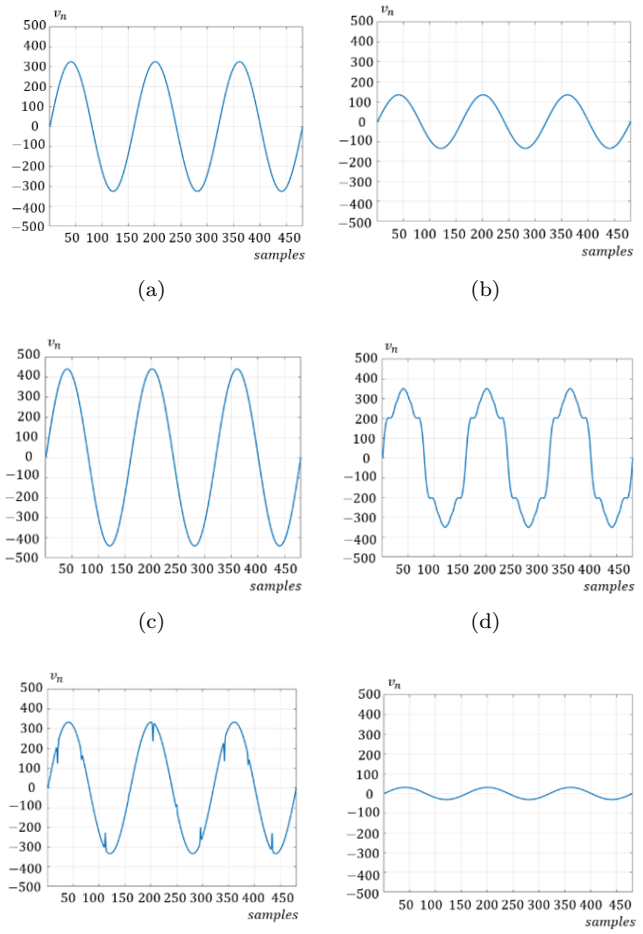

Figure 7.1: PQ disturbances: a) normal; b) sag; c) swell; d) harmonics; e) notch; f) interruption.

ical form of the nominal line voltage (7.1),

$$v(t) = \sqrt{2}V_{RMS}sin(\omega t + \phi) = V_{max}sin(\omega t + \varphi) \tag{7.1}$$

where V_{max} is the maximum amplitude of the waveform in the time domain, V_{RMS} is the root mean square value, ω is the angular pulsation and φ is its

initial phase. Starting from this, it is necessary to create a dataset matrix containing several examples of each disturbance and nominal conditions. In this sense, different examples of voltage sag and voltage swell are obtained by randomly varying the maximum amplitude of the waveform in the range $[(V_{max} - 0.1V_{max}) \div (V_{max} - 0.9V_{max})]$ and $[(V_{max} + 0.1V_{max}) \div (V_{max} + 0.5V_{max})]$ respectively. In order to obtain signals with harmonic distortion, some components with frequencies that are multiple of the fundamental are added in (7.1). For example, in (7.2) the presence of third and fifth harmonic is shown,

$$v_h(t) = v(t) + V_3 sin(3\omega t + \varphi) + V_5 sin(5\omega t + \varphi) \tag{7.2}$$

where the subscript h is used to indicate the presence of the harmonic distortion and the amplitudes V_3 and V_5 are higher than 5% of the rated voltage, which is the limit set by the European standard IEC 61000-2-2. In the case of the voltage interruption, different examples are created by reducing the maximum amplitude of the waveform shown in (7.1) between 0 and 10% of V_{max}. Finally, since the notch is defined as a switching disturbance of the normal voltage, lasting less than 0.5 cycles and having opposite polarity with respect to the nominal waveform, the Simulink model proposed in [72] is used to generate the signals containing these disturbances.

In this work, 5000 voltage signals are generated for each disturbance and additional 5000 voltage signals representing the nominal condition of the grid to create the dataset matrices.

Time Domain Approach

In this case, only one period of the generated voltage signals is considered at a time and it is sampled with a frequency of $8kHz$. Therefore, 160 samples are used as inputs of the neural classifiers in order to obtain the detection of disturbances. This means that the dataset matrix presents 30000 rows and 161 columns, where the last column is used to indicate the desired class in supervised learning algorithms. The structure of the dataset matrix is shown in (7.3), where n_s is the total number of rows and the index of the time sample considered is indicated as a subscript.

$$\begin{bmatrix} V_1^{(1)} & V_2^{(1)} & \cdots & V_{160}^{(1)} & 0 \\ & & \vdots & & \\ V_1^{(n_s)} & V_2^{(n_s)} & \cdots & V_{160}^{(n_s)} & 5 \end{bmatrix} \tag{7.3}$$

Note that the sampled waveforms are normalized with respect to the maximum value of the line voltage. These samples are real numbers and are processed by the complex-valued neural network using two different approaches: *Single Input* mode and *Real-Imaginary* mode. The former, that is the *Single Input* mode, means that each sample belonging to a row is considered as the phase of a complex number with unitary magnitude. Otherwise, in the latter case, that is in the *Real-Imaginary* mode, each pair of successive samples belonging to a dataset row is used to create the corresponding complex number, and this means that the first element of the pair is used as the real part while the second is used as imaginary part.

Frequency Domain Approach

In this case, the complex-valued inputs are obtained from the Discrete Fourier Transform (DFT) of the sampled line voltage with a frequency of $8kHz$. During the training phase, the time-domain samples of the waveforms are processed using a Fast Fourier Transform (FFT) algorithm and each complex term obtained is used as an input of the MLMVN. Figure 7.2 summarizes this procedure.

The structure of the dataset matrix used during the training phase is shown in (7.4),

$$\begin{bmatrix} X_1^{(1)} & X_2^{(1)} & \cdots & X_n^{(1)} & 0 \\ & & \vdots & & \\ X_1^{(n_s)} & X_2^{(n_s)} & \cdots & X_n^{(n_s)} & 5 \end{bmatrix} \tag{7.4}$$

where the last column contains the indexes of the fault classes, n is the number of points used in the fast Fourier transform algorithm and n_s is still the total number of examples. Each term $X_k (k = 1, \cdots, n)$ is calculated by (7.5),

$$X_k = \sum_{i=1}^{N} V_i W_N^{(i-1)(k-1)} \tag{7.5}$$

in which V_i is a voltage sample and W_N is obtained using formula (7.6).

$$W_N = \exp\left(\frac{-j2\pi}{n}\right) \tag{7.6}$$

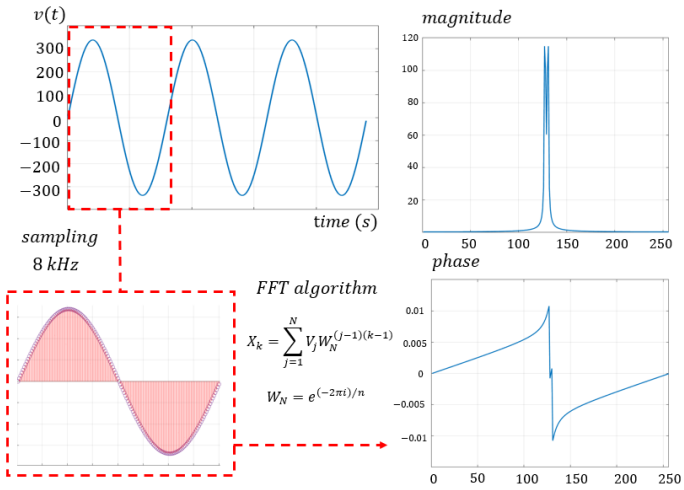

Figure 7.2: Procedure for creating the dataset.

7.3 Set-Up of the Neural Classifiers

In both approaches, the proposed neural classifier is the MLMVN presented in section 3.2, having three layers. In the hidden layer a variable number of neurons can be used and it is defined during the training procedure by means of a heuristic approach. In the output layer, five binary neurons are used, one for each possible disturbance, Figure 7.3(a).

The combination of the output neurons is used to define the global classification results, since each of them has only two possible outputs: $(1+j0)$ or $(-1+j0)$. The first value corresponds to the lower border of the sector $[0, \pi)$ while the second term is that of the interval $[\pi, 2\pi)$. This setting requires the introduction of a specific method for selecting outputs. In fact, the single failure hypothesis is assumed, and this means that only one neuron can be activated by detecting the corresponding disturbance. If, during the training phase, more than one neuron are activated, the *Winner Takes All* rule

is used. This means that only the neuron with the lowest error is kept in the activated state. Figure 7.3(b) shows the functioning of a binary neuron in this type of application.

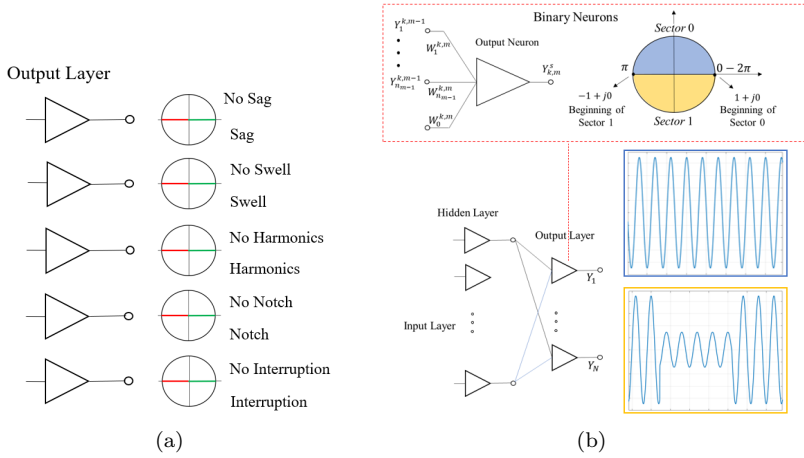

Figure 7.3: MLMVN set-up: a) output layer of the MLMVN-based classifier; b) example of functioning of a binary neuron and output coding.

7.4 Training Results

The training results here presented are obtained through the holdout validation method. This means that 80% of the dataset is used for the correction of the weights and the remaining 20% is used to verify the performance at the end of each training epoch.

7.4.1 Training Results Obtained with Time Domain Samples

In this case it is necessary to distinguish the results obtained in *Single Input* mode and those obtained in *Real-Imaginary* mode. The global classification rates are shown in Table 7.1. The results obtained for each fault class are shown in Figure 7.4(a) and Figure 7.4(b).

	Training	Validation
Real-Imaginary mode	89.43%	89.3%
Single Input mode	80.92%	73.133%

Table 7.1: Global classification results of MLMVN using time-domain samples.

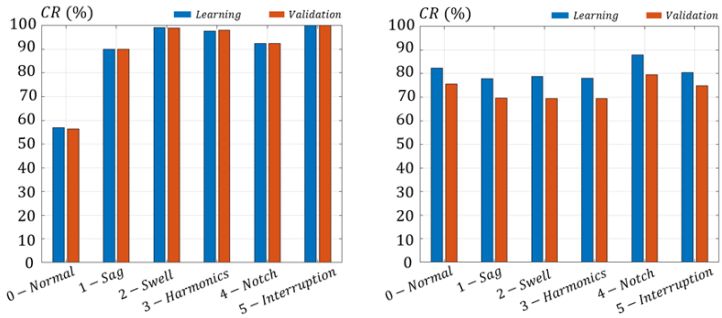

(a) (b)

Figure 7.4: Classification results for each class: a) *Real-Imaginary* mode; b) *Single Input* mode.

From these results, it is possible to state that the *Real-Imaginary* mode offers better performances in terms of classification rate, and the main classification errors are concentrated on class 0. Before considering the test on real measurements, a consideration can be made on the *Single Input* mode: observing the distribution of the input samples on the complex plane it is possible to note that all the possible disturbances belong in a small region. Figure 7.5(a) shows the area of the complex plane that contains the 160 samples of the dataset. In this case the voltage waveform is normalized with respect to its maximum value and this means that only the sector between -1 rad and 1 rad is available to recognize 4 fault classes. Only the swell condition is beyond this limit, but without introducing a quadrant change on the complex plane. The presence of harmonics and notches causes the position inversion of two or more successive samples in a very small area. To improve the classification capability of the MLMVN in *Single Input* mode it is necessary to consider the voltage samples without normalization and

to use degrees as the unit of measurement of the phase. In this way, it is possible to increase the decision area, Figure 7.5(b), and obtain significantly better classification results, as shown in Table 7.2.

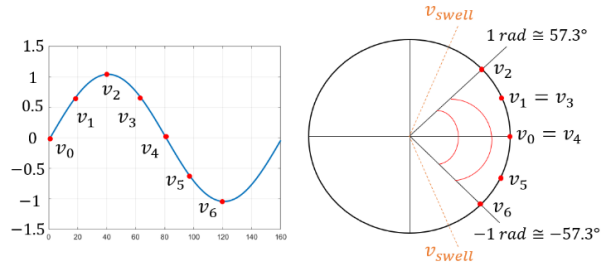

(a)

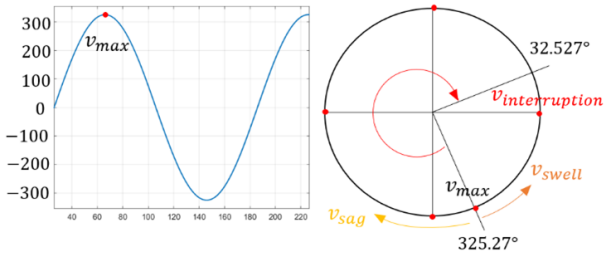

(b)

Figure 7.5: Distribution of the input samples on the complex plane in *Single Input* mode: a) using normalization; b) without normalization.

	Training	Validation
Single Input mode	87.933%	87.43%

Table 7.2: Improvement of the classification results obtained in *Single Input* mode.

7.4.2 Training Results Obtained with Frequency Domain Samples

As previously mentioned, in this case the complex inputs of the MLMVN-based classifier are generated through the discrete Fourier transform of the

sampled voltage waveforms. In this example, 256 points are considered for the DFT. Table 7.3 summarizes the results obtained using 50 neurons in the hidden layer of the neural network. As said before, the output layer contains 5 binary neurons, one for each electrical disturbance, and the nominal conditions correspond to a combination of five zeros.

Fault Class	Training $CR\%$	Validation $CR\%$
0	100	100
1	100	100
2	100	100
3	100	100
4	100	99.19
5	100	100

Table 7.3: Classification results of MLMVN using frequency-domain samples.

7.5 Experimental Validation

This section proposes further validation with real measurements to verify the performance of classifiers. For this reason, many voltage waveforms were extracted directly from the low voltage grid, Figure 7.6(a), and several distortions were generated through the experimental set-up shown in Figure 7.6(b). In this way, it is possible to reproduce multiple network disturbances with different spectral content, duration and amplitude. Measurements are acquired at the load terminals and distortions are introduced via Asterion 4503 A1/3PH programmable AC source by Amtek. It has a maximum power of $4500VA$ and can generate arbitrary waveforms at a frequency of up to 5kHz. The dynamic characteristics of this system make it almost unique in its kind, allowing the simulation of any type of network disturbance. A SIRIUSi-HS-4xHV-4xLV is used to acquire the waveforms of the mains voltage. The acquisition system presents 8 channels with a maximum sample rate of $50kHz$. The purpose of the experimental set-up is to ensure the repeatability of the electrical dynamics and the accuracy of the measurements for each experiment so that the comparison is consistent. Furthermore, thanks to the flexibility of the systems used, it can be adapted to any new configuration required for testing detection and classification algorithms.

(a)

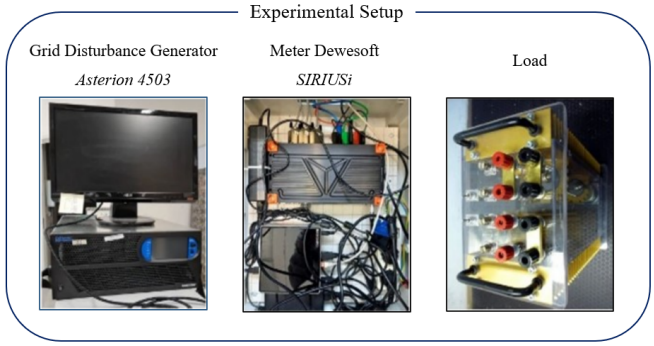

(b)

Figure 7.6: Experimental set-up: a) Test bench for measurements of the real network; b) Test bench for the artificial generation of PQ disturbances.

7.5.1 Validation Using Time Domain Samples

In this case, the first comparison taken into consideration is carried out using five different measurements, each of which contains some normal periods and some periods with a specific PQ disturbance. An example of classification is shown in Figure 7.7, where some normal periods with two interruptions are considered. In general, it can be said that both techniques (*Single Input* mode and *Real-Imaginary* mode) correctly identify and classify samples affected by disturbances. However, the *Single Input* mode results in 20% more errors in class 0 identification. For this reason, the *Real-Imaginary* mode is considered the best choice for classifying samples in the time domain and a complete identification of a signal containing all possible disturbances is proposed (Figure 7.8).The classifier offers excellent results on four categories

of disturbances, while the notch class is not identified in these real measurements. It is necessary to highlight that in some real measurements with larger and more lasting events, the MLMVN is able to identify the notch class but still remains the most critical situation.

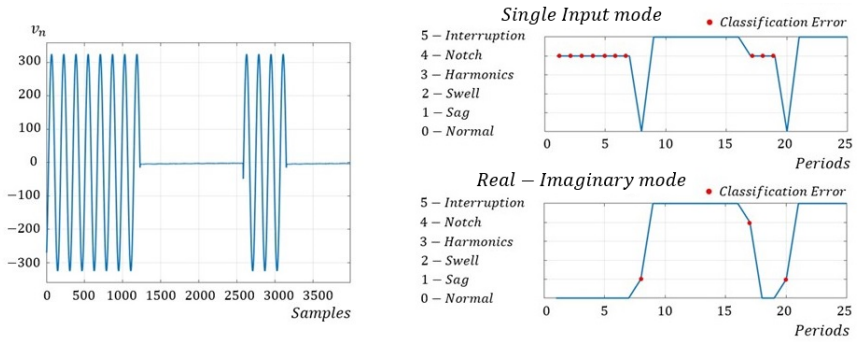

Figure 7.7: Validation example: comparison between MLMVN in *Single Input* mode and *Real-Imaginary* mode.

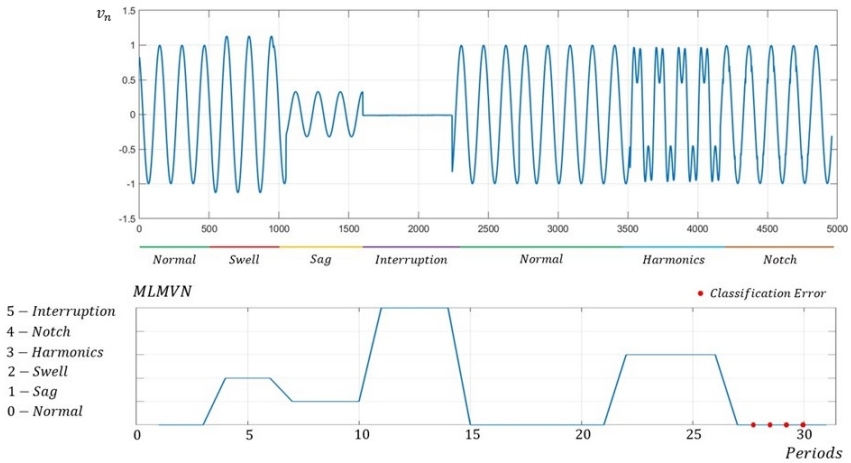

Figure 7.8: Validation example: classification of a signal containing all possible disturbances in *Real-Imaginary* mode.

7.5.2 Validation Using Frequency Domain Samples

The first voltage waveforms used to validate the performance of the MLMVN based classifier in the frequency domain are shown in Figure 7.9(a) and Figure 7.9(b), where the voltage sags and nominal conditions alternate with different durations.

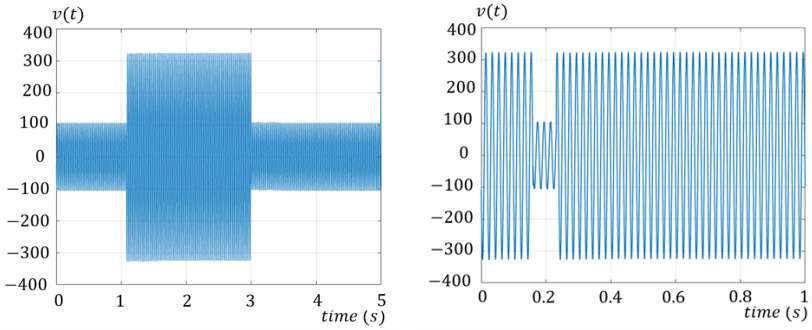

(a) (b)

Figure 7.9: Real voltage waveform used during the validation procedure: a) long-lasting voltage sag; b) short-term voltage sag.

The time window proposed in Figure 7.9(a) has a duration of five seconds and, therefore, it contains 250 sinusoidal periods each of which is made up of 8000 samples. One of the most important aspects in the evaluation of classification results is the time interval taken into consideration. For example, the signal shown in Figure 7.9(a) can be processed using five consecutive time intervals of one second duration. The proposed monitoring method assesses the DFT for each interval and classifies them. As shown in Figure 7.10, this procedure allows the perfect classification of the considered voltage waveform.

However, there are some situations in which the MLMVN makes misclassification, for example in the case of a brief perturbation. Figure 7.9(b) describes this condition: the time interval taken into consideration is classified as normal, but it presents a voltage sag of $60ms$.

To overcome this limitation, it is possible to reduce the duration of the time interval used for the classification procedure. In this way, short disturbances are identified with a high classification accuracy and the exact

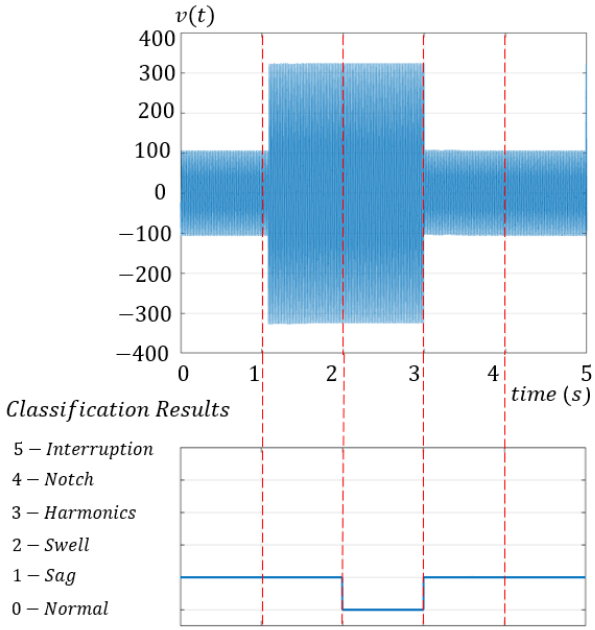

Figure 7.10: Classification results obtained through MLMVN on real measurements using time intervals of one second.

moment they start is detected. Figure 7.11 shows a classification example in which a voltage waveform is processed using $60ms$ time intervals.

Note that the excellent classification results shown in Figure 7.11 can also be obtained by considering the other fault classes. Table 7.4 summarizes the classification performances obtained using different time interval durations.

These results were obtained considering real voltage measurements of 25 seconds and confirm the excellent performance when the waveform is processed using a short time interval. On the other hand, the classification rate decreases as the number of periods processed simultaneously increases. It should be noted that the classification of the harmonic disturbance is slightly better than that of the other perturbations when using time intervals of $1s$ and $2s$. The reason for this result is that the presence of a voltage component with frequency higher than $50Hz$ introduces significant variation in the Fourier analysis. As shown in Figure 7.12(a) and Figure 7.12(b), in the Magnitude representation several lines are introduced with respect to

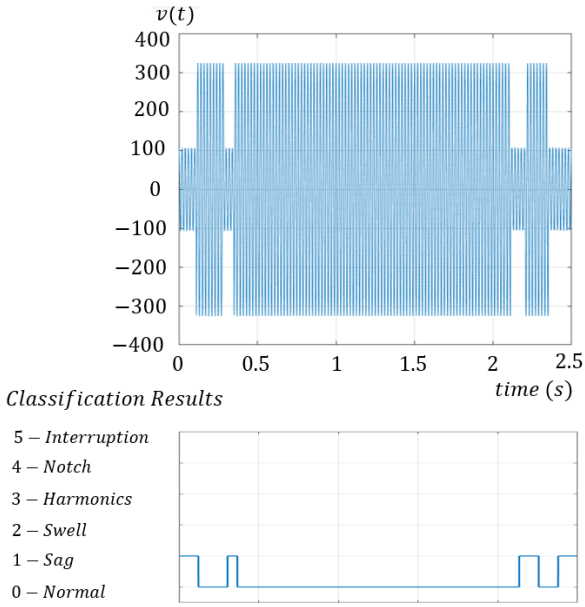

Figure 7.11: Classification results obtained through MLMVN considering time intervals of $60ms$.

Disturbance	Time Interval			
	$0.06s$	$0.6s$	$1s$	$2s$
1-Sag	98.5%	90%	80%	66.6%
2-Swell	97%	87.5%	79.5%	66.6%
3-Harmonics	99.25%	90%	84%	75%
4-Notch	97%	90%	84%	68%
5-Interruption	98.5%	90%	80%	70%

Table 7.4: Global classification results of MLMVN using different time intervals.

the normal condition, each of which corresponds to a frequency component. These contributions are also present in the case of a short duration harmonic perturbation and therefore make the classification slightly easier. As for the other voltage disturbances, they focus on the $50Hz$ component, and this makes it difficult to recognize brief problems.

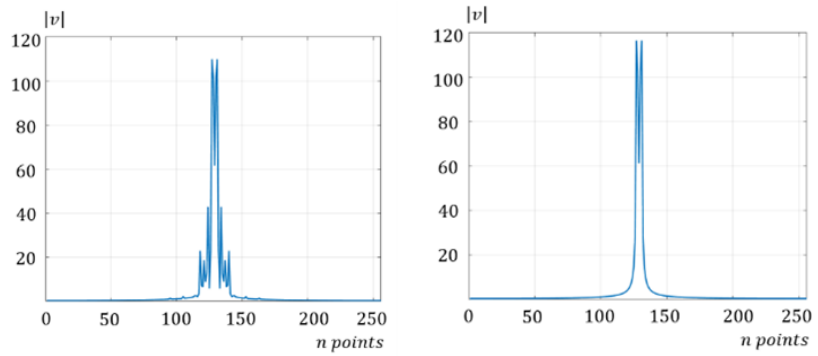

(a) (b)

Figure 7.12: DFT results: a) magnitude in the case of a voltage waveform with harmonic disturbance of $0.15s$; b) magnitude of a normal voltage waveform.

In addition, it should be noted that some of the errors in detecting voltage sags and interruptions using a short time interval ($0.006s$) correspond to class 4 misclassifications. In fact, in the instant in which the voltage drop begins, features very similar to those of a notch can occur. This means that the MLMVN can detect the starting point of these disturbances, but sometimes classifies it as a notch. Figure 7.13 describes this situation. Without considering these errors the classification rate would be over 99%. Finally, a voltage signal containing all 5 categories of disturbances is generated. The voltage waveform is sampled with a frequency of $8kHz$. The goal of the classification is to determine the power quality by studying $60ms$ (3 cycles) at a time. Therefore, the sampled signal is divided into groups of 480 samples and each of them is assigned the corresponding classification. Figure 7.14(a) shows the overall signal and the correct classification of the 16 groups of the analysed samples, while Figure 7.14(b) presents the classification results obtained through the MLMVN-based classifier. The only mistake made is found in the first sample. This is a very complex situation to recognize because the voltage sag situation occurs in the last half-period of the three taken into consideration. Figure 7.14(c) shows this situation. It can be said that by using one FT for each sine cycle, i.e. by analysing one cycle at a time, this type of error can be eliminated by ensuring 100% accuracy.

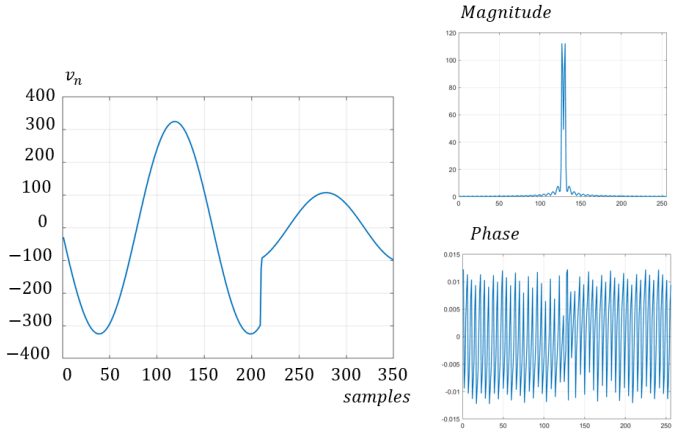

Figure 7.13: Example of a voltage waveform in which the beginning of the voltage sag is classified as notch.

7.6 Conclusion

In conclusion, it can be said that the two proposed techniques allow the monitoring of the power quality in a low voltage distribution network with an excellent level of accuracy. The first proposed classifier processes the samples of the voltage waveform in the time domain. Therefore, the number of inputs depends on the sampling frequency and some classification examples obtained with a frequency of $8kHz$ are proposed. The classification results obtained show the ability to identify power quality disturbances with an accuracy level of 90%. The proposed solution uses two successive samples as real and imaginary parts of a complex number which are then classified by the MLMVN. In this case, to correctly identify the distortions it is necessary to process one sinus cycle at a time or, alternatively, to increase the number of inputs resulting in an increase of neurons in the hidden layer. The second classifier presented offers better performance by exploiting the complex nature of the neural network. In fact, the voltage samples are processed through a DFT and then classified by the MLMVN. In this way, classification results of more than 95% are obtained. The feature extraction phase introduced in this case does not involve an increase in computational cost and does not particularly slow down the classification process.

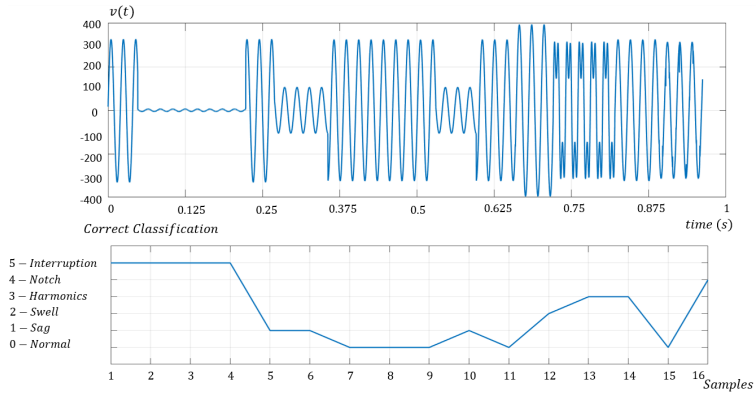

(a)

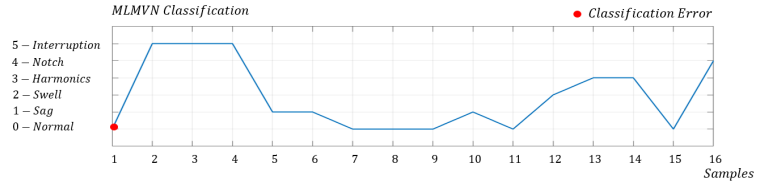

(b)

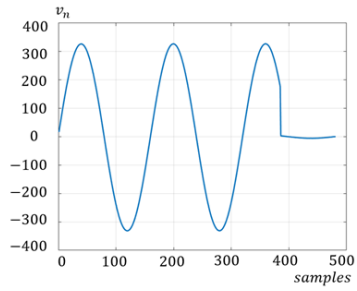

(c)

Figure 7.14: Results obtained with real measurements: a) voltage signal characterized by the five disturbances; b) classification results obtained through MLMVN-based classifier; c) first group of samples not correctly classified.

Chapter 8

Conclusion

This chapter summarizes the contribution of the Thesis and discusses avenues for future research.

8.1 Summary of contribution

In conclusion, it can be said that the prognostic procedure developed during this research activity constitutes an extremely useful and versatile tool for preventing catastrophic failures in many different types of electrical systems. The main fields of application taken into consideration were the following:

- monitoring of electrical infrastructure;
- prognosis of DC-DC power converters;
- detection of Power Quality (PQ) disturbances;

In the field of electrical line monitoring, the preliminary phases of the proposed approach were summarized in three main steps: modelling of the system under test, study of the failure mechanisms, choice of the best test points. In this sense, particular importance has been attributed to the concept of Testability, proposing the main theoretical aspects and the symbolic calculation on SapWin. As for the prognostic analysis, the most important aspect was the development of a Multi-Layer neural network with Multi-Valued Neurons (MLMVN) able to identify the health status of electrical

lines by elaborating frequency response measures. Two different infrastructures were considered: High Voltage (HV) overhead power lines and Medium Voltage (MV) underground networks.

In the proposed methodology for assessing the health status of bolted joints in high voltage overhead lines, the main contributions were:

- lumped parameter modelling of bolted joints;
- definition of the relationships between the most common failure mechanisms and the electrical parameters of the model;
- development of a neural classifier based on MLMVN capable of operating in the hypothesis of multiple failure and multiple severities;
- verification of the classifier operation in identifying the conditions of oxidation and partial breakage of the joints.

In this case, The results obtained show the excellent potential of the prognostic method in the analysis of network branches containing three and four junction regions. The global classification rates are excellent considering the high number of conditions to be classified, 27 in the case of three joints and 81 in the case of four junction regions. Furthermore, by analysing in detail the results obtained for each joint, extremely better performances can be noted. Therefore, the specific analysis reveals the possibility of classifying the health status of each individual joint with an accuracy level greater than 90%.

In the field of underground medium voltage lines, the main objective was to propose a low-level intrusion monitoring system to identify overheated cable sections. Therefore, the use of Power Line Communication devices was considered to extract the frequency response measurements and an experimental procedure for the frequency characterization of MV cables in nominal and overheating situations was developed. In this way, it was possible to increase the accuracy of the simulations approaching real operating conditions. Hence, the most important contributions of this study can be summarizes as follows:

- to propose an overview of the main problems in MV cables and their effects on the equivalent lumped circuit;
- to define an experimental procedure for the frequency characterization of MV cables both in nominal and overheating conditions;

- to develop a neural classifier based on MLMVN capable of locating overheated cable sections using measurements of transmitted signals;

In this case, it can be stated that the prognostic method allows the detection and localization of thermal malfunctions in MV underground networks with a high level of accuracy (96%). It should be noted that the MLMVN-based classifier was focused on the localization of cable over-temperatures $(105 \div 110)°C$ when they concern $250m$ of a $5km$ long line.

In order to verify the effectiveness of the prognostic method from the experimental point of view, the application of the neural classifier for the prognosis of a Zeta converter was proposed. Therefore, after training the neural network using the Simulink/Simscape model of the converter, a real prototype was made and the necessary measurements were extracted to perform the prognosis. Note that the test points used in this application have been selected by the new graphical testability evaluation method proposed in this Thesis. The experimental procedure shows that the neural classifier based on MLMVN results in an excellent performance by using four test points: CR is close to 95% during the training phase and 90% with real measurements. The monitoring method does not use current measurements, which are more difficult to obtain, but only the voltages across all the passive components. Using only the voltages across the capacitors, the intrusive level of the prognostic system is lowered and the accuracy of the classification reduced by 10%. The main theoretical contributions of this application were the following:

- verification of the graphical method for evaluating Testability;
- verification of the operation of the classifier with real data in the time domain;

Finally, the last experimental application of the proposed classifier was the evaluation of the power quality in a low voltage plant. To achieve this goal, a specific test bench was used, capable of creating 5 different types of disturbances. This system involves the use of an artificial distortion generator and some non-linear loads capable of modifying the voltage and current waveforms. In this application, the MLMVN-based classifier was employed in two different configurations:

- in the first case, the samples of the voltage waveform obtained at

$8[kHz]$ were processed directly by the neural network obtaining a classification rate of 90%;

- in the second case, the classifier processes the discrete Fourier transform of the samples and increases the performance reaching 95% accuracy.

8.2 Directions for future work

The prognostic procedure developed during this research activity offers wide possibilities for improvement in all the sectors taken into consideration. In the field of power line monitoring, most of the efforts were concentrated in the modelling phase to find suitable tools for simulating and representing failure mechanisms. Experimental verification of cable behaviour in a wide range of frequencies for both nominal and overheating situations brings the simulation procedure closer to real situations, but further developments need to be addressed to achieve practical application. In fact, from the point of view of the measurement system, the introduction of noise and other effects produced by the line devices will play a fundamental role and will be added to the simulation model. In this sense, a possible approach could be to model the PLC system starting from one actually used for the transmission of information and to introduce high frequency models of transformers and other devices in the simulations as shown in [105]. A first partial step has already been made by identifying a possible target for the capacitive coupling system that would allow the injection of signals in the required frequency range with a low level of intrusion. This is the $CAMS - 10K$ system manufactured by Ziv.

Regarding the prognosis of DC-DC converters, the main future developments can be summarized as follows:

- introduction of parametric failure for active components;
- integration of the prognostic method during converter operation in specific applications;
- Integration of the neural classifier in embedded electronics.

The first two points have already been partially developed. In particular, the monitoring of the active components can be introduced from the simulation point of view considering the increase in internal resistance of the

switches due to the temperature increase. In fact, the deterioration of the performance of the active components leads to an increase in switching losses with consequent production of heat. Therefore, this resistor becomes a variable component of the circuit which can modify the extracted measurements. As for the prognosis of the zeta converter during its use, the photovoltaic production sector was considered (see Figure 8.1).

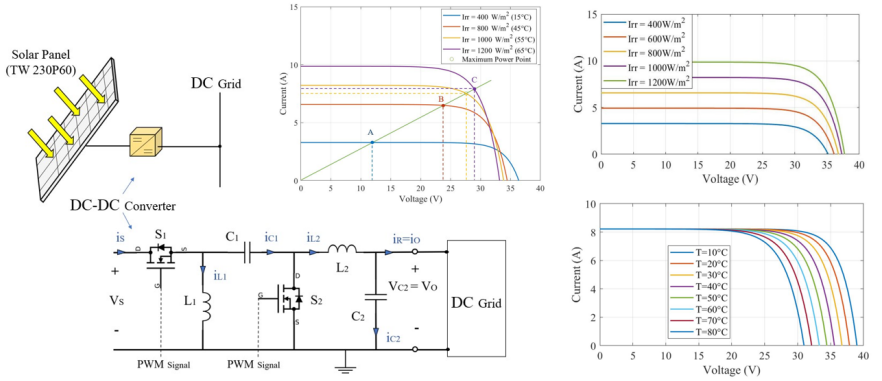

Figure 8.1: Possible integration of the zeta converter presented in Chapter 6 in the photovoltaic sector (partially investigated situation).

In this case, the greatest difficulties are represented by the great variability of the electrical quantities and by the continuous displacement of the operating point. However, early tests indicate that the method is quite robust and maintains excellent performance. However, further developments and analyses are needed to understand the potential of the prognostic approach in this type of application.

Finally, in the field of energy quality, the main developments will concern the neural network's ability to deal with time series and to operate online by identifying the occurrence of a disturbance in real time.

Appendix A

Appendix

This appendix is related to the machine learning methods used as comparison terms with the Multi-Layer neural network with Multi-Valued neurons (MLMVN). Mainly the algorithm taken into consideration is that of the Support Vector Machine (SVM). However, the main theoretical aspects of Decision Tree algorithms are also presented below. Finally, the linear Principal Component Analysis (PCA) used in Chapter 4 to replace the a priori selection of test frequencies is described. Note that the main concepts presented in this section are extracted from [133].

A.1 Support Vector Machine

Support Vector Machines have often been proposed in previous chapters as main competitor of MLMVN. These algorithms, in fact, represent a category of classification tools widely used in literature and usually offer great performances also in the field of regression tasks. From the technical point of view, a SVM is a supervised learning algorithm that constructs a hyperplane or set of hyperplanes in a high- or infinite-dimensional space, which can be used for classification, regression, or other tasks like outliers detection.

A.1.1 Linear SVM

The main theoretical concepts underlying the functioning of linear SVM in classification problems can be easily introduced using two figures extracted from [133] and containing two data classes (Figure A.1(a) and Figure A.1(b)).

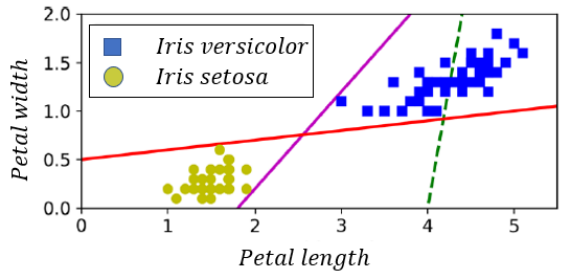

(a)

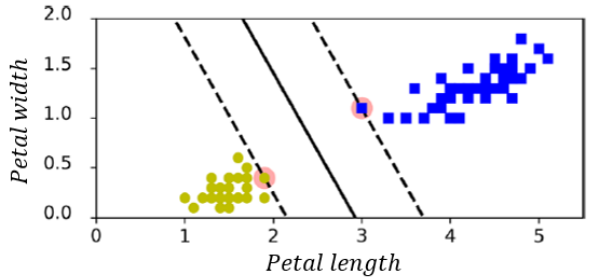

(b)

Figure A.1: Example of classifications used to introduce the operating characteristics of the SVM algorithms in [133].

The two classes can clearly be separated easily with a straight line (they are linearly separable). Figure A.1(a) shows the decision boundaries of three possible linear classifiers. The model whose decision boundary is represented by the dashed line is so bad that it does not even separate the classes properly. The other two models work perfectly on this training set, but their decision boundaries come so close to the instances that these models will probably not perform as well on new instances. In contrast, the solid line in the Figure A.1(b) represents the decision boundary of an SVM classifier; this line not only separates the two classes but also stays as far away from the closest training instances as possible. You can think of an SVM classifier as fitting the widest possible street (represented by the parallel dashed lines) between the classes. This is called large margin classification. Notice that adding more training instances *off the street* will not affect the decision boundary at all: it is fully determined (or supported) by the instances located on the edge

of the street. These instances are called the Support Vectors. Also in these algorithms, as well as in the case of MLMVN, it is possible to distinguish two different approaches: *soft margin* and *hard margin*.

- When it is strictly enforced that all instances must be off the parting surface and properly classified, a hard margin classification is achieved. This approach presents two main problems. First, it only works if the data is linearly separable. Second, it is sensitive to the presence of outliers.

- To avoid these problems, a more flexible approach can be used. The goal is to find a good balance between keeping the road as wide as possible and limiting margin violations. This is called soft margin classification.

A.1.2 Mathematical Description

As mentioned previously, SVM algorithms represent one of the most used Machine Learning techniques for solving classification problems. They were born as binary classifiers of linearly separable multidimensional patterns. The evolution of these techniques makes them applicable also to multi-class non-linear systems. The approach is to define the decision surfaces between the classes.

To deal with these algorithms from a mathematical point of view, it is convenient to start from the simplest case: the application of the SVM technique to two classes of linearly separable multidimensional patterns. In this case, the goal is to define, among all the possible hyperplanes, the one that divides the two classes, guaranteeing the maximum possible margin. It should be noted that the term margin represents the minimum distance of points of the two classes in the training set from the hyperplane identified. Margin maximization is related to generalization: if patterns in the training set are classified by a large margin, it is possible that patterns in the test set near the boundary between classes are also handled correctly. In general, the training set contains n multidimensional pattern samples and the respective classification (A.1). Note that the indexes 1 and -1 are used to indicate the two fault classes considered in this case.

$$(\mathbf{x}_1; y_1) \dots (\mathbf{x}_n; y_n) \quad \mathbf{x}_i \in \Re^d \quad y_n \in \{1, -1\} \tag{A.1}$$

A generic hyperplane is defined by two parameters:$(\mathbf{w}, b)$. The term $\mathbf{w}$ indicates the vector normal to the hyperplane. The quantity $b/\|\mathbf{w}\|$ is the distance from the origin. The basic form of an hyperplane is shown in (A.4).

$$D(\mathbf{x}) = \mathbf{w}^T\mathbf{x} + b \tag{A.2}$$

Note $D(\mathbf{x}) = 0$ indicates the locus of the vectors on the considered hyperplane. So, any vector $\mathbf{x}$ can be written as shown in (A.3) and the distance from the hyperplane is $r = D(\mathbf{x})/\|\mathbf{w}\|$.

$$\mathbf{x} = \mathbf{x}_p + r\frac{\mathbf{w}}{\|\mathbf{w}\|} \quad D(\mathbf{x}_p) = 0 \tag{A.3}$$

$$D(\mathbf{x}) = \mathbf{w}^T\mathbf{x} + b = r\|\mathbf{w}\| \tag{A.4}$$

The hyperplanes separating the training set patterns with minimum distance on each side satisfy the following equations:

$$\begin{cases} \mathbf{w}^T\mathbf{x}_i + b > +1 & if \quad y_i = +1 \\ \mathbf{w}^T\mathbf{x}_i + b \leqslant -1 & if \quad y_i = -1 \end{cases} \tag{A.5}$$

The minimum distance between the separation hyperplane and a pattern of the training set is called the margin τ:

$$\tau = \frac{2}{\|\mathbf{w}\|} \tag{A.6}$$

Figure A.2(a) and Figure A.2(b) summarize the considerations made so far.

Therefore, the optimal hyperplane satisfies the separation constraints and maximizes the τ margin:

$$\begin{cases} \frac{2}{\|\mathbf{w}\|} \quad (margin) \\ y_i[\mathbf{w}^T\mathbf{x}_i + b] - 1 \geqslant 0 \quad i = 1, \ldots, n \quad (separationconstraints) \end{cases} \tag{A.7}$$

the training set patterns found on the edge are called Support Vectors. These patterns completely define the solution to the problem. Therefore, the solution of the problem can be expressed as a function of only these patterns, regardless of the dimensionality of the space d and the number n of elements of the training set. The main application cases of the SVM algorithm are presented below:

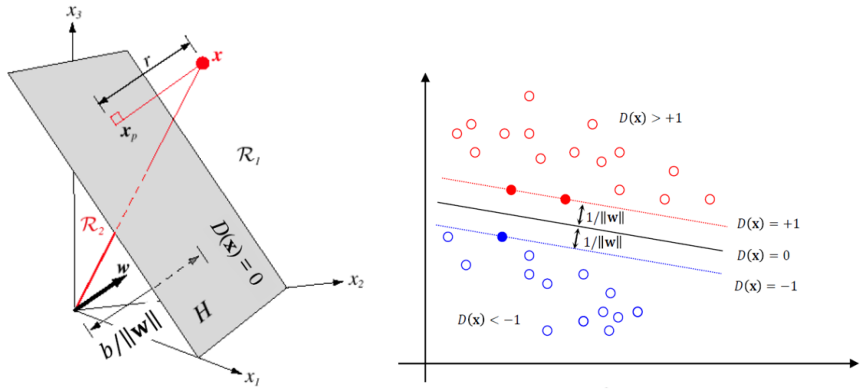

(a) (b)

Figure A.2: General description of SVM algorithm: (a) separation hyperplane; (b)concept of margin.

- **linear SVM and linearly separable patterns:** the main approach consists in introducing a Lagrangian formulation, which involves the introduction of a multiplier $\alpha_i \geqslant 0$ for each constraint equation and the subtraction of the constraint multiplied by α_i from the objective function.

$$Q(\mathbf{w}, b, \alpha) = \frac{1}{2}\mathbf{w}^T\mathbf{w} - \sum_{i=1}^{n} \alpha_i [y_i(\mathbf{w}^T\mathbf{x}_i + b) - 1] \tag{A.8}$$

the term shown in (A.9) must be minimized with respect to **w** and b and maximized with respect to α_i.To simplify the writing, it is advisable to introduce the Karush-Kuhn-Tucker (KKT) conditions which allow the representation of the problem in a dual form by expressing **w** and **b** as a function of the multipliers,

$$Q(\alpha) = \sum_{i=1}^{n} \alpha_i - \frac{1}{2} \sum_{i,j=1}^{n} \alpha_i \alpha_j y_i y_j [\mathbf{x}_i^T \mathbf{x}_j] \tag{A.9}$$

this must be maximized with respect to the terms α_i and this operation can be done using a quadratic programming term algorithm. Therefore, the formulation of the optimal hyperplane is shown in (A.10),

where (x_s, y_s) is a support vector.

$$\begin{cases} \mathbf{w}^* = \sum_{i=1}^{n} \alpha_i^* y_i \mathbf{x}_i = 0 \\ b^* = y_s \sum_{i=1}^{n} \alpha_i^* y_i (\mathbf{x}_i^T \mathbf{x}_s) = 0 \end{cases} \tag{A.10}$$

The distance function from the hyperplane is (A.11),

$$D(\mathbf{x}) = \mathbf{w}^{*T}\mathbf{x} + b^* = \sum_{i=1}^{n} \alpha_i^* y_i (\mathbf{x}^T \mathbf{x}_i) + b^* \tag{A.11}$$

the sign of the function $D(\mathbf{x})$ allows to classify a generic pattern $\mathbf{x}$, the summations are reducible to the support vectors only and, once $\mathbf{w}^*$ and b^* have been calculated, it is not necessary to save the support vectors.

- **linear SVM and non linearly separable patterns:** In this case not all patterns can be separated by a hyperplane and it is necessary to relax the separation constraints so that some patterns (as few as possible) can cross the class boundary (admit some classification errors). Therefore the positive slack variables ξ_i are introduced and the constraints are modified as follows,

$$y_i[\mathbf{w}^T \mathbf{x}_i + b] \geqslant 1 - \xi_i \tag{A.12}$$

this means that the optimal hyperplane must always maximize the margin but, at the same time, minimize the number of classification errors.

$$\begin{cases} \frac{\|\mathbf{w}\|^2}{2} + C \sum_{i=1}^{n} \xi_i \\ y_i[\mathbf{w}^T \mathbf{x}_i + b] \geqslant 1 - \xi_i \end{cases} \tag{A.13}$$

The coefficient C in the previous optimization problem indicates the relative importance of the classification errors with respect to the width of the margin. This is one of the few hyper parameters that the user must choose for SVM tuning. By passing to the Lagrangian form, the same result can be obtained as in the case with linearly separable patterns with a single modification in the constraints.

- **Non linear SVM:** When a very complex separation surface is required, it is possible to extend the initial theory of the search for optimal hyperplanes to the non-linear case. In this case, a non-linear

mapping function is introduced. The patterns are mapped in a larger space than the starting one.

$$\phi : \Re^d \longrightarrow \Re^m \quad \phi(\mathbf{x}) = [g_1(\mathbf{x}), \ldots, g_m(\mathbf{x})] \tag{A.14}$$

Starting pattern	Starting space	Nonlinear mapping function	Final space
x_i	$\Re^d$	ϕ	$\Re^m$

Table A.1: Explanation of the main elements.

Larger space means more degrees of freedom. Patterns in the new space can be more easily separated by a hyperplane using the procedure described above. Analysing the formulation of the Lagrangian problem in this case it can be seen that the vectors of the training set always appear in the form of scalar products between pairs of vectors. Consequently, by appropriately choosing the mapping function, it is possible to reduce the scalar product of two patterns mapped in $\Re^m$ to a function of the two patterns in the space $\Re^d$. This function is called Kernel. This allows to solve the optimization problem without particular complications compared to the linear case. Once the α_i is determined, the separation surface can be expressed as

$$D(\mathbf{x}) = \mathbf{w}^*\mathbf{x} + b^* = \sum_{i=1}^{n} \alpha_i^* y_i K(\mathbf{x}^T\mathbf{x}_i + b) \tag{A.15}$$

the most commonly used Kernel functions are: polynomial of degree q, Radial Basis Function (RBF) and 2-layer neural network.

A.1.3 Non-Linear SVM Classification

As previously mentioned, when the dataset under consideration is not linearly separable, a possible approach is to add more features, such as polynomial features; in some cases this can result in a linearly separable data set. Another example extracted from [133] can be used to easily explain this concept. Figure A.3(a) represents a simple dataset with one feature x_1 and it is not linearly separable. By adding a second feature $x_2 = x_1^2$, the resulting dataset is perfectly linearly separable (Figure A.3(b)).

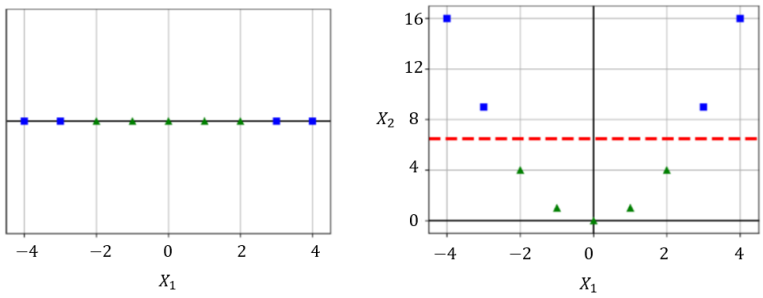

Figure A.3: Use of polynomial features to make the dataset linearly separable [133]: (a) non-linearly separable dataset; (b) linearly separable dataset.

Polynomial Kernel

Adding polynomial features is simple to implement and can work very well. However, at a low polynomial degree, this method cannot handle very complex datasets and, with a high polynomial degree, it creates a huge number of functions, making the model too slow. When using SVM it is possible to apply so-called kernel functions. Using the kernel trick it is possible to obtain comparable results to using many polynomial features without having to add them. So there is not combinatorial explosion of the number of functions.

Similarity Features

Another technique for dealing with non-linear problems is to add calculated characteristics using the similarity function, which measures how much each instance resembles a particular landmark. For example, considering the dataset $1D$ presented in Figure A.3(a) and adding two reference points at $x = -2$ and $x = 1$, it is possible to obtain the situation of Figure A.4(a). So, the similarity function is defined to be the Gaussian Radial Basis Function (RBF) as shown in (A.16).

$$\phi_\gamma(\mathbf{x}, l) = exp(-\gamma\|\mathbf{x} - l\|^2) \tag{A.16}$$

This is a bell-shaped function ranging from 0 to 1 (the reference point). Then, the new features can be calculated ($\gamma = 0.3$ is used in this case). For

example, considering the instance $x = -1$, it is located at a distance of 1 from the first landmark and 2 from second reference point. Therefore, its new characteristics are $x = exp(-0.3 \cdot 1) \approx 0.74$ and $x = exp(-0.3 \cdot 2) \approx 0.30$. The graph in Figure A.4(b) shows the transformed data set (eliminating the original features). Note that the dataset is now linearly separable.

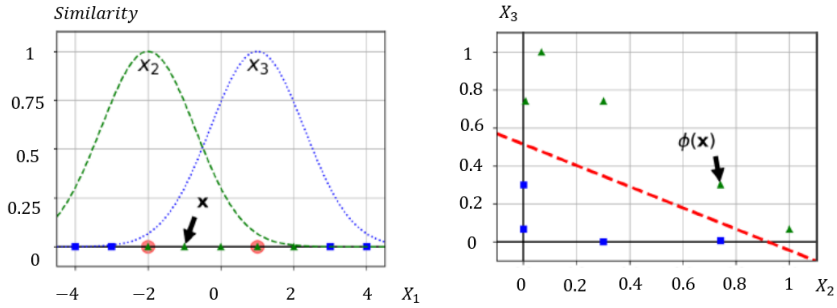

Figure A.4: Similarity features using the Gaussian RBF [133]: (a) initial dataset and reference points; (b) linearly separable dataset.

In this case it is necessary to define a suitable method for setting the reference points. The simplest approach is to create a reference point at the location of each individual instance in the dataset. This creates many size and thus increases the chances that the transformed training set is linear separable. The downside is that a training set with m instances and n functionality is created turned into a training set with m instances and m functions (assuming you delete the original features). If the training set is very large, an equally large number of functions are obtained.

Gaussian RBF Kernel

Just like the polynomial feature approach, the similarity feature method can be useful with any machine learning algorithm, but it can be computationally expensive to calculate all the additional features, especially on large training sets. Once again the use of a kernel function allows to obtain a result similar to the use of many features. Also in this case an example extracted from [133] is shown, where the hyper parameters of the algorithm are varied.

Increasing γ makes the bell-shaped curve narrower (see Figure A.5). As

a result, range of influence of each instance is smaller: the decision boundary ends up being more irregular, wiggling around individual instances. On the other hand, a small value of γ makes the bell-shaped curve wider: instances have a larger range of influence, and the decision boundary ends up smoother. So γ acts like a regularization hyper parameter: if the model is over fitted, it is necessary to reduce it; if the model is under fitted, γ should be increased (similar to the C hyper parameter).

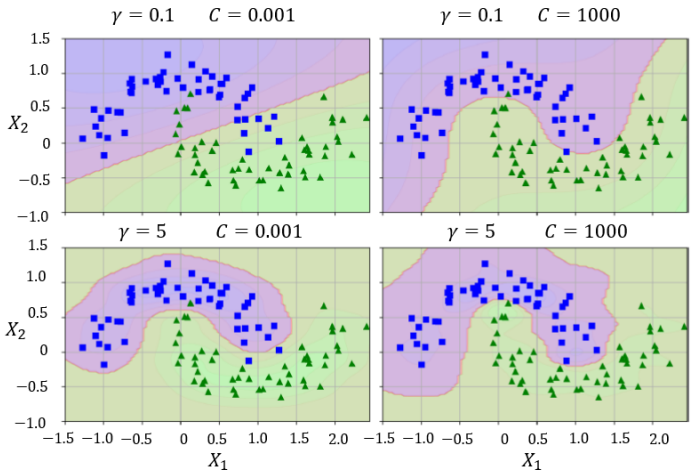

Figure A.5: Example of using an RBF Gaussian kernel with different hyper parameters [133].

A.1.4 Principal Component Analysis

The Principal Component Analysis (PCA) used in the Chapter 4 is one of the most popular dimensionality reduction techniques. The main step in this approach is to identify the hyperplane that is the closest to the data and, subsequently, the entire dataset is projected onto it. To illustrate the main features of this method, a simple $2D$ dataset like the one shown in Figure A.6 can be considered. In the same picture, there are also three different axes (i.e., $1D$ hyperplanes). Figure A.6(b) shows the results of the projection along all these axes. The projection on the solid line retains the maximum variance, while the other two projections do not guarantee the maintenance of high variance values. Therefore, using the axis with the least

loss of variance reduces the loss of information content due to the reduction in dimensionality. Another way to justify this choice is that it is the axis that minimizes the mean square distance between the original dataset and its relative projection on that axis.

The main steps of the algorithm written in Matlab code to reduce the dimensionality of the dataset in the chapter 4 are presented below.

- The first step is the normalization of the dataset matrix; this can be done by subtracting the mean and dividing by the standard deviation for each value of each variable.

- The purpose of the second step is to understand how the variables of the input data set are varying from the mean with respect to each other, or in other words, to see if there is any relationship between them. In fact, sometimes the variables are highly correlated and contain redundant information. Therefore the covariance matrix of the dataset should be calculated. The covariance matrix is a symmetric matrix whose elements are the covariances associated with all possible pairs of the initial variables. Since the covariance of a variable with itself is its variance, the variances of each initial variable are contained in the main diagonal. Also, since the covariance is commutative, all elements are symmetrical with respect to the main diagonal, which means that the upper and lower triangular portions are equal.

- The third phase involves the computation of the eigenvectors and the eigenvalues of the covariance matrix to identify the principal components. Principal components are new variables constructed as linear combinations of the initial variables. These combinations are made in such a way that the new variables are not correlated and most of the information within the initial variables is compressed into the first components. For example, the idea is that 10-dimensional data provides 10 principal components, but PCA tries to put as much information as possible into the first component, then the maximum remaining information into the second, and so on. It is necessary to note that the principal components are less interpretable and do not have any real meaning since they are constructed as linear combinations of the initial variables.

- On the basis of the information expressed in the previous point, the principal components are defined by ordering the eigenvectors in de-

scending order on the basis of their eigenvalues. At this point it is necessary to choose the components to be kept and discard those with the least information content. Those kept form the feature vector. Hence, the feature vector is simply a matrix that has as columns the eigenvectors of the components that are retained.

- In this step, which is the last, the aim is to use the feature vector formed using the eigenvectors of the covariance matrix, to reorient the data from the original axes to those represented by the principal components. This can be done by multiplying the transposition of the original dataset by the transposition of the characteristic vector.

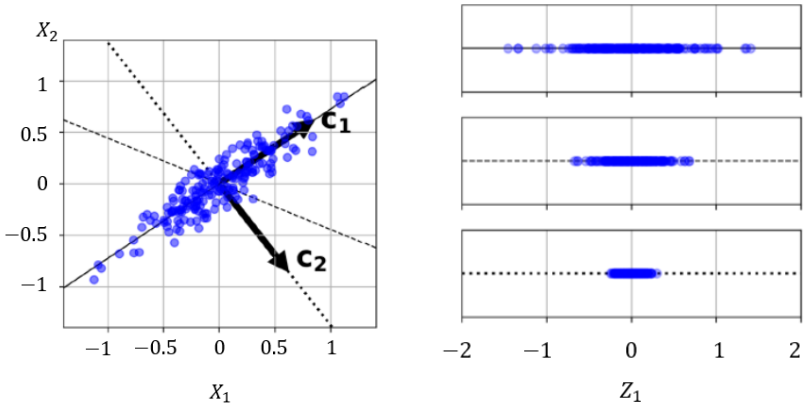

(a) (b)

Figure A.6: Example of Principal Component Analysis [133]: (a) initial dataset; (b) principal components.

Appendix B

Publications

This research activity has led to several publications in international journals and conferences. These are summarized below.[1]

International Journals

1. M. Bindi et al., Failure Prevention in DC–DC Converters: Theoretical Approach and Experimental Application on a Zeta Converter, in IEEE Transactions on Industrial Electronics, vol. 70, no. 1, pp. 930-939, Jan. 2023, doi: 10.1109/TIE.2022.3153827.
2. Bindi, M.; Piccirilli, M.C.; Luchetta, A.; Grasso, F.; Manetti, S. Testability Evaluation in Time-Variant Circuits: A New Graphical Method. Electronics 2022, 11, 1589. https://doi.org/10.3390/electronics11101589.
3. Bindi, M.; Corti, F.; Aizenberg, I.; Grasso, F.; Lozito, G.M.; Luchetta, A.; Piccirilli, M.C.; Reatti, A. Machine Learning-Based Monitoring of DC-DC Converters in Photovoltaic Applications. Algorithms 2022, 15, 74. https://doi.org/10.3390/a15030074.
4. Senzi, A., Bindi, M., Cappellini, I. et al. COVID-19 and VILI: developing a mobile app for measurement of mechanical power at a glance. ICMx 9, 6 (2021). https://doi.org/10.1186/s40635-021-00372-0.
5. Aizenberg, I.; Belardi, R.; Bindi, M.; Grasso, F.; Manetti, S.; Luchetta, A.; Piccirilli, M.C. A Neural Network Classifier with Multi-Valued Neurons for

[1]The author's bibliometric indices are the following: H-index = 5, total number of citations = 54 (source: Scopus on Month 10, 2022).

Analog Circuit Fault Diagnosis. Electronics 2021, 10, 349.
https://doi.org/10.3390/electronics10030349.

6. Aizenberg, I.; Belardi, R.; Bindi, M.; Grasso, F.; Manetti, S.; Luchetta, A.; Piccirilli, M.C. Failure Prevention and Malfunction Localization in Underground Medium Voltage Cables. Energies 2021, 14, 85.
https://doi.org/10.3390/en14010085.
7. M. Bindi, I. Aizenberg, R. Belardi, F. Grasso, A. Luchetta, S. Manetti, M.C. Piccirilli, Neural Network-Based Fault Diagnosis of Joints in High Voltage Electrical Lines, Advances in Science, Technology and Engineering Systems Journal, vol. 5, no. 4, pp. 488-498 (2020).

Submitted

1. Iturrino C.; Bindi M.; Corti F.; Luchetta A.; Grasso F.; Paolucci L.;Picirilli M.C.; Aizenberg I.; Power Quality Analysis Based on Machine Learning Methods for Low Voltage Electrical Distribution Lines, submitted to Electric Power System Research.
2. Bindi M.; Luchetta A.; Lozito G.M.; Carobbi C.F.M.; Grasso F.; Piccirilli M.C.; Frequency Characterization of Medium Voltage Cables for Fault Prevention through Multi-Valued Neural Networks and Power Line Communication Technologies, submitted to IEEE Transaction on Power Delivery.
3. Bindi M.; Luchetta A.; Grasso F.; Piccirilli M.C.; A New Application of Power Line Communication Technologies: Prognosis of Failure in Underground Cables, accepted in the 2nd International Conference on Electrical, Computer, Communications and Mechatronics Engineering (ICECCME).

International Conferences and Workshops

1. M. Bindi et al., Classification of Power Quality disturbances using Multi-Valued Neural Networks and Convolutional Neural Networks, 2022 International Joint Conference on Neural Networks (IJCNN), 2022, pp. 01-08,
doi: 10.1109/IJCNN55064.2022.9892536.
2. M. Bindi, G. Talluri, G. M. Lozito, A. Luchetta, M. C. Piccirilli and F. Grasso, Smart monitoring of DC-DC converters, 2022 IEEE International Conference on Environment and Electrical Engineering and 2022 IEEE Industrial and Commercial Power Systems Europe (EEEIC / I&CPS Europe), 2022, pp. 1-6,
doi: 10.1109/EEEIC/ICPSEurope54979.2022.9854667.
3. M. Bindi, A. Luchetta, L. Paolucci, F. Grasso, S. Manetti and M. C. Piccirilli, Applications of Machine Learning Techniques for the Monitoring of Electrical

Transmission and Distribution lines, 2022 18th International Conference on Synthesis, Modeling, Analysis and Simulation Methods and Applications to Circuit Design (SMACD), 2022, pp. 1-4,
doi: 10.1109/SMACD55068.2022.9816290.

4. M. Bindi, A. Luchetta, P. A. Scarpino, M. C. Piccirilli, F. Grasso and A. Sturchio, Assessment of the health status of Medium Voltage lines through a complex neural network, 2021 AEIT International Annual Conference (AEIT), 2021, pp. 1-6,
doi: 10.23919/AEIT53387.2021.9627068.

5. R Belardi et al 2021 J. Phys.: Conf. Ser. 2022 012007, Thermal Monitoring of Underground Medium Voltage Cables Based on Machine Learning Techniques,
DOI: 10.1088/1742-6596/2022/1/012007.

6. G. Talluri, M. Bindi, A. Luchetta, F. Grasso, L. Luchetti and L. Paolucci, Analysis of Power Losses due to Magnetic Shielding for Electric Vehicle Wireless Charging, 2021 IEEE 15th International Conference on Compatibility, Power Electronics and Power Engineering (CPE-POWERENG), 2021, pp. 1-6,
doi: 10.1109/CPE-POWERENG50821.2021.9501223.

7. M. Bindi et al., Comparison Between PI and Neural Network Controller for Dual Active Bridge Converter, 2021 IEEE 15th International Conference on Compatibility, Power Electronics and Power Engineering (CPE-POWERENG), 2021, pp. 1-6,
doi: 10.1109/CPE-POWERENG50821.2021.9501168.

8. R Belardi et al 2020 IOP Conf. Ser.: Earth Environ. Sci. 582 012001, A complex Neural Classifier for the Fault Prognosis and Diagnosis of Overhead Electrical Lines,
DOI: 10.1088/1755-1315/582/1/012001.

9. M. Bindi, F. Grasso, A. Luchetta, S. Manetti and M. C. Piccirilli, Smart Monitoring and Fault Diagnosis of Joints in High Voltage Electrical Transmission Lines, 2019 6th International Conference on Soft Computing & Machine Intelligence (ISCMI), 2019, pp. 40-44,
doi: 10.1109/ISCMI47871.2019.9004307.

10. I. Aizenberg, M. Bindi, F. Grasso, A. Luchetta, S. Manetti and M. C. Piccirilli, Testability Analysis in Neural Network Based Fault Diagnosis of DC-DC Converter, 2019 IEEE 5th International forum on Research and Technology for Society and Industry (RTSI), 2019, pp. 265-268,
doi: 10.1109/RTSI.2019.8895583.

11. M. Bindi et al 2019 J. Phys.: Conf. Ser. 1304 012006, Modeling and Diagnosis of Joints in High Voltage Electrical Transmission Lines, DOI: 10.1088/1742-6596/1304/1/012006.

National Conferences

1. Bindi M.; Smart monitoring of electrical power systems based on machine learning techniques, Pitch Presentation at XXXVI Riunione Nazionale dei Ricercatori di Elettrotecnica, Ancona, 23-24 june 2022.

Bibliography

[1] I. Aizenberg, R. Belardi, M. Bindi, F. Grasso, S. Manetti, A. Luchetta, and M. C. Piccirilli, "A neural network classifier with multi-valued neurons for analog circuit fault diagnosis," *Electronics (Switzerland)*, vol. 10, no. 3, 2021.

[2] F. Trojan and R. F. M. Marçal, "Proposal of Maintenance-types Classification to Clarify Maintenance Concepts in Production and Operations Management," *Journal of Business and Economics*, vol. 8, no. 7, 2017.

[3] Z. You, E. Sanchez-Sinencio, and J. P. de Gyvez, "Analog System-Level Fault Diagnosis Based on a Symbolic Method in the Frequency Domain," *IEEE Transactions on Instrumentation and Measurement*, vol. 44, no. 1, 1995.

[4] A. Walker, W. E. Alexander, and P. K. Iaa, "Fault Diagnosis in Analog Circuits Using Element Modulation," *IEEE Design and Test of Computers*, vol. 9, no. 1, 1992.

[5] Z. Gao, C. Cecati, and S. X. Ding, "A survey of fault diagnosis and fault-tolerant techniques-part I: Fault diagnosis with model-based and signal-based approaches," 2015.

[6] Z. Gao, C. Cecati, and S. X. Ding, "A survey of fault diagnosis and fault-tolerant techniques-part II: Fault diagnosis with knowledge-based and hybrid/active approaches," *IEEE Transactions on Industrial Electronics*, vol. 62, no. 6, 2015.

[7] M. Tadeusiewicz, P. Sidyk, and S. Hałgas, "A method for multiple fault diagnosis in dynamic analogue circuits," in *European Conference on Circuit Theory and Design 2007, ECCTD 2007*, 2007.

[8] S. Halgas and M. Tadeusiewicz, "Improvement of the search method for parametric fault diagnosis of analog integrated circuits," in *Proceedings of the 23rd International Conference Mixed Design of Integrated Circuits and Systems, MIXDES 2016*, 2016.

[9] S. Tian, C. L. Yang, F. Chen, and Z. Liu, "Circle equation-based fault modeling method for linear analog circuits," *IEEE Transactions on Instrumentation and Measurement*, vol. 63, no. 9, 2014.

[10] D. K. Neitzel, M. E. Simon, R. Widup, and R. J. Schuerger, "IEEE 3007 series: Operation and management, maintenance, and safety of industrial and commercial power systems," in *Conference Record - Industrial and Commercial Power Systems Technical Conference*, 2014.

[11] IEEE, "IEEE Std 3006.3™ -2017 Recommended Practice for Determining the Impact of Preventative Maintenance on the Reliability of Industrial and Commercial Power Systems," tech. rep., 2020.

[12] Y. Zhang, S. Wang, and X. Han, "Research on decision-making process of condition-based maintenance," in *QR2MSE 2013 - Proceedings of 2013 International Conference on Quality, Reliability, Risk, Maintenance, and Safety Engineering*, 2013.

[13] H. M. Hashemian and W. C. Bean, "State-of-the-art predictive maintenance techniques," in *IEEE Transactions on Instrumentation and Measurement*, vol. 60, 2011.

[14] M. Kordestani, M. Saif, M. E. Orchard, R. Razavi-Far, and K. Khorasani, "Failure Prognosis and Applications - A Survey of Recent Literature," *IEEE Transactions on Reliability*, vol. 70, no. 2, 2021.

[15] D. Binu and B. S. Kariyappa, "A survey on fault diagnosis of analog circuits: Taxonomy and state of the art," 2017.

[16] M. U. Farooq, L. Xia, F. A. Hussin, and A. S. Malik, "High level fault modeling and fault propagation in analog circuits using NLARX automated model generation technique," in *ICIAS 2012 - 2012 4th International Conference on Intelligent and Advanced Systems: A Conference of World Engineering, Science and Technology Congress (ESTCON) - Conference Proceedings*, vol. 2, 2012.

[17] S. Wei, Z. Shide, and X. Lijun, "Research on digital circuit fault location procedure based on LASAR," in *Proceedings - ISECS International Colloquium on Computing, Communication, Control, and Management, CCCM 2008*, vol. 2, 2008.

[18] C. Yang, S. Tian, Z. Liu, J. Huang, and F. Chen, "Fault modeling on complex plane and tolerance handling methods for analog circuits," *IEEE Transactions on Instrumentation and Measurement*, vol. 62, no. 10, 2013.

[19] H. Dai and T. M. Souders, "Time-Domain Testing Strategies and Fault Diagnosis for Analog Systems," *IEEE Transactions on Instrumentation and Measurement*, vol. 39, no. 1, 1990.

[20] F. Grasso, S. Manetti, and M. C. Piccirilli, "A symbolic approach to design centering of analog circuits," *Microelectronics Reliability*, vol. 47, no. 8, 2007.

[21] G. Fedi, S. Manetti, M. C. Piccirilli, and J. Starzyk, "Determination of an optimum set of testable components in the fault diagnosis of analog linear circuits," *IEEE Transactions on Circuits and Systems I: Fundamental Theory and Applications*, vol. 46, no. 7, 1999.

[22] F. Grasso, A. Luchetta, S. Manetti, and M. C. Piccirilli, "A method for the automatic selection of test frequencies in analog fault diagnosis," *IEEE Transactions on Instrumentation and Measurement*, vol. 56, no. 6, 2007.

[23] G. Fedi, A. Liberatore, A. Luchetta, S. Manetti, and M. C. Piccirilli, "Symbolic approach to the fault location in analog circuits," in *Proceedings - IEEE International Symposium on Circuits and Systems*, vol. 4, 1996.

[24] G. Fedi, A. Luchetta, S. Manetti, and M. C. Piccirilli, "A new symbolic method for analog circuit testability evaluation," *IEEE Transactions on Instrumentation and Measurement*, vol. 47, no. 2, 1998.

[25] G. Fedi, R. Giomi, A. Luchetta, S. Manetti, and M. C. Piccirilli, "On the application of symbolic techniques to the multiple fault location in low testability analog circuits," *IEEE Transactions on Circuits and Systems II: Analog and Digital Signal Processing*, vol. 45, no. 10, 1998.

[26] G. Fontana, F. Grasso, A. Luchetta, S. Manetti, M. C. Piccirilli, and A. Reatti, "A new simulation program for analog circuits using symbolic analysis techniques," in *2015 International Conference on Synthesis, Modeling, Analysis and Simulation Methods and Applications to Circuit Design, SMACD 2015*, 2015.

[27] N. Sen and R. Saeks, "Fault Diagnosis for Linear Systems Via Multifrequency Measurements," *IEEE Transactions on Circuits and Systems*, vol. 26, no. 7, 1979.

[28] G. Fontana, A. Luchetta, S. Manetti, and M. C. Piccirilli, "A Testability Measure for DC-Excited Periodically Switched Networks with Applications to DC-DC Converters," *IEEE Transactions on Instrumentation and Measurement*, vol. 65, no. 10, 2016.

[29] G. Fontana, A. Luchetta, S. Manetti, and M. C. Piccirilli, "A Fast Algorithm for Testability Analysis of Large Linear Time-Invariant Networks," *IEEE Transactions on Circuits and Systems I: Regular Papers*, vol. 64, no. 6, 2017.

[30] R. S. Berkowitz, "Conditions for Network-Element-Value Solvability," *IRE Transactions on Circuit Theory*, vol. 9, no. 1, 1962.

[31] N. Navid and A. N. Willson, "A Theory and an Algorithm for Analog Circuit Fault Diagnosis," *IEEE Transactions on Circuits and Systems*, vol. 26, no. 7, 1979.

[32] W. H. Huang and C. L. Wey, "Diagnosability analysis of analogue circuits," *International Journal of Circuit Theory and Applications*, vol. 26, no. 5, 1998.

[33] D. Grzechca, T. Golonek, and J. Rutkowski, "Simulated annealing with fuzzy fitness function for test frequencies selection," in *IEEE International Conference on Fuzzy Systems*, 2007.

[34] Z. Ding, J. Zhou, B. Liu, and W. Bai, "Research of Intelligent Fault Diagnosis Based on Machine Learning," in *Proceedings - 2021 International Conference on Computer Network, Electronic and Automation, ICCNEA 2021*, 2021.

[35] A. Ethem, *Introduction to Machine Learning Second Edition Adaptive Computation and Machine Learning.* 2015.

[36] A. C. Ian Goodfellow, Yoshua Bengio, *Deep Learning - Ian Goodfellow, Yoshua Bengio, Aaron Courville - Google Books.* 2016.

[37] K. L. Priddy and P. E. Keller, *Artificial Neural Networks: An Introduction.* 2009.

[38] R. O. Duda, P. E. Hart, and D. G. Stork, *Pattern Classification.* 2000.

[39] M. Lapan, *Deep Reinforcement Learning Learning Hands-on (TOP Reference).* 2019.

[40] A. Eskandari, J. Milimonfared, and M. Aghaei, "Fault Detection and Classification for Photovoltaic Systems Based on Hierarchical Classification and Machine Learning Technique," *IEEE Transactions on Industrial Electronics*, vol. 68, no. 12, 2021.

[41] A. F. Novelo, E. Q. Cucarella, E. G. Moreno, and F. M. Anglada, "Fault diagnosis of electric transmission lines using modular neural networks," *IEEE Latin America Transactions*, vol. 14, no. 8, 2016.

[42] A. Luchetta, S. Manetti, M. C. Piccirilli, A. Reatti, F. Corti, M. Catelani, L. Ciani, and M. K. Kazimierczuk, "MLMVNNN for Parameter Fault Detection in PWM DC-DC Converters and Its Applications for Buck and Boost DC-DC Converters," *IEEE Transactions on Instrumentation and Measurement*, vol. 68, no. 2, 2019.

[43] R. Lasri, "Clustering and classification using a self-organizing MAP: The main flaw and the improvement perspectives," in *Proceedings of 2016 SAI Computing Conference, SAI 2016*, 2016.

[44] M. A. Kramer, "Nonlinear principal component analysis using autoassociative neural networks," *AIChE Journal*, vol. 37, no. 2, 1991.

[45] H. Gao, W. Hong, J. Cui, and Y. Xu, "Optimization of principal component analysis in feature extraction," in *Proceedings of the 2007 IEEE International Conference on Mechatronics and Automation, ICMA 2007*, 2007.

[46] F. Grasso, A. Luchetta, S. Manetti, M. C. Piccirilli, and A. Reatti, "SapWin 4.0-a new simulation program for electrical engineering education using symbolic analysis," *Computer Applications in Engineering Education*, vol. 24, no. 1, 2016.

[47] I. Aizenberg, M. Bindi, F. Grasso, A. Luchetta, S. Manetti, and M. C. Piccirilli, "Testability Analysis in Neural Network Based Fault Diagnosis of DC-DC Converter," in *5th International Forum on Research and Technologies for Society and Industry: Innovation to Shape the Future, RTSI 2019 - Proceedings*, 2019.

[48] Y. Q. Chen, O. Fink, and G. Sansavini, "Combined Fault Location and Classification for Power Transmission Lines Fault Diagnosis With Integrated Feature Extraction," *IEEE Transactions on Industrial Electronics*, vol. 65, no. 1, 2018.

[49] Y. Huang, M. Chen, and J. Zhai, "High impedance fault identification method of the distribution network based on discrete wavelet transformation," in *2011 International Conference on Electrical and Control Engineering, ICECE 2011 - Proceedings*, 2011.

[50] W. Li, Y. Liu, Y. Li, and F. Guo, "Series arc fault diagnosis and line selection method based on recurrent neural network," *IEEE Access*, vol. 8, 2020.

[51] C. Prévé, *Protection of Electrical Networks.* 2006.

[52] J. M. Gers and E. J. Holmes, *Protection of electricity distribution networks, 3rd edition.* 2011.

[53] Z. Melhem, *Electricity Transmission, Distribution and Storage Systems.* 2013.

[54] F. M. Gatta, *Impianti Elettrici.* 2014.

[55] V. Visvanathan and A. Sangiovanni-Vincentelli, "Diagnosability of Nonlinear Circuits and Systems -Part I: The dc Case," *IEEE Transactions on Circuits and Systems*, vol. 28, no. 11, 1981.

[56] R. Saeks, A. Sangiovanni-Vincentelli, and V. Visvanathan, "Diagnosability of Nonlinear Circuits and Systems Part II: Dynamical Systems," *IEEE Transactions on Circuits and Systems*, vol. 28, no. 11, 1981.

[57] L. Wang, Z. Qin, T. Slangen, P. Bauer, and T. Van Wijk, "Grid Impact of Electric Vehicle Fast Charging Stations: Trends, Standards, Issues and Mitigation Measures - An Overview," 2021.

[58] A. Latheef, M. Negnevitsky, K. Muttaqi, and S. Perera, "Present understanding of the impact of distributed generation on power quality," in *2008 Australasian Universities Power Engineering Conference, AUPEC 2008*, 2008.

[59] CENELEC, "En 50160," *European Standard*, vol. 2007, 2005.

[60] CEI/IEC, "61000-4-30:2003, International Standard "Electromagnetic Compatibility (EMC) - Part 4-30: Testing and Measurement Techniques - Power Quality Measurement Methods," *IEC Standard*, 2003.

[61] Institute of Electrical and Electronics Engineers, *IEEE Std 1159 - IEEE Recommended Practice for Monitoring Electric Power Quality.*, vol. 2009. 2009.

[62] J. V. Milanovic and M. Negnevitsky, "Power quality problems and solutions: Current understanding," in *Proceedings of International Conference on Harmonics and Quality of Power, ICHQP*, vol. 1, 1998.

[63] Mohibullah and S. H. Laskar, "Power quality issues and need of intelligent PQ monitoring in the smart grid environment," in *Proceedings of the Universities Power Engineering Conference*, 2012.

[64] Y. Zheng, F. Meng, J. Liu, B. Guo, Y. Song, X. Zhang, and L. Wang, "Fourier Transform to Group Feature on Generated Coarser Contours for Fast 2D Shape Matching," *IEEE Access*, vol. 8, 2020.

[65] W. Qiu, Q. Tang, J. Liu, and W. Yao, "An Automatic Identification Framework for Complex Power Quality Disturbances Based on Multifusion Convolutional Neural Network," *IEEE Transactions on Industrial Informatics*, vol. 16, no. 5, 2020.

[66] M. Garrido, "The Feedforward Short-Time Fourier Transform," *IEEE Transactions on Circuits and Systems II: Express Briefs*, vol. 63, no. 9, 2016.

[67] B. Zhao, Q. Li, Q. Lv, and X. Si, "A Spectrum Adaptive Segmentation Empirical Wavelet Transform for Noisy and Nonstationary Signal Processing," *IEEE Access*, vol. 9, 2021.

[68] S. Santoso, E. J. Powers, W. M. Grady, and A. C. Parsons, "Power quality disturbance waveform recognition using wavelet-based neural classifier - Part 1: theoretical foundation," *IEEE Transactions on Power Delivery*, vol. 15, no. 1, 2000.

[69] I. W. Lee and P. K. Dash, "S-transform-based intelligent system for classification of power quality disturbance signals," in *IEEE Transactions on Industrial Electronics*, vol. 50, 2003.

[70] R. Gong and T. Ruan, "A New Convolutional Network Structure for Power Quality Disturbance Identification and Classification in Micro-Grids," *IEEE Access*, vol. 8, 2020.

[71] M. Valtierra-Rodriguez, R. De Jesus Romero-Troncoso, R. A. Osornio-Rios, and A. Garcia-Perez, "Detection and classification of single and combined

power quality disturbances using neural networks," *IEEE Transactions on Industrial Electronics*, vol. 61, no. 5, 2014.

[72] C. I. Garcia, F. Grasso, A. Luchetta, M. C. Piccirilli, L. Paolucci, and G. Talluri, "A comparison of power quality disturbance detection and classification methods using CNN, LSTM and CNN-LSTM," *Applied Sciences (Switzerland)*, vol. 10, no. 19, 2020.

[73] I. Aizenberg, "Complex-valued neural networks with multi-valued neurons," *Studies in Computational Intelligence*, vol. 353, 2011.

[74] X. Ying, "An Overview of Overfitting and its Solutions," in *Journal of Physics: Conference Series*, vol. 1168, 2019.

[75] M. A. Salam, A. T. Azar, M. S. Elgendy, and K. M. Fouad, "The Effect of Different Dimensionality Reduction Techniques on Machine Learning Overfitting Problem," *International Journal of Advanced Computer Science and Applications*, vol. 12, no. 4, 2021.

[76] I. Aizenberg, A. Luchetta, and S. Manetti, "A modified learning algorithm for the multilayer neural network with multi-valued neurons based on the complex QR decomposition," *Soft Computing*, vol. 16, no. 4, 2012.

[77] S. Khanom and M. R. Islam, "Performance analysis of QR-decomposition RLS and householder sliding window RLS for noise elimination of EEG," in *5th IEEE Region 10 Humanitarian Technology Conference 2017, R10-HTC 2017*, vol. 2018-Janua, 2018.

[78] I. Aizenberg, "MLMVN with soft margins learning," *IEEE Transactions on Neural Networks and Learning Systems*, vol. 25, no. 9, 2014.

[79] M. H. Azarian, E. Lando, and M. Pecht, "An analytical model of the RF impedance change due to solder joint cracking," in *2011 IEEE 15th Workshop on Signal Propagation on Interconnects, SPI 2011 - Proceedings*, 2011.

[80] F. De Paulis, C. Olivieri, A. Orlandi, G. Giannuzzi, F. Bassi, C. Morandini, E. Fiorucci, and G. Bucci, "Exploring remote monitoring of degraded compression and bolted joints in HV power transmission lines," *IEEE Transactions on Power Delivery*, vol. 31, no. 5, 2016.

[81] M. Z. Heider, M. M. Rahman, and A. A. Al-Arainy, "Study of frequency variant tan delta diagnosis for MV cables insulation status assessment," *2019 5th International Conference on Advances in Electrical Engineering, ICAEE 2019*, pp. 260–264, 2019.

[82] L. Lampe, A. M. Tonello, and T. G. Swart, *Communications Principles , Standards and Applications From Multimedia.* 2016.

[83] A. Cataliotti, A. Daidone, and G. Tinè, "A medium-voltage cables model for power-line communication," *IEEE Transactions on Power Delivery*, vol. 24, no. 1, pp. 129–135, 2009.

[84] A. Cataliotti, D. Di Cara, and G. Tinè, "Model of line to shield power line communication system on a Medium Voltage network," *2010 IEEE International Instrumentation and Measurement Technology Conference, I2MTC 2010 - Proceedings*, pp. 1459–1462, 2010.

[85] G. Fontana, F. Grasso, A. Luchetta, S. Manetti, M. C. Piccirilli, and A. Reatti, "Testability Analysis Based on Complex-Field Fault Modeling," in *SMACD 2018 - 15th International Conference on Synthesis, Modeling, Analysis and Simulation Methods and Applications to Circuit Design*, 2018.

[86] M. Bindi, I. Aizenberg, R. Belardi, F. Grasso, A. Luchetta, S. Manetti, and M. C. Piccirilli, "Neural network-based fault diagnosis of joints in high voltage electrical lines," *Advances in Science, Technology and Engineering Systems*, vol. 5, no. 4, 2020.

[87] I. Aizenberg, R. Belardi, M. Bindi, F. Grasso, S. Manetti, A. Luchetta, and M. C. Piccirilli, "Failure prevention and malfunction localization in underground medium voltage cables," *Energies*, vol. 14, no. 1, 2021.

[88] A. Sturchio, G. Fioriti, M. Pompili, and B. Cauzillo, "Failure rates reduction in SmartGrid MV underground distribution cables: Influence of temperature," in *2014 AEIT Annual Conference - From Research to Industry: The Need for a More Effective Technology Transfer, AEIT 2014*, 2015.

[89] Y. Jiang, "Data-driven fault location of electric power distribution systems with distributed generation," *IEEE Transactions on Smart Grid*, vol. 11, no. 1, 2020.

[90] N. Bayati, H. R. Baghaee, A. Hajizadeh, M. Soltani, Z. Lin, and M. Savaghebi, "Local Fault Location in Meshed DC Microgrids Based On Parameter Estimation Technique," *IEEE Systems Journal*, vol. 16, no. 1, 2022.

[91] P. Dehghanian, M. Fotuhi-Firuzabad, F. Aminifar, and R. Billinton, "A comprehensive scheme for reliability centered maintenance in power distribution systems - Part i: Methodology," *IEEE Transactions on Power Delivery*, vol. 28, no. 2, 2013.

[92] E. S. Kapareliotis, K. E. Drakakis, H. P. K. Dimitriadis, and C. N. Capsalis, "Fault recognition on power networks via SNR analysis," *IEEE Transactions on Power Delivery*, vol. 24, no. 4, 2009.

[93] J. Nsengiyaremye, P. C. Bikash, and M. M. Begovic, "Low-Cost Communication-Assisted Line Protection for Multi-Inverter Based Microgrids," *IEEE Transactions on Power Delivery*, vol. 36, no. 6, 2021.

[94] A. N. Milioudis, G. T. Andreou, and D. P. Labridis, "Enhanced protection scheme for smart grids using power line communications techniques - Part I: Detection of high impedance fault occurrence," *IEEE Transactions on Smart Grid*, vol. 3, no. 4, 2012.

[95] A. N. Milioudis, G. T. Andreou, and D. P. Labridis, "Enhanced protection scheme for smart grids using power line communications techniques-Part II: Location of high impedance fault position," *IEEE Transactions on Smart Grid*, vol. 3, no. 4, 2012.

[96] J. Borghetto, G. Pirovano, C. Tornelli, and A. Contin, "Frequency Dielectric Spectroscopy and Dissipation Factor Measurements during Thermal Cycles on Different Types of MV Cable Joints," in *2021 Electrical Insulation Conference, EIC 2021*, 2021.

[97] A. Ghaderi, A. Mingotti, F. Lama, L. Peretto, and R. Tinarelli, "Effects of temperature on mv cable joints tan delta measurements," *IEEE Transactions on Instrumentation and Measurement*, vol. 68, no. 10, 2019.

[98] A. Zhao and L. Gu, "Study on the temperature distribution of the outer surface of the cable intermediate joint based on ANSYS simulation," in *Proceedings of 2018 IEEE 4th Information Technology and Mechatronics Engineering Conference, ITOEC 2018*, 2018.

[99] L. Calcara, S. Sangiovanni, and M. Pompili, "MV underground cables: Effects of soil thermal resistivity on anomalous working temperatures," in *2017 AEIT International Annual Conference: Infrastructures for Energy and ICT: Opportunities for Fostering Innovation, AEIT 2017*, vol. 2017-Janua, 2017.

[100] C. H. Lee, J. J. Kwon, J. H. Byoun, D. Y. Wee, S. H. Nam, J. H. Lee, K. I. Sohn, J. T. Cho, and J. Y. Kim, "Medium voltage optical fiber composite power cable system for smart grid," in *IET Conference Publications*, vol. 2013, 2013.

[101] M. Aihara, Y. Ebinuma, M. Minami, and M. Murakawa, "Insulation monitoring system for XLPE cable containing water sensor and optical fiber," 1991.

[102] R. Papazyan, "Technique for localization of degraded cable insulation regions using TDR measurement artefacts," in *2021 13th Electrical Engineering Faculty Conference, BulEF 2021*, 2021.

[103] W. McDermid, M. Partyka, and T. Black, "Water Tree Detection in Medium Voltage XLPE Cables," in *2019 IEEE Electrical Insulation Conference, EIC 2019*, 2019.

[104] A. Cataliotti, A. Daidone, and G. Tinè, "Power line communication in medium voltage systems: Characterization of MV cables," *IEEE Transactions on Power Delivery*, vol. 23, no. 4, 2008.

[105] A. Cataliotti, V. Cosentino, S. Guaiana, D. Di Cara, N. Panzavecchia, and G. Tinè, "Experimental investigation on PLC signal crossing of power transformers," *Conference Record - IEEE Instrumentation and Measurement Technology Conference*, pp. 1235–1239, 2014.

[106] A. Cataliotti, V. Cosentino, D. Di Cara, P. Russotto, and G. Tinè, "On the use of narrow band power line as communication technology for medium and low voltage smart grids," *2012 IEEE I2MTC - International Instrumentation and Measurement Technology Conference, Proceedings*, pp. 619–623, 2012.

[107] A. O. Adeniyi, J. J. Walker, and C. Nyamupangedengu, "Influence of temperature on tan-delta of XLPE cables," in *Proceedings - 2019 Southern African Universities Power Engineering Conference/Robotics and Mechatronics/Pattern Recognition Association of South Africa, SAUPEC/RobMech/PRASA 2019*, 2019.

[108] H. Tarzamni, F. P. Esmaeelnia, M. Fotuhi-Firuzabad, F. Tahami, S. Tohidi, and P. Dehghanian, "Comprehensive Analytics for Reliability Evaluation of Conventional Isolated Multiswitch PWM DC-DC Converters," *IEEE Transactions on Power Electronics*, vol. 35, no. 5, 2020.

[109] H. Givi, E. Farjah, and T. Ghanbari, "A comprehensive monitoring system for online fault diagnosis and aging detection of non-isolated DC-DC converters' components," *IEEE Transactions on Power Electronics*, vol. 34, no. 7, 2019.

[110] L. Wen, X. Li, L. Gao, and Y. Zhang, "A New Convolutional Neural Network-Based Data-Driven Fault Diagnosis Method," *IEEE Transactions on Industrial Electronics*, vol. 65, no. 7, 2018.

[111] Y. Lei, F. Jia, J. Lin, S. Xing, and S. X. Ding, "An Intelligent Fault Diagnosis Method Using Unsupervised Feature Learning Towards Mechanical Big Data," *IEEE Transactions on Industrial Electronics*, vol. 63, no. 5, 2016.

[112] T. Dragicevic, P. Wheeler, and F. Blaabjerg, "Artificial Intelligence Aided Automated Design for Reliability of Power Electronic Systems," *IEEE Transactions on Power Electronics*, vol. 34, no. 8, 2019.

[113] Z. Li, Y. Gao, X. Zhang, B. Wang, and H. Ma, "A Model-Data-Hybrid-Driven Diagnosis Method for Open-Switch Faults in Power Converters," *IEEE Transactions on Power Electronics*, vol. 36, no. 5, 2021.

[114] S. Dusmez, S. H. Ali, M. Heydarzadeh, A. S. Kamath, H. Duran, and B. Akin, "Aging precursor identification and lifetime estimation for thermally aged discrete package silicon power switches," *IEEE Transactions on Industry Applications*, vol. 53, no. 1, 2017.

[115] M. S. Haque and S. Choi, "Sparse Kernel Ridge Regression Assisted Particle Filter Based Remaining Useful Life Estimation of Cascode GaN FET," *IEEE Transactions on Industrial Electronics*, vol. 68, no. 8, 2021.

[116] M. Tadeusiewicz and S. Halgas, "A Method for Local Parametric Fault Diagnosis of a Broad Class of Analog Integrated Circuits," *IEEE Transactions on Instrumentation and Measurement*, vol. 67, no. 2, 2018.

[117] S. Kiranyaz, A. Gastli, L. Ben-Brahim, N. Al-Emadi, and M. Gabbouj, "Real-Time Fault Detection and Identification for MMC Using 1-D Convolutional Neural Networks," *IEEE Transactions on Industrial Electronics*, vol. 66, no. 11, 2019.

[118] S. H. Kim, D. Y. Yoo, S. W. An, Y. S. Park, J. W. Lee, and K. B. Lee, "Fault Detection Method Using a Convolution Neural Network for Hybrid Active Neutral-Point Clamped Inverters," *IEEE Access*, vol. 8, 2020.

[119] G. Fontana, A. Luchetta, S. Manetti, and M. C. Piccirilli, "An unconditionally sound algorithm for testability analysis in linear time-invariant electrical networks," *International Journal of Circuit Theory and Applications*, vol. 44, no. 6, 2016.

[120] K. Woranetsuttikul, K. Pinsuntia, N. Jumpasri, T. Nilsakorn, and W. Khan-Ngern, "Comparison on performance between synchronous single-ended primary-inductor converter (SEPIC) and synchronous ZETA converter," in *2014 International Electrical Engineering Congress, iEECON 2014*, 2014.

[121] A. M. Khatab, M. I. Marei, and H. M. Elhelw, "An Electric Vehicle Battery Charger Based on Zeta Converter Fed from a PV Array," in *Proceedings - 2018 IEEE International Conference on Environment and Electrical Engineering and 2018 IEEE Industrial and Commercial Power Systems Europe, EEEIC/I and CPS Europe 2018*, 2018.

[122] V. Bist and B. Singh, "Power factor correction in a brushless DC motor drive using an isolated-Luo converter," in *Proceedings of 6th IEEE Power India International Conference, PIICON 2014*, 2014.

[123] J. A. Ziani, M. J. B. Ghorbal, and S. Moussa, "Comparative study of Boost and Zeta converters in DC microgrid applications," in *6th IEEE International Energy Conference, ENERGYCon 2020*, 2020.

[124] F. L. Luo, "Luo-converters, voltage lift technique," in *PESC Record - IEEE Annual Power Electronics Specialists Conference*, vol. 2, 1998.

[125] D. K. Papakostas and A. A. Hatzopoulos, "A unified procedure for fault detection of analog and mixed-mode circuits using magnitude and phase components of the power supply current spectrum," *IEEE Transactions on Instrumentation and Measurement*, vol. 57, no. 11, 2008.

[126] E. A. Mertens, L. F. Dias, F. A. Fernandes, B. D. Bonatto, J. P. Abreu, and H. Arango, "Evaluation and trends of power quality indices in distribution system," in *2007 9th International Conference on Electrical Power Quality and Utilisation, EPQU*, 2007.

[127] Y. H. Chung, G. H. Kwon, T. B. Park, H. J. Kim, and J. I. Moon, "Voltage Sag, Swell and Flicker Generator with series injected inverter," in *2005 IEEE Power Engineering Society General Meeting*, vol. 2, 2005.

[128] D. Galzina, "Economic approach to power quality mitigation," in *Proceedings of International Conference on Harmonics and Quality of Power, ICHQP*, vol. 2018-May, 2018.

[129] V. Gali, N. Gupta, and R. A. Gupta, "Mitigation of power quality problems using shunt active power filters: A comprehensive review," in *Proceedings of the 2017 12th IEEE Conference on Industrial Electronics and Applications, ICIEA 2017*, vol. 2018-Febru, 2018.

[130] D. Ivan, G. Lazaroiu, G. Ungureanu, and O. Udrea, "Influence on the power quality of the connection of wind power into the electricity grid transmission," in *Proceedings of International Conference on Harmonics and Quality of Power, ICHQP*, 2014.

[131] N. Mohan, K. P. Soman, and R. Vinayakumar, "Deep power: Deep learning architectures for power quality disturbances classification," in *Proceedings of 2017 IEEE International Conference on Technological Advancements in Power and Energy: Exploring Energy Solutions for an Intelligent Power Grid, TAP Energy 2017*, 2018.

[132] S. Alshahrani, M. Abbod, B. Alamri, and G. Taylor, "Evaluation and classification of power quality disturbances based on discrete Wavelet Transform and artificial neural networks," in *Proceedings of the Universities Power Engineering Conference*, vol. 2015-Novem, 2015.

[133] A. Géron, *Hands-on machine learning with Scikit-Learn and TensorFlow : concepts, tools, and techniques to build intelligent systems.* 2019.